1989

Structural analysis/design of large robotic manipulators

Udaykumar G. Parshionikar
Lehigh University

STRUCTURAL ANALYSIS/DESIGN

OF LARGE ROBOTIC MANIPULATORS

by

Udaykumar G. Parshionikar

A Thesis

Presented to the Graduate Committee

of Lehigh University

in Candidacy for the Degree of

Master of Science

in

Mechanical Engineering and Mechanics Department

Lehigh University

1989

Certificate of Approval

This thesis is accepted and approved in partial fulfillment of the requirements for the degree of Master of Science.

5/16/89

Date

Professor in Charge

Dr. N. Duke Perreira

F. Erdogan

Chairman of Department

Dr. Fazil Erdogan

Acknowledgements

The analyses and results reported herein form part of an investigation on the "Automated All-Weather Cargo Transfer System" financially sponsored by the US Army, Belvoir RD&E Center, and carried out by the joint venture of Mr. Donald E. Lee and August Design and Development, Ardmore, PA. The work reported in this paper was conducted under the guidance of Professor N. Duke Perreira of the Mechanical Engineering Department and Manufacturing Systems Engineering program.

The author wishes to express his sincere gratitude to Professor N. Duke Perreira whose guidance and expertise proved immensely important in working on the problem of large robotic manipulators. Sincere thanks and appreciation are also due to Mr. Donald E. Lee, the Principal Investigator of the Ben Franklin Partnership project # 14.6 "Design/Analysis of a Large Robot Arm for AACTS", for his valuable and creative suggestions throughout the project. He has also been very helpful in providing whatever material and data needed to conduct the analyses. It has been, on the whole, an educating experience for the author to meet regularly with them, both of whom are experts in their own field.

Special thanks are again due to Mr. Donald Lee for his help and extreme patience in proof-reading and correcting the manuscripts of the project report to make it more readable and understandable.

Table of Contents

List of Tables

List of Figures

Abstract

This thesis report presents a methodology for design and analysis of "large" robotic manipulators. A definition for "large"ness of a manipulator is proposed. "Large" robotic manipulators have been treated as mechanisms as well as structures in suggesting a design and analysis procedure. Problems anticipated with increase in the size of the robots are discussed and guidelines have been set forth to overcome them. The general concepts developed were applied to a particular application.

A conceptual design of a 140 ft long SCARA type robotic manipulator arm with a lift capacity of 70,000 lb, developed by August Design and Development (ADD) for an Automated All-Weather Cargo Transfer System (AACTS), was analyzed. A tenth scale model, which will be built by ADD as a proof of concept and for experimental testing purposes, was also analyzed. The manipulator arm, consisting of space-frame structures, was analyzed using the Finite Element Analysis code - ANSYS. Both static and dynamic types of structural analysis were used to evaluate the structure under conditions which simulate off-shore working conditions. The static analysis included force, stress and displacement calculations for the manipulator arm in different orientations, and a linear and non-linear buckling analysis. The dynamic analysis included modal analysis, harmonic response analysis and transient force response analysis.

A preliminary design was developed for both the tenth scale and the full scale arm, using results from the conceptual design analysis. Static and dynamic analysis of the improved designs have shown that the present design achieves the required structural rigidity with lower weight and significantly lower stress levels. The fully extended full scale arm deflects less than 2.5 inches when lifting a 70,000 lb load at a distance of 140 ft. High structural rigidity can be attributed to the space frame nature of the manipulator.

1. Introduction

1.1 Definition of Design Process for Structures

Many engineers and most students often confuse design with calculation of the size of a beam, the thickness of a plate, diameter of the bolts to be used, and numerous other similar calculations. Though such detail calculations are an essential part of the design process, such calculations only should come towards the end of the process. For structural design, the design process is more aptly defined in the words of D. J. Fraser as "an essentially trial and error procedure consisting of three interacting aspects : conceptual design or decision making; structural analysis and proportioning members; and subsequent detailed design" [1]. These three aspects or stages are explained as in the following sections.

1.1.1 Conceptual Design or Decision Making

Fundamental engineering knowledge alone is not sufficient to create a structure. A conceptual process of logical thinking is needed in which the engineering techniques are the base from which the logic operates. This is the process of conceptual design, the first stage of the design process. Conceptual design, requires:

i) the recognition of constraints and parameters relevant to the project,

ii) the assembly of constraints and the identification of their interrelationship,

iii) the devising of a structure to comply with the demands of the constraints.

1.1.2 Preliminary Analysis and Design

Design is an iterative process. As any other iterative procedure, the usefulness of design procedure depends on its "rate of convergence", that is the number of iterations or trials needed in reaching the final design. This rate of convergence can be greatly

increased if the procedure starts with trial answers that are reasonable estimates of the final solution. The preliminary analysis and design stage of the process aims at obtaining reasonable estimates of the member sizes and/or analytical results, so that a minimal number of detailed analyses and design checks are required in arriving at the final solution. This stage also provides quick evaluation of several conceptual design solutions, hence facilitating design making in the conceptual design process.

1.1.3 Detailed Design

During conceptual design, the designer resorts to thinking on broad terms rather than succumbing to the detailed mathematics of the final design. Preliminary Analysis and Design involves approximate methods of analysis in order to get reasonable estimates for the final solution. In the third stage of design, the detailed design, the designer has to draw upon all of his engineering expertise to perform an exhaustive analysis of the structure devised and detail its each and every single part. These three phases of the design process, however, are not totally independent. Detailed design analyses may lead to results which may require a complete reexamination of the conceptual design.

1.2 Design Procedure for Robotic Manipulators

B. O. Nnaji[2] details a procedure for design of robots as follows :

1. Use workplace/task information to determine the number of links and degrees of freedom at each joint.

2. Use load and number of links to determine the physical properties of links (sizes in discrete form) and nature of joints.

3. Using production (throughput) requirements, determine speed of the skeleton robotic setup.

4. With load and mass of the links, determine the torque, relative velocity and

position using kinematic and/or dynamic equations for motion and position.

5. Choose the gripper mechanism based on load size and fragility.

6. Using the energy requirements, torque and velocity, go to the drive system block and choose a motor setup.

7. Choose sensory system based on the complexity of tasks.

8. Using the speed, motor type, workplace and complexity of tasks, choose a control system.

9. Evaluate the feasible configurations, (the combinations of joint types), to determine an appropriate robot(s).

10. Using a mathematical evaluating system, determine the best robot.

In this thesis report, we are concerned only with the structural design of a robot. Hence, only steps 1 through 4 detailed above, will be of interest. With reference to the Fraser[1] definition of design of structures, steps #1 through 3 belong to the decision making or conceptual design stage; whereas step #4 and part of step #2 (sizes of links) belong to both the preliminary analysis as well as detailed design stage.

1.2.1 Structural Design of Robotic Manipulators

The prime objective of this thesis report is to elaborate the design/analysis procedure used for a 70 kip payload and 140 ft. long robotic manipulator; and to set some guidelines for design/analysis of very large robotic manipulators, using the experience obtained during the design work. We are concerned about robots of sizes larger than those currently found in a typical automated manufacturing facility. These robots generally measure between 3-13 ft in size, robots of sizes in the order of 100 ft have to be given special treatment in their structural analysis. We adapt the Fraser definition of structural design, which was devised for (large) civil engineering structures, as a basis for organizing the methods required for the purpose of structural design of a robotic manipulator. The structural design of robots can be then described as :

1.2.1.1 Conceptual Design

The conceptual design stage is one of the most creative steps of the design process. Many would recommend "brain-storming" without concern about feasibility, to come up with ideas. During the latter portions of this design stage the designs are limited to those which meet the constraints.

Step 1) Recognition of Relevant Constraints and Parameters

Constraints are the factors that confine design choices whereas parameters are the factors that define a feasible scheme. For example, while designing a robot to do pick and place inside cylindrical workspace, a constraint might be the shape of the workspace (hence perhaps a cylindrical coordinate linkage arrangement) whereas a parameter might be the height of that cylindrical work space. Similarly, if a situation dictates that a RRR manipulator be used then the RRR design would be a constraint whereas the actual lengths and cross-sectional dimensions of the links would be the parameters involved.

Vukobratovic [25] mentions four constraints in design of robots : reachability constraint, elasticity constraint, actuator constraint and stress constraint. Economic constraint (that the proposed design be cost-effective, [2]) is also a contributing factor in the design. However, using the first axiom of Suh's Axiomatic Design Method [47] we concentrate our work using only the most important - the "reachability constraint". Others constraints are left for later stages.

The Reachability Constraint states that a manipulator should be able to be configured to perform the required task. This means that it should be able to reach all the points in space where the task needs to be performed and should be able to have certain amounnt of dexterity at each of those points. The volume and shape of the workspace is defined by the basic kinematics of the manipulator. Factors like structural tolerances, thermal conditions of the links, payload being manipulated, velocities and

accelerations of the links are of lesser importance during this design stage [30]. The dexterity is defined by the range of degrees of orientation the robot has at any of the reachable points. Degree of redundancy may be important if points in the workspace need to be reached in more than one way (so as to avoid obstacles and to overcome degeneracy problems). The reachability constraint basically refers to the kinematic capabilities of the manipulator. These capabilities are decided by various parameters :

1. Physical Linkage Arrangement

Arrangements based upon different coordinate systems have advantages and disadvantages of their own with respect to their workspace shapes, dead zones, clearance volume requirements, dexterity and ease of programming and visualization. These can be tabulated as in table 1.1 [4].

Table 1.1 -- Robot Linkage Arrangements : Advantages and Disadvantages

Advantages	Disadvantages
i) Cartesian Coordinates	
• Moves in three linear directions and thus is easy to visualize.	• Requires large volume to operate in, even though whole space is not used.
• Easy Computation.	• Largest surface area required of all configurations.
• Most rigid structure for given length, since it is supported at both ends.	• Exposed guiding surfaces require covering or boots in dusty or corrosive atmosphere.

ii) Cylindrical Coordinates

- Easy to visualize and compute.
- Linear drives well suited to use of hydraulic drives. Therefore, can provide great power.
- Good access into cavities and machine openings.
- Restricted volume of access. Cannot reach cylindrical volume near vertical support or floor.
- Both radius drive and vertical drive are exposed. Difficult to seal from dust and liquids.
- Possible to have rear clearance volume overlap with work envelope.

iii) Spherical Coordinates

- Covers large volume from one central support.
- Two rotary drives can easily be sealed.
- Covers a large volume.
- Complex coordinates difficult to visualize and control.
- One linear drive. May be sealing and protection problems.
- Restricted volume coverage.

iv) Revolute Coordinates

- All joints are rotary. Maximum flexibility, since any location in the total volume can be reached.
- Joints can be completely sealed. Useful in dusty or corrosive locations, or under water.
- Require more expensive drives when using hydraulics, but well suited to electric motor drives.
- Visualization and control are most difficult in this configuration.
- Restricted volume coverage.

2) Dexterity of the Robot

i) Degrees of Freedom (d.o.f.) -- of the robot decide the ability and flexibility of a robot in reaching out points in space with varying orientations. At least six degrees of freedom are needed to emulate the human arm, that is, reach all the points in the workspace and acheive many desired orientations at each of these. Some tasks may need less than six d.o.f.s while some might need more for redundancy to avoid obstacles.

ii) Arm and Body motions -- needed to acheive a prescribed task may involve vertical, radial and rotational traverses. Vertical traverse is the up-and-down motion of the arm, radial traverse is the extension or retraction of the arm allowing change of effective length of the arm, whereas rotational traverse is the rotation about the vertical axis.

iii) Wrist motions -- such as swivel, bend and yaw may be required to acheive certain tasks. Again some would need several continuous rotations to occur (like screwing in a bolt), while others would find limited rotations sufficient.

Step 2) Assembly of constraints and the identification of their interrelationship

Conceptual structural design of a robotic manipulator should only be concerned with the reachability constraint. This gives one the ability to exercise his/her imagination and creativity to design a manipulator mechanism to acheive the given task(s). Detailed kinematic analyses is performed during the design stage while feasiblity analysis is done during the preliminary analysis stage of design.

R. C. Dorf[5] suggests that the range of tasks for which the robot is being built should be defined before the actual task of devising the structure. This range of tasks should be specified as clearly as possible so that detailed manipulator properties and feature specifications may be developed. No single robot linkage arrangement will perform well on tasks of widely varying description. Therefore a robot should be designed to have only the flexibility it needs to perform the range for which it is

intended.

Step 3) Devising of a structure to comply with the demands of the constraints

Kinematic chains used to form the structure of a robotic manipulator, can be classified as simple or complex. Complex chains are formed by combining several simple ones. Simple kinematic chains can be open or closed. In a closed chain, each member enters into two two kinematic pairs, while in an open chain, the last member enters into only one kinematic pair. With complex chains, the individual members may enter into three or more kinematic pairs [25]. Examples of simple and complex chains are given in Fig. 1.1.

A very large majority of the existing industrial manipulators are of simple, open kinematic chains. However, closed kinematic chains are also becoming popular because of their property of their reduced overall inertia of moving components and increasing the payload. These improvements are gained at a loss of reachability and dexterity. Examples of such manipulators are "parallelogram structure" and "five-bar mechanism" as shown in Fig. 1.2[3]. The parallelogram structure shown has five joints but only three d.o.f.s. The heavy motor-transmission units are stationary and motion is delivered to the end of the arm by the additional power transmitting links. This requires a more complicated design and higher manufacturing costs. The additional links and kinematic redundancy increase structural stiffness and may require stricter manufacturing tolerances. In order to achieve the same reachability, closed kinematic chains require a larger number of links. For example, the five-bar linkage shown in Fig. 1.2(b) a proportioning of its links in order to achieve the same reachability as of the much simpler three-bar mechanism shown in Fig. 1.2(c). Although closed chain systems can generally speaking hold a greater payload, they are more difficult to analyze and program than open chain systems.

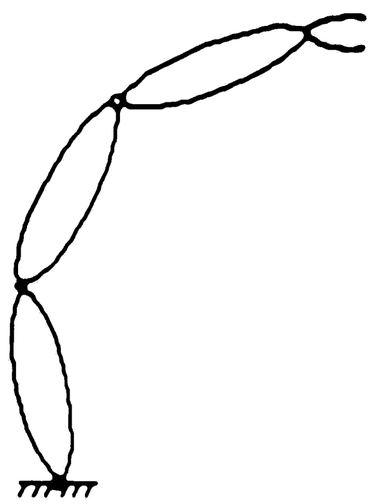

(a) Open Chain

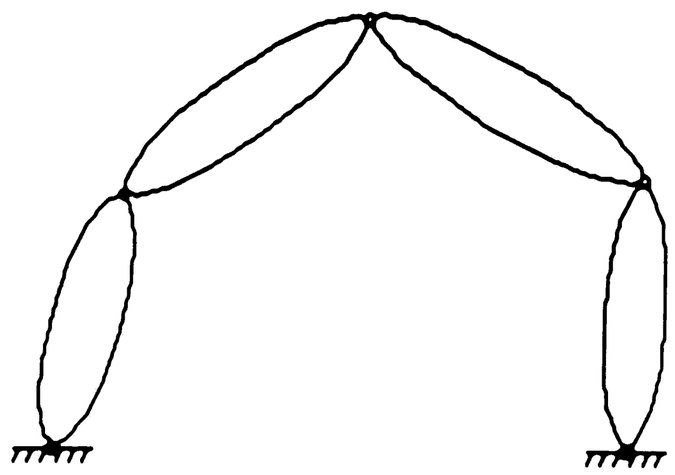

(b) Closed Chain

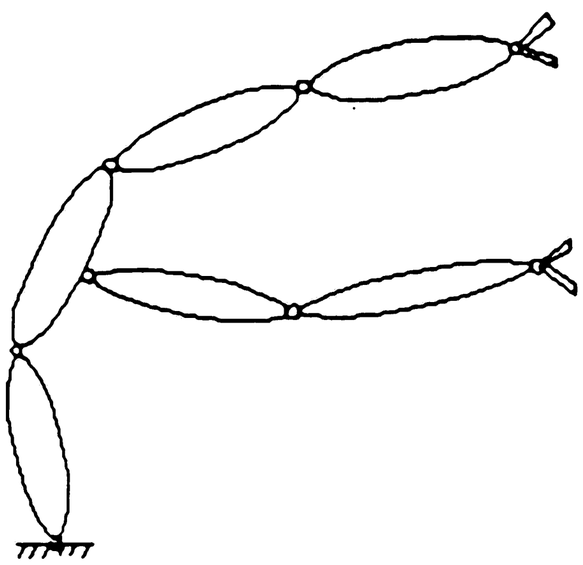

(c) Branched Chain

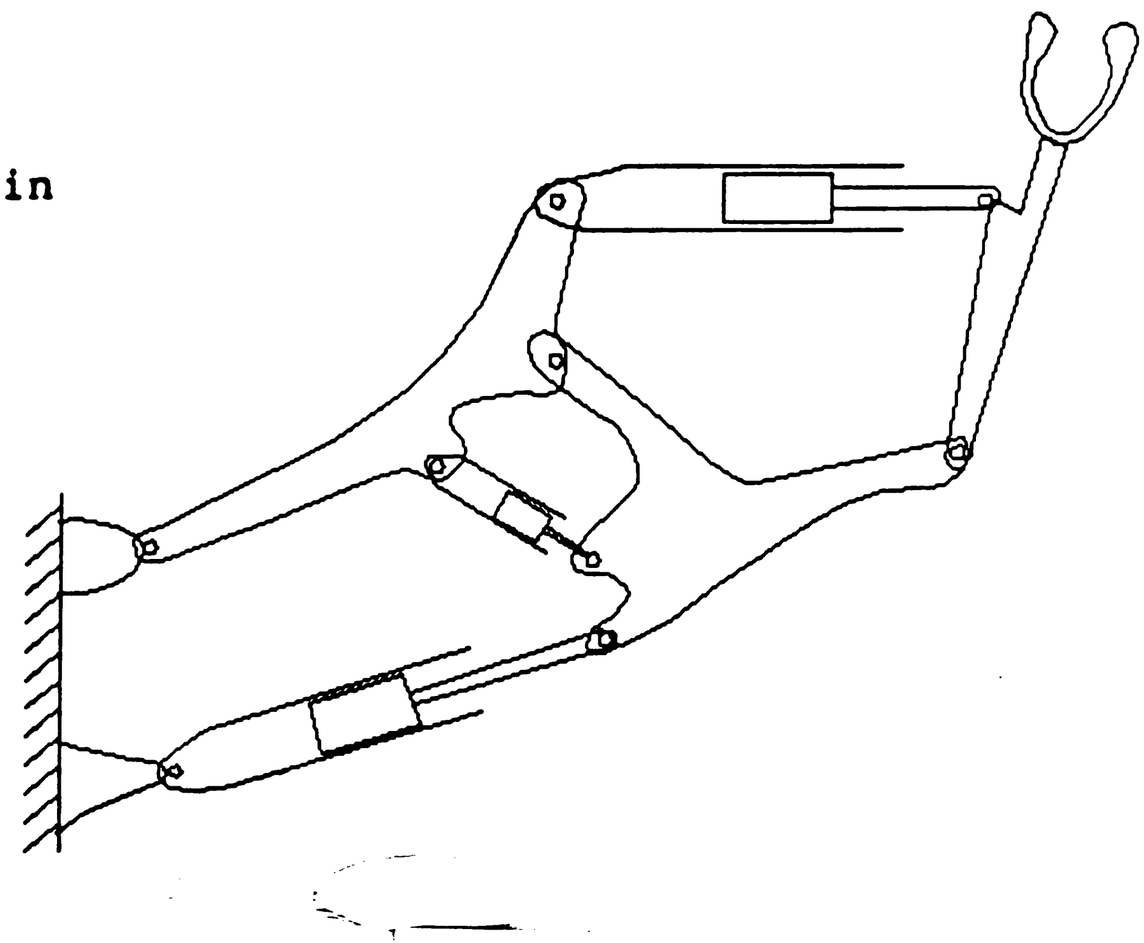

Complex Chain

Fig. 1.1 : Simple (a-Open, b-Closed and c-Branched) and Complex Kinematic Chains

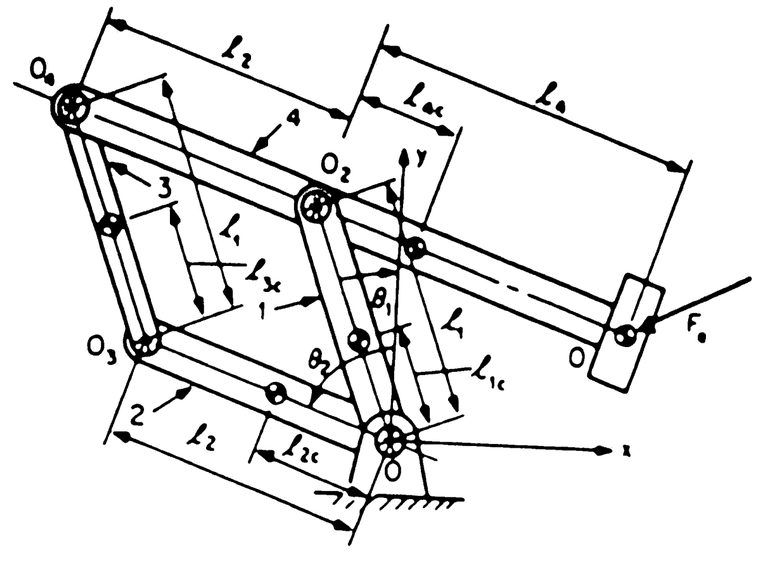

(a) Parallelogram Linkage

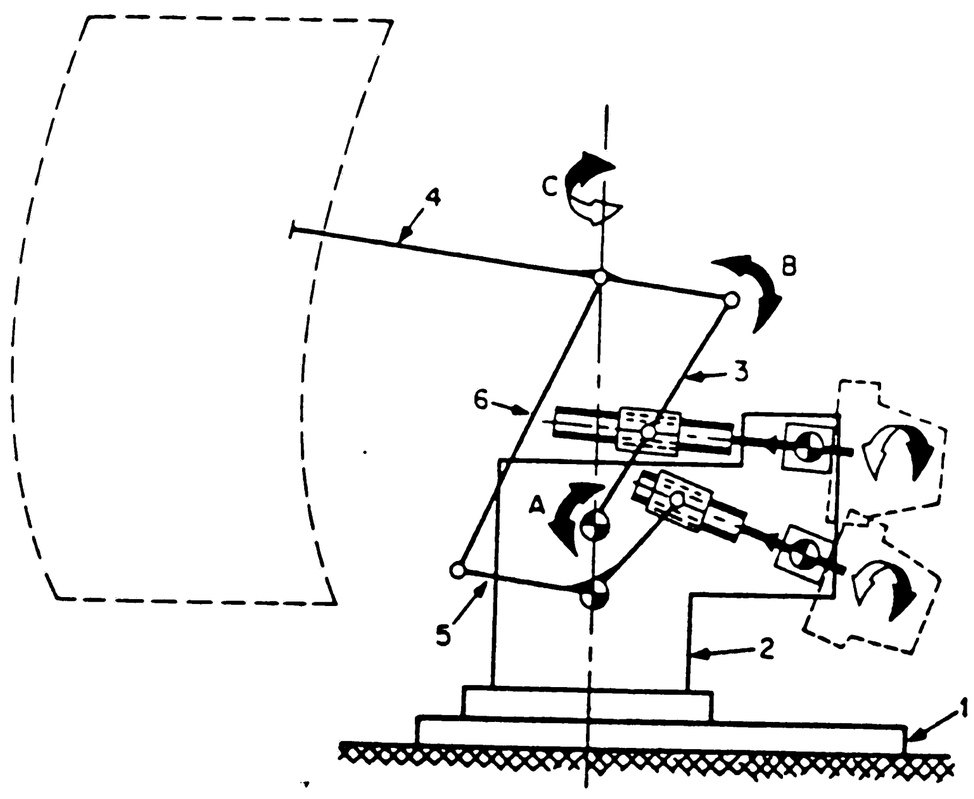

(b) Five-Bar Linkage

Fig. 1.2 : "Parallelogram structure" and "five-bar mechanism"

Mobility and design features of the arm depend on the type and placement of joints. Fig. 1.3 [33] shows possible kinematic configurations of three P and/or R joints together with their idealized workspace shapes. Rivin [3] specifies the following three conditions on the relative positioning of the joints of the linkage, at least one of which should be satisfied, to move the end-point of the arm in three-dimensional space --

i) There are two revolute joints with nonparallel axes.

ii) There are two revolute joints with parallel axes and one prismatic joint whose axis is not perpendicular to the revolute joint axes.

iii) There are two prismatic joints with nonparallel axes and one revolute joint whose axis is not perpendicular to the plane containing the axes of the prismatic joints or the third prismatic joint whose axis is nonparallel to that plane.

K.C. Gupta and B. Roth [23] introduce some basic concepts regarding workspace of manipulators which are of the form of series of links joined by revolute axes. They deal with the two basic issues of kinematics : Given the structure, what is the workspace? And, given a desired workspace, what should be the manipulator structure? The paper discusses the relationship between the twist angles and transverse dimensions of the adjacent links on the workspace, and identifies conditions when holes and voids are introduced in the workspace. The effects of the size of the hand (end effector) on the primary (dextrous) workspace and effects of introducing a spherical joint in the linkage on the primary workspace are also discussed.

A complete discussion of the linkage arrangement types applicable to most processes is given in Perreira and Colson [46]. Some kinematic structures for use in manipulator designs are constructed in terms of components. C. F. Earl and J. Rooney discuss general properties of kinematic structures and a method for combining two given structures in [31]. Two types of components, actuation and distribution components, are specified. Modification of the structures is effected by transfer of drives. Existing designs for manipulators are examined and some new designs are generated.

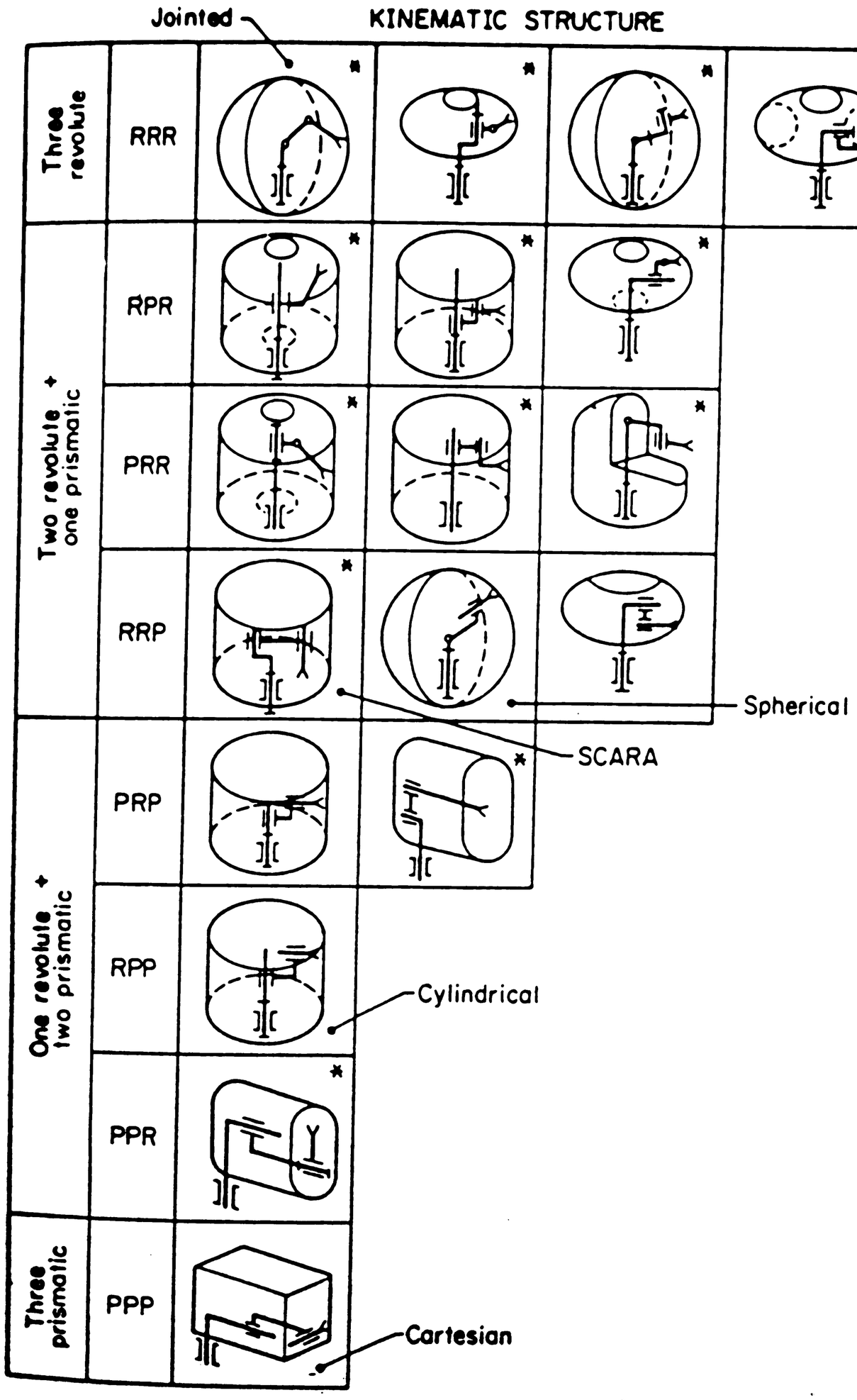

Fig. 1.3 : Possible kinematic configurations of three-jointed robot manipulators.

M. A. Shaik and P. Datseris [23] approach manipulator design as an optimization problem. They propose a method for calculation of workspace volume of generalized manipulators which include both revolute and prismatic joints. It is seen that for a fixed length of generalized manipulator, optimization of workspace volume leads to specific manipulator configurations. These optimized configurations are seen to resemble the configurations used in industrial robotic manipulators, and when the first three joints are revolute, they resemble animal links.

1.2.2.2 Preliminary Structural Analysis and Design

The preliminary design stage aims at arriving at trial answers that are reasonable estimates of the final solution. Efforts are made to obtain reasonable estimates of the member sizes and/or analytical results, so that minimum number of detailed analyses and design checks area required in arriving at the final solution. These analyses may involve the following three types of analyses :

i) Kinematic analyses -- involve calculations for determining the end-effector velocity given the various joint velocities (Direct Kinematics problem); and calculations for determining various joint velocities to obtain the desired end-effector velocities (Inverse Kinematics problem).

ii) Static analyses -- involve calculations for forces and moments which act on the manipulator structure, when it is at rest. Effects of gravity and forces arising from interaction with the environment are considered. The magnitude of deflection observed at the end-effector is also of interest for purposes of determining strength and accuracy of the manipulator.

iii) Dynamic analyses -- involve calculations for determining time rate of change of the manipulator configuration for given joint torques and forces (Direct Dynamics problem); and calculations for determining the joint torques and forces to obtain desired time rate of change of manipulator configuration (Inverse Dynamics problem). Effects of inertia,

centripetal, coriolis and vibratory forces are considered.

In this thesis report, we are concerned only with the latter two, namely, static and dynamic analyses. Conventional robot manipulators are basically composed of cantilevered beams forming a sequence of arm links connected by hinge joints. This structure gives them an inherent poor mechanical stiffness and accuracy. Hence, static and dynamic analyses are very important to determine the behavior of the manipulator structure under working conditions.

E. I. Rivin [3] provides a lucid and simple to understand discussion on static and dynamic calculations for a variety of rigid planar manipulator structures such as : Cartesian frame, Polar frame, Jointed or Articulated, Parallelogram structures. He also discusses the nonrigid calculations for the first three structures. Three dimensional static and dynamic models are, however, very cumbersome to formulate and solve. In fact, calculation of exact dynamic model is not possible if it is to be done by hand. Hence computers have to be used to set up the exact dynamic equations and solve them.

1.2.1.2.1 An Interactive Procedure for Computer-Aided Design of Manipulators[25]

M. Vukobratovic discusses algorithms for complete dynamic analysis of manipulator motion in [25], and proposes a computer-aided method for design of manipulators based on it. The analysis is started with some trial values for the parameters (selected based upon previous experience) and the results are checked for the satisfaction of following constraints --

a) Actuator Constraint --

The performance specification of a task many times includes the time allowed or speed of execution for the task. Actuator constraint is the requirement that the driving motors in the manipulator joints can produce the forces and torques necessary to

acheive the required speed of execution. Structural designers should also be concerned about this constraint since the actuators and drive systems add up to the self-weight of the manipulators and can play a significant role in the dynamic characteristics of the manipulator.

b) Stress Constraint --

This constraint states that the stresses generated in the links of the manipulator during operation, do not exceed certain permissible values so that the structure does not fail. Such values are normally determined based upon the yield and fatigue failure criteria. Stresses in the manipulators are generated either during the performance of the task (due to payload, self-weight and inertial loads of the links) or when the manipulator is maintaining certain configuration in space.

c) Elasticity Constraint --

This constraint requires that the elastic deformations of the links do not exceed certain prescribed permissible values so that errors in positioning and orientation are within certain limits. Accuracy is important both for point-to-point operation or trajectory-generating (continuous path following) operation of the robot. Accuracy specifications are generally determined by requirements of the task to be performed. Repeatability can also be greatly influenced by the complicance of the structure since elastic deformations change with payloads and configuration of the manipulator.

On violation of any of the above constraints, the following measures can be adopted as corrective action [25] --

i) Violation of actuator constraint :.

1. Choose a new actuator;
2. Change reduction ratio in that joint;

3. Reduce mass of working object;

4. Reduce some masses of manipulator itself;

5. Increase task execution time;

ii) Violation of stress constraint :

1. Increase cross-section dimension of the segment;

2. Choose new cross-section form;

3. Reduce mass of working object;

4. Reduce some concentrated masses of manipulator device (motors, reducers, etc.)

iii) Violation of elasticity constraint :

1. Increase cross-section dimensions of one or several manipulator segments;

2. Choose new forms of cross-sections;

3. Reduce masses of working objects;

Note that violation and correction of the first two constraints, that is actuator and stress constraints, are applicable to specific joints or segments. However, when elasticity constraint is violated, the whole manipulator is responsible and corrections become more complicated.

Once parameters such as length and cross-sectional dimensions of the links, mass of actuators, payload, etc. are specified, the static and dynamic analyses can be carried by some computer based algorithm. Vukobratovic describes such algorithms in [25] which are based on the methods for setting and solving mathematical models of active mechanisms in robotics, based on general theorms of dynamics and Newton-Euler equations, Lagrange equations, Gauss' principle, etc [24].

1.2.1.2.2 Finite Element Methods for Dynamic Analysis of Mechanisms

Apart from the conventional methods of setting up models by means of dynamics equation, nowadays finite element methods are also in vogue, especially for the study of manipulators with elastic links with complex geometry and under going spatial, three-dimensional motion. W. Sunada and S. Dubowsky apply finite element methods for analyzing a flexible linkage mechanism in [15] and claim that the technique can be used for robotic manipulators also. In [15] they use the finite element analysis package, NASTRAN, to generate a set of time-invariant matrices describing the mechanism independent properties of the links. These matrices are then reduced in size by a structural dynamic reduction method called "Component Mode Synthesis". The reduced matrices for individual links are then assembled using a 4 x 4 matrix method into a set of equations using compatibility matric transformations and numerically integrated to obtain time response of the mechanism. An explicit application of the above technique to flexible robotic manipulators appears in their work in [14]. Links with distributed flexiblity and mass, and complex geometry are readily analyzed and a good correlation with experimental data is seen.

M. Dado and A. H. Soni present a generalized approach for forward and inverse dynamics of elastic manipulators using finite element methods in [22]. They use the FEM technique to solve for internal system forces as well as joint deflections. In the forward analysis, the inertial loads are determined using the known acceleration vector. In the inverse analysis, the accelerations of the driven coordinates is determined by solving the dynamic equilibrium equations of the system. The position and velocity vectors are obtained by integrating the acceleration vector. It is shown that this integration procedure can be generalized for multidegree of freedom systems.

1.2.1.2.3 Commercially available Finite Element Analysis software

Finite Element Methods of analysis are nowadays being used commercially to solve a variety of engineering problems. One can find considerable number of commercially available FEM packages in the market today covering a wide range of solution capabilities. One among them is ANSYS Engineering Analysis System, a self-contained general purpose FEM program with the following types of solution capabilities [6],[37]--

i) Linear and Nonlinear Static analysis

Used to solve for displacements, stresses, strains, and forces under the action of applied loads. Capabilities include elastic, plastic, large deflections, stress stiffening, and geometrically non-linear elements. These capabilities are sufficient for static analysis of robotic manipulators to find deflections and internal stresses generated under the action of gravity and applied loads. A nonlinear buckling analysis can also be performed.

ii) Buckling analysis (Linear)

Used to calculate critical loads and buckling modes (Eigen Buckling). Assumes linear behavior therefore of academic interest only. However, can be used to provide an upper-limit on the critical load for a structure. (Nonlinear buckling analysis is a better choice.)

iii) Modal analysis

Used to calculate natural frequencies, mode shapes (both reduced and expanded), and participation factors. Both spectrum and non-spectrum options can be used. It can be very useful in determining the lowermost natural frequencies and mode shapes of the robotic manipulator and hence get an insight to the dynamic behavior of the manipulator structure.

iv) Full Harmonic Response analysis

Used to determine steady state response of a linear structure to a set of harmonic loads of known amplitudes and frequencies. This capability can be

very useful in determining the response of a manipulator structure to a harmonic excitation force being applied to it externally or internally.

v) Nonlinear Transient Dynamic analysis

This is an extension of the Static analysis that solves for the dynamic response of the structure under the action of applied time dependent loads. Inertia and damping effects can also be included alongwith all the other nonlinear capabilities mentioned under static analysis. Therefore this can be used for both forward and inverse dynamic problems.

vi) Linear Transient Dynamic analysis

This is a linear version of the previous item, and thus does not allow nonlinearities like large deflection. Also it necessitates that the integration time step be constant throughout the analysis. This renders it of limited use for solving most of the dynamic problems of robotic manipulators.

vii) Reduced Harmonic Response analysis

Used to determine the steady-state response of linear structures to a set of harmonic loads of known amplitudes and frequencies.

viii) Heat Transfer analysis

Used to solve for the steady-state or transient temperature distribution in a body. Conduction, convection, radiation, and internal heat generation may also be included. Material properties may be orthotropic and temperature dependent.

The above capabilities of ANSYS makes it quite suitable for both static and dynamic analysis of robotic manipulators. In fact, even kinematic problems can be solved using the large deflection nonlinear option in static analysis, and use of large rotation joint elements. However this not recommended since that would be quite inefficient computationally.

1.2.1.3 Detailed Design and Analysis

The techniques mentioned in the previous section (Preliminary analysis and design) can be used for detailed design also. The difference being that before the detailed analysis is conducted, the structure satisfying the governing constraints should have been determined, and additional conceptual and preliminary design iterations are not expected. Here considerable depth and detail of analysis as demanded by the problem at hand are used. It is expected that this stage will be the last and the structure can be built without any requirement for further design analyses.

2.0 Large Robotic Manipulators

2.1 Need for Large Robotic Manipulators

A simplistic definition of a "large" manipulator, is a manipulator quite large compared to a human arm. Robotic arms have traditionally been developed to emulate the human arm and mimic its capabilities. Seering[39] criticizes this saying that the human arm was designed for throwing stones and climbing trees, and not for doing factory work. He further emphasizes that robots are machines and they should be designed, treated and controlled as such. They should be designed not to emulate the human arm but to outperform it. Robots can outperform the human arm in situations needing dextrous handling of large and heavy payloads over a large workspaces or in the other extreme case of very small and light payloads over small workspaces. One example of such an application is Remote Manipulator System on board the NASA space shuttle which consists of a 50 ft long jointed manipulator designed for payload capacity of 300 lbs under no gravity condition. Whereas micromanipulators have been designed and used to test micro-electronic circuits and have the potential for use in medical operations, for example connecting small nerves. Many of the techniques indentified in this thesis are applicable to both extremes but only large robots are addressed here.

2.2 Definition of a "Large" Robotic Manipulator

E. I. Rivin provides an interesting comparison of human arm and existing industrial robotic arms in [3] as follows. The total mass of the linkage of the human arm (lower and upper arm and wrist) is about 10 to 20 lb with which it can handle rather precisely loads of about 10 to 20 lb; with slightly lower speeds it can handle 30 to 50 lb; and it can make simple movements with loads up to 200 to 300 lb. These payloads far exceed the weight of the linkage which carries it. Whereas industrial robots have payload

limitations which amount to one-twentieth to one-fiftieth of their masses, more than 10 times less effective than a human arm.

For the sake of comparison between various robotic manipulators, the size of a robotic manipulator, in terms of "largeness" or "smallness", can be defined in relation to its largest dimension compared to the size of the arm of an average human being. Manipulators with their largest dimensions of the same order of magnitude of a human arm can thus be termed as a "Normal" size manipulator. Each higher order of magnitude then relates to the "Largeness" of the arm: one order refers to a "Large" robot, two orders to a "Very Large" robot; and so on. Similarly "Small" and "Very Small" manipulators can be defined as those with their largest dimensions one or more orders of magnitude smaller than the human arm.

2.3 "Large"ness Related Problems

A typical robotic manipulator is designed to perform functions which a human operator normally would perform. This calls for mobility and dexterity typically not required in more traditional machine tools. Most manipulators are designed to resemble the human arm in order to achieve this mobility and dexterity. Hence a robot structure is basically composed of cantilevered beams, forming a sequence of arm links connected by hinge joints. Such a structure inherently has poor stiffness and accuracy, and is not appropriate for the heavy-duty, high-precision applications required of machine tools. These inherent problems become more prominent as the size of the manipulator increases. The structural problem in manipulators some what parallels that of biological systems, very small animals have no skeleton, while small creatures are exoskeletal and medium to large animals are endoskeletal. Very large animals do not exist and thus do not give as a model for structure within large or very large robots. We will see that models for such structures are available from the building construction area.

2.3.1 Self-weight Related Problems

2.3.1.1 Effect on Stresses

Consider the following cantilever problem. The stresses generated due to its self-weight and externally applied load can be calculated as follows --

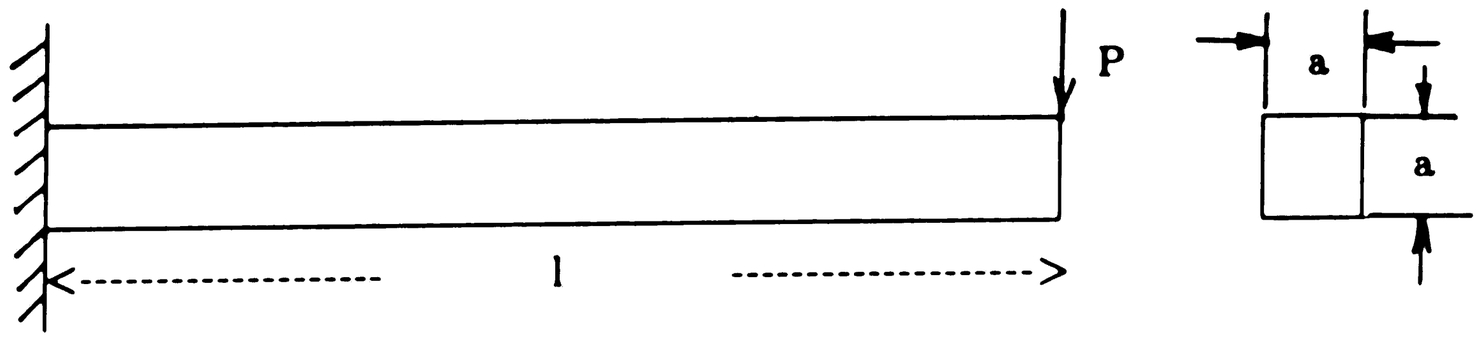

Self-weight, W, of the beam = $a^2 l \rho g$

Bending moment, M, due to self-weight = $\rho g \int_0^l a^2 x \, dx = a^2 \rho g \frac{l^2}{2}$

Maximum tensile stress, σ_{bmax}, due to Moment M = $\frac{M \, y_{max}}{I} = \frac{3\rho g l^2}{a}$

Maximum Shear force, V, at O (due to self-weight) = $a^2 l \rho g$

Maximum stress due to shear V, $\sigma_{shear} = \frac{3 \, V}{2 \, A} = \frac{3 \, l \rho g}{a}$

Now, the maximum principal stress, $\sigma_1^{s.w.}$, is

$$\sigma_1^{s.w.} = (\sigma_{bmax}^2 + \sigma_{shear}^2)^{1/2}$$
$$= 3 l \rho g \, (\, (l/a)^2 + 1/4 \,)^{1/2}$$

As (l/a) >> 1/4 for slender cantilevers,

$$\sigma_1^{s.w.} \rightarrow \frac{3\rho g l^2}{a} = \sigma_{bmax}$$

While, for a weightless cantilever beam, the bending stress, σ_1^{ext}, under the action of external transverse load P is

$$\sigma_1^{ext} = \frac{M\, y_{max}}{I}$$

$$= \frac{(6\ Pl)}{a^3}$$

The stress σ_1^{ext} varies as l, whereas $\sigma_1^{s.w.}$ varies as l^2. Hence the effect of self-weight becomes predominant as the size of the cantilever increases. Thus, increases in size leads to more dominant self-weight generated stresses in the robot structure. We will find these higher stresses not only reduce the factor of safety but will reduce the stiffness of the structure and thus increase the deflections within. To get a better physical understanding, we look into the following comparison --

Case i) "Normal" Size Cantilever :-

l	=	2.5 ft	(length of a human arm)
P	=	5 lb	(manipulatable payload for human arm)
a	=	1 in.	(arbitrary)

For a cantilever beam made out of steel, $\rho = .00073$ lbm/in^3, $\sigma_{safe} = 30$ ksi (approx).

Therefore, stress generated in a weightless beam under the externally applied load is

$$\sigma_1^{ext} = \frac{6\ Pl}{a^3}$$

$$= \frac{6 * 5\ lb * 30\ in}{1^3}$$

$$= 900\ psi$$

Whereas, stress generated due to the self-weight of the beam is

$$\sigma_1^{s.w.} = \frac{3\rho g l^2}{a}$$

$$= \frac{3 * .00073 * 386 * 30^2}{1}$$

$$= 760.8 \text{ psi} \qquad \text{(this is about 84.5 \% of } \sigma_1^{ext})$$

The factor of safety hence obtained is = 30 ksi / (900+760.8) psi = <u>18.07</u>

<u>Case ii) Large Size Cantilever (10 times larger)</u> :-

$l = 25 \text{ ft} = 300 \text{ in}$

$P = 5000 \text{ lb}$ (in proportion with increase in mass)

$a = 10 \text{ in.}$ (in proportion with increase in length)

Now, stress generated in a weightless beam under the externally applied load is

$$\sigma_1^{ext} = \frac{6\,Pl}{a^3}$$

$$= \frac{6 * 5000 \text{ lb} * 300 \text{ in}}{10^3}$$

$$= 9000 \text{ psi}$$

Whereas, stress generated due to the self-weight of the beam is

$$\sigma_1^{s.w.} = \frac{3\rho g l^2}{a}$$

$$= \frac{3 * .00073 * 386 * 300^2}{10}$$

$$= 7608 \text{ psi} \qquad \text{(this is also about 84.5 \% of } \sigma_1^{ext})$$

The factor of safety hence obtained is = 30 ksi / (9+7.6) ksi = <u>1.807</u>

The stresses generated in the two cases are tabulated below.

	External Load	Self-weight
Normal Size	900 psi	760.8 psi
Large Size	9000 psi	7608 psi

Hence, when the size (length dimension) of the beam is increased by a factor of 10 and we increase the material invested in the beam by a factor of 1000 in order to increase its payload capacity, the factor of safety actually dropped 10 times! This example provides a flavor of the predicament of the designer who will be trying to design a "large" manipulator with higher payload capacity. Obviously, this problem will be accentuated as the size of the manipulator is increased further.

2.3.1.2 Effect on Deflections

Considering further the cantilever problem discussed in the previous section, let us investigate deflection of the beam under externally applied load and self-weight. Using standard formulas for cantilever beam, as in [40], the deflections can be given as --

Deflection of a weightless cantilevered beam under the action of external load P,

$$f^{ext} = \frac{Pl^3}{3\,EI}$$

Deflection of a cantilevered beam under its own self-weight,

$$f^{s.w.} = \frac{(V\rho g)\,l^3}{8\,EI} \qquad \text{(V being volume of the beam)}$$

Taking the dimensions provided in the previous section for "normal" and "large" beams, we get the following deflections (inches)--

	External Load	Self-weight
Normal Size	0.018	0.0114
Large Size	1.8	1.14

Even if 1000 times more material is put in the beam in order to keep it stiff, increasing the size of the beam 10 times leads to 100 times increase in deflection (irrespective of weight consideration of the beam).

Stiffness of the manipulator structure is a prime consideration for purposes of accuracy and repeatability of the robot. Since increase in size of the manipulator increases deflections at a faster rate than the increase in size, increasing stiffness of the structure for a given weight (to limit self-weight induced stresses and deflections) becomes a prime desin objective.

2.3.2 Dynamic Characteristics

All transient processes of real robotic manipulators, such as acceleration and deceleration, are accompanied by vibrations. The intensity of vibrations is different at different configurations and directions of motion. Low frequency vibrations are frequently observed during the starting and stopping of motion. This causes a need to allow for settling time for the structure before it can proceed with the next operation, hence increasing the execution time.

Structural dynamic characteristics of a structure are largely determined by its stiffness, inertia, damping and natural frequencies. Though the characteristics are highly interrelated, stiffness can be singled out as one of the most important factors in their determination [3]. This is because inertia characteristics are to a greater degree determined by the payload; natural frequencies are a derivative of stiffness and inertia; and damping of the most important fundamental modes can be frequently influenced by relatively modest modifications of actuators and/or control systems. Higher stiffness (and natural frequencies) is basically desired for better accuracy and repeatablity. A manipulator with higher stiffness and natural frequency can follow the prescribed paths with reduced overshoot at higher speeds. Increase in accuracy can also lead to less need

for complex feed-forward control systems and a faster settling time.

Determination of the dynamic characteristics of relatively large manipulators with the assumption of rigid links would be highly unrealistic. Nonrigid analyses (considering the elastic deformations of links of the manipulator) are highly essential for a proper determination of the dynamic behavior of the structure. As detailed in the previous two sections, an increase in dimension generally results in reduction in stiffness. Reduction in stiffness leads to lowering of natural frequencies. Further, the increase in dimesions of a system is generally accompanied by increase in its mass and therefore leads to further reduction in natural frequencies. The traditional approach of beefing up the cross-sections is not effective in enhancing the stiffness as it may lead to increase in inertia which can in turn lead to higher dynamic deflections.

Lower natural frequencies are not desirable since they are relatively easier to be excited, and in absence of sufficient damping, can lead to large amplitudes of vibration and even instability of the structure. Larger robotic manipulators will generally be expected to work outdoors or under tough working environments. Thus, lower natural frequencies will make them more prone to wind excitation, and also ground/base excitation in case the robot is on a moving foundation.

Reduction of stiffness and increase in mass, both have adverse effect on the natural frequencies of the system. Considering the cantilever beam problem described in the previous sections further, let us investigate the effects of largeness on the natural frequencies of the beam.

Meirovitch [43] provides calculations for the natural frequencies of a beam with one clamped end (cantilever). The first natural frequency is given by --

$$\omega_1 = 1.875^2 \sqrt{\frac{EI}{mL^4}}$$

where I is moment of inertia of the section,

m is mass per unit length for the beam,

L is the length of the beam.

We know from the previous example that,

$$I_{large} = 10000 * I_{normal}$$

$$m_{large} = 100 * m_{normal}$$

$$L_{large} = 10 * L_{normal}$$

and thus we can see that,

$$\omega_{large} = 0.01 * \omega_{normal}$$

Hence a 10 fold increase in size leads to a 100 fold decrease in the natural frequencies.

Large inertias can further slow down the working of large manipulators by imposing limits on acceleration and decelerations during operation. These limits may be set for purposes of limiting the dynamic stresses and/or the deflections. (Remember that stresses generally do not pose a problem in smaller robots). Powerful actuators will also be needed, causing a further addition to the cost. Better (lighter but stronger and stiffer) materials will hence be required to reduce the inertias and hence contain stresses and deflections.

2.3.3 Other largeness related problems

Robotic manipulators generally require reduction systems to convert the high speed and low torque input provided by motors into low speed but high torque output for the links. As the size of the links increase, their masses increase along with the increase in the moment arm acting at the rotational joints. This results in a more acute need for high torque low speed actuators, and/or a light efficient reduction system. Electrical

motors with these characteristics are only now becoming available. Hydraulic systems, although available, tend to be very compliant, increasing the vibration problems.

Large manipulators will generally expected to work outdoors, handling large and heavy payloads over large workspaces. However, this working environment can introduce a whole new range of dynamic loading conditions such as wind loads, vibrations due to equipment mounted on the structure on which the robot is mounted, wave impact loads on the mounting structure, earthquake excitation, etc. This would not only lead to necessitation of more complex dynamic analyses but also increase the complexity of the control system due to the unpredictability of dynamic loads (such as wind loads or wave impact loads, which are highly transient in nature). Hence off-line programming maynot be of much help with large manipulators unless specific care to extremely noisy environment are made when designing the system controller.

2.4 Design Methodolgy for Large Robotic Manipulators

Most of the robots today (except Cartesian frame type robots) emulate the human arm in some manner and thus end up being in the shape of a cantilevered chain of links. This cantilever type of structure however leads to several mechanical deficiencies. When the size of links is increased to increase the reach of the manipulator, these deficiencies are highly accentuated. The problems that can be expected while designing large manipulators are as summarized in Fig. 2.1. It can be seen that all the noted problems result from excess mass or self-weight of the large manipulator or simply from the "large"ness of the manipulator. Even an increase in the self-weight can be attributed to the "large"ness of the manipulator. Since "large" dimensions are needed in order to have larger workspaces and payloads, the major ways to improve the static and dynamic performance and thus reduce static and dynamic stresses and deflections are --

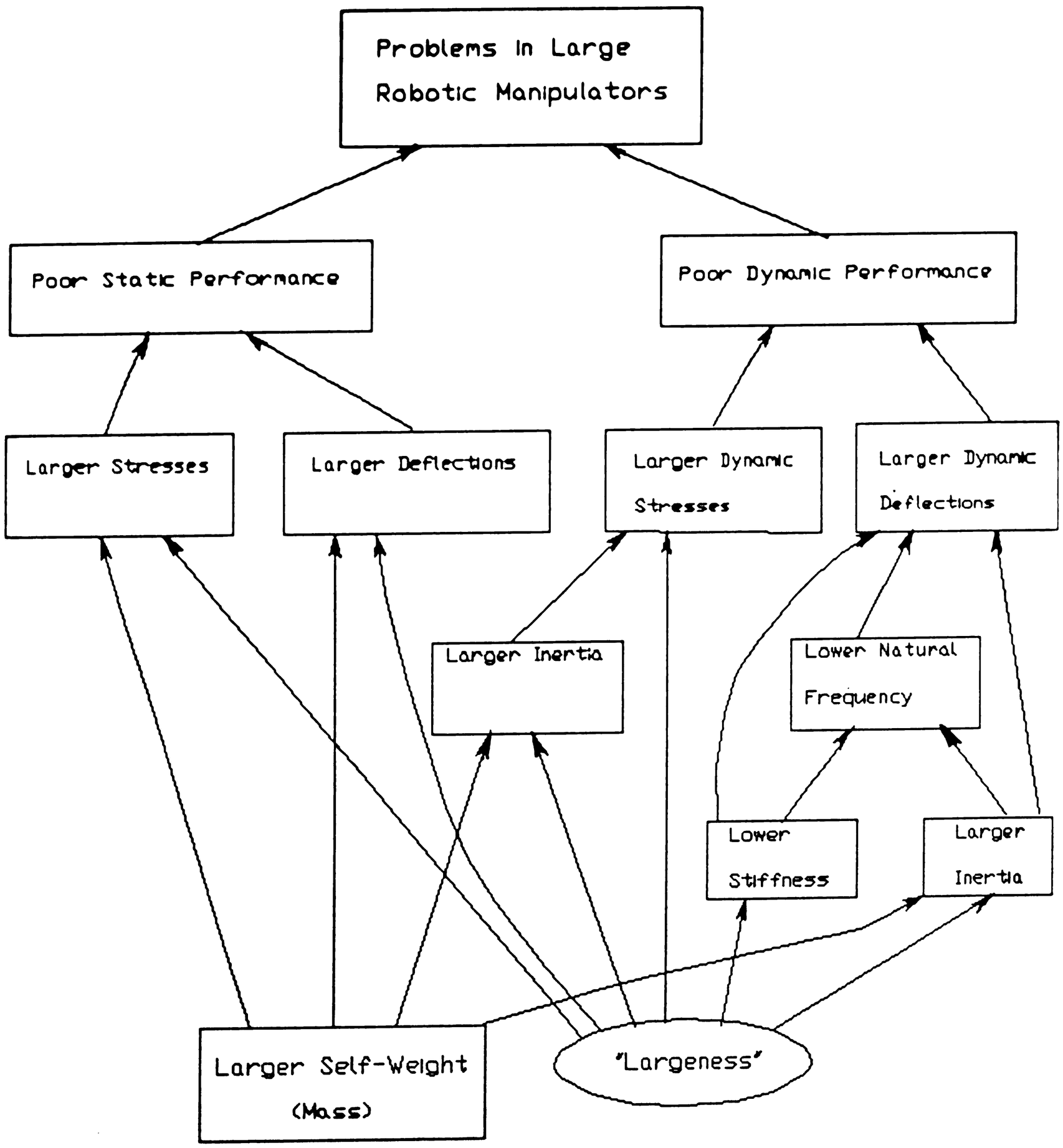

Fig 2.1 : Expected problems in Large Robotic Manipulators if designed traditionally.

1. **Increase the stiffness/self-weight ratio of the manipulator**

    i) **By using superior material**

    ii) **By conventional and unconventional structural techniques**

2. **Reducing structural vibrations by damping.**

2.4.1 Increasing Stiffness/Weight ratio by Superior Materials

For any given robot, the static and dynamic performances can be improved if a lighter, stiffer and stronger material is available. High stiffness (or elastic modulus E) to self-weight (or specific gravity ρ) ratio materials would be very desirable. Table 2.1 compares E/ρ ratios of some materials with steel. Ceramics like boron carbide and alumina have a very good E/ρ ratio compared to steel however they are brittle in nature and difficult to manufacture. Berrylium also has a good E/ρ ratio but it is too expensive. Researchers have been able to increase the strength of metal alloys by increasing their yield and ultimate strengths but not much success has been obtained in increasing the elastic modulii substantially at the same time. Hence, one might as well have to choose between materials such as Magnesium, Aluminium or Titanium which have about the same E/ρ ratio as steel but are quite lighter.

Unconventional materials such as carbon-fiber-resin matrix composites can be used to obtain a significant improvement over steel and aluminium both in strength-to-density and stiffness-to-density ratios. With proper selection and placement of fibers, composites can be stronger and stiffer than steel parts and weigh 40-70% less. Also, in contrast to metals for which there are only three variable input parameters of geometry, moment of inertia, and tensile strength available to the designer, carbon fiber composites offer three more design degrees of freedom : modulus of elasticity, Poissons ratio, and strength of modulus direction[5]. Each of the materials are fairly expensive when compared to steel.

Table 2.1 : Comparison of E/ρ Ratio of Various Materials[3]

Material	E, 10^5 MPa	ρ, 10^3kg/m^3	E/ρ, 10^7m^2/s^2
Boron Carbide	4.50	2.4	19.0
Beryllium	2.90	1.9	15.3
Alumina	3.0-4.0	3.7-3.8	7.9-11
Lockalloy	1.90	2.1	9.1
Titanium Carbide	4.0-4.5	5.7-6.0	7.0-9.1
Tungsten Carbide	5.50	16.0	3.4
Molybdenum	3.20	10.2	3.0
Steel	2.1	7.8	2.7
Titanium	1.16	4.4	2.6
Aluminium	0.72	2.8	2.6
Magnesium	0.45	1.9	2.4
Tungsten + 2-4% Ni, Cu	3.5	18.0	1.9

2.4.2 Conventional and Unconventional Methods for Increasing Stiffness/Weight ratio

Increase in stiffness has a very salubrious effect on the overall performance of a manipulator. The accuracy and repeatability is enhanced due to the reduction in deflections. Increase in natural frequencies leads to reduction in overshoot, hence enabling the manipulator follow paths more accurately and settle at the final position faster. Faster end-of-arm speeds are also made possible due to the enhanced dynamic characteristics.

There are various methods for increasing the stiffness of a structure. We can classify them as conventional and unconventional depending their past utilization in design of robotic manipulators. The so-called "unconventional" methods have long been in use in engineering, but seldom in the context of robots. We will see why those would come handy in case of large robotic manipulators.

2.4.2.1 Conventional Methods

Compliance, that is reciprocal of stiffness, or deflection divided by the force causing

this deflection, can be attributed to the following : Structural deformation of load transmitting components (links of the mechanism), Contact deformations (inside joints of the mechanism) and Deformations in the energy transforming devices (motor or actuators of the mechanism)[3]. These factors can be dealt with as follows.

2.4.2.1.1 Reducing deformations in the links

Reduction by means of efficient cross-section

Since most of the links of the manipulator mechanism are mostly beams experiencing some kind of bending action, stiffness can be increased by increasing their cross-sectional moment of inertia (without increasing their cross-sectional area). Hollow cross-sections such as circular and rectangular enhance the bending and torsional stiffness without increasing the weight. Other structural sections such as 'I', 'C' or 'T' sections can also be utilized if found convenient. Enhancement of bending stiffness of links can also be acheived by means of axial preloading. Infact, tensile axial preload also increases the torsional stiffness.

Efficient design of beams of links loaded in bending and torsion leads to a hollow stressed-skin concept of their structure. However this leads to a reduction in their resistance to buckling failure. Kiedrzynski [8] presents general criteria for the efficient cross-section geometry of links by means of a mass/stiffness analysis including buckling resistance. Based on his analysis, open cross-section link design can be qualified as inefficient for torsion. Also, aluminium alloy shells may be recommended against steel shells for their buckling resistance.

Reduction by means of efficient link shapes

Beams with built-in ends experience maximum bending stresses near the built-in end and minimum bending stress away from it. Also, deflection at the free end is mostly

determined by the bending stress at the fixed end. The highest intensity of inertia forces is generated in sections adjacent to the end which is the center of rotation. This leads to the a design rule that the links can be tapered at the ends away from built-in ends and centers of rotations without much reduction in rigidity but with considerable reduction in weight.

2.4.2.1.2 Reducing contact deformations

Even if contact deformation in joints can be beneficial with respect to more uniform stress distribution (in joints) and damping of vibrations, they can lead to considerable overall compliance of the structure. When such joints are pre-loaded, most of them behave as linear angular springs stiffening with increasing preload. Preload can thus be used to increase stiffness.

Contact deformations in cylindrical joints can be decreased by reducing the clearance between the mating parts, since that increases the area of contact. Contact stiffness for vibratory loads (dynamic stiffness) can be increased by lubrication, as the viscous resistance to fast squeezing of oil from the contact area can lead to up to 50% enhanced stiffness in dynamic mode as compared to static. For cases of moment loading, optimization of the shape of contacting surfaces can be undertaken to increase their moment of inertia.

2.4.2.1.3 Reducing deformations in motors and actuators

Pneumatic actuators have reduced stiffness and hence lower natural frequencies by the virtue of the compressibility of air. Stiffness of such actuators can be enhanced by increasing the cross-sectional area of the piston and decreasing the working pressure. Total internal volume reduction by means of shortening of hoses, pipes, etc., and use of additional stages of reduction at output can also be quite effective.

Although oil is more incompressible than air, very high pressure in hydraulic actuators can lead to a significant absolute compression of oil as well as deformation of containing walls (like those of cylinders, pipes and hoses). Introducing a mechanical reduction stage is again helpful in reducing the compliance.

2.4.2.2 Unconventional Methods

2.4.2.2.1 Trusses and Spaceframes

It is well known that parts are much stiffer in tensile or compressive loading than in bending or torsion. In fact, bending deflections may exceed tensile or compressive deflections by several orders of magnitude. Hence, if by some way the manipulator structure could be altered such that its links experience tensile/compressive stresses in place of bending, the stiffness can be enhanced considerably. Consider the problem shown in Fig. 2.2. The cantilever beam in Fig 2.2(a) experiences bending stresses hence undergoes bending deflections. But when replaced by a simple triangular "truss" (as in Fig 2.2(b)), the bending stresses are eliminated and replaced by pure tensile and compressive stresses. This idea can be carried further and a "space-frame" can be used as shown in Fig. 2.2(c). This can not only increase the stiffness but also significantly reduce the weight of the structure. This principle has a tremendous potential and has been already used by civil engineers in design of large structures and there is no reason why it cannot be applied for large manipulator structures.

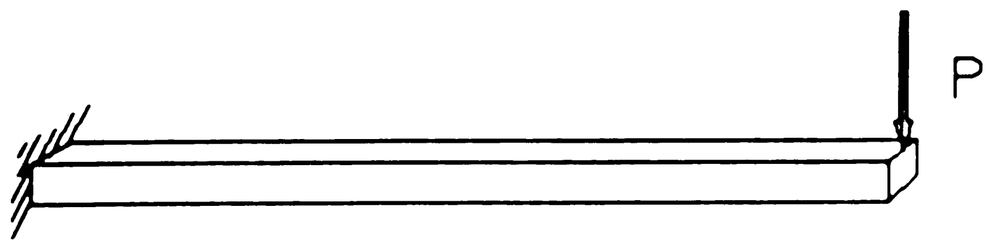

a) Cantilevered Beam

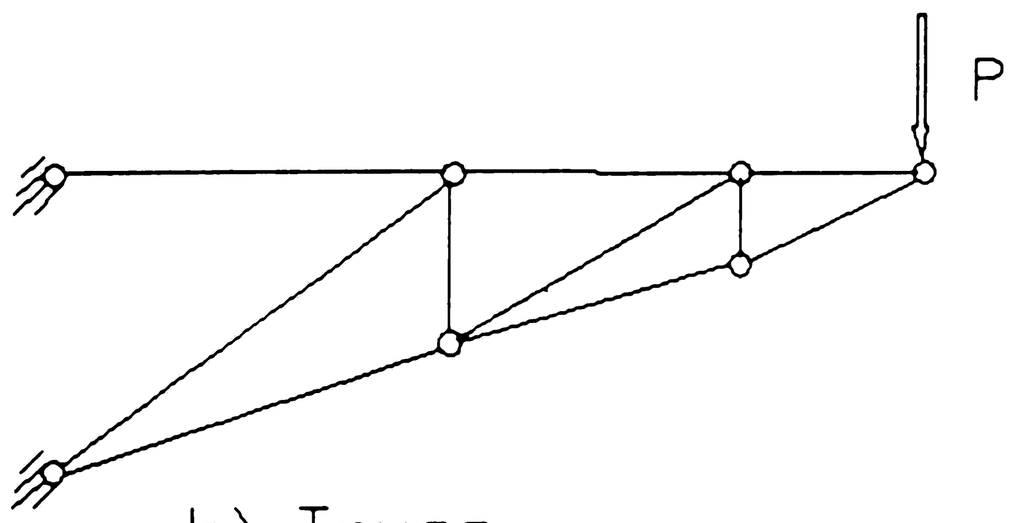

b) Truss

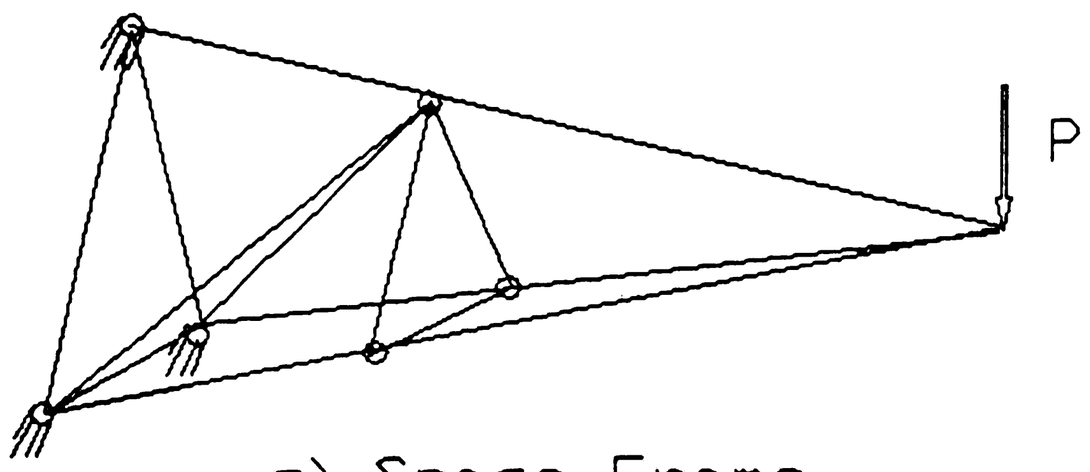

c) Space Frame

Fig. 2.2 : Avoiding Bending Stresses by using Space Frames.

According to Corkill [28], a truss can be defined as a structural system which distributes loads to support through a linear arrangement of various sized members placed within a single plane. These members, each shorter than the total span, resist either tensile or compressive force. Whereas, a space frame is a structural system which distributes loads to supports through a linear arrangement of members placed in more than one plane. It is also designed to transmit loads by direct tension or compression without bending. The space frame is a three dimensional truss.

The inherent property of a truss or a space frame, that is the one of transmitting loads by direct tension or compression, can be used to considerable advantage in large robotic manipulators. Links of a manipulator, instead of being designed as beams can instead be designed as space frames and lot of material saving as well as an increase in rigidity as well as natural frequency can be expected. The basic components of a space frame, that is pyramids and tetrahedrons, can be used to make the structure of the manipulator. Some examples are as shown in Fig. 2.3.

One disadvantage of the above arrangements is that as the size of the component tetradedron or pyramid is increased with respect to the length of the link is increased, the relative rotation between two links is restricted. For example, the height of the pyramid units used in Fig. 2.3(a) should be so designed as to not to pose excessive restrictions on the rotation as well as not to be too shallow to resist torsion loads arising from out-of-plane loading. Other disadvantage is the complications in static and dynamic analyses due to the space frame structure of the links. (Note that for large manipulators, it is critical to consider the effects of elastic deformation). The problem of structural optimization will now be more time consuming.

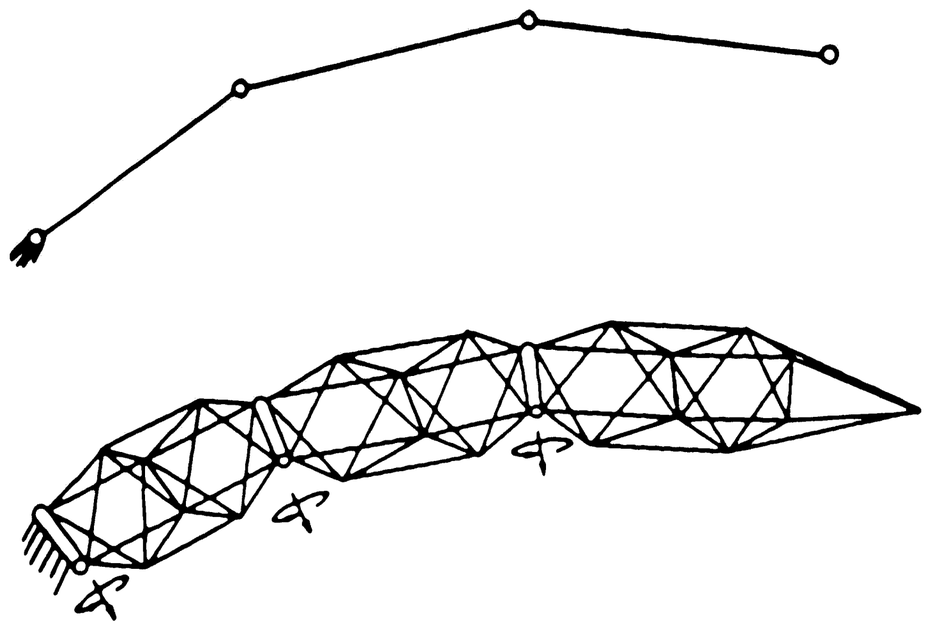

(a) RRR Design : All Axes Parallel

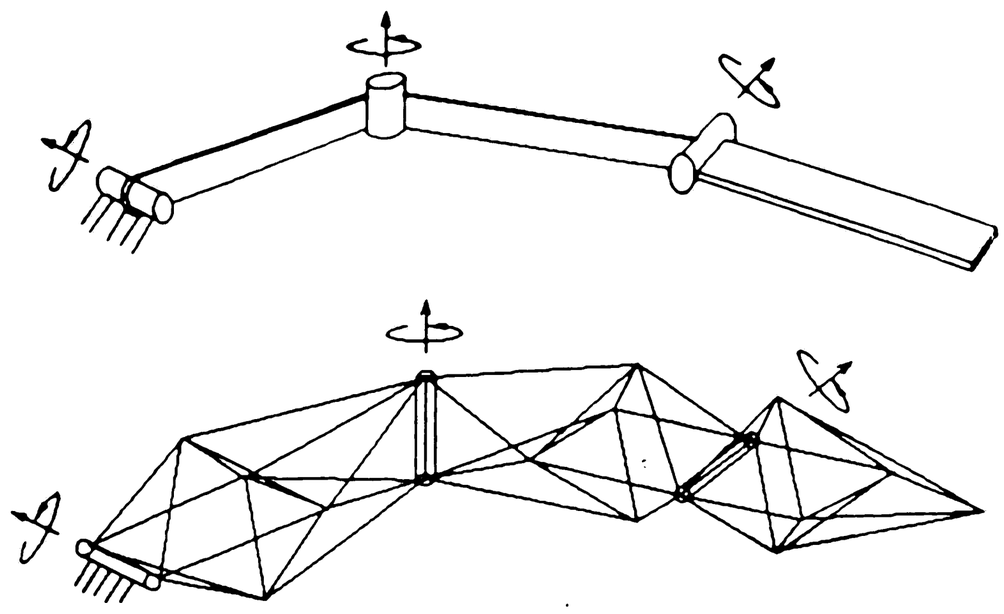

(b) RRR Design : Perpendicular Axes

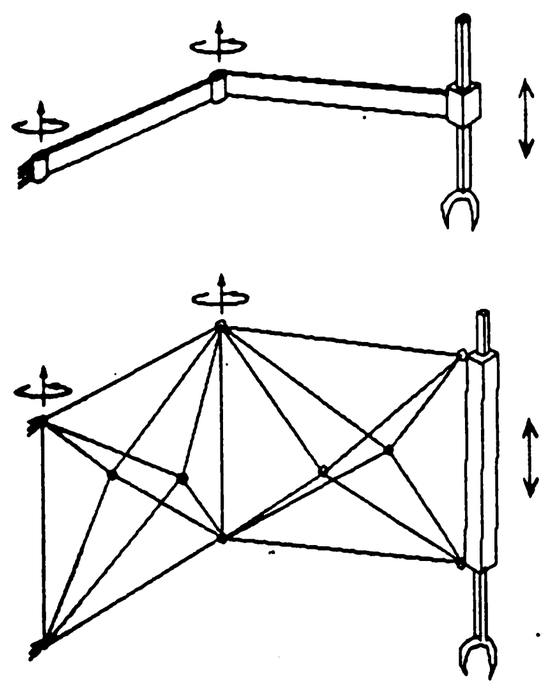

(c) SCARA Design

Fig. 2.3 : Examples of use of space frames for manipulator linkage design.

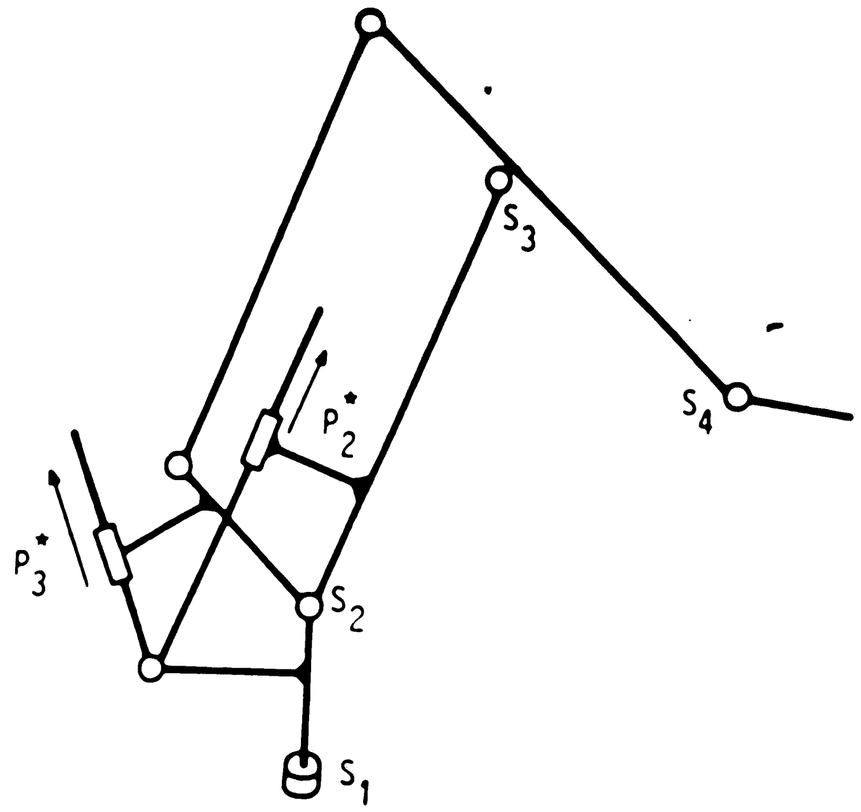

(a) Mechanism with a Parallelogram [26]

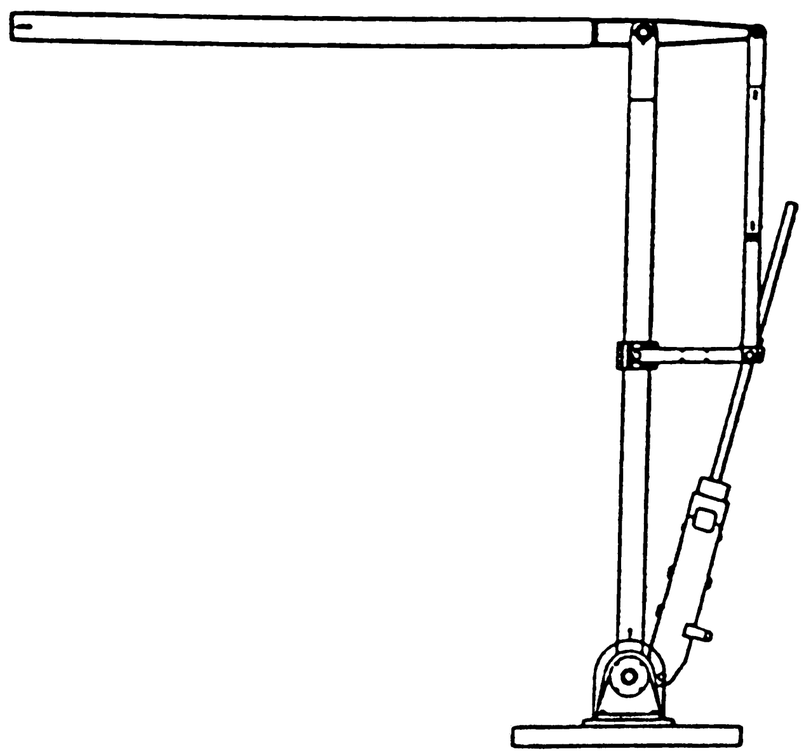

(b) A 2 dof Lightweight Robot Arm [6]

Fig 2.4 : Embedded closed mechanisms in manipulators [6], [24].

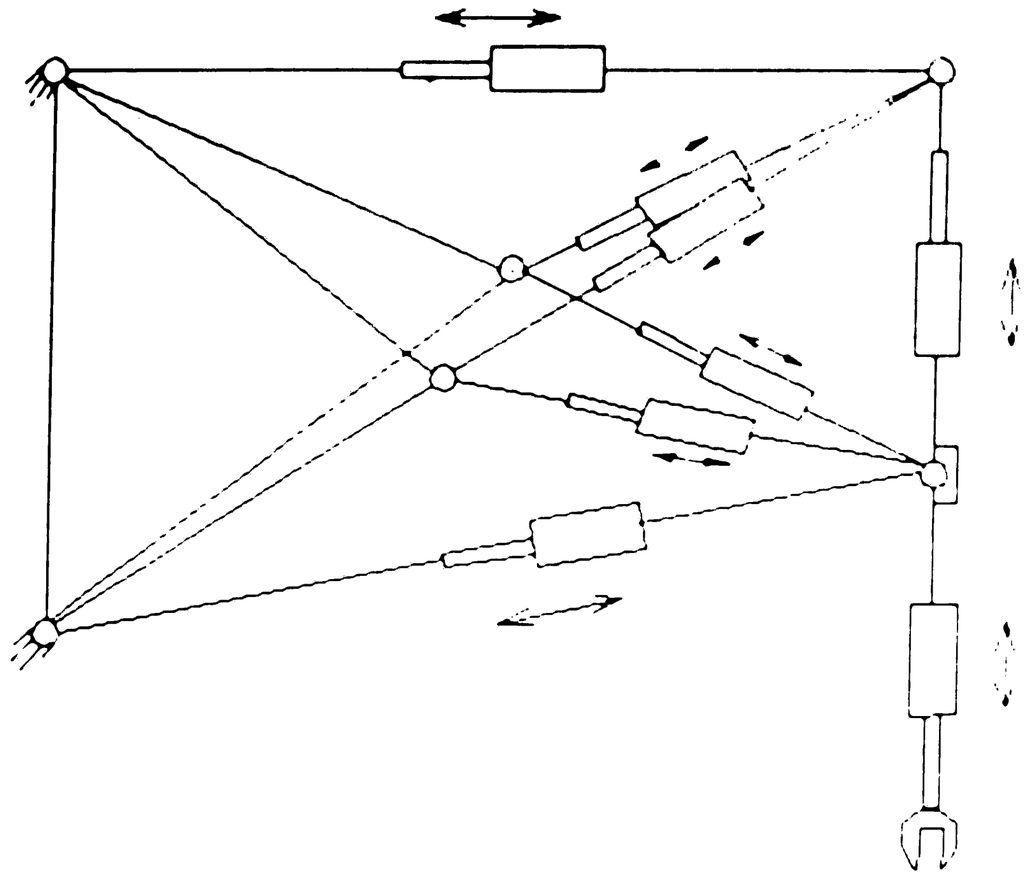

(a) Space Frame based on AACTS Robot Arm

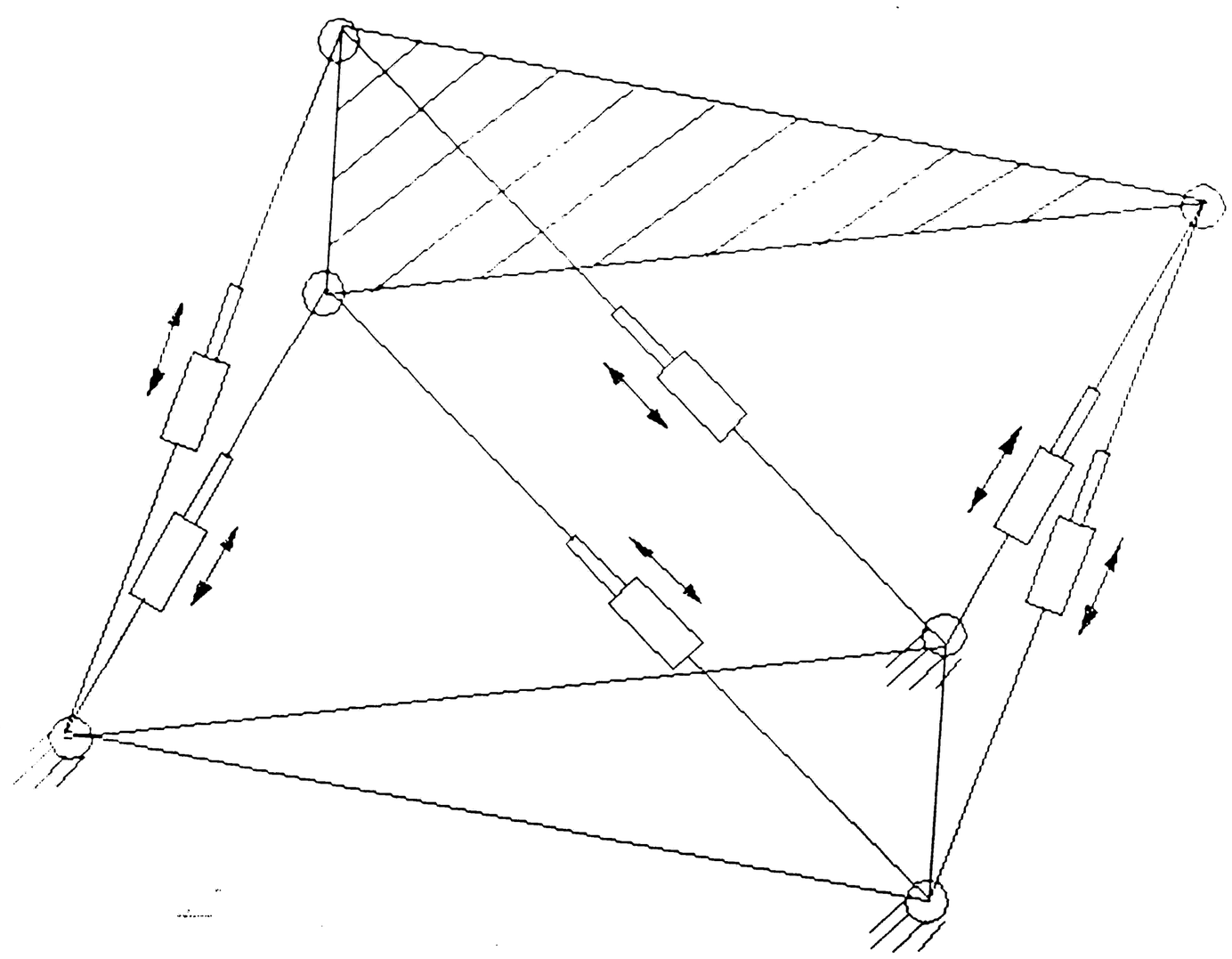

(b) Stewart's Platform

Fig. 2.5 : Space Frame with Variable Size Members [47].

2.4.2.2.2 Embedded Closed Chains

Embedded closed chains can be introduced in manipulator mechanism to not only bring the actuators near the foundation (and thereby reducing the inertia), but also to convert some of the bending action into direct tension and compression. The freely suspended span of the last link can be reduced (and hence the amount of material experiencing bending stresses leading to an opportunity to reduce weight), whereas the cantilevering of previous beams can be totally eliminated. One indirect advantage can be increase in natural frequencies due to reduction in length of freely hanging spans. If suitably designed, the embedded linkdage can also provide some amount of counterbalancing. See Fig. 2.4 for examples. Fig. 2.4(b) shows a 2 dof lightweight robotic arm designed by M. P. Hennessey, et. al. [6], with a weight to payload ratio of 2:1 with a horizontal reach greater than 10 ft and payload capacity 100 lbs. Obvious disadvantages of these arrangements are those of increased complexity of kineamtic, static and dynamic analyses and increase in dead-spaces in the workspaces of the manipulators.

2.4.2.2.3 Space Frames with Variable Size Members

The concepts in the previous two sections can be extended further by having space frame like manipulator with variable link sizes. In fact a fusion of the concepts can be used to design totally unconventional manipulators. Fig. 2.5 [47] shows one such robot with the basic pyramid constitution but variable member sizes. The number of variable members can be increased for extra flexibility. It is expected to inherit both the advantages and disadvantages of the previous two concepts.

2.4.2.2.4 Use of Cables for Tension members

Many a space frames have the property that some of their members always experience same kind of load (tensile or compressive) for given type of payload (static

and dynamic). In such cases, the tensile members can be replaced by cables. Steel cables normally have higher strength than structural steel and therefore will be lighter in resisting given tensile load. However the decrease in cross-sectional area can lead to reduction in stiffness, which can be overcome by preload. Preload can also compensate for decrease in natural frequencies. However, the exact effect of having cables in the structure can only be determined by detailed dynamic analysis.

2.4.2.2.5 Kinematic Refinement for Stiffness

Generally in design of flexible mechanisms, once the mechanism is decided upon the satisfaction of deflection constraints is reached by changing the cross-sectional areas of the links, using some optimization procedure. However Zhang and Grandin [41] propose an optimization scheme in which geometrical parameters as well as cross-sectional parameters are used. Hence satisfaction of deflection constraints is reached by mainly changing the geometrical parameters, such as lengths of the links and positions of the pivot points, and not by increasing the cross-sectional areas. This results in mechanisms possesing less weight.

2.4.3 Methods for Reducing Vibrations by Damping

N. C. Singer and W. P. Seering classify seven distinct approaches being used for robot vibration reduction research in [12]. Few of those approaches, most relevant to the problem of large robotic manipulators, can be stated as in following sections.

2.4.3.1 Structural Damping Components

Permanently applied brakes in the actuators can be used as very efficient dampers of low frequency vibrations of links. These dampers continuously dissipate a certain fraction of installed power of the actuator but provide sufficient amount of friction. Other method of actuator damping can be use of surge tanks (in pneumatic actuators).

These techniques are effective for relatively low frequencies.

Mechanical damping of links assure more uniform damping of both the low and high frequencies. Materials with high internal damping can be used for "extensional" and "constrained layer" damping treatment of links[3]. Extensional damping involves applying a layer of viscoelastic material with high energy losses to the external surface of a structural member loaded in bending. This is helpful for damping bending vibrations. A much more pronounced effect can be achieved by constrained-layer treatment. A rigid constraining layer is attached atop the viscoelastic layer on the link. Bending of the link then generates a significant shear deformation in the viscoelastic layer.

Low mass, all welded construction techniques produce structures with low inherent damping. Usually over 90 percent of the inherent damping of fabricated civil engineering structures originate from joints. Vibrational energy is dissipated by frictional forces when small relative movements take place at the joint interfaces. C. F. Beards and A. Woovat[42] present the effects of friction damping occurring in joints on the frequency response of a portal frame, under varying clamping force (and hence friction) at joints. They found that the vibration response of the frame tested could be changed by altering the joint clamping forces; both the amplitude of the resonant response and the resonance frequencies could be controlled to certain extent. It was found that although reduction in the clamping force led to maximum damping, it also led to a reduction in the stiffness of the structure. However, this should not be a problem for structures designed as space frames where the basic component of the structure is a triangle or one that can be triangulated, and joints are not designed to carry any moments (pin joints). Since space frame structure has been recommended for large robotic manipulators, friction joints can be a very effective way of damping.

2.4.3.2 Control System

In this approach, one would directly measure the absolute position of the end-point

of the manipulator, which would then be used in a conventional feedback loop to control out endpoint vibrations. It is of course assumed that noise-free measurement of the endpoint location, without interfering in the robot's task is possible. This approach can be easier in larger manipulators than smaller one due to the relative ease in endpoint location measurement and relatively less stringent requirements of positioning accuracy. In fact, if a control system could be designed to work on the above approach, the stiffness requirements of the manipulator can be made less stringent and some costs can be cut.

2.4.3.3 Shaping of Manipulator Commands[12]

The shaping of the input commands can be implemented in three ways. First, commands can be colored so that energy is not introduced above the first mode. Second, energy may be put into the system above the first mode, but selectively so that resonances are avoided. Third, allow some modes to "wind up" at the beginning of the move and then remove energy at the end of the move. Singer and Seering used the second approach in [12], and were successful in obtaining a reduction in a large space shuttle arm (50 ft long). The reduction was obtained by eliminating those frequencies in the input command which were close to the structural modes, by means of acausal filter. This prevents any energy being put near the resonances. It can be seen that the process of elimination of unwanted frequencies is some kind of a "pre-processing" action, and therefore there is no need for real-time processing.

2.4.4 Other Design Guidelines for Large Robotic Manipulators

2.4.4.1 Mechanism Design

2.4.4.1.1 Macro- and Micro-positioners

Large robotic manipulators are basically needed to access large areas and to handle heavy payloads. This makes the design of the manipulator very demanding in terms of

stiffness, accuracy, repeatability, vibration and control requirements. However, this requirements can be made less stringent if the manipulator can be designed as a combination of two components -- the macro-positioning component and the micro-positioning component. The macro-positioning component would provide upto 95-99% of the movement for the endpoint location and the micro-positioning component, located on the last link of the macro-positioner, would do the fine positioning and orientation. It is also recommended that this micro-positioner have as much dexterity as is required (for the execution of the task) so that the macro-positioner can be made simple but stiff. Position sensors may be fitted on the micro-positioner (for feedback to the control-system of both the macro- and micro-positioner) so that an accurate location is obtained. This can also help to nullify the effect of small amplitude vibrations of the macro-positioner.

2.4.4.1.2 Bracing Technique

The concept of macro- and micro-positioners in large robotic manipulators can be further extended as described by W. J. Book in [7]. He suggests that large motions be assigned to joints that move the major links. When these motions are completed, the arm is "braced" against the workpiece or a passive workbench. The small motions are assigned to other degrees of freedom which are referenced to the workpiece rather than the base of the robot. In this way lighter arms are possible without their disadvantages for fast and accurate motions. The feasibility of this technique depends on the nature and environment of the task to be performed. The workpiece or some other structure near the workpiece should be available to act as a "brace".

2.4.4.2 Considerations for Analyses

Static Analysis

In normal size robots, the basic intention of static analysis is to find the deflections

at the endpoint of the manipulator. However, in large size robots, the stresses generated are also of interest. These analyses can be done in various critical configurations of the robots to see the transmission of load through the manipulator structure, and hence give the designer an idea of the critical areas of the manipulator during the dynamic analysis.

Stability Analysis

Stability analysis of manipulator structure becomes critical as its size increases because of increasing mass and reducing stiffness. P. Mullord [19] reviews the various approaches currently used for space frames. They are detailed as follows.

1) Plastic Mechanism Approach

This involves finding a plastic mechanism within a structure such that the structure is in equilibrium and no member carries load greater than its squash load. A particular structure may have various mechanisms and the analyst must find the mechanism corresponding to the lowest applied load. A plastic mechanism analysis can only accomodate stability effects in a very approximate manner and should really be restricted to structures such as single layer structures where failure is dominated by member bending.

2) Elastic Stability Approach

Elastic stability analysis concerns with the calculation of certain critical states at which the stiffness of a structure with respect to a small disturbing force becomes zero or negative. The stability problem is considerably simplified if we assume that all displacements are insignificant when compared with the dimensions of the structure. This is the "Linear" stability problem. The linear problem can be posed as a eigenvalue problem with 'n' solutions where 'n' is the number of degrees of freedom. The eigenvalues will be the critical or buckling loads whereas the eigenvectors are the buckled

shapes. This analysis is normally cheaper computationally but may not produce necessarily accurate results. In fact, the results should only be used as limiting values (upper limit) for the actual critical loads. This is because the analysis does not consider the effect of displacement on stiffness of the structure. Also, it assumes that the structure is perfect.

Elastic stability analysis done without the assumption of small displacements is called the "Nonlinear" stability analysis. It can also be used for determining post-buckling behavior as well as imperfection sensitivity of the structure. The numerical approach to non-linear analysis uses incrementation and iteration to accomodate the changing stiffness of a structure as loading is applied. The iteration technique involves repeated improvements to displacement and stresses due to given loading so as to reduce the error in the equilibrium equations.

Of all the approaches listed above, the nonlinear approach shows greatest promise for large manipulators. It should be used for buckling and imperfection sensitivity analysis of the structure. The imperfection sensitivity analysis can be used to establish the manufacturing tolerance for the structure. It is not necessary that the whole structure be analysed. These analyses can only be performed for critical regions of the manipulator (e.g. members with high elongation ratio under compressive stress).

Modal Analysis

Modal analysis should normally be the first dynamic type of analysis performed for a structure. Since it provides natural frequencies and mode shapes as results, a basis of determining the integration step sizes for the numerical dynamic analyses is obtained. Also, one could see the effect of particular modes in dynamic reponse of the structure. It is also recommended that modal analysis be performed both with and without brakes

(where feasible) at the actuator joints, with and without payload at the end-effector, and with joint stiffnesses if possible. Modal analysis of manipulators is complicated by the fact that thier natural frequencies and mode shapes change with joint variables, that is with endpoint location.

Dynamic Analysis

Large manipulators can be expected to withstand a variety of dynamic loads as --

i) Transient torques and forces at the actuator joints.

ii) Step, impact, and ramp loads occuring upon loading and unloading of payloads.

iii) Vibrations developed by oscillating motion of its foundation by earthquake, wave impact, etc.

iv) Wind loading when in an outdoor environment.

Analyses should be done under above loading with and without payload on the endeffector of the manipulator, as the dynamic characteristics can be substantially different in those cases. Results of static should be considered before going for dynamic analysis in various endpoint locations.

Norris, et. al. detail conditions when wind loads should be considered as static or dynamic (transient) in [34]. Some reasons for considering wind loading to be static may be briefly mentioned as : nonperiodic and localized nature of wind (absence of sustained periodic component in wind); insensitivity of wind-load stresses to local force variations; general insensitivity of structures to rapid wind force changes; concurrent existence of nonwind forces of significant magnitude (e.g. gravity), etc. However, in cases where dynamic nature of winds cannot be ignored, numerical as well as experimental (wind-tunnel tests, etc.) analyses should be resorted.

J. G. Giannotti [44] present an analytical model for predicting wave impact loads

for the design of offshore platforms. If the robotic manipulator is mounted on such platform, the effects of wave loading can be studied.

Experimental Analysis

Large robotic manipulators can be expected to be quite costly to fabricate and experimental testing may be required on scaled down models. C. W. Burckhardt and D. Helms [36] discuss some scaling laws for manipulators and present relation between shock and elastic forces, and breaking strength while varying size of a manipulator. Wind tunnel tests on the scaled model may also be considered.

3.0 Design/Analysis of a Large Robotic Manipulator

3.1 The Problem -- Large Robotic Manipulator for AACTS

The problem of design/analysis of a large robotic manipulator, dealt with in this thesis report, forms a part of the design of an Automated All-Weather Cargo Transfer System (AACTS). The conceptual design for AACTS was developed by August Design and Development under a SBIR Phase I Contract from the U S Army Belvoir R D & E Center, Fort Belvoir, VA. It was conceived as an advanced cargo handling system for offshore transfer of cargo under seastate 3 (SS3) conditions or higher in a LOTS environment[50]. Offloading of containerized cargo from large oceangoing ships using existing equipment is hazardous during periods of rough weather and high seas. Conventional cargo handling systems are not designed to cope with the relative motion between ships and lighters in such conditions. While vertical descent rates and load pendulation can be nominally controlled, heavy seas create significant motion on the lighter in six degrees of freedom. In SS3 or higher, present methods and resources used for safe control of lighterage-cargo interface exceed human capabilities. AACTS attempts to provide a solution to these problems.

A key component of the AACTS is the robotic manipulator arm, two of which are mounted on each end of the AACTS structure for offloading cargo from containerships. Each manipulator arm has a maximum lift capacity of 35 tons at a horizontal reach of 140 ft, and a vertical reach of 120 ft. Two arms servicing a containership can thus access over 300 ft of deck space, handling containers both on deck and in the ship's cargo hold.

3.2 Conceptual Design

The conceptual design of the robotic manipulator was done by August Design and

Development, PA as given in [50]. Fig. 3.1 shows a simplified picture of AACTS with the robotic manipulators attached. The conceptual design shows a strong effect of the "reachability constraint" and the "stiffness constraint". The RRP design of the linkage mechanism of the manipulator originates from the workspace requirements and the action to be performed in the workspace. Each arm needs to reach about 100 ft on the far side of the deck of a 100 ft wide containership and lift containers over a height of about 80 ft. From the dimensions given, it can be seen that the manipulator arms are 140 ft long and 70 ft in height; and can cover 300 ft on the far side of the deck of a 100 ft wide containership. The revolute joints give sufficient reach whereas the prismatic joint gives the necessary lift. The space-frame nature of the manipulator indicates the effect of stiffness constraint considerations.

The manipulator arms attached to each corner of AACTS are made up of four major subsystems: the upper arm, the forearm, the vertical hydraulic hoist, and the "intelligent" spreader bar (Fig 3.2). The first three are the links of the kinematic chain of macro-positioning part of the robotic manipulator; whereas the spreader bar is the micro-positioning part. The upper arm and the forearm provide movement in the horizontal plane, forming a SCARA-type robot similar to those used in industry. (SCARA refers to arms which are Selectively Compliant Assembly Robot Arm.) By rotating the "shoulder" (juncture of the upper arm and AACTS frame) and the "elbow" (juncture of the upper arm and the forearm) the arm can reach a large area of the ship. The spreader bar is a Stewart platform type mechanism capable of producing all translatory as well as rotational motions in a workspace of about 3' x 3' x 3'.

The vertical rigid hoist is a 120 ft long three-stage telescoping member with good rigidity in the vertical direction. It provides for a vertical lift of approximately 120 ft. from the hold of a ship to a clearance over the maximum height of containers stacked on

deck. In addition to its vertical movement, the vertical hoist provides rotation about the vertical axis to properly orient the spreader bar, with respect to container placement.

Fig 3.2 is a simplified view of the elements of the structure. The upper and fore arms are space frame type structures in the shape of octahedrons. Each edge of these octahedrons is a space frame by itself (which we will call basic-frame member). Fig 3.3 explains how tetrahedrons meet to form octahedrons, which in turn form the basic-frame member. Note that the design at hand now is actually a space-frame type SCARA manipulator.

3.3 Design Analysis

3.3.1 Approach for analysis

3.3.1.1 Use of Finite Element Methods

The space frame nature of the manipulator makes the structural (static and dynamic) analysis quite complex. Theoretical closed forms solutions are not available and hence numerical solutions are pursued. Finite element methods are hence used for the above structural analyses. Various commercially developed finite element analysis packages are available at Lehigh University including ANSYS, MSC/NASTRAN, GTSTRUDL, and SUPERB (from I-DEAS). ANSYS was selected for analysis because of its varied capabilities to perform linear and non-linear static and dynamic analyses.

3.3.1.2 Some Considerations for Analyses

The manipulator arm operates in a complex dynamic environment, necessitating the use of both static and dynamic analysis. The arm assumes various configurations while acquiring and transfering containers, and the stress distribution in the basic-frame

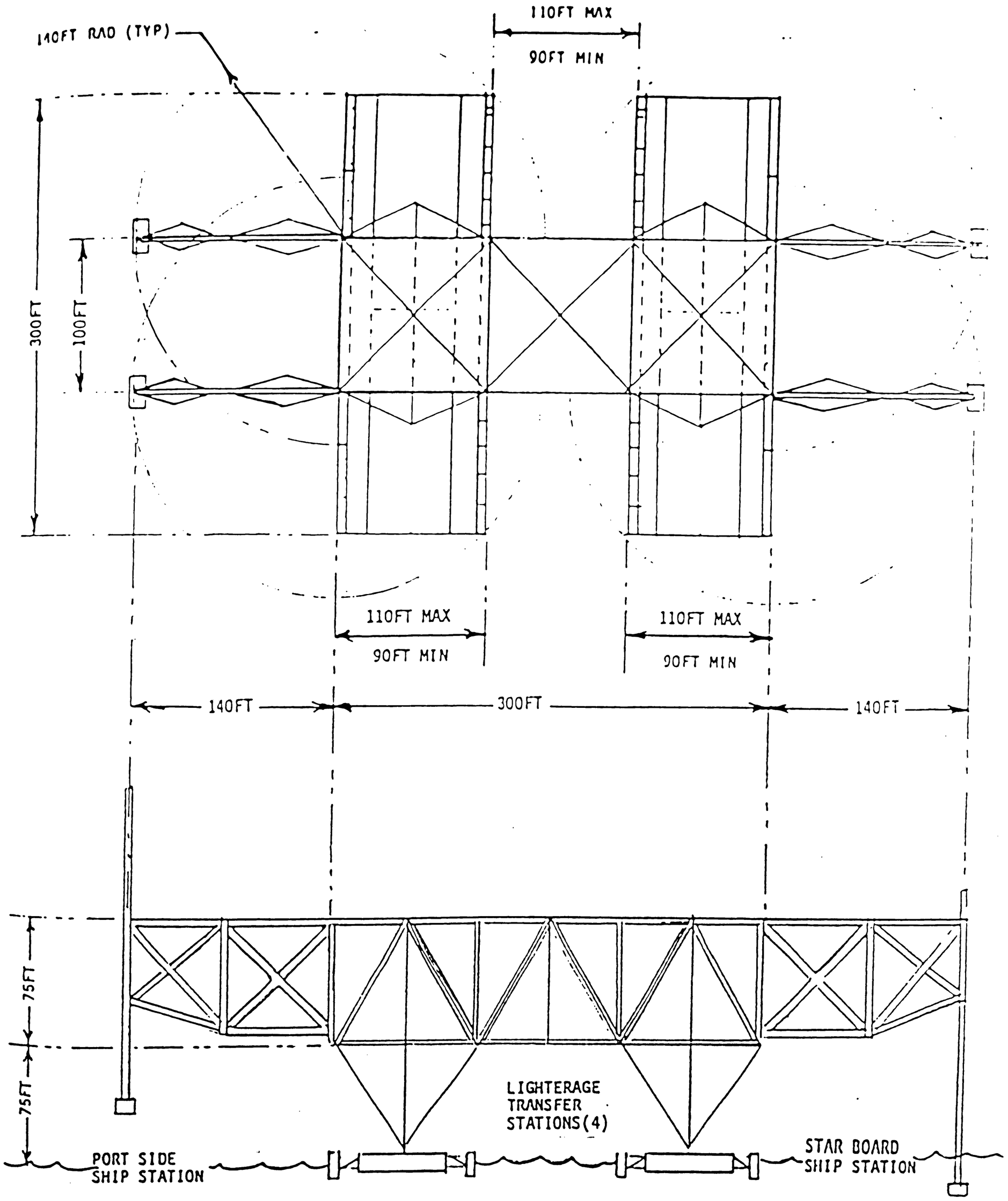

Fig 3.1 : AACTS Dimensions.

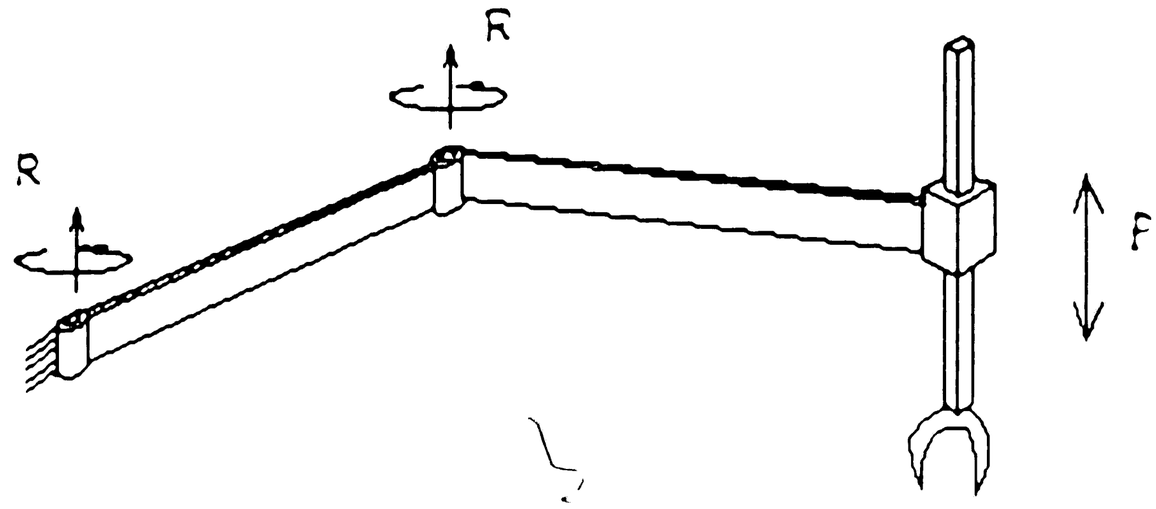

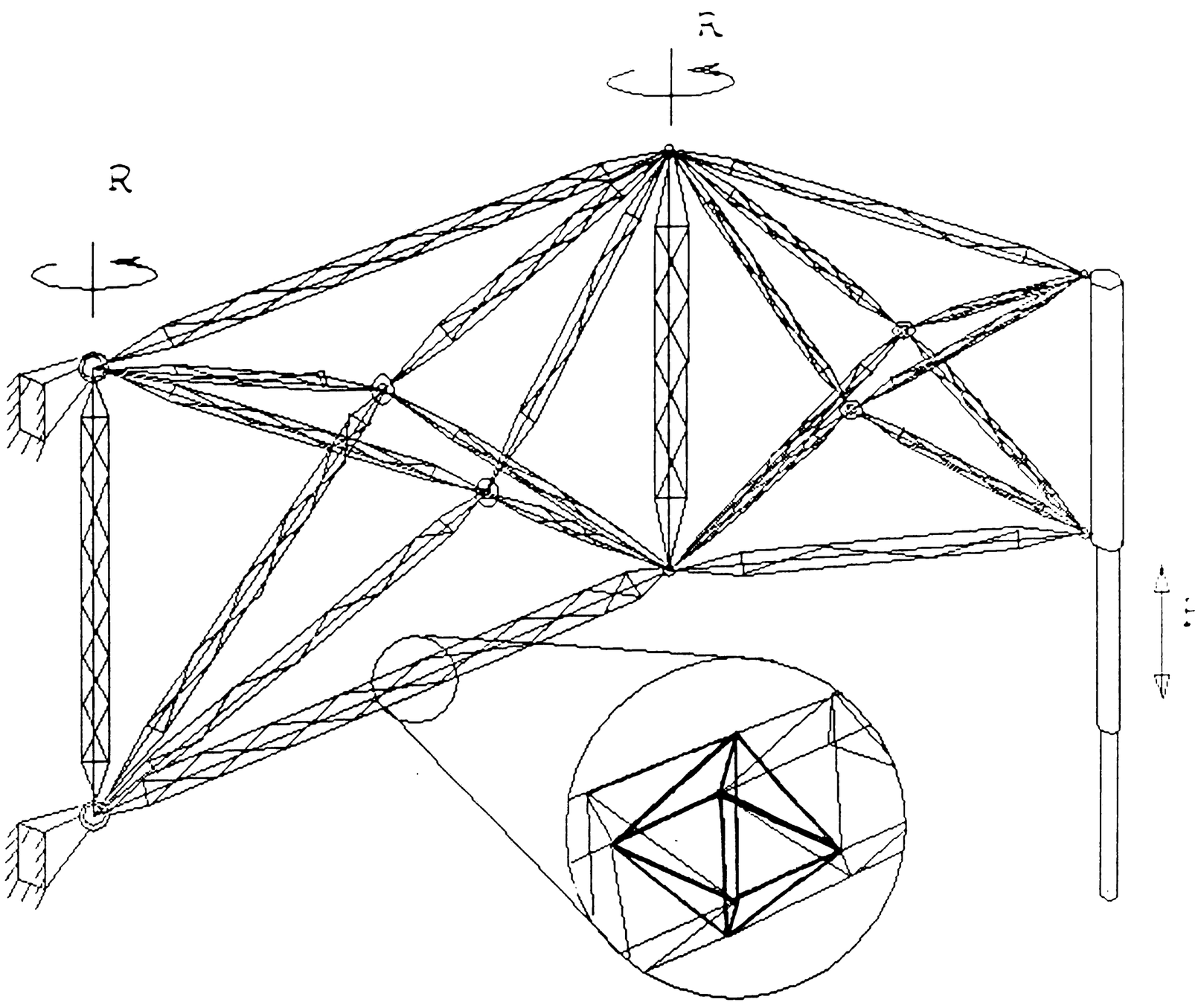

Fig 3.2 : Robotic Manipulator.

Two Tetrahedrons

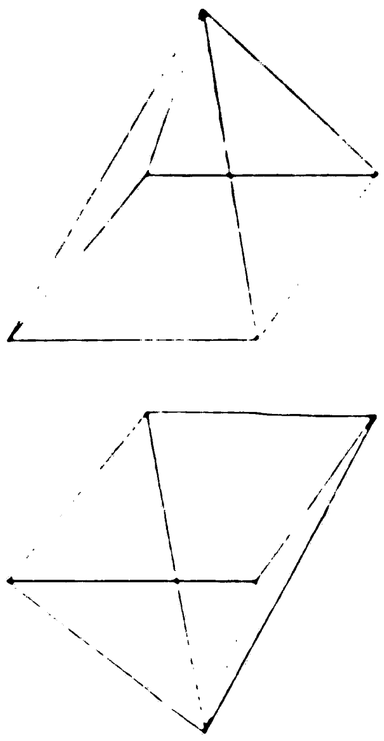

One Octahedron

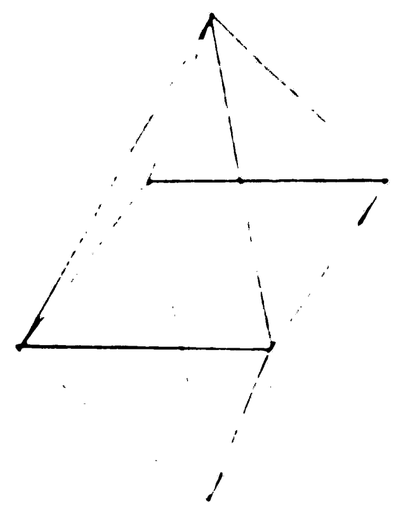

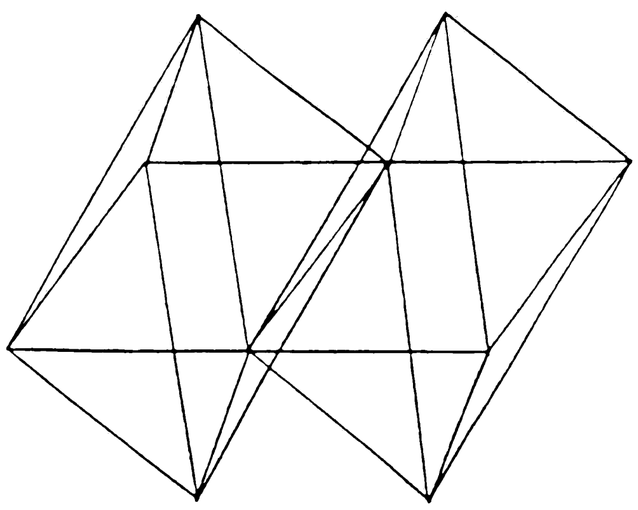

Two Octahedrons

Series of octahedrons making up the structure of the basic-frame

Fig 3.3 : Use of tetrahedrons and octahedrons in building up the structure of each individual member / link.

members will change as the forearm rotates from fully extended or coplanar with the upper arm to a position at 90° with respect to the upper arm. In the rotated position the upper arm has to resist a large torque caused by the out-of-plane loads. The static and dynamic analyses should therefore be performed for all critical arm configurations. The two most important orientations are : i) both arms in the same plane; and ii) both arms at right angles to each other.

When the container (i.e., the load) is lifted, it becomes a part of the manipulator structure. The mass of the container will be comparable to the total mass of the arm. This will significantly affect the dynamic behavior of the structure. The container is a concentrated mass attached to the end of the hoist, a slender rod, accentuating the lateral springiness. Proper consideration will be given while modeling the arm under this action.

The report includes suggested design modifications for both a full-scale manipulator arm and a tenth-scale version based on Finite Element Analysis results. Although the two different designs have dimensions that differ by a factor of ten, the basic layout is maintained. Design changes found necessary in one analysis are incorporated in the design prior to the next run. The general flow of analyses is full-scale conceptual design analysis, then tenth-scale conceptual and preliminary analysis, followed by full-scale preliminary design analyses.

3.3.2 Analysis of Conceptual Full Scale Manipulator Design

3.3.2.1 Finite Element Model of the Arm

The load carrying elements of the manipulator arm are the long slender basic-frames fabricated from rolled structural steel angles. Since it would be computationally expensive and time-consuming to represent each structural element in each basic-frame, a single equivalent beam element (ANSYS element type STIF4), was used in the model

to represent each of the basic-frames. Each equivalent beam element then carries all the loads and moments, and reacts in the analysis in a manner equivalent of the original basic-frame assembly.

To properly define the equivalent beam elements, it is necessary to clearly describe the mass, effective cross-sectional area, moments of inertia, and end connections for each of the basic-frame assemblies in the manipulator arm. Since all basic-frames were pin connected in the conceptual design, the only external forces possible were axial, i.e. tension or compression loads.

A detailed analysis of a typical basic-frame member verified that only the main longitudinal structural angles were effective in carrying the tensile and compressive loads. Transverse and diagonal elements, on the other hand, are active in carrying any shear loads and moments. Hence the basic-frame assemblies are modeled using equivalent beam members which had areas and moment of inertias equal to sum of the corner members of the detailed section. If the cross-sectional area and moment vary between two nodes of an equivalent element, average values are used.

The user is reponsible for using proper and consistent units when using ANSYS. The units adopted for the analyses performed in this project are as follows :

Length -- in

Force -- lb (Note : In this analysis, lb has been taken to mean lb_f, i.e unit of force)

Time -- sec

Accel -- in/sec^2

Mass -- $lb\text{-}sec^2/in$

Stress -- lb/in^2

Fig 3.4 : Approximation of Detailed Basic-frame Structure by beam element

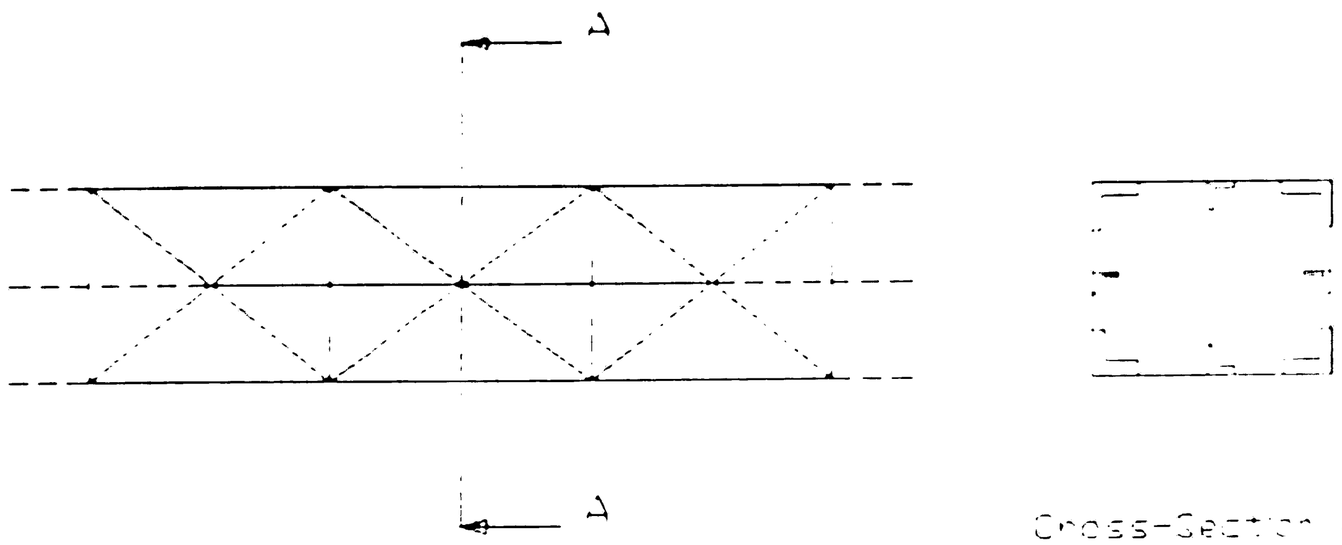

Fig 3.5 : Simulation of Pin/Universal Joints using Coupling

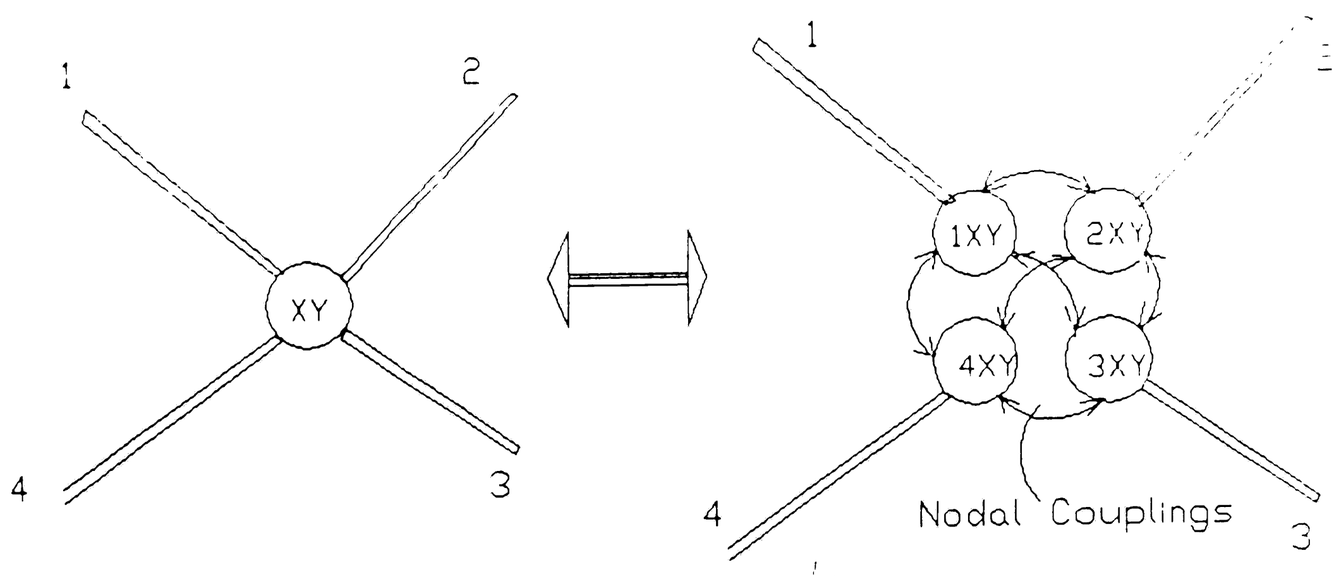

ANSYS calculates the mass of beam members based on volume of the beam and mass density specified for the beam material. For volume calculations, it is assumed that the cross-sectional area remains constant. The load induced by self-weight of the members is then calculated using the mass value and specified acceleration. When we approximate the total cross-sectional area of a detailed basic-frame structure by its major load bearing area (i.e. the sum of corner elements), the stresses generated by external loads are quite accurate but the self-weight generated loads are under estimated as the approximation fails to account for the weight of the non-load bearing elements of the detailed section. This problem was overcome by increasing the mass density of the equivalent members so as to correctly compute the self-weight of the basic-frame.

The forearm is connected to the upperarm, and the upperarm is connected to the fixed support (ground) by means of pin-joints. The basic-frames of the arms are connected by universal joints. Simulation of a pin or a universal joint is done as in Fig 3.5. Instead of defining one node 'XY' which would be shared by four elements, four overlapping nodes 1XY, 2XY, 3XY, 4XY are defined and attached separately to each element. To simulate a universal joint, a coupled set is defined where all the overlapping nodes move together (acquire same coordinates in space) without any constraints on rotation of individual elements (joined at node XY). If a pin joint is required with rotational freedom about a single axis, rotation about the other directions may be constrained (i.e. all the overlapping nodes assume same rotational displacements about those axes).

Fig 3.6 shows node location designations which were used throughout the analysis. The origin of the global coordinate system is located at node #3 throughout the analysis.

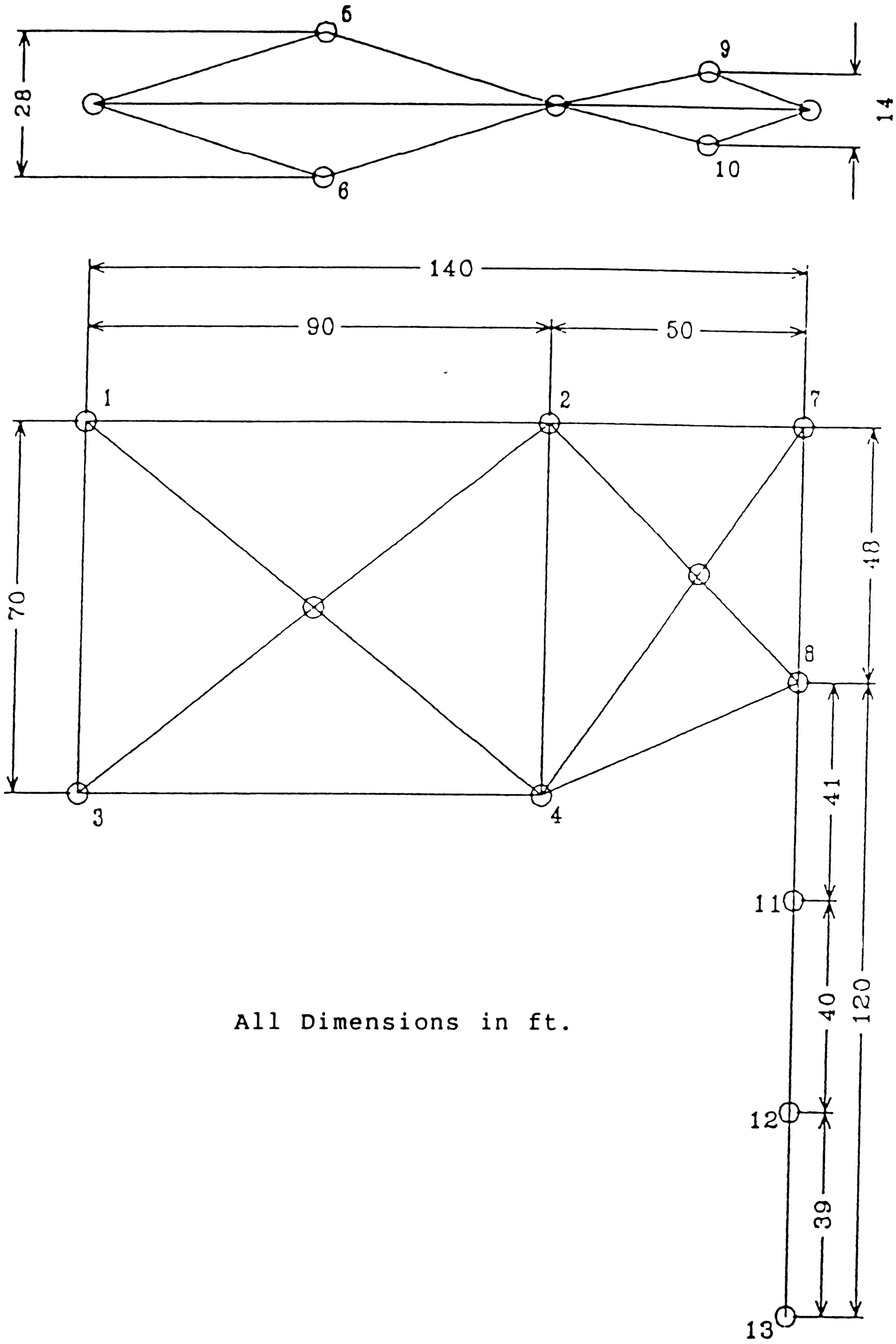

All Dimensions in ft.

Fig 3.6 : Manipulator Arm Arrangement.

3.3.2.2 Static Analysis

The static analysis consists of force/stress/displacement calculations for the manipulator in different configurations and evaluation of the forearm and upperarm assemblies. The results in sections 3.3.2.2.1 through 3.3.2.2.3.2 do not correctly represent the manipulator arm characteristics because of design changes and improvements which were made as the study progressed. The early results are included in this section for completeness of reporting , and to correctly represent the flow of the analysis and the improvements made to the conceptual design.

3.3.2.2.1 Forearm Analysis

The forearm portion of the manipulator was selected for analysis first to provide a less complex structure at the beginning of the study. The results obtained from the forearm analysis were applied to the later analysis of the upper arm, and both results were then available for comparison with the full manipulator arm performance. Fig 3.6 shows the arrangement of the manipulator arm.

For separate forearm analysis, the external load is applied at node # 13, but the support points are shifted to nodes 2 & 4. Nodes 2, 4, 7, 8, 9, and 10 are all simulated as universal-joint connections whereas nodes 11, 12, 13 are defined as welded connections. This model is as shown in Fig 3.7.

The static analysis (force/stress/displacement calculations) of the forearm (for conditions given below) using ANSYS yields the displacement shape as shown in Fig 3.8.

Support Location

Nodes : 2, 4 (Pin joints, NO rotational constraints)

Applied Load

Self-weight, & External force : 70,000 lb at node #13

Non-support pin joints

All are Universal Joints.

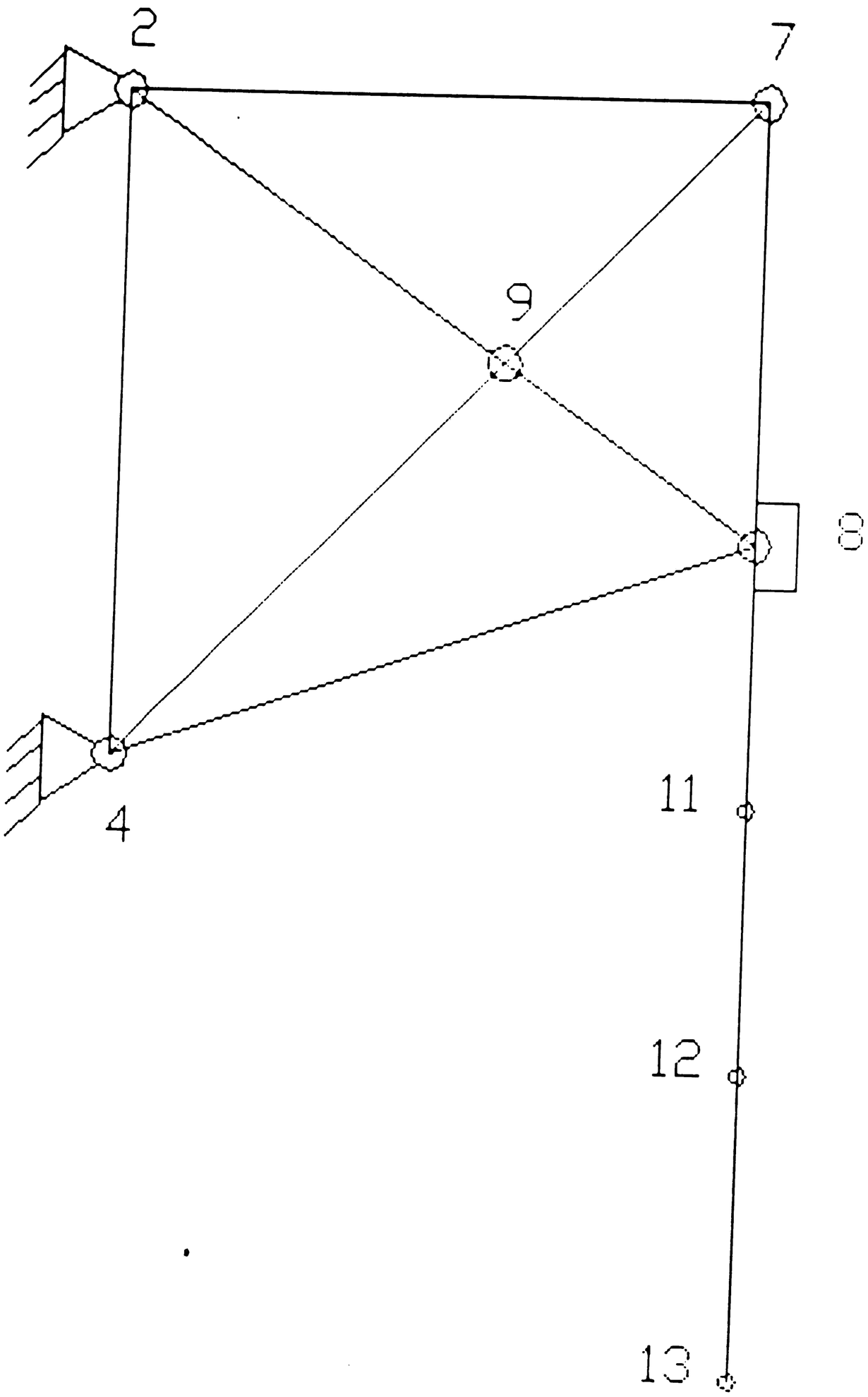

Fig 3.7 : Schematic of Forearm model

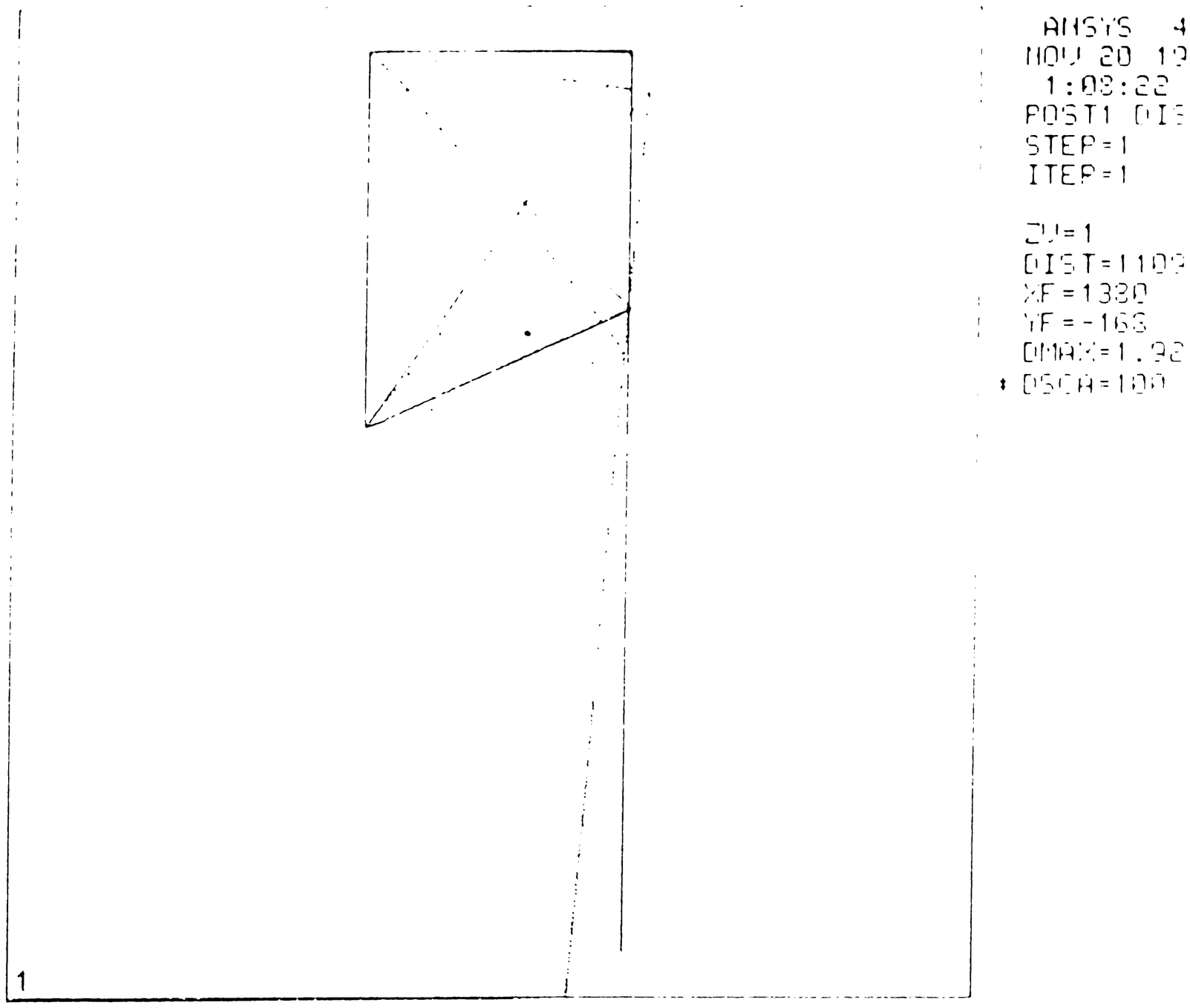

Fig 3.8 : Distortion of Forearm under self-weight and external load of 70,000 lb applied at node #13.

Fig 3.8 shows the displacements (change in the node locations under the action of load) magnified 100 times, for clarity purposes. This technique is very helpful in observing the movement of the nodes under action of a load, but it may lead to unrealistic distortion of the overall shape. To get a more realistic view, the plots should be drawn with a distortion scale closer to one (1.0).

The distorted shape in Fig 3.9 shows clockwise rotations about support nodes 2 and 4. This was expected since both the applied external load and self-weight are acting to produce a clockwise moment at the support points. A maximum deflection of 1.92 inches is obtained at node #13.

Examples of several alternative conditions which could be evaluated are as follows :

Self-weight	-	present or absent
External weight	-	present or absent
Support nodes	-	rotational constraints or not
Non-support nodes	-	pin joints, universal joints, or moment-carrying joints
Design details	-	selective

A specific design change which was investigated was the addition of a beam element between nodes 9 & 10. Although the forearm structure is stable without the 9-10 member, its addition provides a degree of redundancy and could possibly have a stiffening effect. The results of the forearm analysis are as shown in table 3.1.

Table 3.1 : Forearm Analysis -- Comparison of Results.

Type of Analysis		LOADING CONDITIONS		
		Self-weight of the structure	External load of 70 kip at #13	Cumulative (Self-weight+70kip)
1) Moment Carrying Joints	Max. Displ. (in.)	-.816, -.720, -.110 (#13) (#13) (#9)	-.997, -.740, -.078 (#13) (#13) (#9)	-1.81, -1.46, -.188 (#13) (#13) (#9)
	Max. Rotation ($\times 10^3$)	-.255, -.126, -.943 (#9) (#9) (#2)	-.060, -.094, -.641 (#9) (#9) (#8)	-.315, -.220 (#9) (#9)
	Max. Element-Force (t)	36.1, -53.3, 5.7 (4-8) (8-11) (9-7)	27.2, -70.0, 4.0 (4-8) (8-11) (9-7)	63.3, -123.3, 9.7 (4-8) (8-11) (9-7)
	σ_1 (kpsi)	Compr. : -2.09 (4-8) Tensile : 2.0 (2-9)	Compr. : -1.25 (4-8) Tensile : 1.21 (8-9)	Compr. : -3.34 (4-8) Tensile : 3.14 (8-9)
2) Pinned Joints	Max. Displ. (in.)	-.80, -.74, -.26 (#13) (#13) (#9)	-.61, -.75, -.18 (#13) (#13) (#9)	-1.41, -1.49, -.44 (#13) (#13) (#9)
	Max. Rotation ($\times 10^3$)	-4.59, -5.43, -3.19 (#9) (#9) (#4)	-2.3, -2.7, -.65 (#9) (#7) (#7)	
	Max. Element-Force (t)	34.3, -53.3, 5.9 (4-8) (8-11) (9-7)	25.0, -70.0, 4.3 (4-8) (8-11) (9-7)	57.3, -123.3, 10.2 (4-8) (8-11) (9-7)
	σ_1 (kpsi)	Compr. : -1.4 (4-8) Tensile : 1.23 (2-7)	Compr. : -.98 (4-8) Tensile : .9 (2-7)	Compr. : -2.38 (4-8) Tensile : 2.13 (2-7)

Table 3.1 continued :

Type of Analysis		LOADING CONDITIONS		
		Self-weight of the structure	External load of 70 kip at #13	Cumulative (Self-weight+70kip)
3) With a Stiffener	Max. Displ. (in.)	-.89, -.75, -.0005 (#13) (#13) (#9)	-.71, -.74, -.00034 (#13) (#13) (#9)	-1.6, -1.49, -.00085 (#13) (#13) (#9)
	Max. Rotation ($\times 10^3$)	-4.25, -5.64, -3.17 (#9) (#9) (#4)	-2.18, -2.25, -.64 (#8) (#7) (#7)	
	Max. Element Force (t)	41.0, -53.3, 7.0 (4-8) (8-11) (8-9)	29.6, -70.0, 5.07 (4-8) (8-11) (8-9)	70.6, -123.3, 12.07 (4-8) (8-11) (8-9)
	σ_1 (kpsi)	Compr. : -1.64 (4-8) Tensile : 1.35 (2-9)	Compr. : -1.16 (4-8) Tensile : 0.79 (11-12)	Compr. : -2.80 (4-8) Tensile : 2.09 (8-9)

The first two columns of the above table were calculated using ANSYS, whereas the third was obtained by summing the first two. The three figures represent the x, y, z components of the variables indicated in the leftmost column. The parenthetical number preceded by # is the node number, and the two numbers separated by a dash represent the nodes identifying the beam element. The underlined node is the node to which the calculations apply.

Two conclusions can be made from the results of the forearm static analysis. First, the forearm analysis clearly shows that there is no advantage in using moment carrying (rigid / welded) joints over the pinned joints in the design. This clearly demonstrates an important characteristic of the basic design of the space-frame configuration. All reaction forces are directly converted to tension or compression loads in the individual basic-frames. Hence the use of moment-carrying joints does not lead to any significant improvement in the performance of the forearm.

Another conclusion is that the beam element added between the two diagonal member cross-joints makes no significant change in the performance of the structure. Again the space frame configuration of the forearm is such that without the stiffening beam element the nodes 9 and 10 do not show any significant increase in separation in the Z direction. Hence the use of the extra beam element is not very helpful. As noted earlier, the cross member may be added as a reliability improvement if this was found to be worthwhile in the final design of the arm. Additionally, the added beam element may be helpful during assembly and disassembly of the space-frame structure.

Operational conditions of the manipulator arm suggest the use of applied displacement analysis. For this analysis, an external load is applied to a particular node of the model by means of a specified displacement. This is can simulate conditions

when the spreaderbar at the tip of the vertical hoist becomes entangled with containers or other equipment on a containership. An applied deflection of 10" was selected as a "unit value" since it can be considered a reasonable deflection for a 120 ft rod extension. Effects of larger or smaller deflections can then be estimated in relationship to this value. The analysis is done with following conditions --

Relative orientation of two arms

N/A

Support Location

Nodes : 2, 4

Joints : Pin joints, rotational constraint about Y axis.

Applied Load

Self-weight : NO

External force : 0.0

Applied displ. : 10 in. (in Z and X directions separately)

Non-support pin joints

All are Universal Joints.

Figs 3.9 & 3.10 represent the distortion shapes which results from a displacement applied in the positive Z axis and X axis respectively. Figs 3.12 & 3.13 indicate the induced stresses for the above two conditions respectively. The maximum induced stress (σ_1: maximum principal stress) are 0.81 and 0.93 kpsi respectively, both conditions at node #13, the point where the displacement is applied. The maximum induced stresses at node 13 are quite low, and the resulting stresses elsewhere in the structure are practically nonexistant. Clearly, this shows that whenever a displacement is applied at the tip of the spreader bar, being slender and relatively soft than the rest of the structure, it deforms absorbing most of the applied deflection/strain and passing a very little of it to the rest of the arm. The limited stiffness of thevertical hoist can present a problem in accurately positioning the spreaderbar over a container on a moving deck.

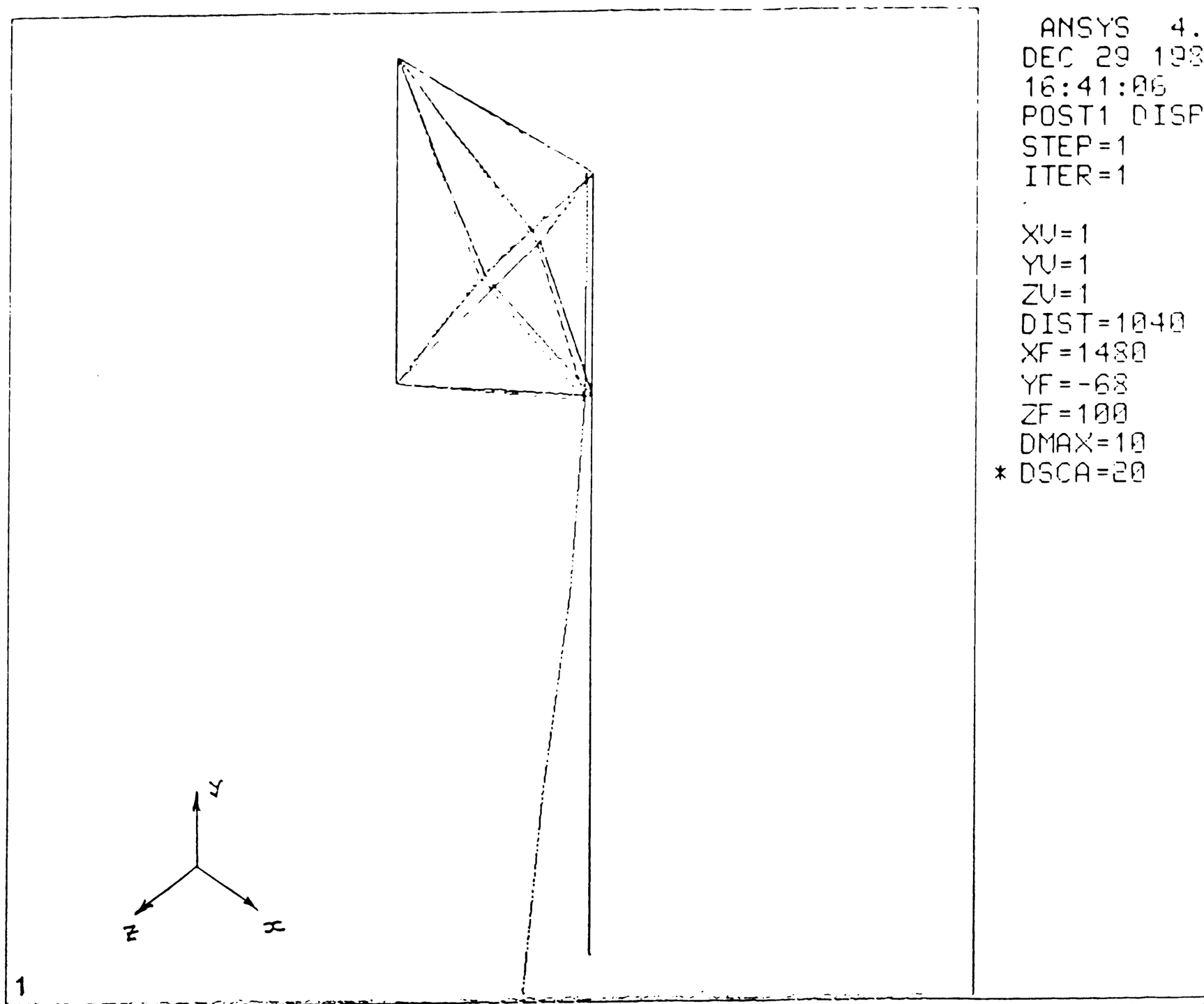

Fig 3.9 : Distortion of Forearm under applied displacement of 10 in. in the Z direction.

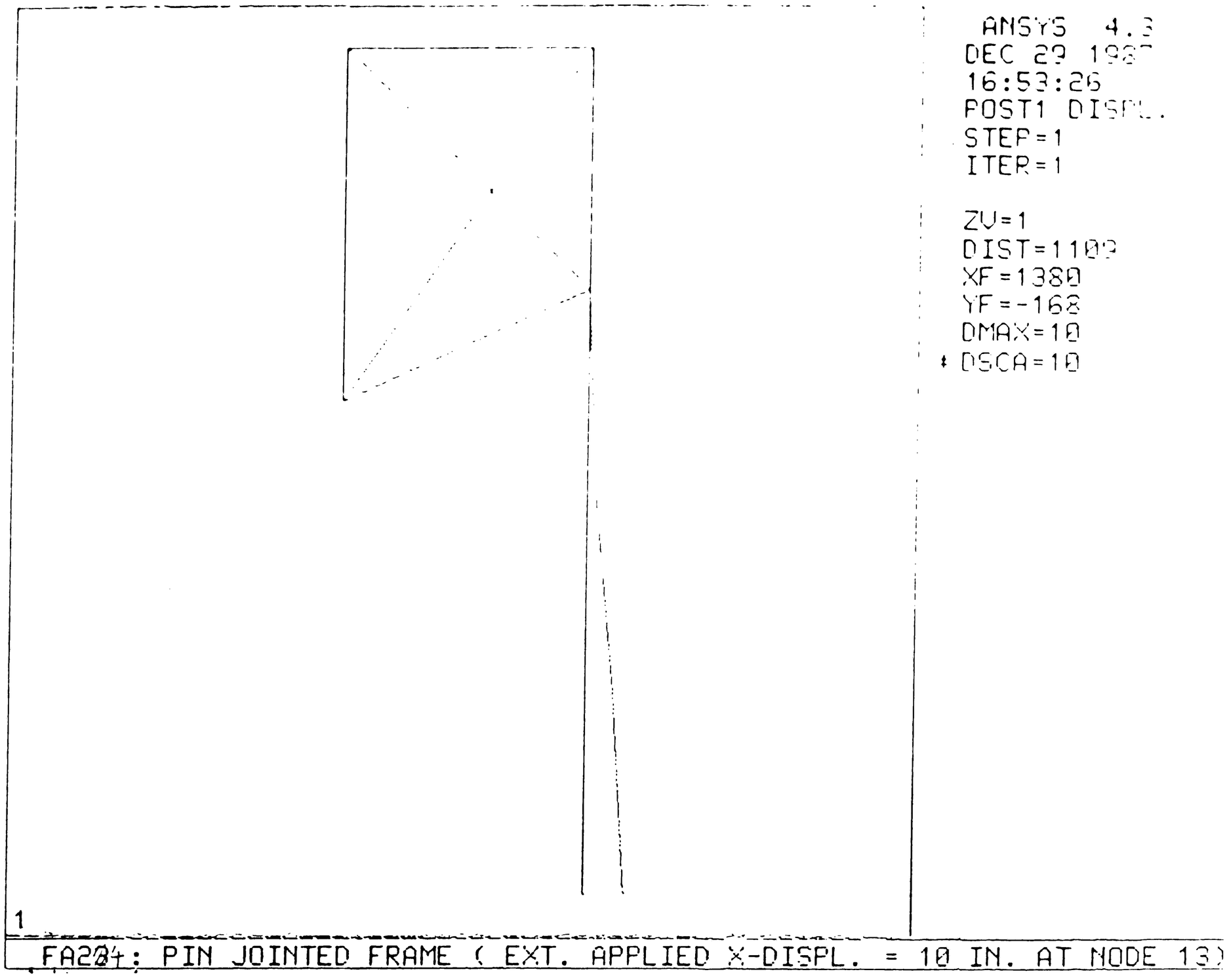

Fig 3.10 : Distortion of Forearm under applied displacement of 10 in. in the X direction.

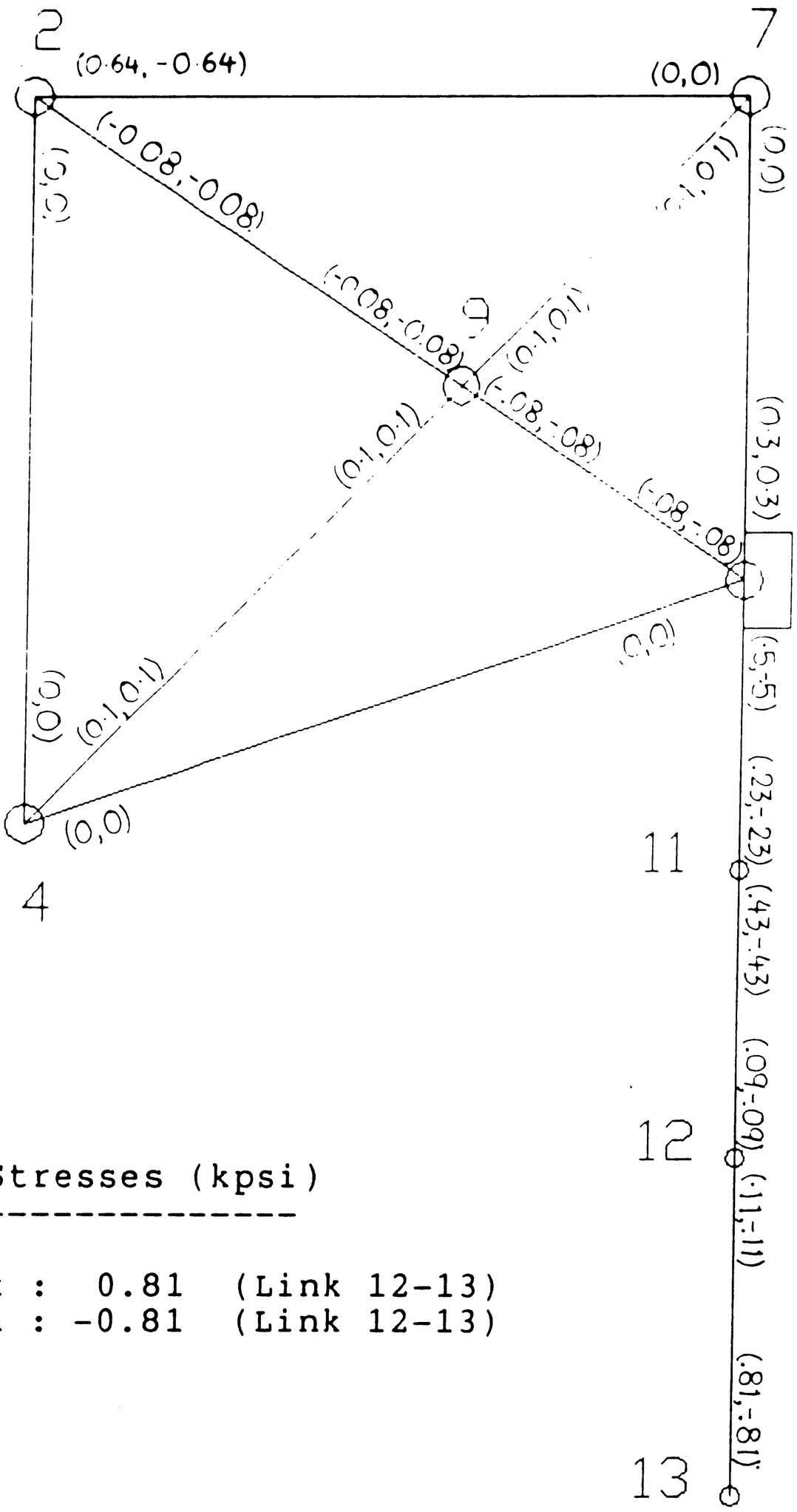

Fig 3.11 : Stress Distribution in Forearm under applied displacement of 10 in. in the Z direction.

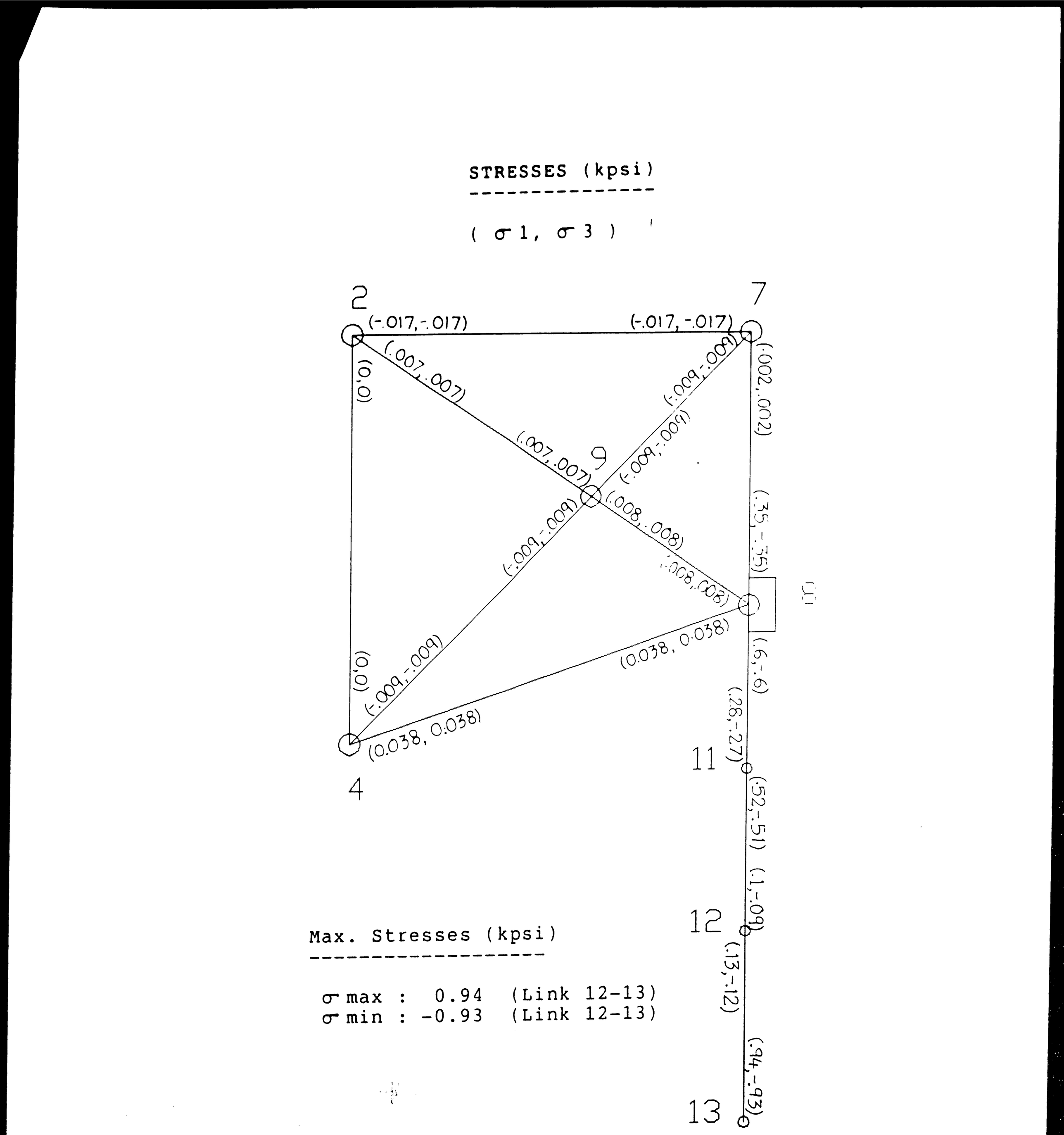

Fig 3.12 : Stress Distribution in Forearm under applied displacement of 10 in. in the X direction.

3.3.2.2.2 Upper Arm Analysis

A frame representation of the upper arm was analyzed for the following two load conditions --

Relative orientation of two arms

N/A

Support Location

Nodes : 1,3

Joints : Pin joints, No rotational constraints.

Applied Load

Self-weight : i) YES ii) NO

External force : i) 0.0 ii) Weight of Forearm and 70,000lb load

Applied displ. : None.

Non-support pin joints

All Universal Joints.

Fig 3.13 and 3.14 show the induced stresses in the upper arm for the indicated conditions. Maximum stress of .79 kpsi occurs in the diagonals 1-5 and 3-5 when only self-weight is acting. Whereas, under the action of external load only (i.e. the 70 kip load & the weight of the forearm), the top and bottom members are stresses the most, up to a stress of 9.1 kpsi. Considering that the yield-stress of steel is in the order of 35 kpsi, the stresses induced in the upperarm are quite reasonable.

STRESSES (kpsi)

(σ1, σ3)

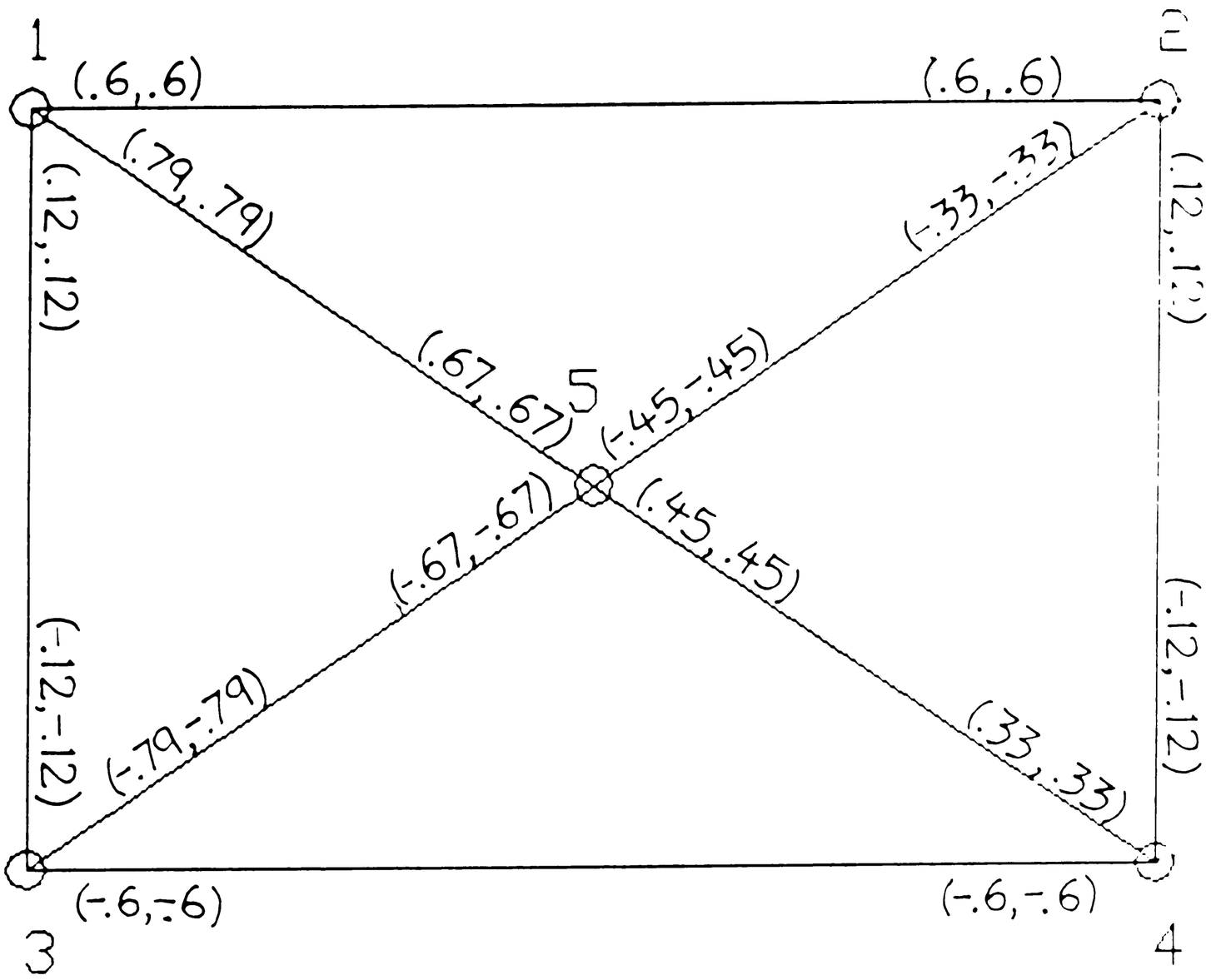

Max. Stresses (kpsi)

σ max : 0.79 (Link 1-5)
σ min : -0.79 (Link 3-5)

Fig 3.13 : Stress Distribution for Upper arm - Self-weight only

STRESSES (kpsi)

(σ 1, σ 3)

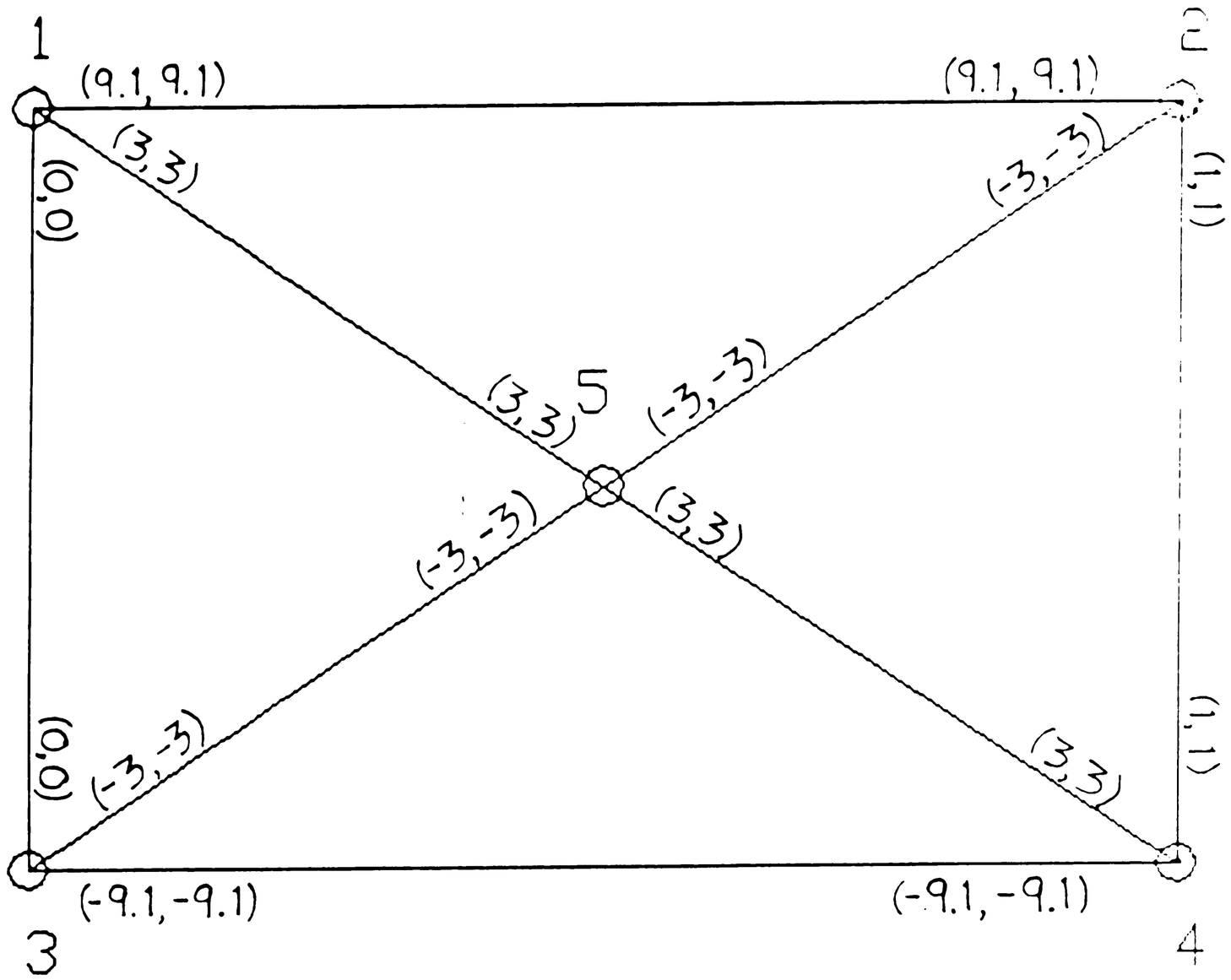

Max. Stresses (kpsi)

σ max : 9.1 (Link 1-2)
σ min : -9.1 (Link 3-4)

Fig 3.14 : Stress Distribution for Upper arm with no self-weight,
But with Reaction forces at nodes 2 & 4 to represent forearm loads

3.3.2.2.3 Complete Manipulator Arm Analysis

The analyses of the forearm and upperarm provided an assurance that the basic design of each was sound. Analysis of the full manipulator arm can be done for various relative angular positions of the two parts of the arm. The most important positions to be evaluated are the fully extended position (i.e. both arms lie in the same plane) and 90° rotated position (in which the arms lie in planes at right angles to each other).

3.3.2.2.3.1 Fully Extended Position

The manipulator arm was analyzed in the fully extended position for the following listed two load conditions --

Relative orientation of two arms

0.0° rotation

Support Location

Nodes : 1,3

Joints : Pin joints, NO rotational constraints.

Applied Load	Case #
Self-weight :	i) YES ii) NO
External force :	i) 0.0 ii) 70,000 lb load at node #13

Non-support pin joints

All Universal Joints.

The stress distributions obtained for the above two conditions are as shown in Fig 3.15 and 3.16 respectively. If these two stress fields are added, we get the distribution for that of a combined loading (i.e. both self-weight and external load of 70,000 lb at the spreader bar) as shown in Fig 3.17. This can then be compared with the cumulative

effect of self-weight and forearm reactions on upper arm (as in Fig 3.13 and Fig 3.14). The stress distributions compare within 1% and hence give a good self-check. The distorted shape of the arm under combined load is as given in Fig 3.18.

Link 3-4, one of the longest members, experiences a high compressive stress because of the combined moments of the self-weight and external loading. (Shear loads are carried by the diagonal members). Buckling load calculations for link 3-4 were done as follows :

By Rankine's formula (for slenderness ratios 20 to 100),

for steel columns with both ends rounded,

Ultimate column load in kpsi --

$$p_{buckling} = \frac{S}{(1 + l^2/ (6250*r^2))}$$

where,

S is the ultimate compressive strength in kpsi

l is the length of column in inches

r is the radius of gyration in inches.

Using 60 kpsi as the ultimate compressive strength of steel, the buckling load of link 3-4 comes out to be 48.9 kpsi (353 tons). Note that the link experiences a stress of 9.56 kpsi (under combined load) which is quite low with respect to buckling considerations. However the section modulus of the top and bottom beams of the upper arm may still be increased to reduce arm deflection and to increase the ultimate load capacity of the arm.

3.3.2.2.3.2 Rotated Position

The forearm is required to be rotatable with respect to the upperarm to permit the spreaderbar to have access to the containers at less than 140 ft radial disttance. The conceptual design provides for rotation upto approximately +/- 135° from the fully extended position, thus allowing the spreaderbar (node 13) to access any point from a radius of 140 ft down to about 65 ft. The rotated position produces a high torsional load on the upperarm which is resisted entirely by the upper arm diagonal members. At 90° rotation, the stresses in the diagonal members from the torsional moment are at a maximum.

At this juncture of analysis, a few data errors are detected. A data error occurred in the definition of the 3"x3" diagonal angles (in the detailed configuration of individual link). The thickness was given as 5/8 in, whereas the correct value calculated for the original conceptual design was 5/16. This error caused the stresses in the diagonal members to be incorrect (lower) by a factor of two. Another error was use of an incorrect (lower) value of Young's Modulus for steel. The result of the lower E value was an excessive strain and large displacements. Correction of the E value lowered the strains / displacements for any given value of stress or loads. An analysis of the structure with the correct E value gave a maximum displacement of 7.9 inches as a result of the combined effect of self-weight and an external load of 70,000 lb. The total displacement at the spreader bar, when the load is picked up, is now only 3.0 inches indicating a very stiff structure. Fig 3.19 shows a distortion amplified shape of the arm under the combined action of self-weight and external load. Fig 3.20 shows the resulting stresses.

STRESSES (kpsi)

(σ 1, σ 3)

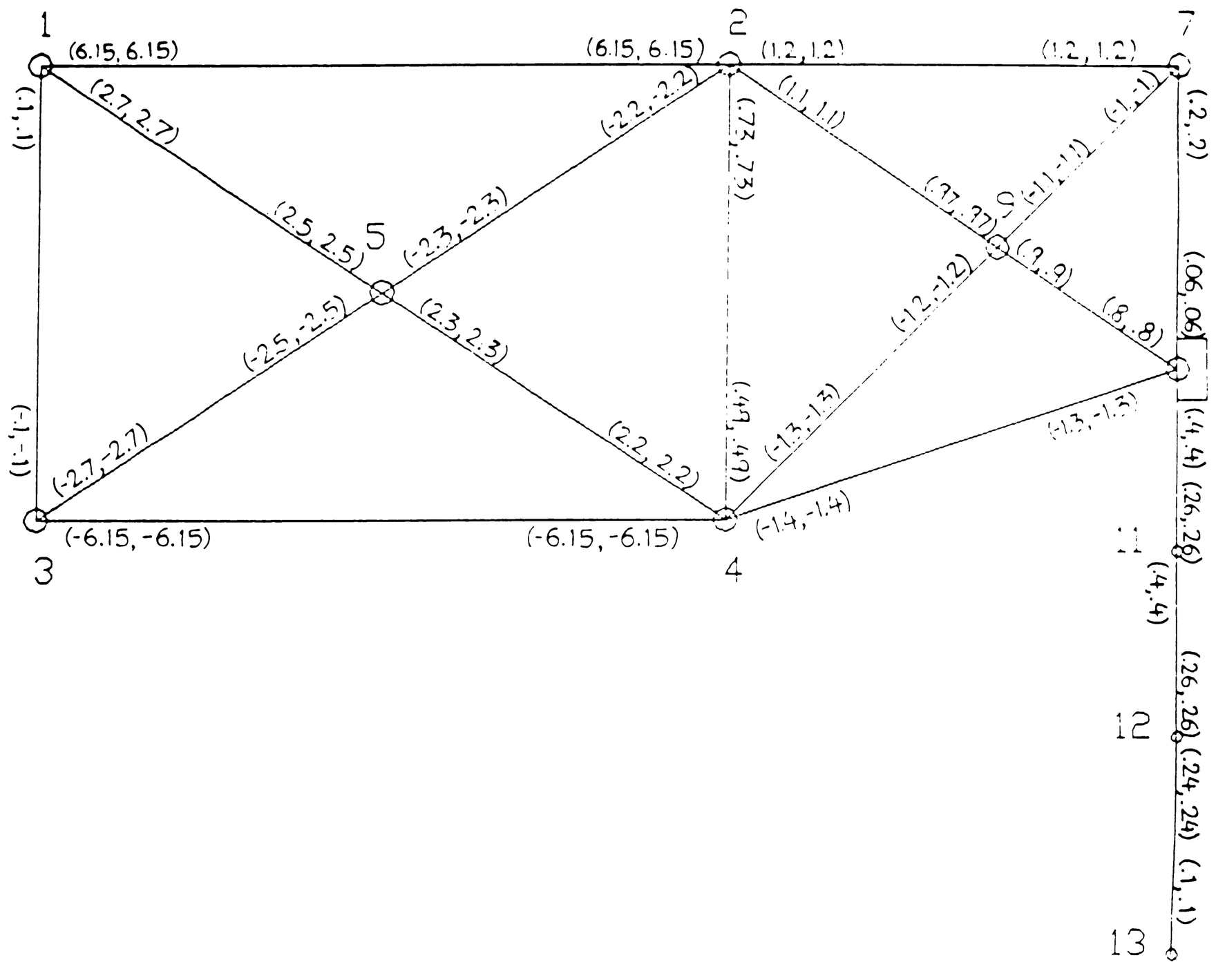

Max. Stresses (kpsi)

σ max : 6.15 (Link 1-2)
σ min : -6.15 (Link 3-4)

Fig. 3.15 : Stress Distribution for Fully extended Arm [Self-weight only]

STRESSES (kpsi)

(σ 1, σ 3)

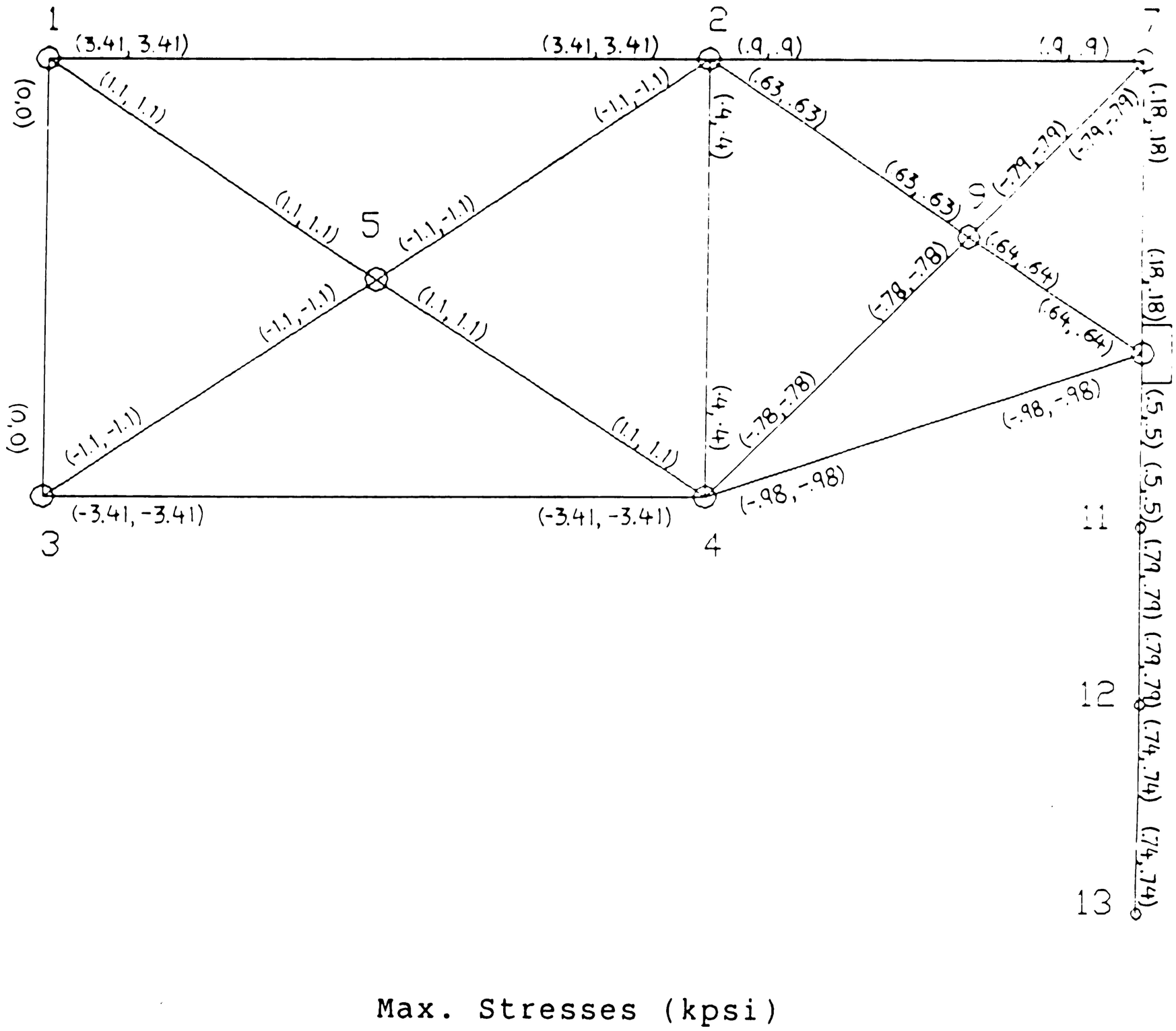

Max. Stresses (kpsi)

σ max : 3.41 (Link 1-2)
σ min : -3.41 (Link 3-4)

Fig. 3.16 : Stress Distribution for Fully extended Arm [No Self-weight But External load of 70,000 lb at node #13]

STRESSES (kpsi)

(σ 1)

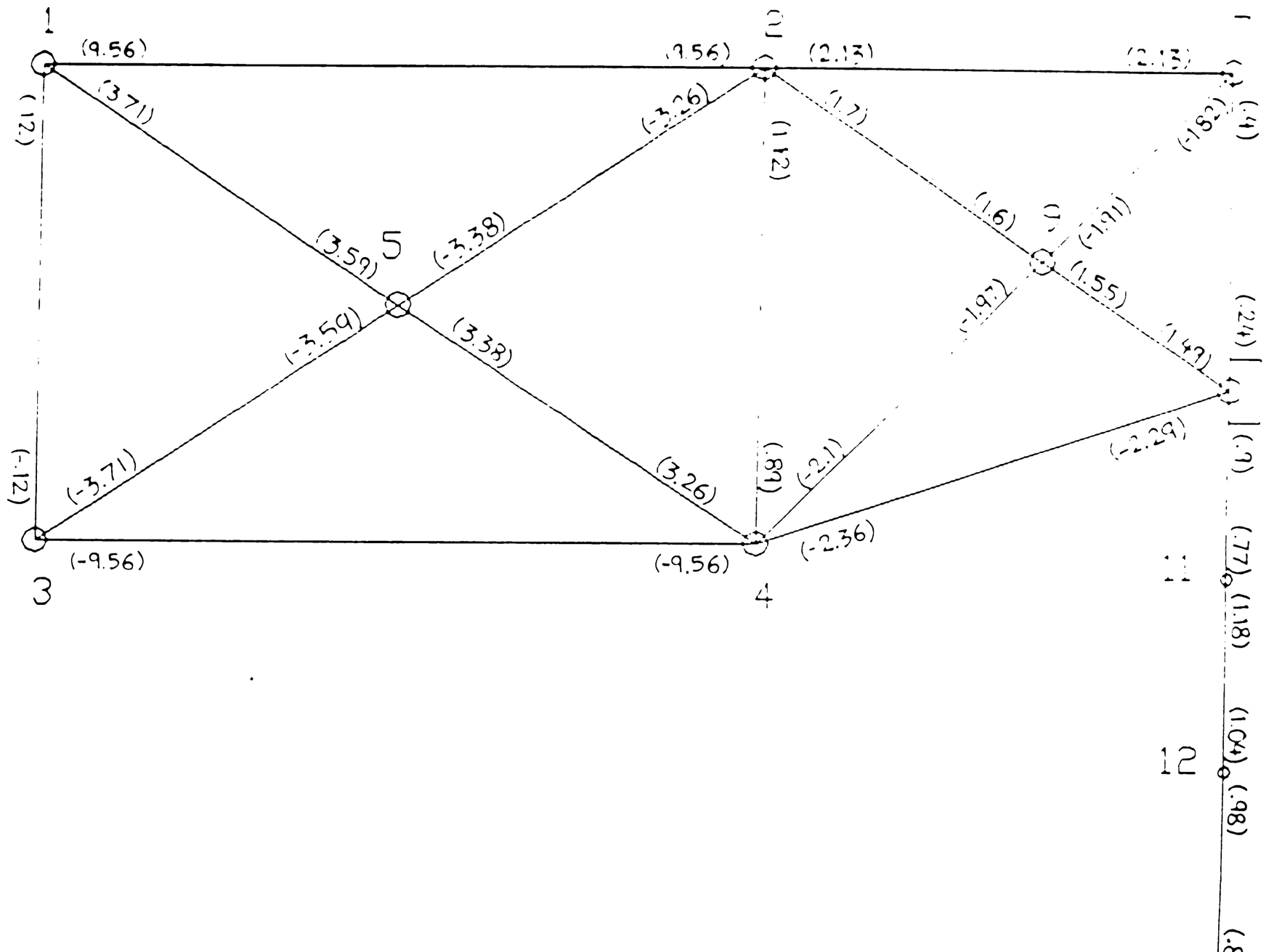

Max. Stresses (kpsi)

σ max : 9.56 (Link 1-2)
σ min : -9.56 (Link 3-4)

(Note : For above load condition, $\sigma 1 = \sigma 3$)

Fig. 3.17 : Stress Distribution for Fully extended Arm [Both Self-weight & External load of 70,000 lb]

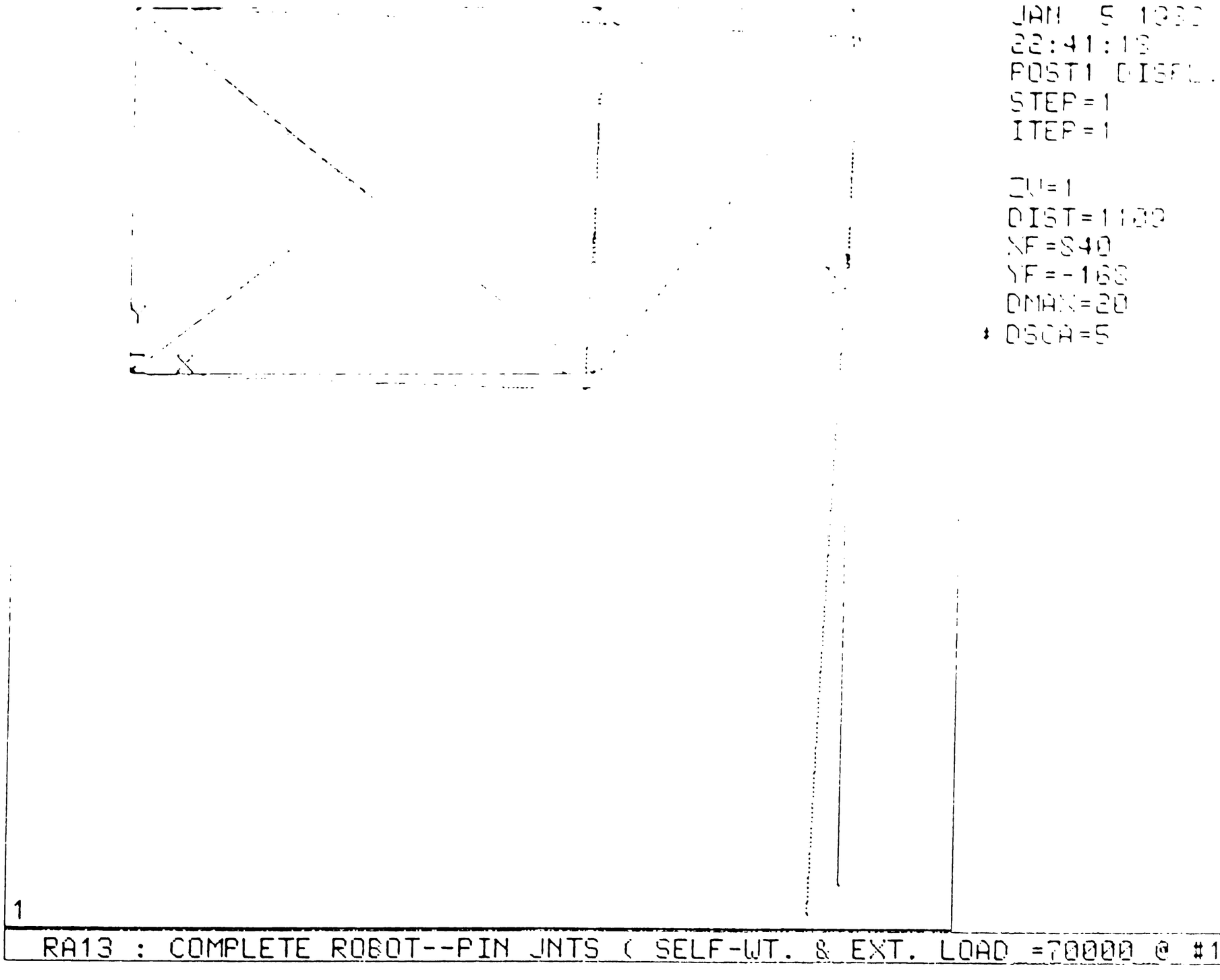

Fig. 3.18 : Distorted shape of Fully extended Arm [Both Self-weight & External load of 70,000 lb]

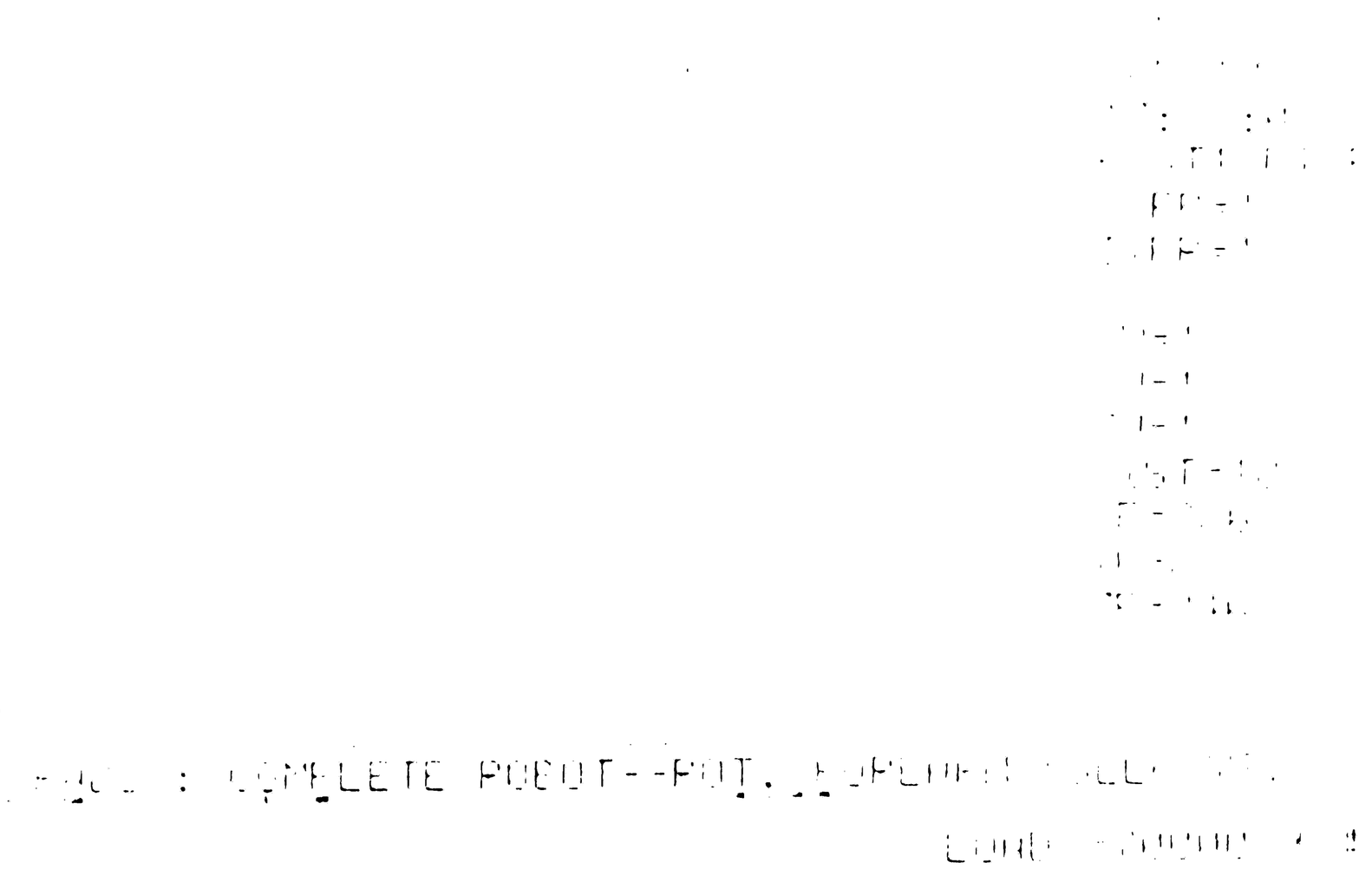

Fig 3.19 : Distortion of Rotated Arm [Self-weight & External load of 70,000 lb]
View (a)

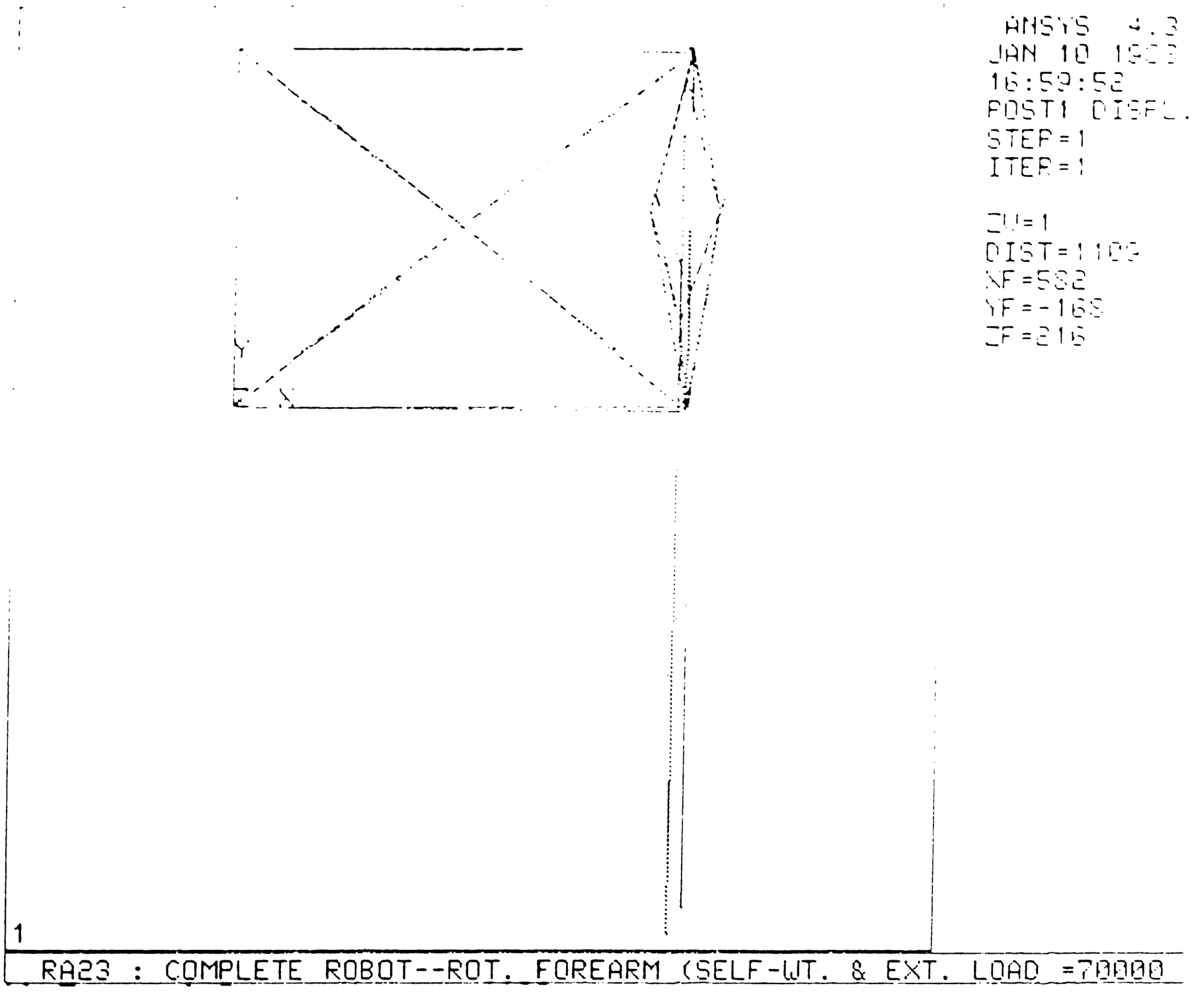

Fig 3.19 : Distortion of Rotated Arm [Self-weight & External load]

View (b)

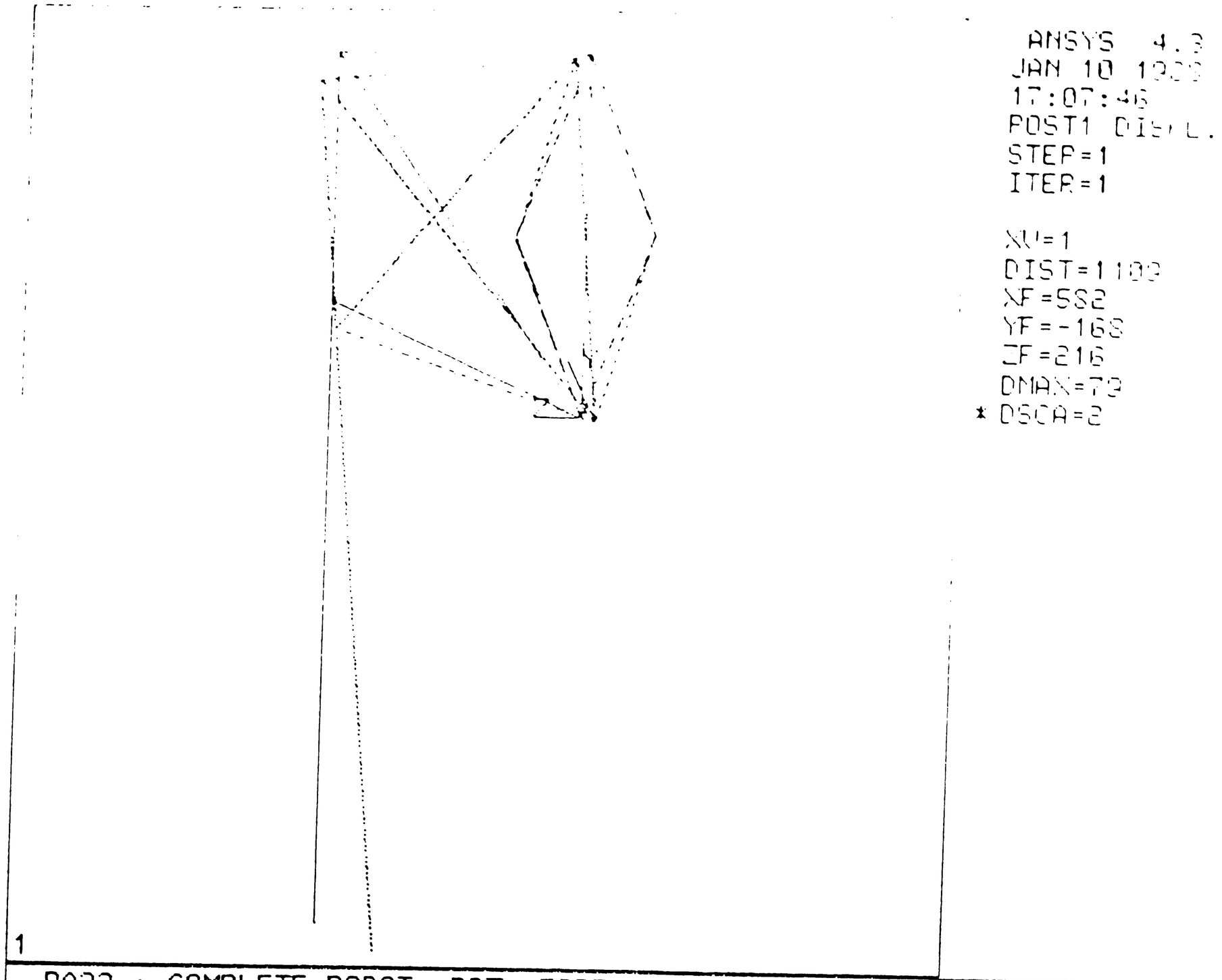

Fig 3.19 : Distortion of Rotated Arm [Self-weight & External load

View (c)

STRESSES (kpsi)

(σ 1, σ 3)

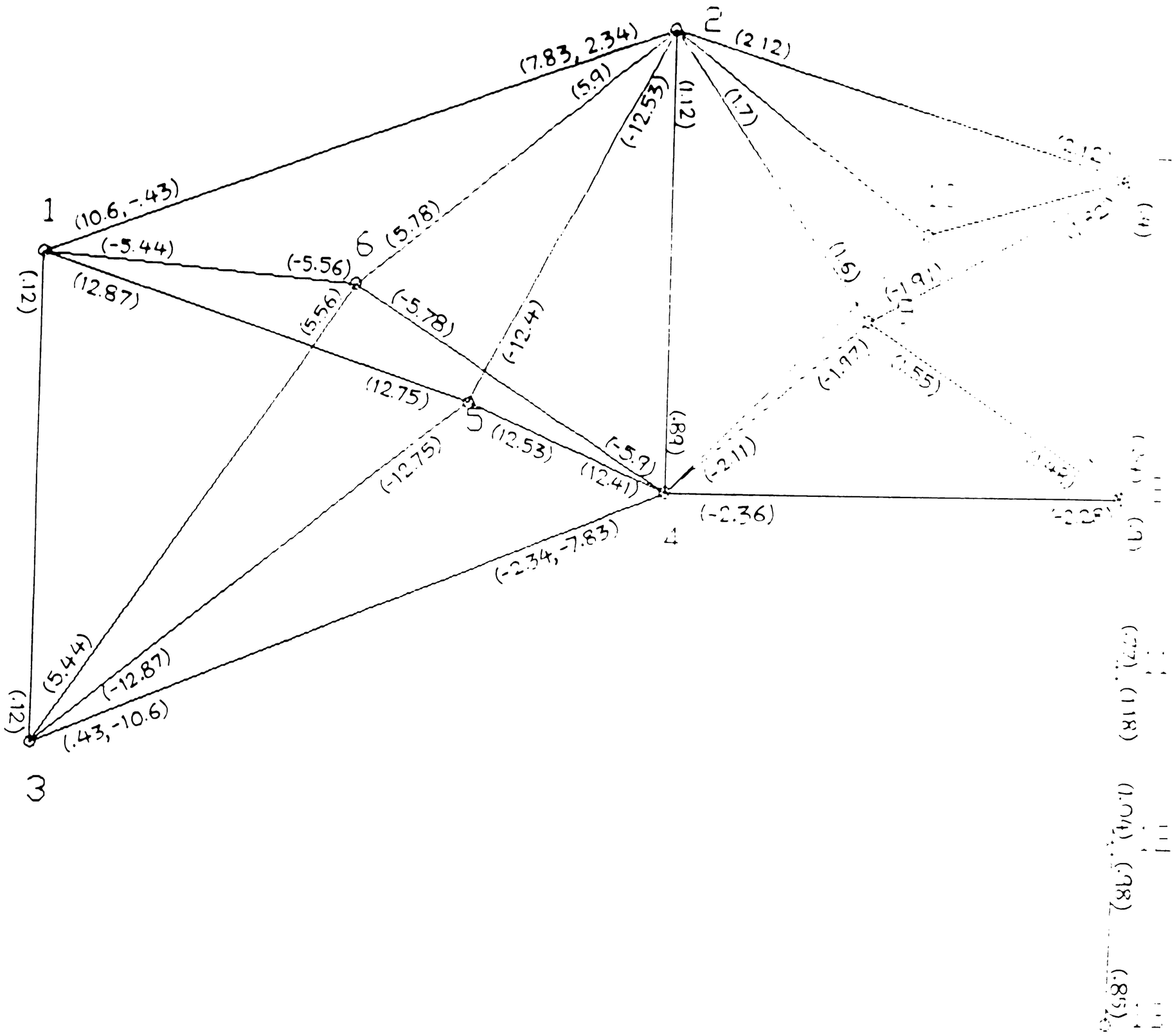

Max. Stresses (kpsi)

σ max : 12.87 (Link 1-5)
σ min : -12.87 (Link 3-5)

Fig 3.20 : Stress Distribution in Rotated Arm [Self-weight & External load of 70,000 lb]

3.3.2.2.4 Design Improvements

Three categories of design changes were investigated to see if the structural design should be improved, i.e. stresses, weight or displacements, could be reduced. The first change was the addition of a stiffening member connected between nodes 5 and 6 on the upperarm. The second was to change the horizontal distance between nodes 5 and 6. The third was to reduce the mass of the structural members in the forearm.

i) Stiffener member

A stiffener beam is connected between nodes 5 and 6 on the upper arm and the static analysis was rerun to see if there were any improvements in the performance of the arm. Fig 3.21 and 3.22 show the displacements and stresses of the modified structure in rotated position under combined loading, respectively. No change is noted with this modification, and the stresses in the stiffener beam 5-6 remain close to zero.

ii) Variation of Distance between nodes 5 and 6

When the forearm is turned at an angle with respect to the upperarm, a torque is generated in the upperarm by the out-of-plane mass of the forearm multiplied by the distance from the plane of the upperarm to the center of the mass of the forearm. External loads increase the torque significantly since the moment arm is at the end of the forearm.

The diagonal members of the upperarm react to the externally applied torque by an appropriate tension and compression forces which result in an equal and opposite torque/moment on nodes 2 and 4, effectively transmitting the torque/moment reaction forces to the support structure through nodes 1 and 3. The absolute value of the reaction forces is a function of the relative orientation of the diagonal members of the upperarm with respect to nodes 2 and 4. Changing the distance between nodes 5 and 6 changes this orientation. Four static analyses were therefore made to determine the effect of changing the distance between nodes 5 and 6 from 21 ft to 56 ft.

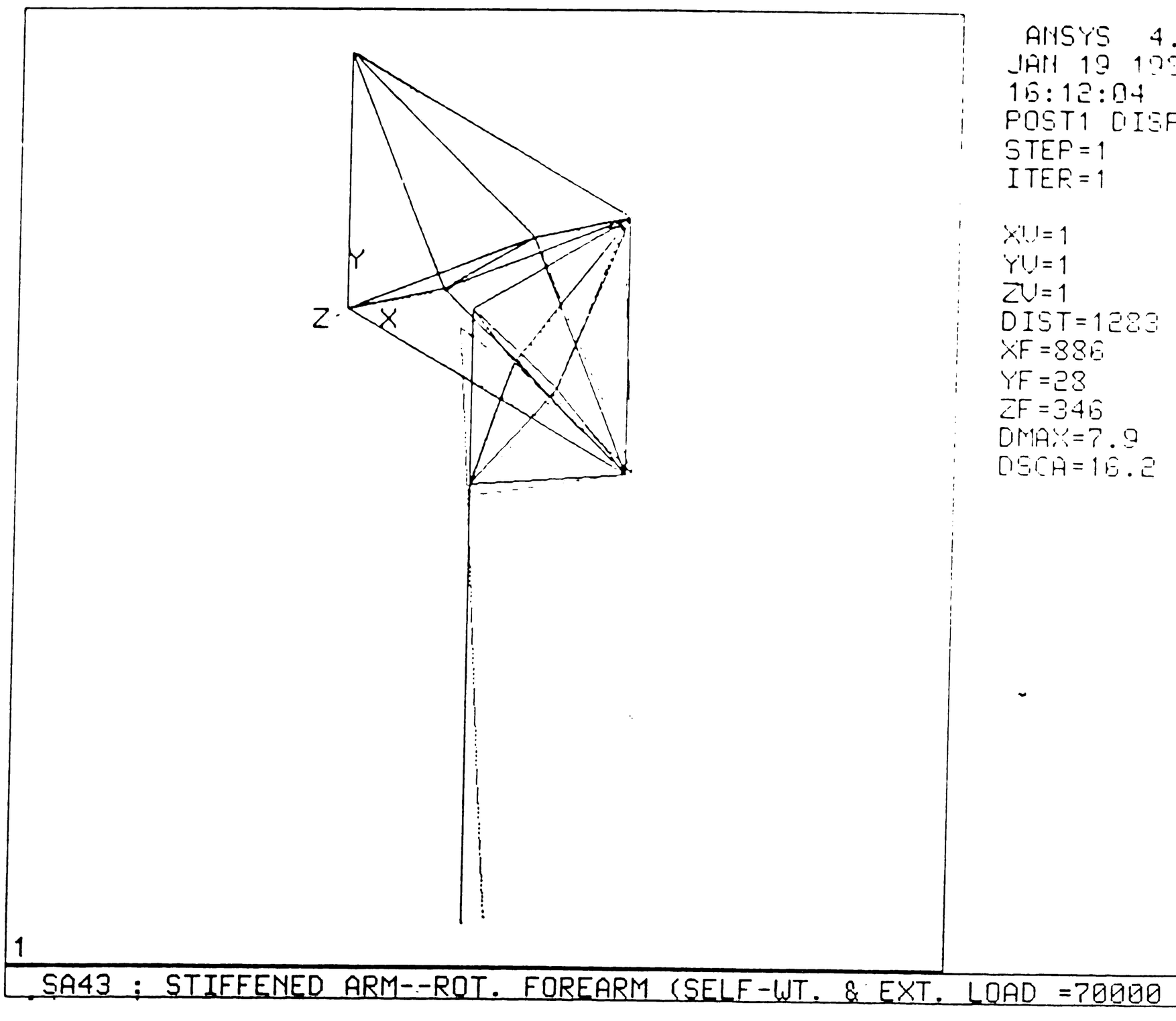

Fig 3.21 : Displacement for rotated arm with stiffener beam

[Self-weight and external load]

STRESSES (kpsi)

(σ1, σ3)

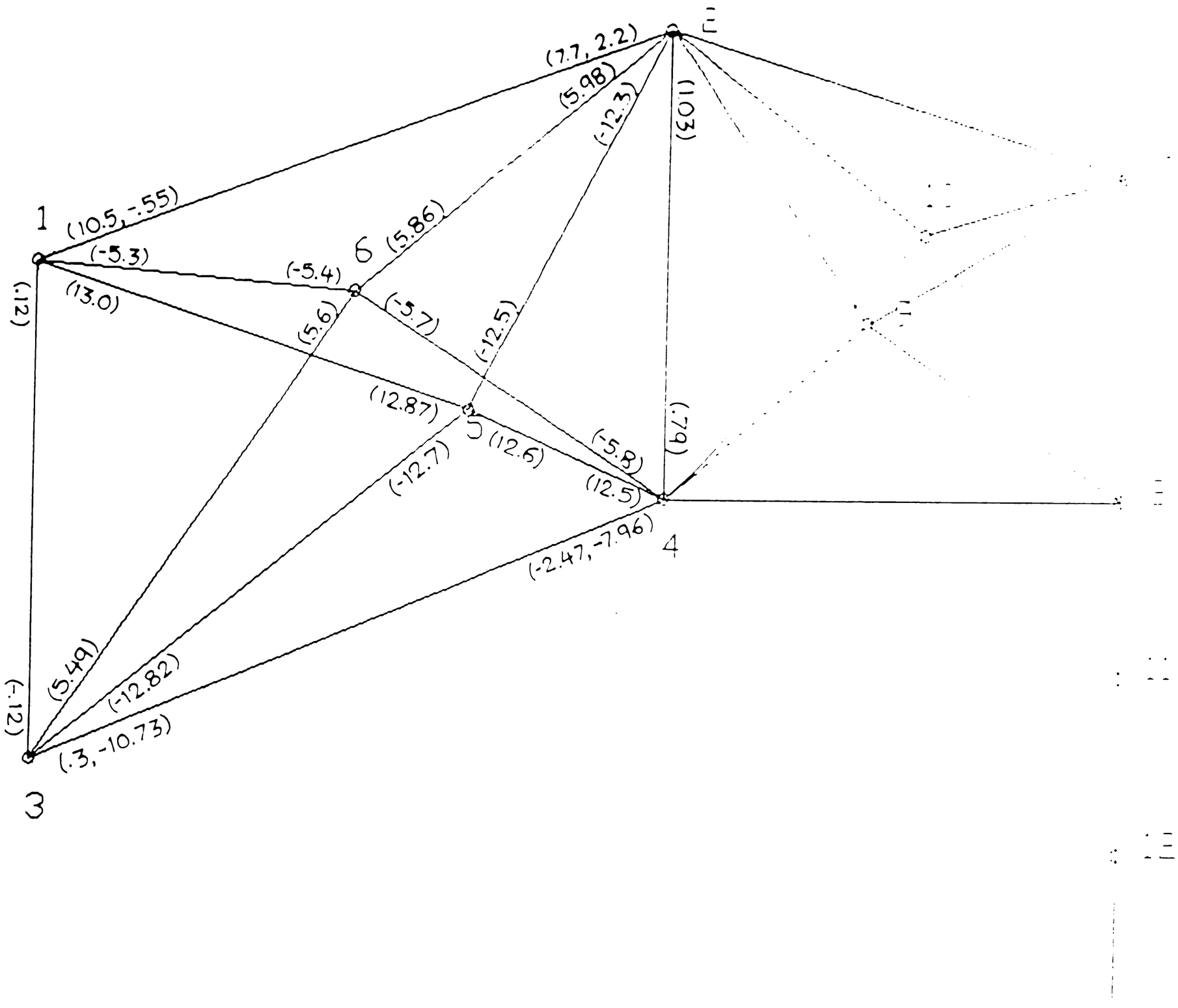

Max. Stresses (kpsi)

σmax : 13.0 (Link 1-5)
σmin : -12.82 (Link 3-5)

Fig 3.22 : Stress Distribution for rotated arm with stiffener beam [Self-weight and external load]

The displacement at the spreader bar and the maximum stresses changes as in follows:

Table 3.2 : Max. Stress and Displacement Variation with Change in Distance Between Nodes 5 and 6.

Distance between Nodes 5 & 6	Displacement at Node 13	Max Stress
252 in (21 ft)	12.9 in (1.63x)	15.5 kpsi(1.19x)
336 in (28 ft)	7.9 in (1.00x)	13.0 kpsi (1.00x)
420 in (35 ft)	5.5 in (.70x)	11.3 kpsi (.87x)
672 in (56 ft)	3.0 in (.38x)	9.1 kpsi (.70x)

The rigidity of the upper arm increases as the distance between nodes 5 and 6 is increased. The stress level and displacement increases as the node distance is decreased. The stiffness characteristic is highly nonlinear and an increase of spacing from 28 to 35 ft might be warranted to make a 30% reduction in the movement of node 13.

iii) Reduced Forearm

In the initial conceptual design, a "standard" basic-frame section was used for all members throughout the forearm and the upperarm. It was recognized that some optimization could be expected following more extensive analysis than was possible during the SBIR Phase I study.

The forearm cross-sectional dimensions were reduced as follows : Mass and areas of the top and bottom beam elements were reduced by a factor of three; and mass and area

of the diagonals were reduced by a factor of five. The major loads on the top and bottom members of the upper arm are due to the bending moment caused by the weight of the forearm structure, the hoist, the spreader bar and the external load. The loads on the diagonal are from the vertical shear and torques resulting from these loads. Since the mass of the forearm represents a significant portion of the load on the upper arm, any reduction in the forearm mass will reduce the stresses and deflections in the upper arm. Analysis was performed for the "optimized" version and the original version with the following conditions --

Relative orientation of two arms

90.0° rotation

Support Location

Nodes : 1,3

Joints : Pin joints, Rotational constraint at 1 (about Y)

Applied Load

Self-weight : YES

External force : 70,000 lb load at node #13

Non-support pin joints

All Universal Joints.

A rotational constraint about Y axis was applied at node #1 for purposes of easy comparison of displacements between the original and "optimized" version. The table on the following page compares results before and after "optimization". As was expected, the results produce higher (but not excessive) stresses in the forearm, with the diagonals being more heavily loaded than horizontal members. The reduced mass of the forearm produce stress reductions of about 10 percent in the upper arm diagonal beams and 16 percent in the top and bottom members. Stress distribution for the "optimized" version is as in Fig 3.23.

Table 3.3 : Complete Arm Analysis -- Comparison of Results before and after "optimization".

	"Optimized" Values	Original Values
Node #13 Displacement	8.46 inches	9.09 inches
Beam 4-8 stresses	-6.66 kpsi	-2.36 kpsi
Beam 2-7 stresses	6.06 kpsi	2.12 kpsi
Beam 2-9 stresses	7.31 kpsi	1.70 kpsi
Beam 4-9 stresses	-9.03 kpsi	-2.11 kpsi
Beam 3-5 stresses	-11.68 kpsi	-12.98 kpsi
Beam 3-4 stresses	-5.99 kpsi	-7.18 kpsi
Beam 1-5 stresses	11.68 kpsi	12.98 kpsi
Self weight	164103 lb	198933 lb

3.2.2.5 Detailed Basic-Frame Structure Analysis

The detailed basic-frame structure analysis is needed for the following reasons :

1. To verify whether the effective area of the basic-frame structure can be fairly approximated by using the sum of areas of its four longitudinal structural angles;
2. To determine stress distribution and identify any potential problem areas.

Fig 3.24 shows a detailed basic-frame structure geometry. The detailed structure is mainly composed of two types of elements : the long corner elements (5" x 5" x 3/8" angles) which are the main axial load bearing elements, and the diagonal elements (3" x 3" x 5/16" angles) which hold the main elements together and provide structural integrity. The basic-frame is an assembly of octahedrons placed one beside other (as explained in Fig. 3.3).

STRESSES (kpsi)

(σ1, σ3)

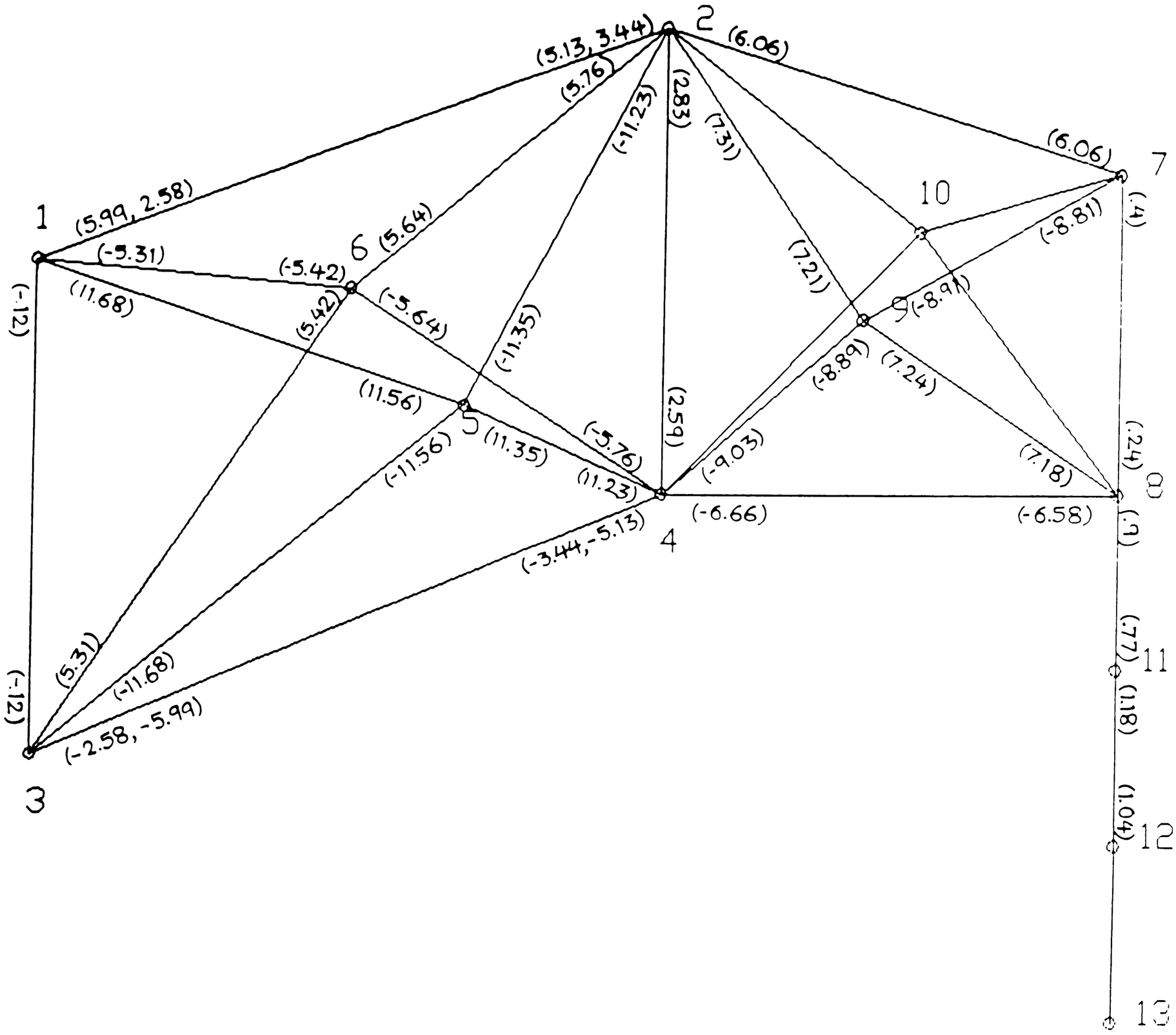

Max. Stresses (kpsi)

σmax : 11.68 (Link 1-5)
σmin : -11.68 (Link 3-5)

Fig 3.23 : Stress distribution for Arm with reduced/"optimized" forearm.

[Both self-weight and external load]

REF.#	X	Y	Z
1	0	0	0
2	96	12	0
3	96	-42	0
4	138	0	42
5	138	0	-42
6	180	42	0
7	180	-42	0
8	222	0	42
9	222	0	-42
10	264	42	0
11	264	-42	0
12	306	0	42
13	306	0	-42
14	348	42	0
15	348	-42	0
16	390	0	42
17	390	0	-42
18	432	42	0
19	432	-42	0
20	474	0	42
21	474	0	-42
22	516	42	0
23	516	-42	0
24	558	0	42
25	558	0	-42
26	600	42	0
27	600	-42	0
28	642	0	42
29	642	0	-42
30	684	42	0
31	684	-42	0
32	726	0	42
33	726	0	-42
34	768	42	0
35	768	-42	0
36	810	0	42
37	810	0	-42
38	852	42	0
39	852	-42	0
40	894	0	42
41	894	0	-42
42	936	42	0
43	936	-42	0
44	978	0	42
45	978	0	-42
46	1020	42	0
47	1020	-42	0
48	1062	0	42
49	1062	0	-42
50	1104	42	0
51	1104	-42	0
52	1200	0	0

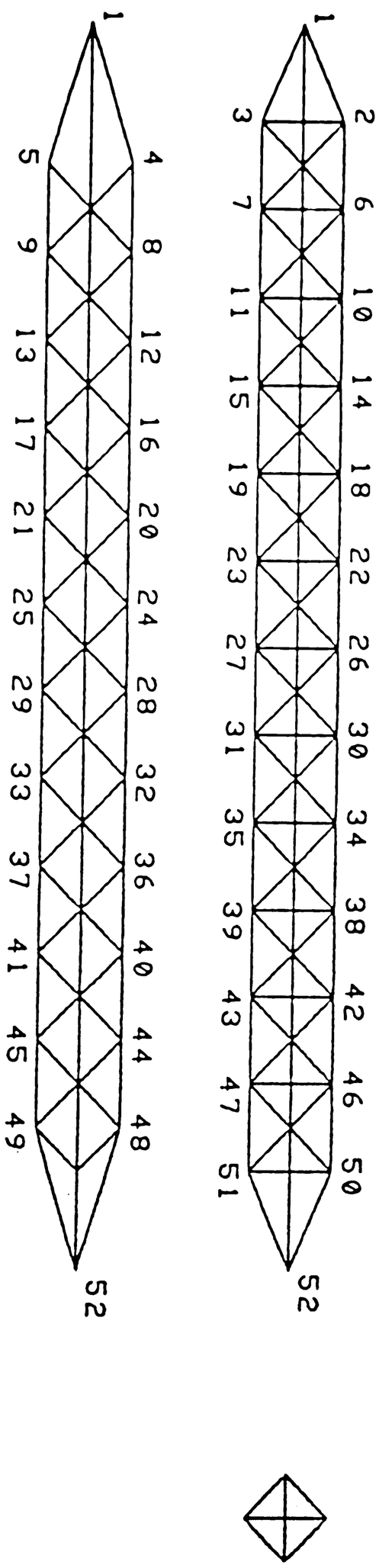

All Dimensions in inches

Fig 3.24 : Detailed Basic-Frame Geometry.

3.3.2.2.5.1 Force/Stress/Displacement Analysis

The detailed basic-frame structure is first tested using a hypothetical problem wherein a 100 ft basic-frame is kept in a horizontal plane and then subjected to a tensile load. Applying a tensile load of 100 kip, fixing one end and making other a roller support, where the load is applied along the axis of the member. With action of gravity, the following results are obtained --

i) The basic-frame sags .62" in under its own weight.

ii) Average strain is .298"/(100'*12 in/ft) = .00025 in/in.

iii) Maximum tensile stress is 11.9 kpsi between nodes 23-31 (mid bottom main member).

iv) Maximum compressive stress is 3.3 kpsi between nodes 2-3 (first transverse member).

To better understand the behavior of a detailed basic-frame structure under pure axial loading, a rerun is made of the analysis without self-weight to eliminate the bending effect. Under these conditions, the following results are obtained :

i) Average axial strain was .299"/(100'*12 in/ft) = .00025 in/in.

ii) Tensile stress in the long main members (4 corner elements) is 6.93 kpsi.

A comparison of the maximum tensile stress in the basic-frame structure shows that approximately 40 % of the maximum stress is caused by the self-weight of the structure. The maximum stress can be reduced by either increasing the effective cross-section of the longitudinal members or by increasing the depth of the basic-frame. The recommended solution was to fabricate the basic-frame with a taper, such that the longer basic-frames would have greater depth in the mid-section. The calculated average strain in the steel column with the 100 kip load permitted the effective area to be calculated as follows :

$$\text{Stress} = \text{Force / Area} = E * \text{Strain}$$

Hence,

$$\text{Area} = \text{Force} / (E * \text{Strain})$$

$$= 100{,}000 \text{ lb} / (30E6 \text{ psi} * .00025)$$

$$= 13.3333 \text{ in}^2$$

The calculated effective area of 13.3333 in^2 is within 8% of the area (of 14.44 in^2) of the four longitudinal structural members.

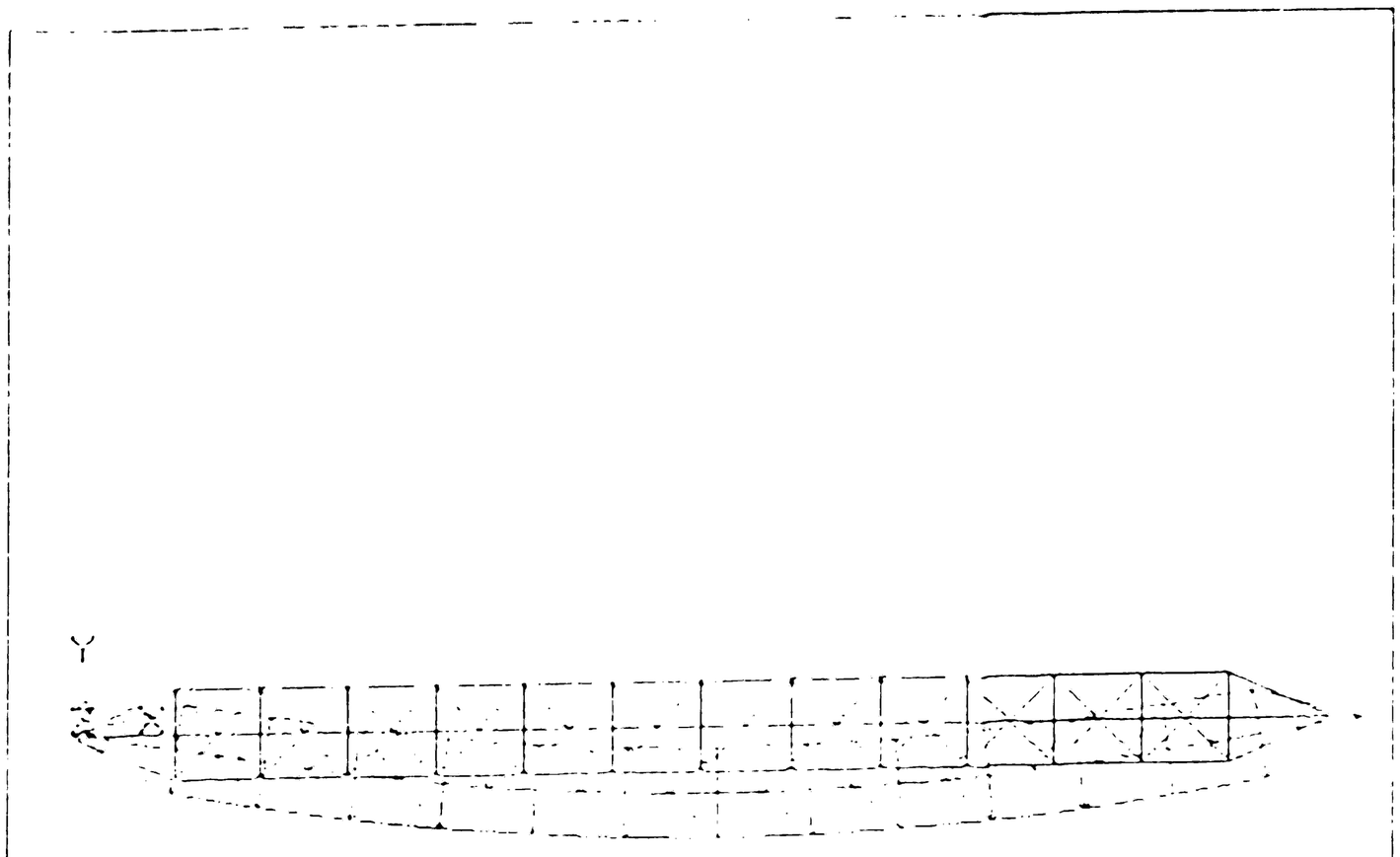

Fig 3.25 : Distortion of the Detailed Basic-Frame Structure [Self-weight & Ext. load].

The next step in the analysis was to make a direct comparison of the behavior of an equivalent beam element in the manipulator arm model subjected to normal working conditions (self-weight & external load) and a corresponding detailed basic-frame structure subjected to the same loads. Extra nodes were introduced in link 1-2 of the maipulator arm model so as to permit the examination of stresses at internal locations on the equivalent beam element. Static analysis was done with following conditions --

Relative orientation of two arms

0° rotation

Support Location

Nodes : 1,3

Joints : Pin joints, Rotational constraint at 1 (about Y)

Applied Load

Self-weight : YES

External force : 70,000 lb load at node #13

Non-support pin joints

All Universal Joints.

Fig 3.26 indicates the stress distribution for the manipulator arm with above loading conditions with extra nodes. The area of the equivalent beam member is equal to the area of the four main structural angles in the basic-frame structure. The density used in the equivalent beam member is appropriately increased to allow for the self-weight of the remaining basic-frame elements. The main subject of interest in this analysis is link 1-2 and its intermediate nodes, which is to be compared with the stress patterns in the detailed basic-frame structure.

STRESSES (kpsi)

(σ 1 , σ 3)

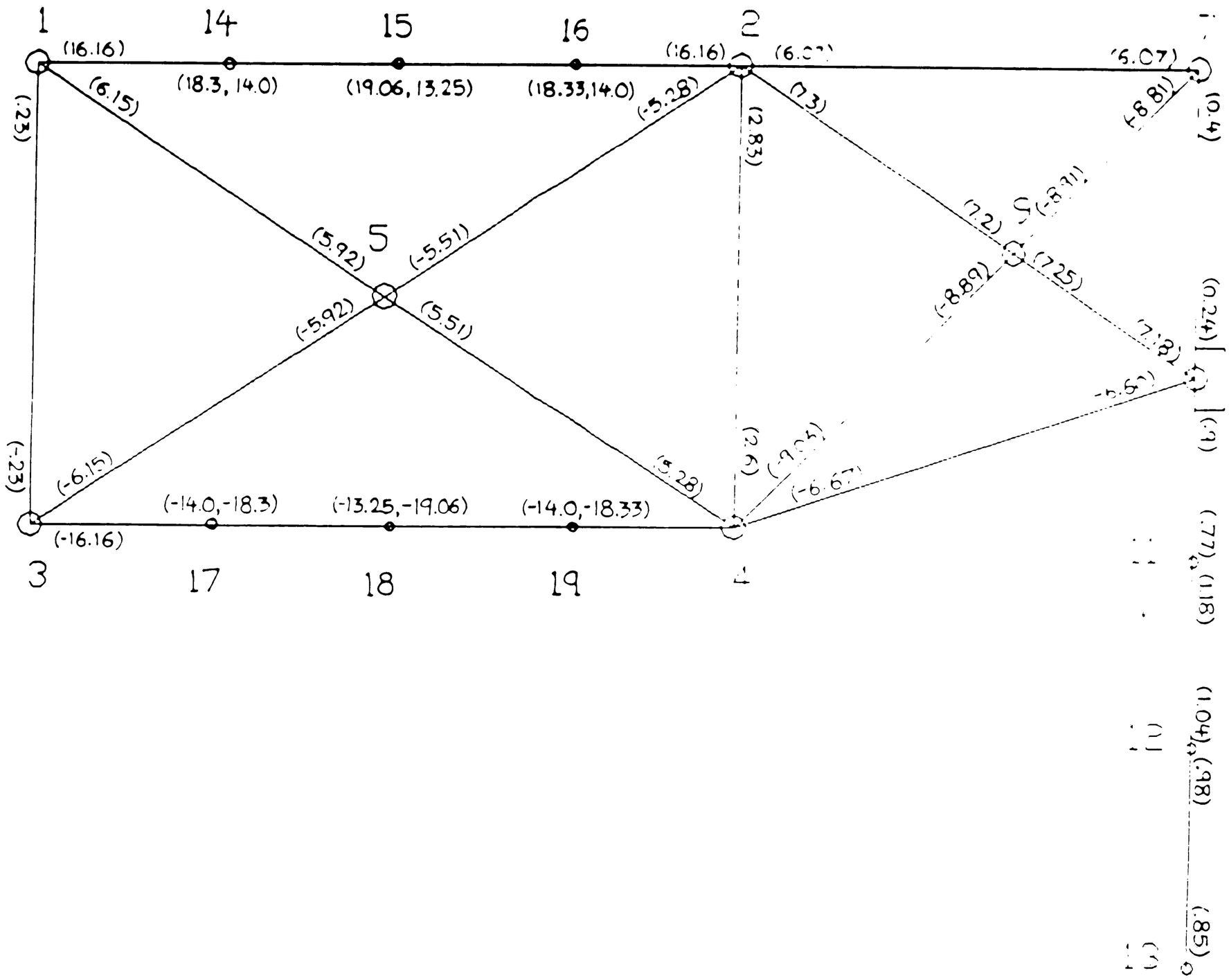

Max. Stresses (kpsi)

σ max : 19.06 (Link 1-2)
σ min : -19.06 (Link 3-4)

Fig 3.26 : Stress distribution for the arm with extra nodes

[Self-weight & external load]

The end conditions at nodes 1 and 2 were applied to a 90 ft detailed basic-frame structure and the internal stresses and displacements were analyzed. This gave a maximum tensile stress of 20.3 kpsi and maximum compressive stress of -8.0 kpsi.

A comparison of the stress levels at the mid-point of the link 1-2 in the previous two analyses shows that the stresses (19.95 and 12.22 kpsi) obtained in the detailed basic-frame structure analysis compare well with the stresses (19.06 and 13.25 kpsi) obtained in the equivalent beam element in the full-scale arm. This verifies that the area of the four longitudinal members in the basic-frame structure is, in fact, the effective area to be used for the equivalent beam element.

3.3.2.2.5.2 Buckling Analysis

Stability or buckling analysis is used to determine if a structure is stable under any specified load or at what level the structure might become unstable. Two types of buckling analyses can be performed in the ANSYS program : Linear Buckling, and Nonlinear Buckling.

Linear buckling analysis is used to calculate critical loads and buckling mode shapes. It is also known as the Eigenvalue Buckling analysis, since the results of the analysis are given in terms of eigenvalues and eigenvectors. The eigenvalues represent scaling factors on the applied load. If the applied load is unity, the eigenvalues are the buckling loads. The eigenvectors are the buckled shapes. Only the first eigenvalue and eigenvector are of interest. Linear buckling analysis is considered to be somewhat academic in nature since it cannot account for any nonlinearity or initial imperfections in the structure. Linear buckling theory can thus only predict the upper bound on the buckling load, whereas usually the lower bound is desired. Its main advantage is that it is a relatively inexpensive (computationally fast) method for determining a rough order of magnitude estimate of the stability of a structure.

Nonlinear buckling analysis uses the large deflection theory. It is useful for predicting snap-through phenomena, a condition in which a structure snaps through one stable configuration to a second stable configuration. Snap-throughs cannot be predicted using the linear theory and only large deflection analysis can properly determine the limit load. Also, if initial imperfections (as existing in real structures) are considered, the buckling loads are much smaller than the loads determined by linear analysis. Only large deflection analysis can account for such imperfections or nonlinearities. The actual limit load is usually dependent on the amount of initial imperfections.

Nonlinear buckling analysis was used more extensively for evaluating the manipulator arm structure. Non-linear analysis involves iterative solutions to determine stability of the structure. A static solution is first found with the given loading conditions and constraints. Using the thus computed reactions and displacements, the nodal coordinates are updated and stress-stiffening effects are applied. This is now taken as a new set of initial conditions, the loads are reapplied and a second static solution is found. This process is continued until the structure reaches equilibrium conditions. The solution is then said to have converged. If the structure does not reach an equilibrium, no convergence is reached, and the structure is considered to have buckled. Nonlinear analysis can thus determine if a structure would buckle under a certain load, but it cannot explicitly calculate the critical load. However a close estimate of the critical load can be had by doing a "binary search", using as the upper limit the value calculated by Eigenvalue Analysis.

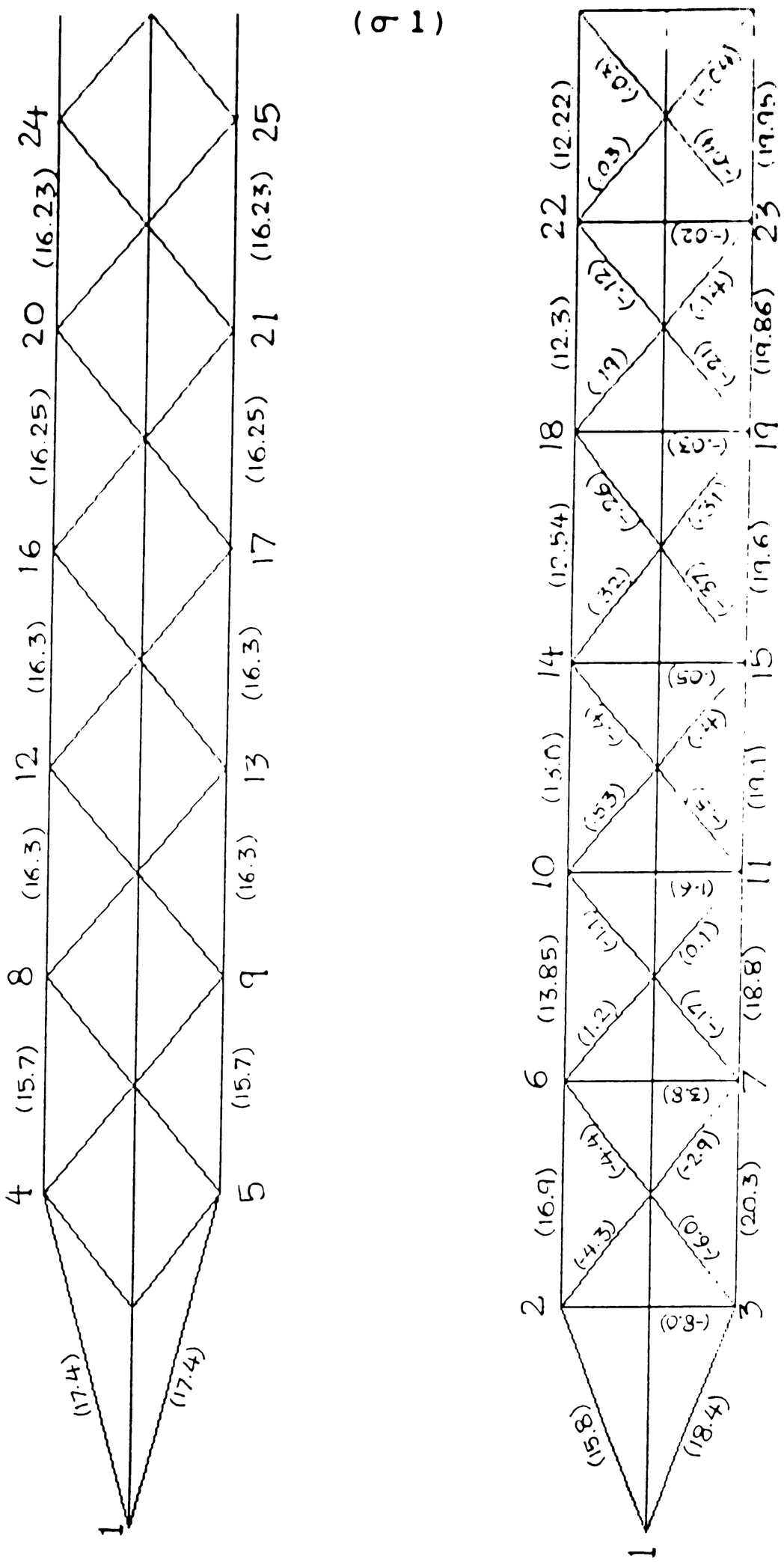

Fig 3.27 : Stress distribution for detailed basic-frame structure [Same end conditions & loads as link 1-2 in Fig 3.26]

The behavior of detailed basic-frame structure 3-5 was studied under the action of forces obtained from a static analysis of the manipulator arm with the forearm rotated 90°, with self-weight and 70 kip external load at spreader bar. The analysis indicated that link 3-5 had the maximum compressive stresses and since it is the longest basic-frame structure, it was selected for buckling analysis. The compressive load from the manipulator arm analysis, calculated at 324,200 lbs, is applied to the detailed basic-frame buckling analysis. The solution converged in 3 iterations, indicating that the system is stable. The maximum displacements in the X, Y and Z directions are (-.5973,-.0802,.0591) inches respectively. The maximum tensile and compressive stresses are 12.49 and -25.99 kpsi respectively. Further buckling analysis with four times the actual load also indicates stability of the structure, with maximum tensile and compressive stresses of 48.79 and -100.97 kpsi respectively. Since these stresses are well above the yield stress of steel, the structure will fail by yielding rather than by buckling.

The above calculations assume perfect symmetry of the detailed structure. However this may not be the case when the structure is manufactured because of the manufacturing tolerances. Hence the buckling analysis was rerun with an eccentricity of 1" at the one end (in a direction perpendicular to the axis of the basic-frame) and the solution diverged (i.e. the structure buckled) with 400% of actual load. This indicates that the structure could buckle at four times rated load if the basic-frame loading conditions were not properly centered. Further calculations indicated that the structure buckled with an eccentricity of 0.5 in. but is stable with an eccentricity of 0.25 in., with 400% the actual load.

3.2.3 Dynamic Analysis

Dynamic analysis is used to determine the performance of the manipulator arm under conditions simulating the working environment. In dynamic analysis, as defined earlier, the structures are subjected to loads that vary with time. Dynamics also includes the study of free vibrations, i.e. the oscillations of a structure after the force causing the motion has been removed or has ceased to vary.

3.2.3.1 Modal Analysis

Modal Analysis is used to determine the natural frequencies and mode shapes of a structure. Free undamped vibrations and linear elastic structural properties are assumed. ANSYS provides two options for modal analysis : spectrum and non-spectrum. Both options produce natural frequencies, mode shapes (both reduced and expanded), and participation factors. The nonspectrum option includes unit displacement spectra (displacement amplitude v/s frequency variation) in order to calculate participation factors. Since the calculated mode shapes are relative, no stress output are calculated.

Modal Analysis was performed using the non-spectrum option, in which ANSYS internally assumes a unit-displacement spectra. The program simulates a unit displacement condition of the entire manipulator arm in all directions at all frequencies, after which the structure is allowed to vibrate. The results indicate the mode frequencies and shapes and the participation factors obtained with the above starting conditions. The participation factor is a measure of relative amplitude of a particular mode shape with respect to the mode shape with the maximum amplitude.

The spectrum option of Modal Analysis can compute either of two types of analysis: Base excitation analysis, and Force excitation analysis. In the base excitation method, a displacement spectrum can be defined at the base or the support nodes, and

the response of the structure to this specific input can be obtained. This could be very useful for the current problem, for example, since the base of the manipulator arm may experience base excitations caused by action of sea waves or other environmental factors. The second method, force excitation, involves excitation at non-support points, by application of a force spectra. This could be, for example, the reaction forces on the vertical hoist from handling a container with the spreaderbar. Both types of analysis are suggested for future study of specific manipulator arm applications.

A limited amount of modal analysis was performed on the full-scale conceptual design. The mode frequencies (eigenvalues) obtainable from any analysis is equal to the number of Degrees of Freedoms (DOFs) of the problem. However, all of the modal frequencies are not required to provide a fairly accurate indication of the dynamic behavior of the structure. Rotational DOFs are specified to be eliminated from the eigenvalue extraction since the corresponding rotational or torquing vibrations of individual members are not of interest. Also, since the lowest frequencies play the most important role in the dynamic response of a structure, only a few lowermost frequencies are needed to be extracted. The following results were obtained from the modal analysis:

Mode #	Freq. (Hz)	Brief description of Mode shape
1	0.165	Rotation about the shoulder axis
2	0.461	Vertical hoist bending in XY plane
3	0.503	Vertical hoist bending in YZ plane
4	1.36	Rotation about the shoulder axis
5	2.00	Vertical hoist bending in YZ plane
6	2.19	Vertical hoist bending in XY plane

Mode shapes obtained are as shown in Fig. 3.28 (a-f).

(a) Mode Shape #1

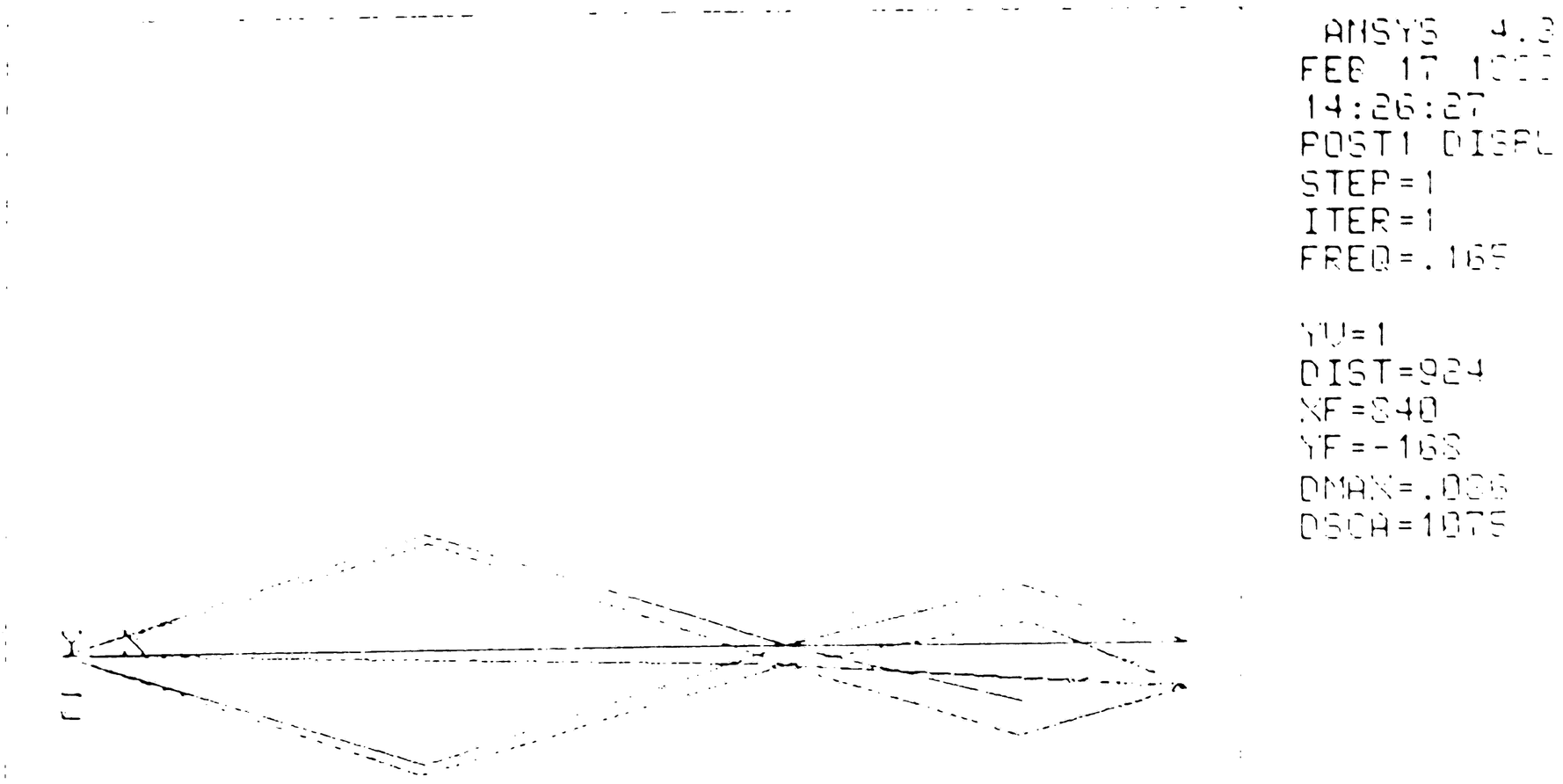

Fig. 3.28 : Mode shapes for the Full-scale manipulator arm.

(b) Mode Shape #2

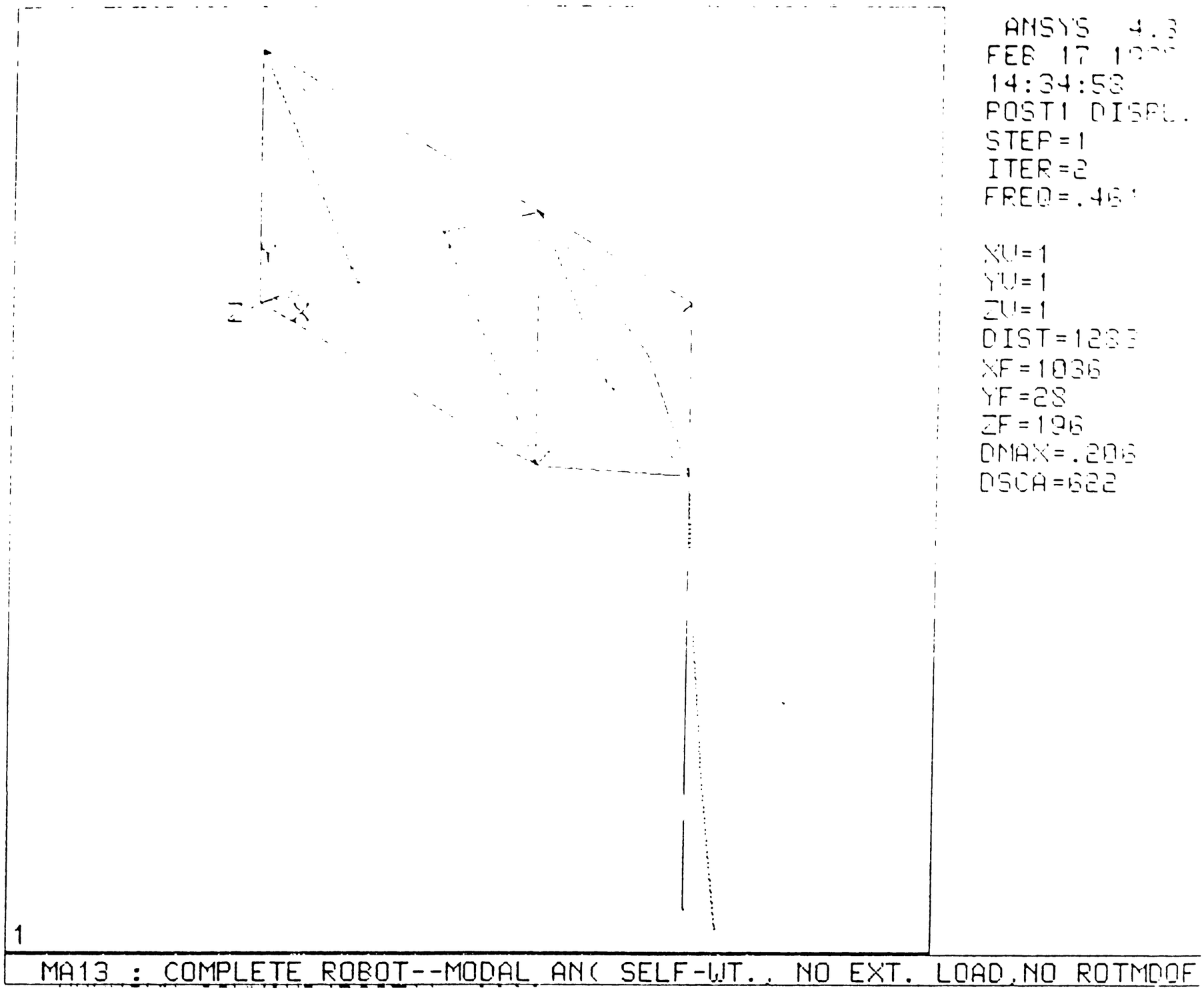

Fig. 3.28 : Mode shapes for the Full-scale manipulator arm.

(c) Mode Shape #3

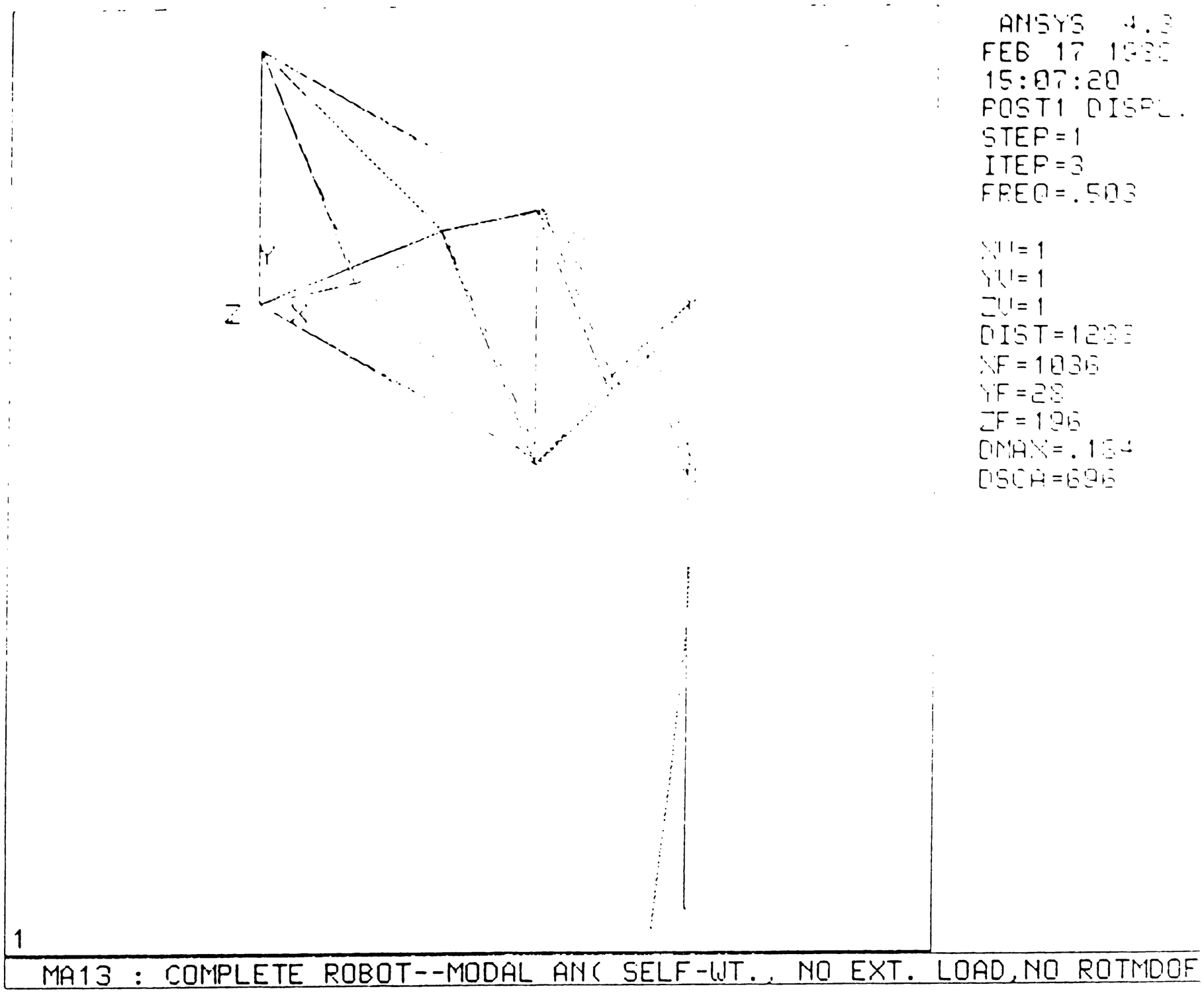

Fig. 3.28 :. Mode shapes for the Full-scale manipulator arm.

(d) Mode Shape #4

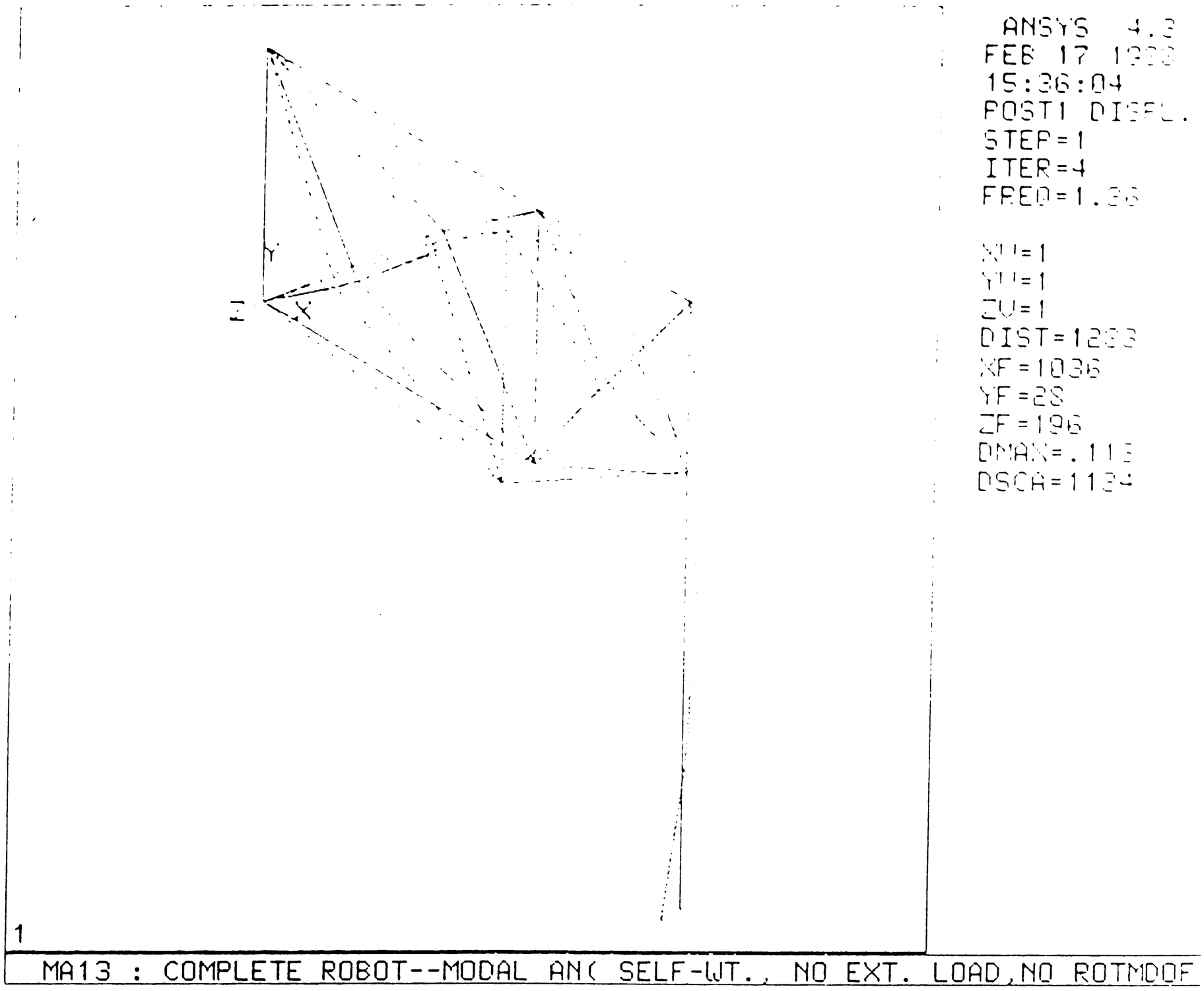

Fig. 3.28 : Mode shapes for the Full-scale manipulator arm.

(e) Mode Shape #5

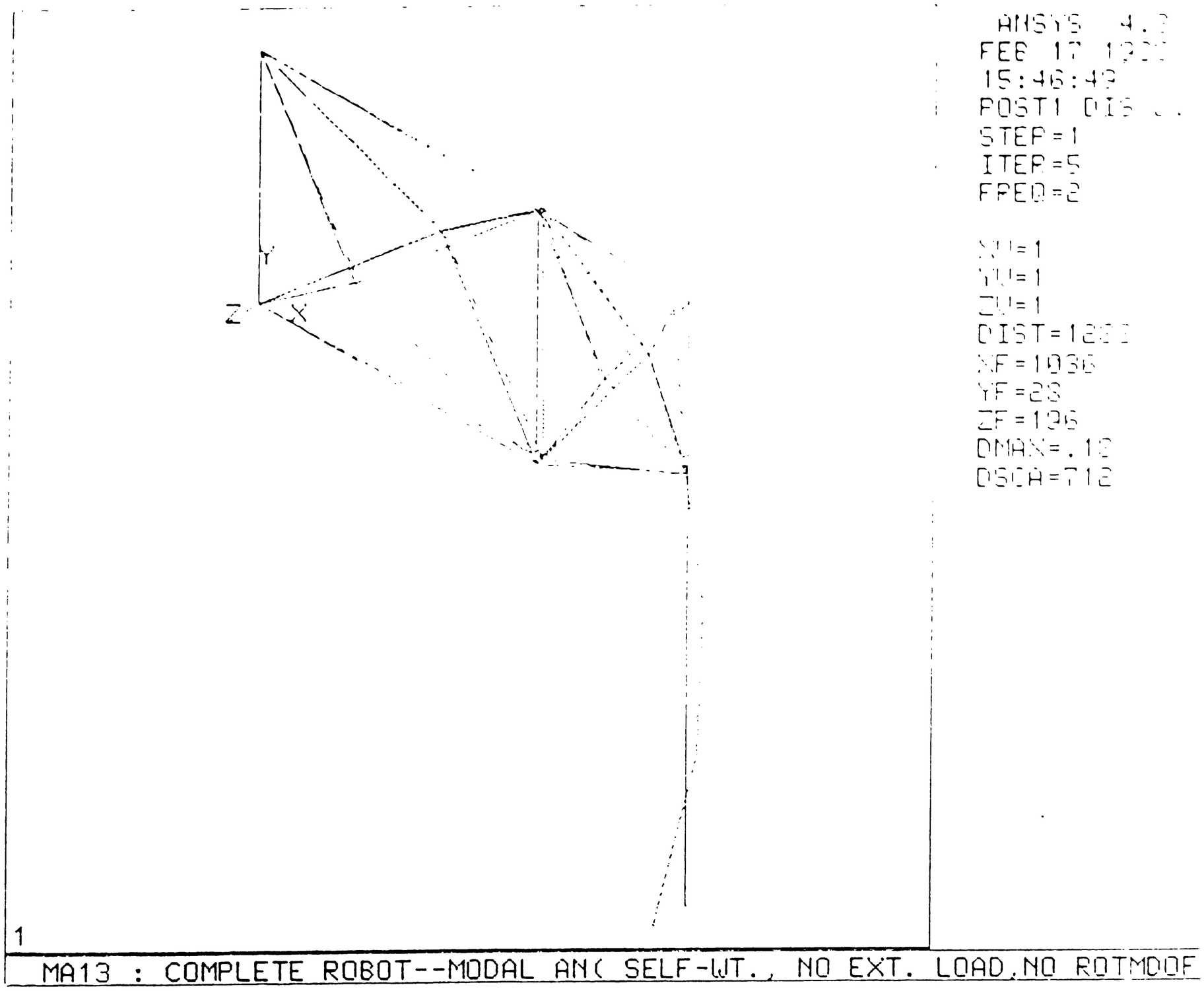

Fig. 3.28 : Mode shapes for the Full-scale manipulator arm.

(f) Mode Shape #6

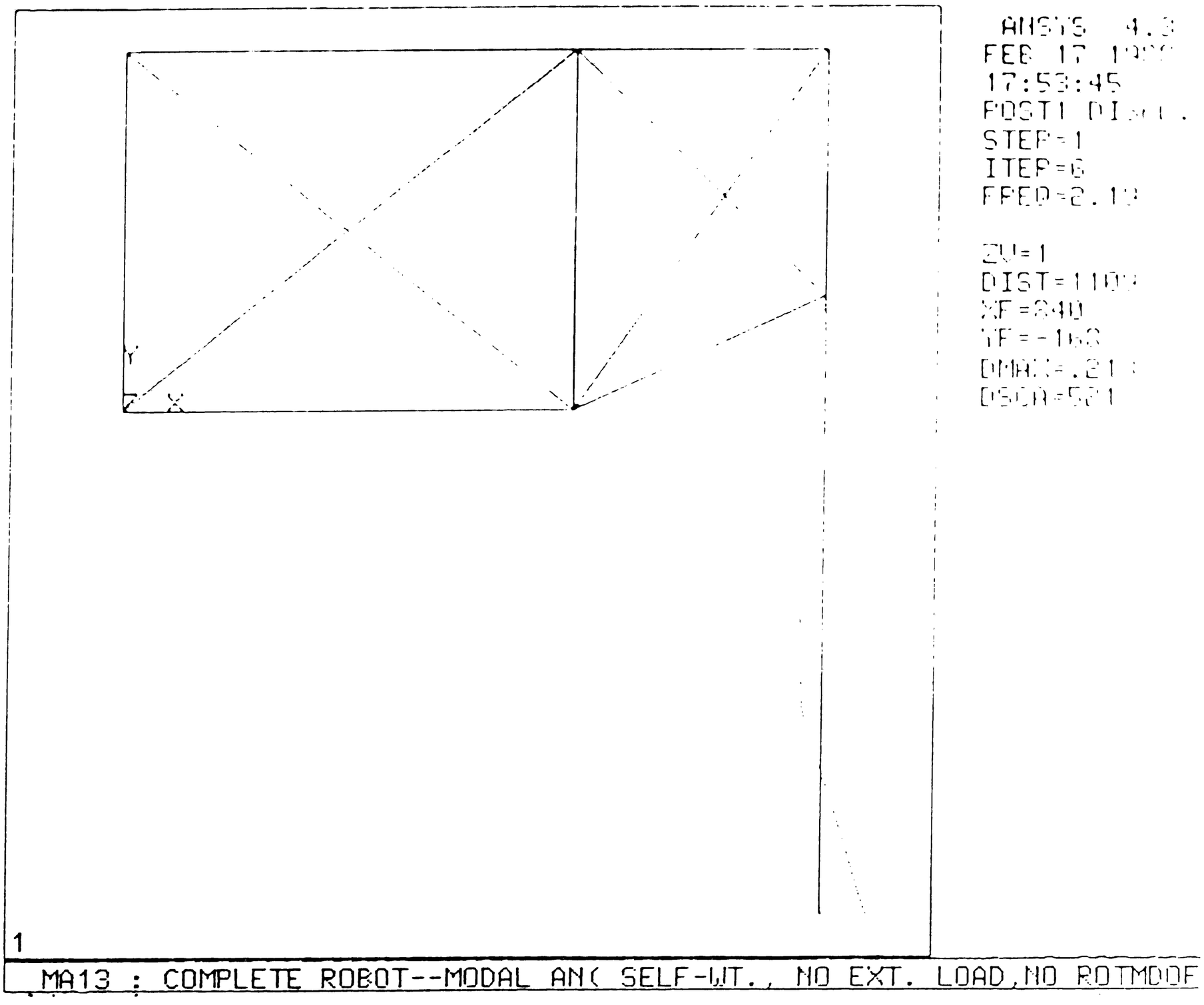

Fig. 3.28 : Mode shapes for the Full-scale manipulator arm.

Modal analysis was initially performed with a reduced number of DOFs (equal to 200). Further modal analysis runs were made to see the effect of further reduced number of DOFs on the results. No significant changes resulted when the number of DOFs was dropped to 35. Small changes were observed with DOFs at 25.

Additional modal analyses were run for the "optimized" structure in various orientations, both with or without external load of 70,000 lb represented by an equivalent mass element. The frequencies (Hz) obtained are as tabulated below :

Table 3.4 : Modal Analysis of Fullscale Arm -- Frequencies in Hz.

Mode #	Extended Position		Rotated Position	
	W/O 70 klb	With 70 klb	W/O 70 klb	With 70 klb
1	0.164	0.161	0.203	0.199
2	0.517	0.457	0.353	0.330
3	0.530	0.468	0.585	0.520
4	1.320	1.305	0.726	0.681
5	1.872	1.811	1.262	1.615

Wave periods for ocean seastate 3 conditions range from 2.0 to 8.8 seconds, equivalent to wave frequencies of .1135 to .5 Hz. Since the first two or three modal frequencies are within the range of ocean disturbances for SS3 conditions, steps will have to be taken to damp out the ocean caused movement of the manipulator mounting or otherwise limit the structural response to these frequencies.

3.2.3.2 Harmonic Force Response Analysis

The Harmonic Response Analysis was used to determine the steady-state response of a structure to harmonic (sinusoidally varying) external force of a specified amplitude and frequency. Multiple forcing functions of different frequencies, amplitudes and phase-

shifts can also be specified. Damping may be specified for the structure, and harmonic loads can be specified either in terms of applied force or displacements. The analysis, however, does not permit nonlinearities and element load vectors such as pressures, gravity, etc.

As noted in the previous section, excitation caused by seastate 3 conditions falls in the range of .1135 to .5 Hz. Since two or three of the lower-most modal frequencies fall in this range, the structure was excitated in the range of .1 to .3 hz to analyze its response. A damping ratio of 2.0 % was considered appropriate and was used for the purpose of analysis[51]. The following two methods for excitation were used:

1. Excitation was first developed by means of harmonic displacements applied at node 13 in each of the three directions X, Y, Z. This condition could occur if the spreaderbar is attached to a container or a hatch cover which is fixed to the ship and thus not movable. Fig 3.29 shows a stress plot of the manipulator arm with harmonic displacement of +/- 1 inch in the vertical direction at 0.1 hz, without the 70 kip load on. Maximum tensile stress was about 8700 psi (in top member of the upper arm), and the maximum compressive stress was about 4170 psi (in bottom member of the upper arm). Further analyses with excitation frequencies of .2, .3, .4 and .5 hz and with 90° rotated position showed stress values that compared with the expected stresses from static analysis, since the frequencies did not exactly match the mode frequencies for resonance. However, excitation in proper direction at a precise modal frequency can lead to much higher stresses.

2. Excitation was then developed by means of harmonic displacements applied at the support nodes (# 1 & 3) in each of the three directions X, Y, Z. This condition could occur when the support structure for the robot arm moves with the sea waves. Fig 3.30 shows the stress plot for the arm with a harmonic displacement of +/- 1 in. in the

vertical direction at 0.1 hz (at nodes #1 & 3), without the 70 kip load on. Maximum tensile stress was about 12,500 psi (in top member of the upper arm), and the maximum compressive stress was about 7,400 psi (in bottom member of the upper arm). These values are nearly 50 percent higher than those obtained by exciting at the spreader bar. With the forearm rotated at 90°, the maximum tensile and compressive stresses in the diagonals of the upper arm was about 15,000 and 11,000 psi respectively. These values are almost three times higher than the stresses observed when the spreader bar is moved vertically. The increased stresses which result from excitation applied at the support nodes is caused by the large moments (and torques in the rotated position) due to the inertia of the manipulator arm.

The results of other harmonic analyses are tabulated in Table 3.5. The frequencies of excitation are selected to be close to mode frequencies so as to observe the behavior of the structure at near resonating conditions.

Table 3.5 : Harmonic Response Analysis of Fullscale Arm.
Stress Comparison with 70 klb mass attached to spreader bar

(Min. stress, Max. stress) kpsi

Excitation Location	Fully Extended		Rotated
	Freq = 0.168 hz	Freq = 0.5 hz	Freq = 0.5 hz
X :	-	-	(-1.7, 4.0)
Spreader Y :	(-1.3, 3.5)	(-1.2, 3.2)	(-4.6, 5.6)
Bar Z :	-	-	(-1.7, 4.0)
X :	-	(-19.4, 20.0)	(-27.3, 90.9)
Support Y :	-	-	(-28.1, 93.3)
Nodes Z :	(-20.2, 24.1)	-	(-27.3, 90.0)

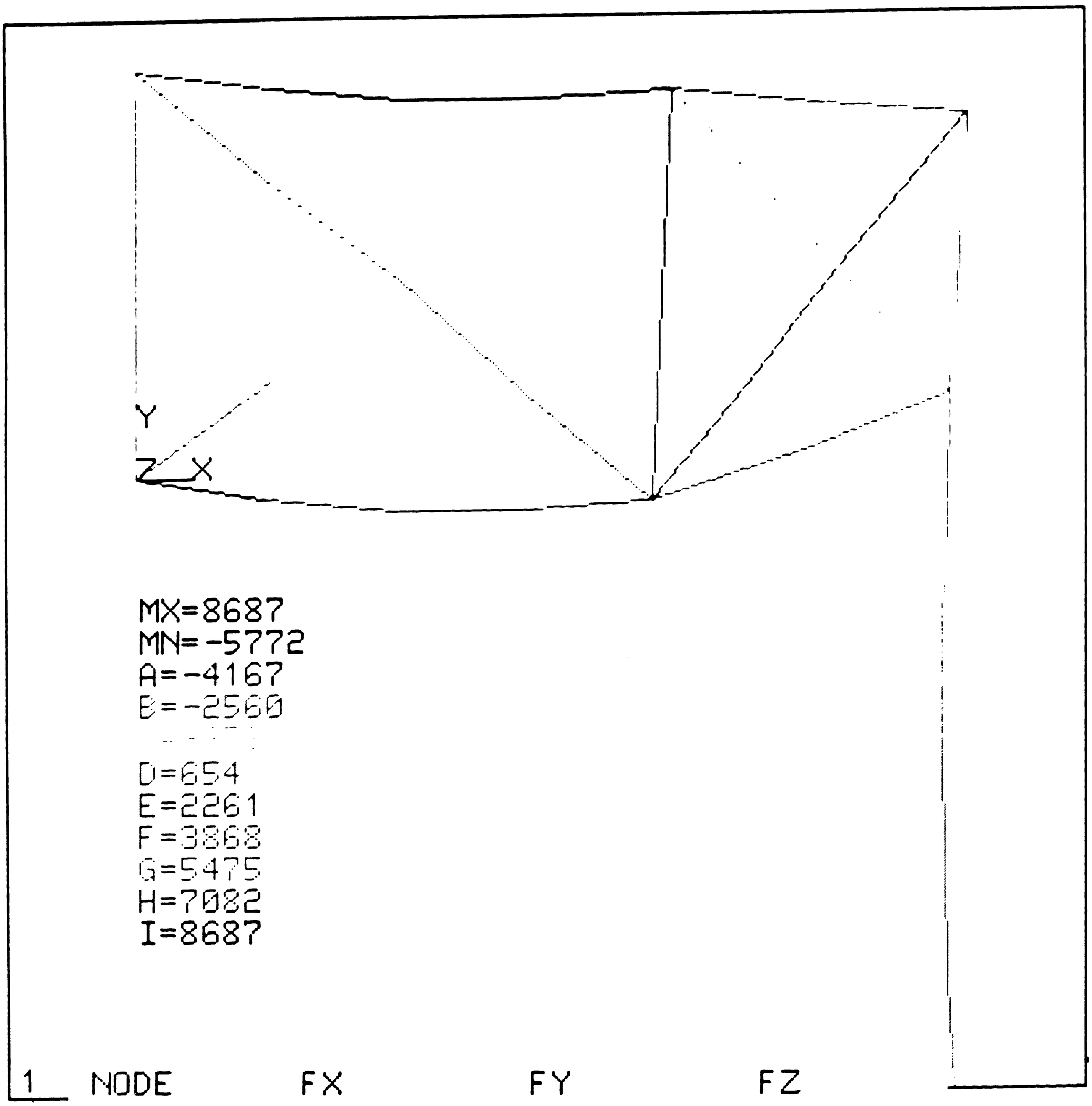

Fig 3.29 : Harmonic Analysis -- Stress Distribution for Arm excited at Node#13 in vertical direction at frequency 0.1 hz with 1 in. displacement load.

The above tabulation confirms the tendency for the induced stresses to rise significantly when the support nodes are excited, due to the reasons discussed previously. A more disturbing fact is that the maximum stress values rise very significantly up to 24 kpsi in the fully extended position and to 93 kpsi in the rotated position. This clearly means that the 2% damping factor, normally used for steel structure calculations, is not adequate for the present structure. Additional damping provisions must be made in the final design if the manipulator arm operating environment will see harmonic forces at modal frequencies. Further analysis should be run with different damping ratios to determine the ratios which can limit the induced stresses within safe limits.

3.3.2.3.3 Transient Dynamic Analysis

Transient Dynamic Analysis is used to determine the response of a structure to a variety of time-varying or transient force functions and harmonic analysis is only a small subset of these. The structural response can be evaluated for any arbitrarily varying force functions, eg. impulse forces, step forces, or force history for achieving a particular kinematic behavior. All of these types of analysis can be performed using either linear or nonlinear methods. The linear type of Transient Dynamic analysis was used for evaluating the manipulator arm, neglecting the effect of geometric and material non-linearities.

ANSYS uses a direct-integration technique to solve transient analysis problem. This means that the equilibrium is satisfied only at discrete time-points instead of continuously. These time-points must specified by the user by defining time-intervals or size of a time-step. These time-steps may be equally spaced or otherwise. Linear analysis requires that the time-step size be maintained constant through out the analysis, whereas nonlinear analysis can work with unequal time-step size. The force,

stress, displacement values are only calculated at the specified time-points.

Transient Dynamic Analysis solves the general equation of motion using an implicit, unconditionally stable integration scheme, in which the size of the time-step, called as the integration step size (ITS) is of vital importance. The accuracy of the solution increases with decreasing ITS. Large values of ITS tend to introduce a numerical error which effectively dampens out the dynamic response of the higher modes, whereas a very small size may make the problem too computationally intensive. Therefore, the ITS should be chosen to be small enough for an accurate solution but without requiring excessive use of computational resources. Various guidelines for choosing an ITS are given in Ref. [52]. Among the relevant items discussed are :

1. Resolution of input curve -- The ITS should be small enough to characterize the input force or displacement curve. If an erratic curve is to be followed, it is recommended that at least 7 time-points be along the shortest side of the curve.

2. Resolution of frequency of response -- The ITS should be small enough to resolve the motion of the structure. An ITS small enough to resolve the highest frequency of interest should be selected. For a frequency f, the ITS may be calculated from ITS = 1/(20f), i.e. 20 steps per cycle of frequency f.

According to the above rule, since the highest frequency of interest to for the manipulator arm is 0.5 hz (corresponding to the upper limit of SS3, i.e. waveperiod of 2 sec),

$$\text{ITS} = 1/(20 * .5) = 0.1 \text{ sec}$$

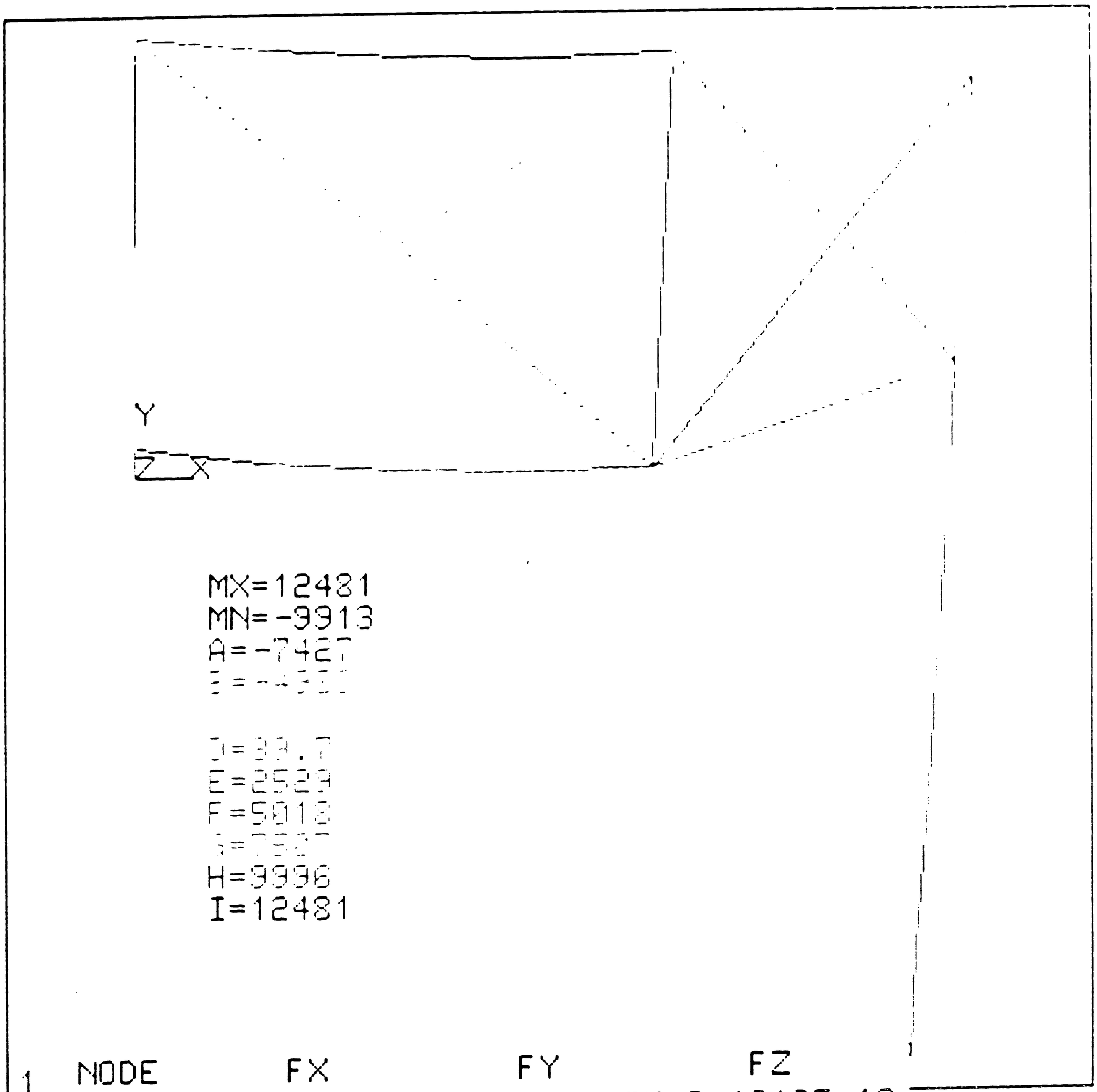

Fig 3.30 : Harmonic Analysis -- Stress Distribution for Manipulator Arm excited at Nodes1 & 3 in vertical direction at frequency 0.1 hz with 1" displacement load.

3.3.2.3.3.1 Impact Load

A linear transient analysis was run for an impulse loading of 140 kips in the -Y direction at node #13. A load of 140 kips was applied for 0.1 second and released. Fig 3.31 shows the variation of X, Y and Z displacements of node # 13 as a function of time. No displacement is observed in the Z direction due to symmetry. However significant ringing was observed both in X and Y directions at about 0.5 hz. The amplitude in the -Y direction is about twice the dead weight displacement, indicating a stress level near twice the static full load stress. Damping elements will be required to limit the ringing of the structure unless it can be shown that impulse loads of this type cannot be encountered during arm operation.

3.3.2.3.3.2 Step Load

A transient analysis was made of the arm with forearm extended with a step load of 70 kips. This condition may arise when a load (container) is lifted suddenly. The variation of displacement of node # 13 in X, Y, Z versus time was obtained for 0.1 sec and 0.05 sec ITS, as shown in Fig 3.33 (a) & (b). The general shape of in the two figures is the same though the one with the smaller ITS shows much more details and more pronounced peaks.

A plot of the stress variations observed in several of the more highly stressed elements was made. These highly stressed elements are as identified in Fig 3.33. The stress variations are plotted over a period of 1 second in Fig 3.34. Tensile stresses in beam elements 5 and 40 vary from about 8 to 26 kpsi, while compressive stresses in beam elements 15 and 31 range from about 9 to 24 kpsi.

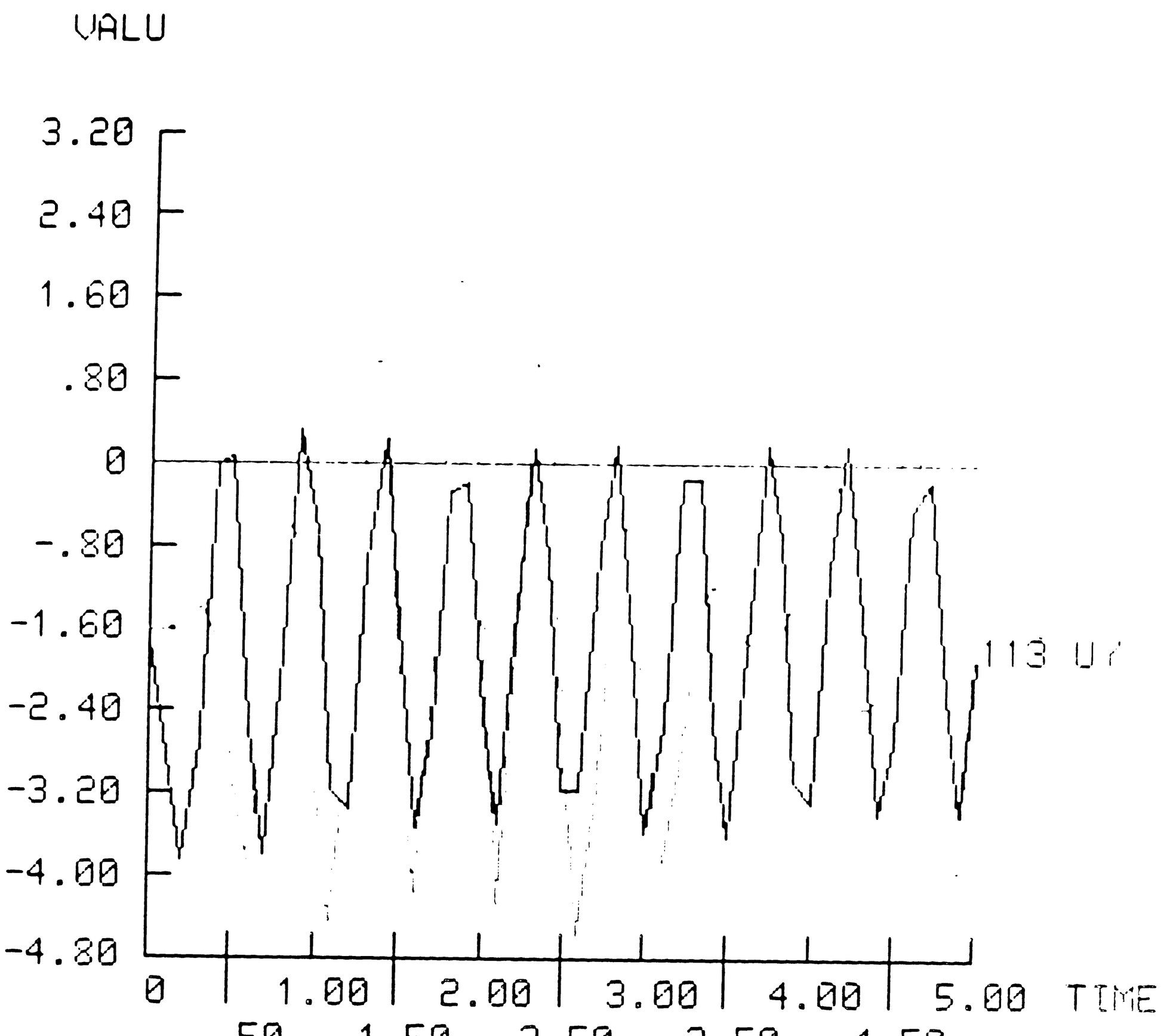

Fig 3.32 : Transient Dynamic Response -- Impulse load of 140 kips

Time Variation of X, Y, Z displacement of node #13

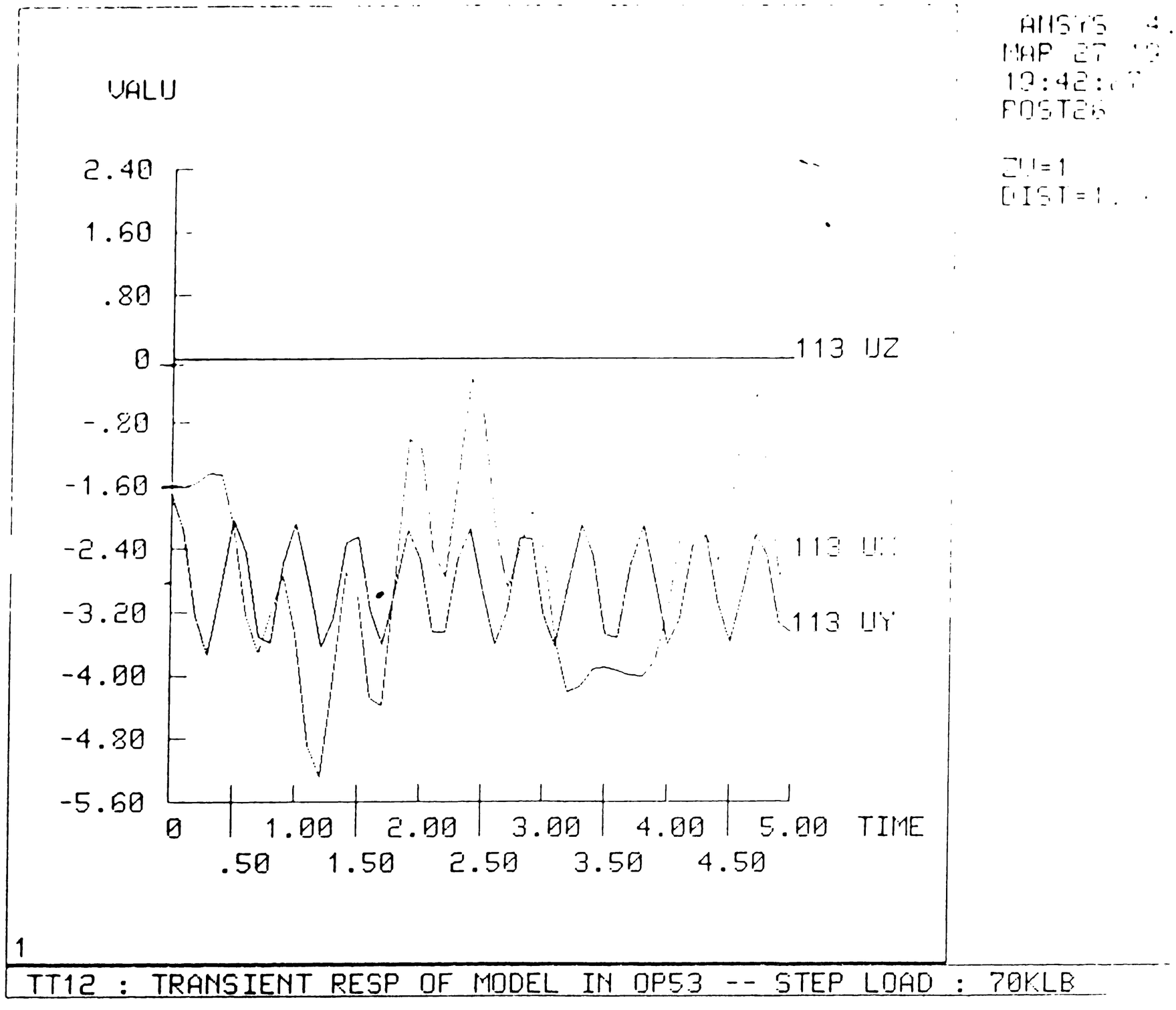

Fig 3.33 : Transient Dynamic Response -- Step load of 70 kips

Time Variation of X, Y, Z displacement of node #13

(a) 0.1 sec ITS

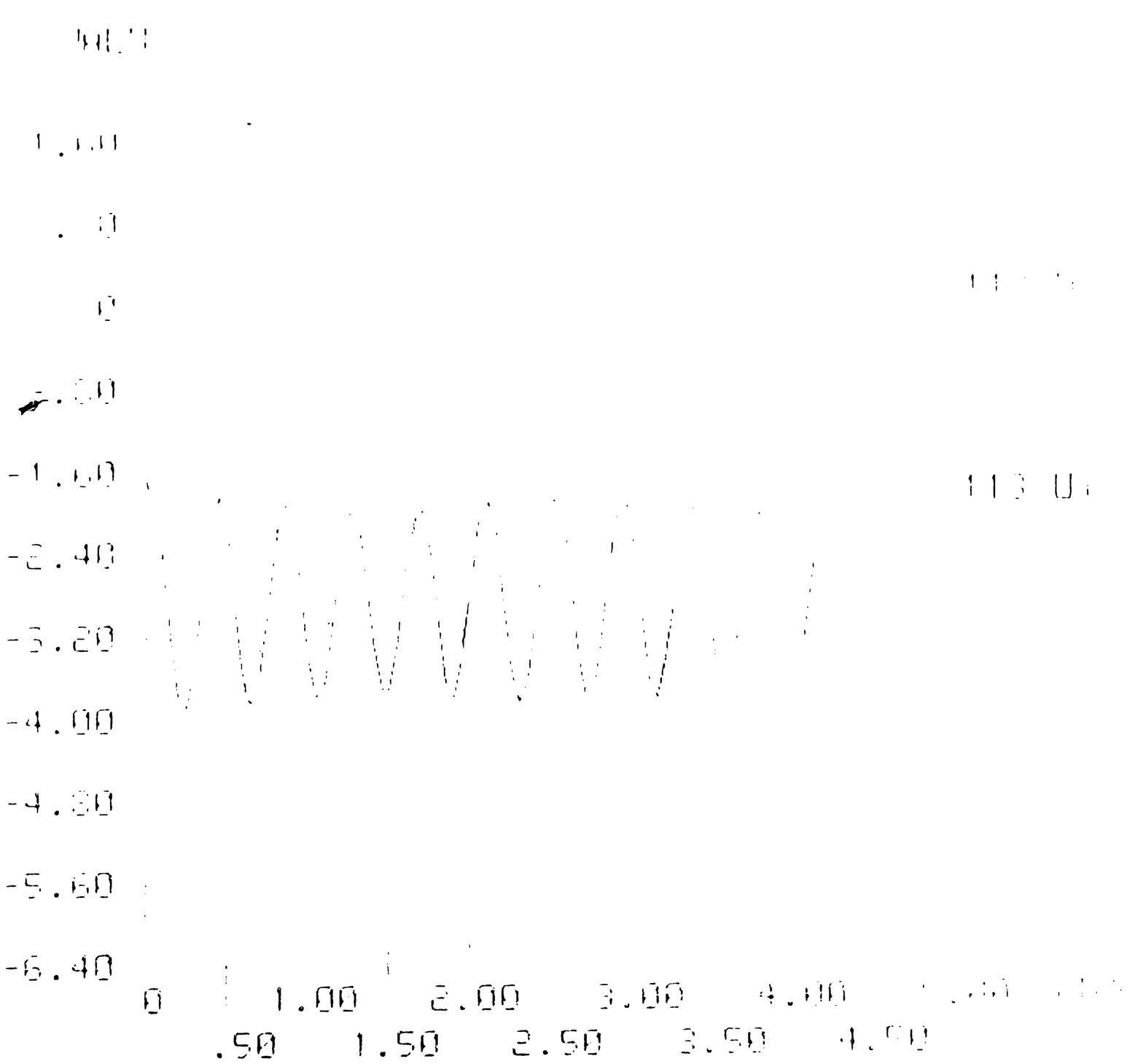

Fig 3.33 : Transient Dynamic Response -- Step load of 70 kips

(b) 0.05 sec ITS

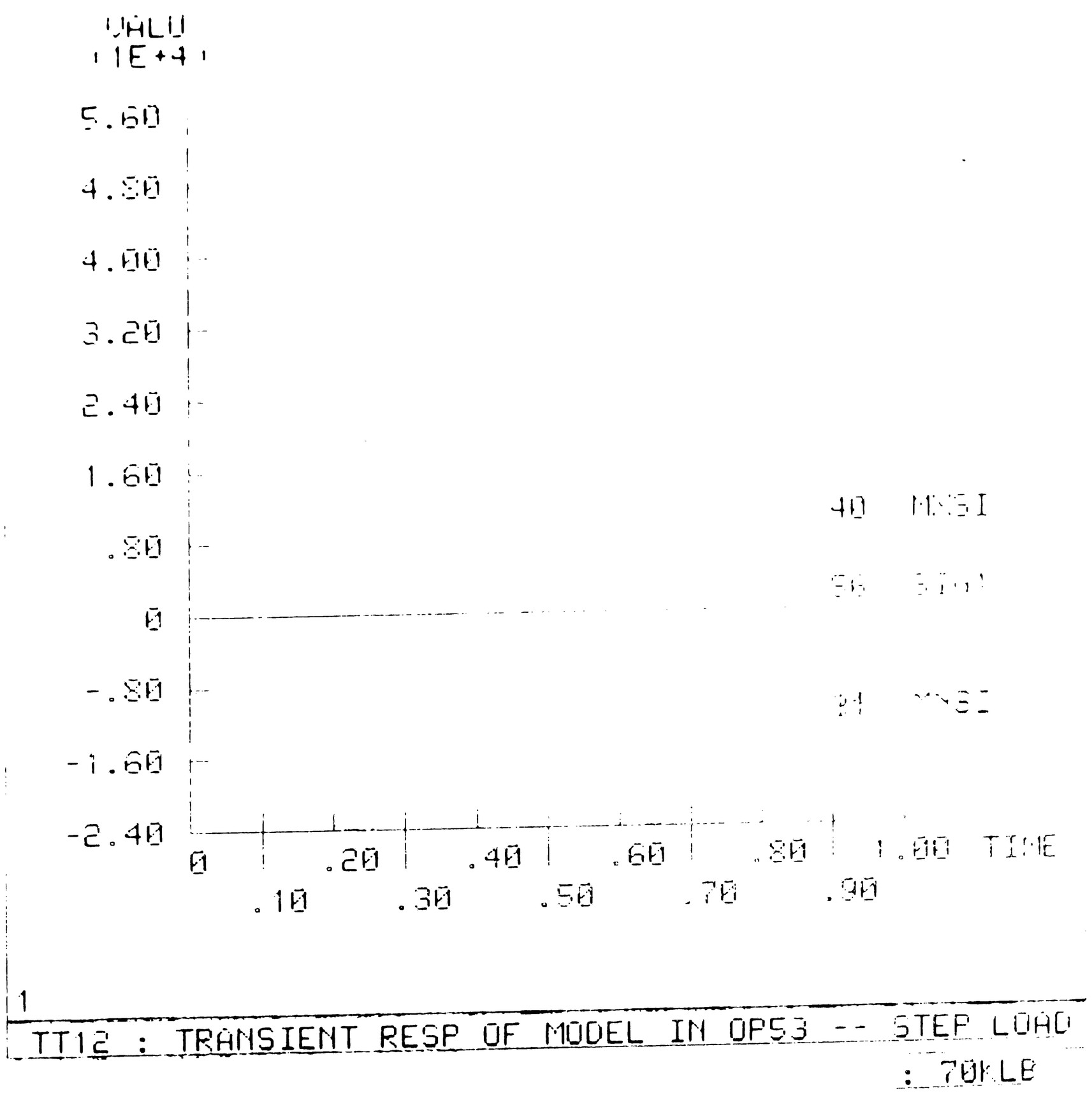

Fig 3.34 : Transient Dynamic Response -- Step load of 70 kips

Time Variation of Stresses

3.3.3 Tenth Scale arm Analysis

Testing of fullscale model was not considered to be feasible in the case of the manipulator arm for AACTS. A tenth scale design was therefore selected for experimental testing purposes, as a proof of concept.

3.3.3.1 Suggested Design

The 1/10th scale design is shown in Fig 3.35. As a convenience for initial studies, it was decided to consider the structure to be a scalar reduction of the conceptual design in all dimensions by a factor of ten. The resulting reduction of areas was by 100 times and of volumes by 1,000 times. Hence the self-weight was reduced by 1,000 times, and the payload for the tenth scale model was also reduced by 1,000 times. Since the section modulus varies as the fourth power of the length dimension, a reduction of 10,000 times was expected in the section moduli for the tenth-scale design. However, after selecting the available standard structural components, the section moduli were smaller by a factor of 6000.

3.3.3.2 Approach for Analysis

The tenth scale analysis was started after much of the analysis for the full-scale arm was done. Hence the individual arm analysis (forearm and upperarm), was omitted, as was the analysis of detailed basic-frame structure of the tenth-scale arm.

3.3.3.3 Static Analysis

The tenth-scale conceptual design was only analyzed in the fully extended position for stresses and displacements under the combined action of self-weight and an external load of 70 lb. A maximum displacement of 0.02 inches occurred at the spreader bar (Fig 3.36). A maximum compressive stress of 0.96 kpsi occurred in link 3-4, and a maximum

tensile stress of the same magnitude occured in link 1-2 (Fig 3.37). The displacements obtained seemed to be too small and the structure stiffness seemed too high. However, hand calculations on the free body system of the vertical hoist suggested that the stress and displacement figures are quite reasonable.

3.4 Preliminary Design

3.4.1 Tenth Scale Design

3.4.1.1 Tenth Scale Design Details

The tenth scale model of the manipulator arm was developed before the full-scale arm because it is to be built for use in a project to test and evaluate scale models of key AACTS components. More extensive analysis of the preliminary design was therefore performed on the tenth scale model.

Four significant features distinguish the preliminary design from the conceptual design. The first design change was the use of 6061 T6 Aluminium instead of steel. The significant weight reduction more than compensated for the reduction in the ultimate strength. The resulting reduction in stress levels kept the arm deflections (i.e. strains) to reasonable levels.

A second change in the preliminary design was the use of pipe sections instead of structural angles to fabricate the basic-frame sections for the full-scale manipulator arm. For the scale model, a decision was made to simulate the basic-frame shapes with square aluminium tubing. The sides of the square shapes could have been milled out to duplicate the stress patterns in the diagonal basic-frame members, but it was decided to keep the full cross section for purposes of analysis and initial testing.

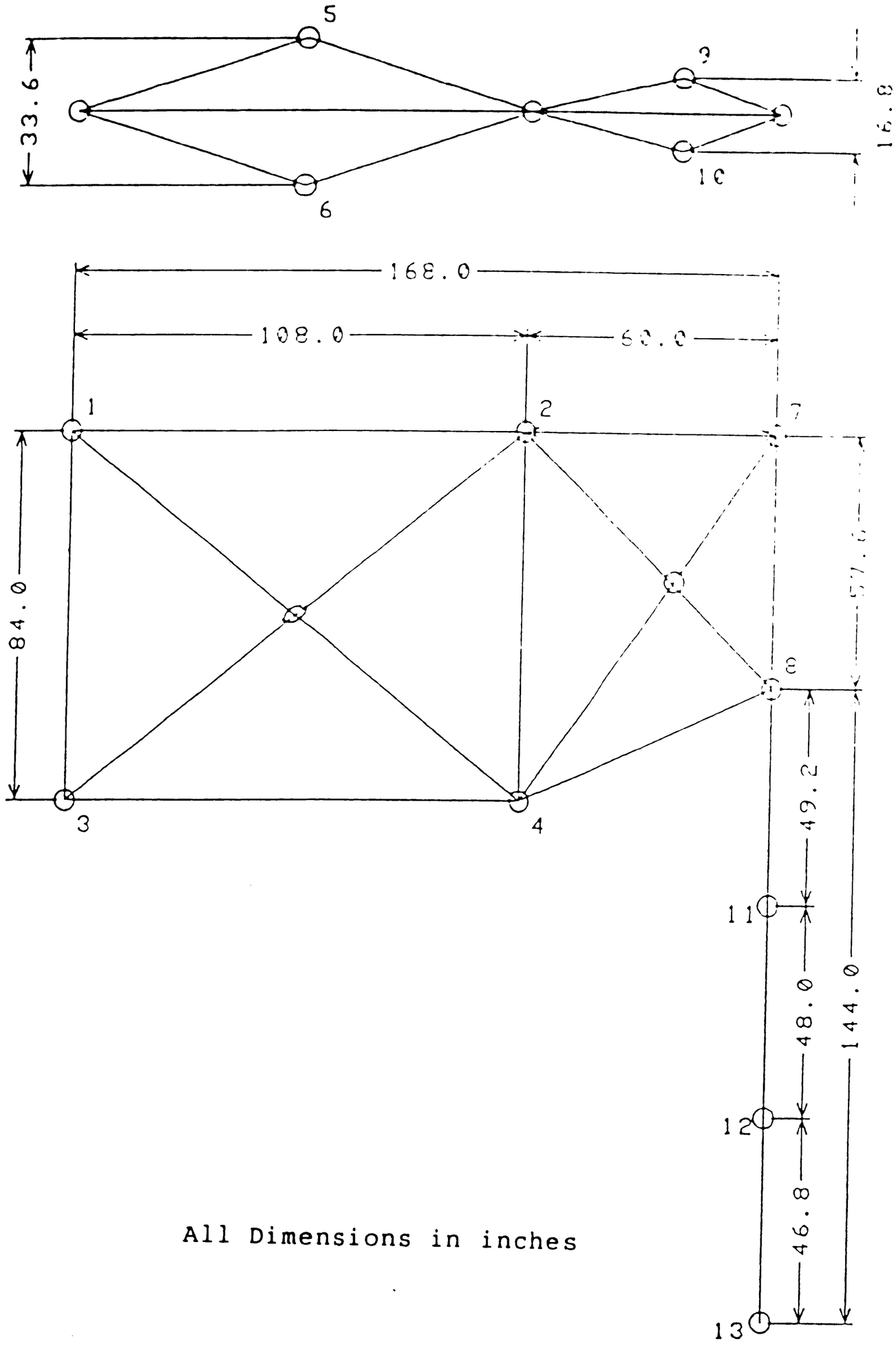

All Dimensions in inches

Fig 3.35 : Tenth scale Conceptual Design.

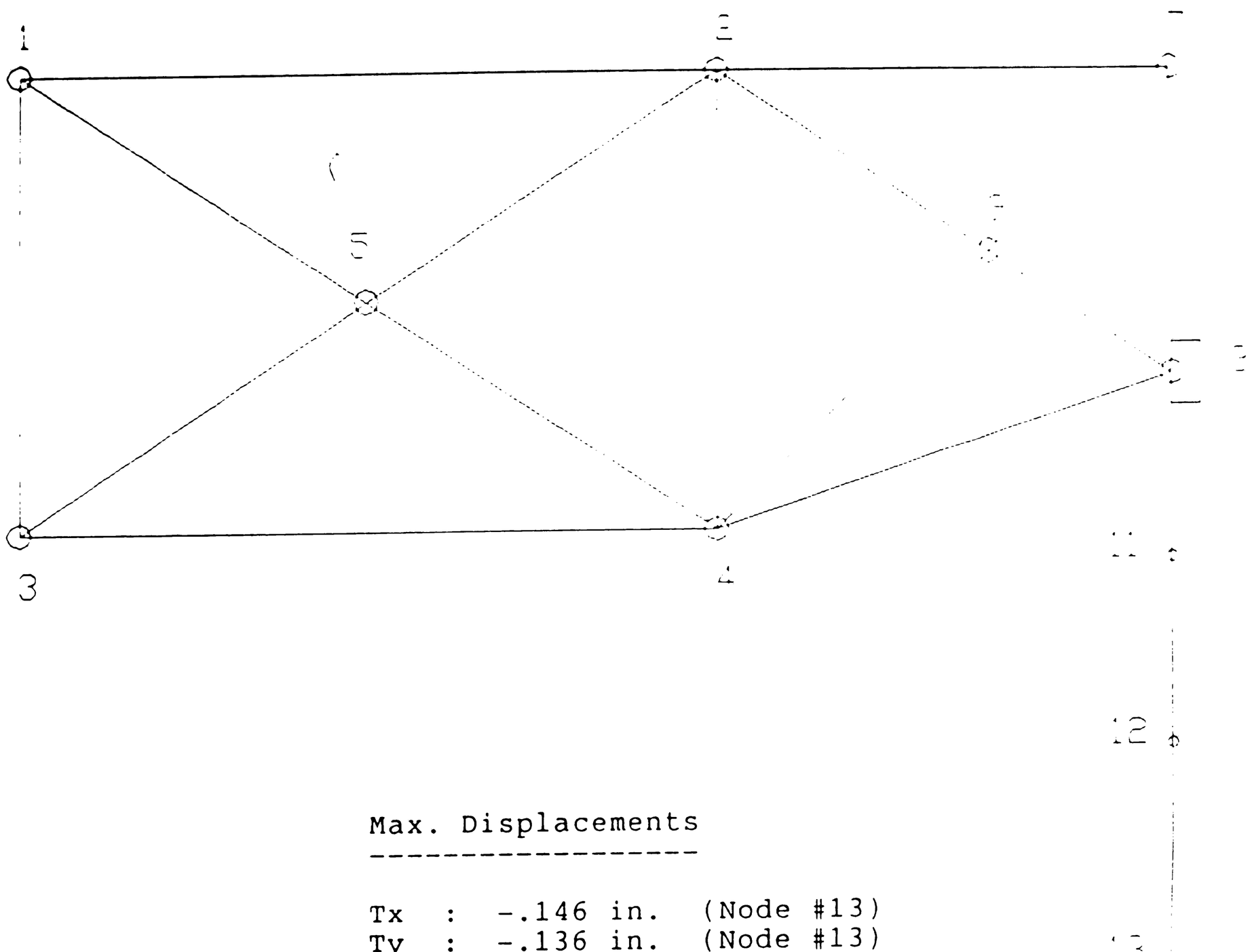

Max. Displacements

Tx : -.146 in. (Node #13)
Ty : -.136 in. (Node #13)
Tz : -.0068 in. (Node #9)

Rx : -.003 rad. (Link 9-8)
Ry : -.004 rad. (Link 9-7)
Rz : -.001 rad. (Link 2-7)

Fig 3.36 : Tenth scale -- Displacements with Self-weight and 70 lb load.

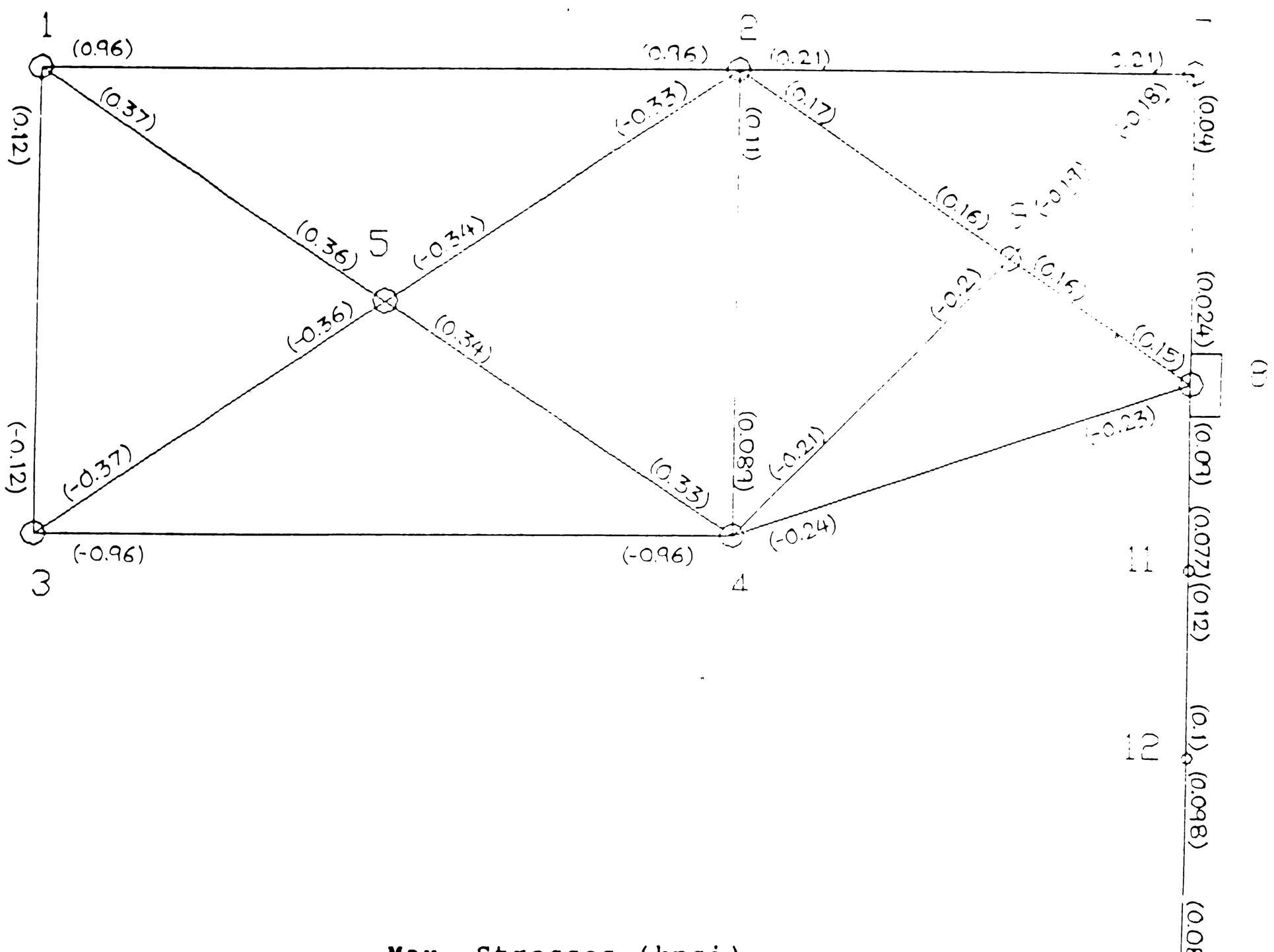

Max. Stresses (kpsi)

Tensile : 0.96 (Link 1-2)
Compr. : -0.96 (Link 3-4)

Fig 3.37 : Tenth scale -- Stresses with Self-weight and 70 lb load.

A third change in the preliminary design was the addition of a support structure to which the manipulator arm could be attached. By including the support structure in the analysis, the computed displacements could all be determined with respect to ground, and the values could be checked later in the experimental test program. A steel support structure, generally following the basic-frame design principles, was used for the manipulator arm. Some design weaknesses have been identified, principally in the use of cantilever type bearing supports and a torque tube to resist the resulting moments. As a result of static analysis, the support structure has been redesigned to completely eliminate all non-basic-frame construction. These changes will probably be analyzed at a later date.

A fourth change in the preliminary design was the addition of a drive system for both the upperarm and the forearm. Modal analysis of the conceptual design identified a low frequency vibrational mode which resulted from the low section modulus in rotation about the two drive axes. The drive systems were therefore designed to include a drive pulley at the axis of rotation with a diameter approximately equal to the spacing between the diagonals (node 5 and 6 in the upperarm, nodes 9 and 10 in the forearm). By rigidly attaching the drive pulleys to the support structure and the forearm, drive motors for both the systems could be mounted on a cross member between the diagonals on the upperarm (nodes 5 and 6). Fig 4.1 shows the tenth scale manipulator arm with the torque tube support structure and the drive cables connected to the two drive pulleys. Take up pulleys for both drive system cables are mounted on the upperarm cross members (between nodes 5 and 6). Each arm can rotate +/- 135° from the straight out position.

The structural changes made to the tenth-scale conceptual manipulator design to arrive at the preliminary design are summarized in the following table :

Table 3.6 : Tenth-scale Arm Design Changes

	CONCEPTUAL DESIGN	PRELIMINARY DESIGN
MATERIAL	Steel	Aluminium
SUBASSEMBLIES		
* Main Members	1/2x1/2x1/16 angle	
. Min. rad of gyration	0.153 in	
. Area	0.06 in^2	N/A
. Moment of Inertia	0.0014 in^4	
. Weight	0.21 lb/ft	
* Auxiliary Members	3/8x3/8x1/16 angle	
. Min. rad of gyration	0.112 in	
. Area	0.043 in^2	N/A
. Moment of Inertia	0.00054 in^4	
. Weight	0.16 lb/ft	
* basic-frame Structure	6 in square	4x4x.25 square tube
. Min. rad of gyration	2.45 in	1.54 in
. Area (Effective)	0.24 in^2	3.75 in^2
. Moment of Inertia	2.185 in^4	8.83 in^4
. Weight	1.90 lb/ft	4.5 lb/ft

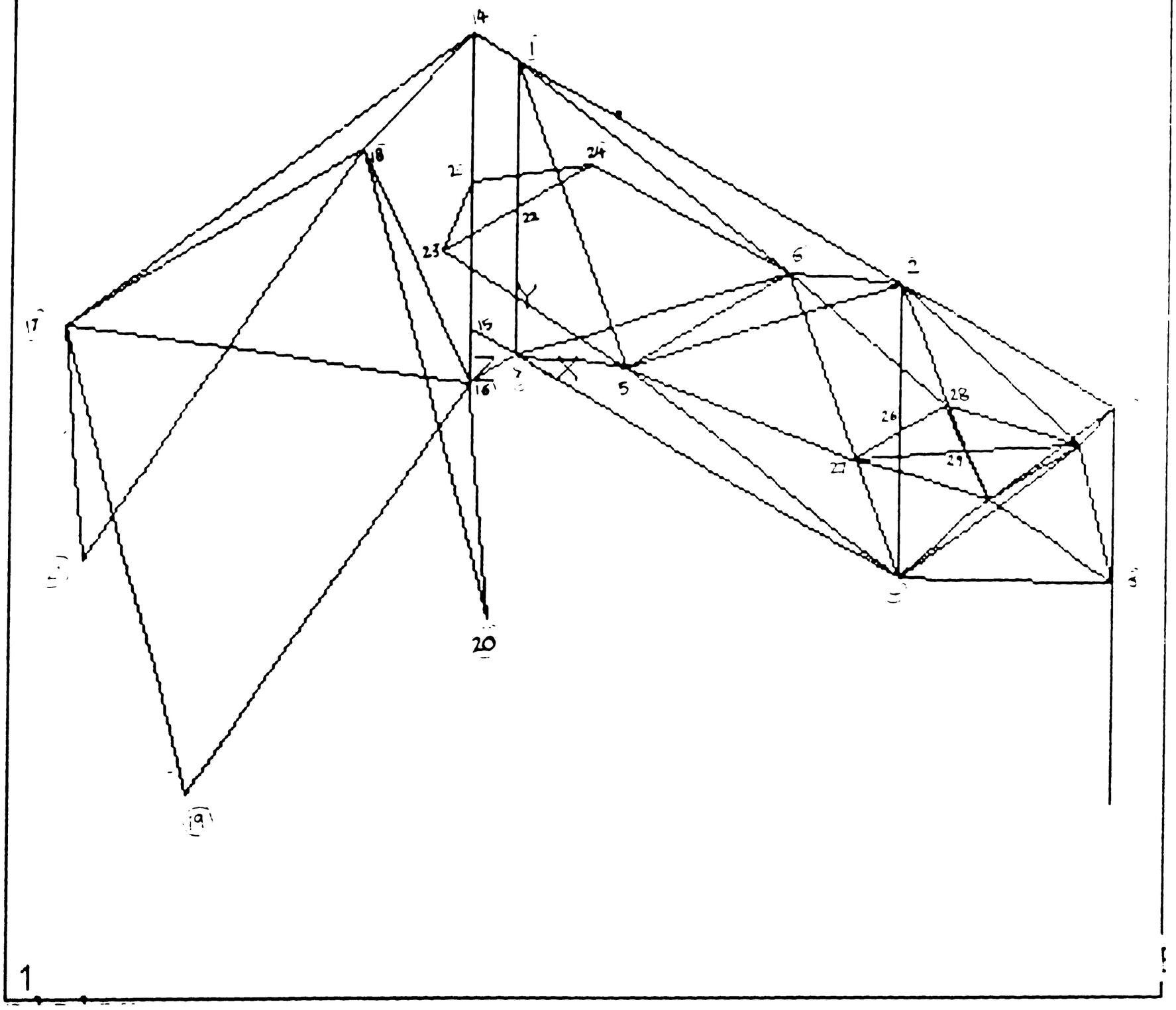

Fig 3.38 : Tenth scale arm with torque tube support structure and cable drive system.

3.4.1.2 Tenth Scale Design Analysis

3.4.1.2.1 Static Analysis

In the initial stages of static (force / stress/ displacement) analysis, it was seen that modeling the drive pulleys with plate elements was somewhat complex computationally. Hence, for purposes of simplicity and speed, the drive pulley plate on the forearm was modeled as a framework of beams. Also, the pulleys were replaced by beams as seen in Fig 3.38(b). Various conditions were analyzed in terms of configuration (0°, 90° rotations), and loads (none, 70 lb, 700 lb). A drive cable preload of 100 lb was consistently used. The results are summarized as follows :

Table 3.7 : Tenth Scale Preliminary Design -- Static Analysis Results.

LOAD CONDITION	NO LOAD		70 lb	700 lb
Forearm Position	Extended	Rotated	Extended	Extended
Max. σ psi	2803	4127	3536	5874
Min. σ psi	-3387	-4530	-3897	n/a
Y Disp. @ 13 inch	-.0526	-.077	-.062	-.139

The calculations indicate that the maximum direct stresses are at a reasonable level even with ten times the rated loads. The calculated displacements at the spreader bar are approximately 1/32 inch with no load, 1/16 inch with 70 lb load (rated), and 1/8 inch with ten times the rated load of 700 lb. Fig 3.39 and 3.40 show the displacements and stresses obtained with a fully extended arm under the action of self-weight and a 700 lb load.

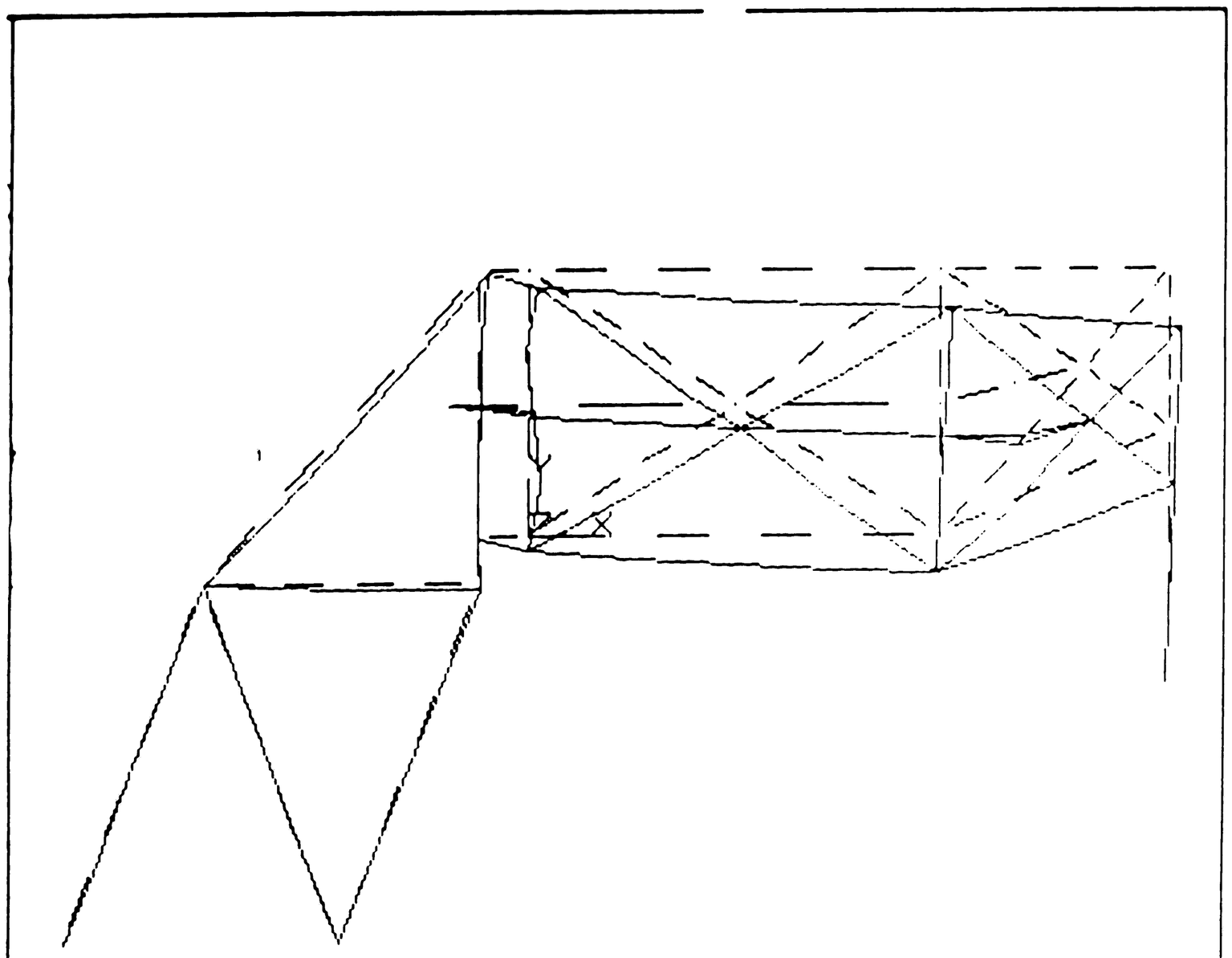

119	661.5	2982.	-1019.
120	661.5	2982.	1019.
121	-1323.	-3436.	-0.8527E-13

Fig 3.39 : Tenth scale arm -- Displacements with 10 times the rated load.

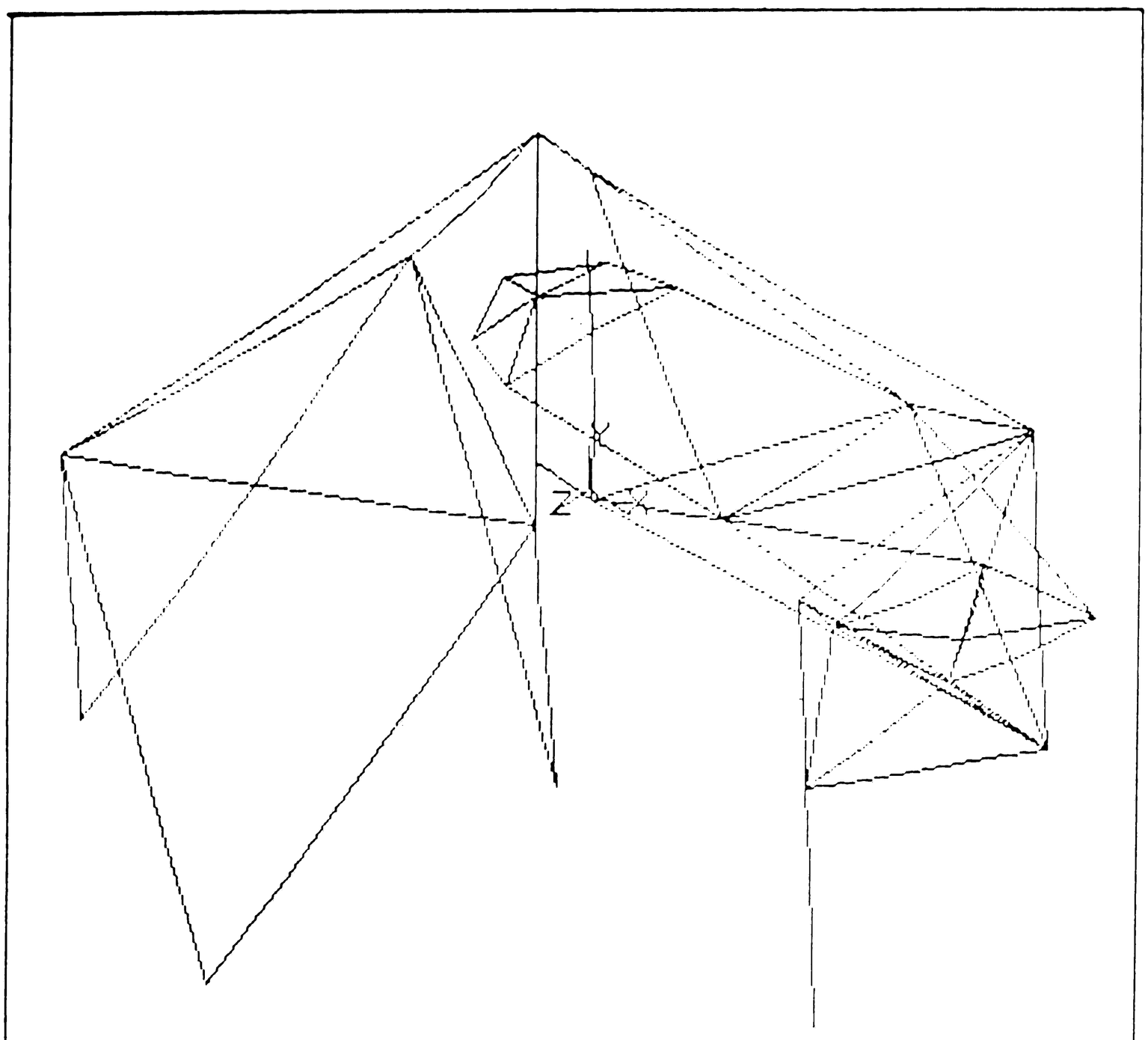

119	190.7	1654.	-453.7
120	260.2	1284.	413.2
121	-450.8	-1110.	40.55

Fig 3.40 : Tenth scale arm -- Stresses with 10 times the rated load.

As a design simplification, nodes 9 and 10 were relocated to bring them in line with nodes 5 and 6. This would improve alignment for the drive system. A rerun of the static analysis (see Fig 3.41 and 3.42) under fully extended condition with no load indicated a displacement of 0.0531 in. at the spreader bar, compared to the previously obtained value of 0.0526 in. The maximum stress in a structural member was 2801 psi, the same as was obtained before relocation of nodes. Therefore, the relocation of the nodes did not cause any significant increase in displacements or stresses.

4.1.2.2 Modal Analysis

Modal Analysis was the only dynamic analysis done for the tenth scale manipulator preliminary design. It was performed for three load conditions (No load, rated load, 10 times rated load), and two braking conditions (ON or OFF on all arm support joints). Braking conditions used were actually rotational constraint conditions at nodes 1, 2, 3, and 4 about the Y-axis. In actual practice, there would be bearings at these points and also some provision for restricting the rotational motion of the arm about the pivots there. Brakes would normally be ON there except when the manipulator is changing configuration by relative rotation. When the brakes are ON, the manipulator rotary joints are constrained to maintain the same configuration. Hence the arm is stiff. However, it becomes relatively limber while changing configuration since the cables are the only member preventing free rotation. Different dynamic characteristics are therefore obtained with brakes ON or OFF.

A sample of the various mode shapes obtained (for 45° rotated, No load and Brakes OFF) is shown in Fig 3.43 (a-f). The mode shapes can be generalized to some basic shapes, regardless of the arm configuration, load or braking condition, as shown in Table 3.8.

Using the mode shape categories established in Table 3.8, plots were made to see the effect of various loading, braking and configuration conditions on the mode frequencies.

Fig 3.44 indicates the variation of mode frequencies for mode I under various conditions. Note that Mode I has the lowest mode frequency for any possible configuration or load/braking condition. The lowest possible mode frequency is 0.14 hz in the fully extended position, with brakes off and at 10 times the rated load.

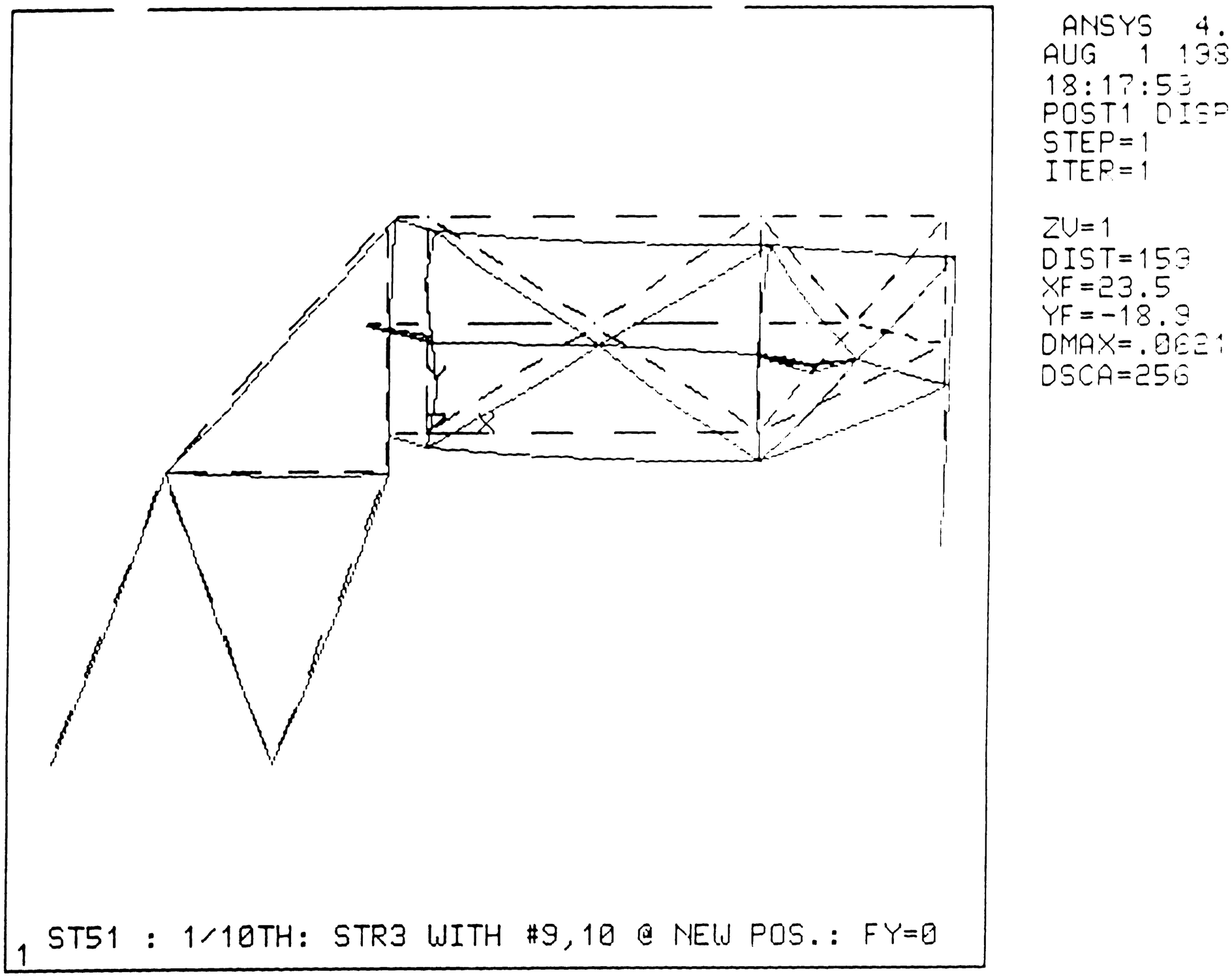

Fig 3.41 : Tenth scale arm -- Displacements with relocated nodes under no load.

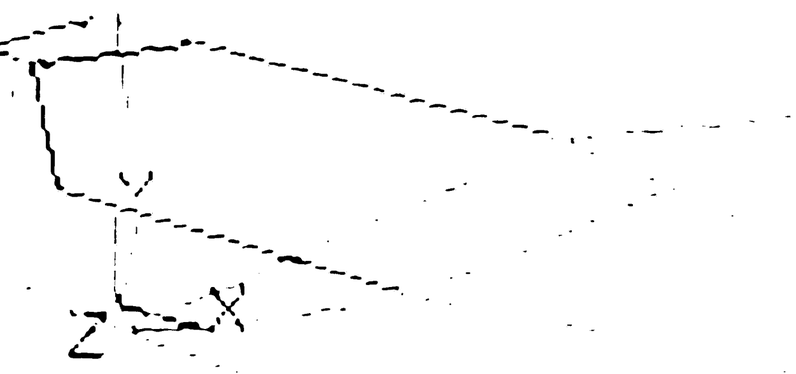

MX=3952
MN=-1231

H=3377
I=3952

ST51 : 1/10TH: STR3 WITH #9,10 @ NEW POS.: FY=0

119	266.0	1578.	-480.9
120	266.0	1578.	480.9
121	-531.9	-1326.	0.4120E-04
TOTAL	0.1642E-09	1829.	-0.8527E-13 0.0000E+00

Fig. 3.42 : Tenth scale arm -- Stresses with Relocated Nodes under no load.

(a) Mode Shape #1

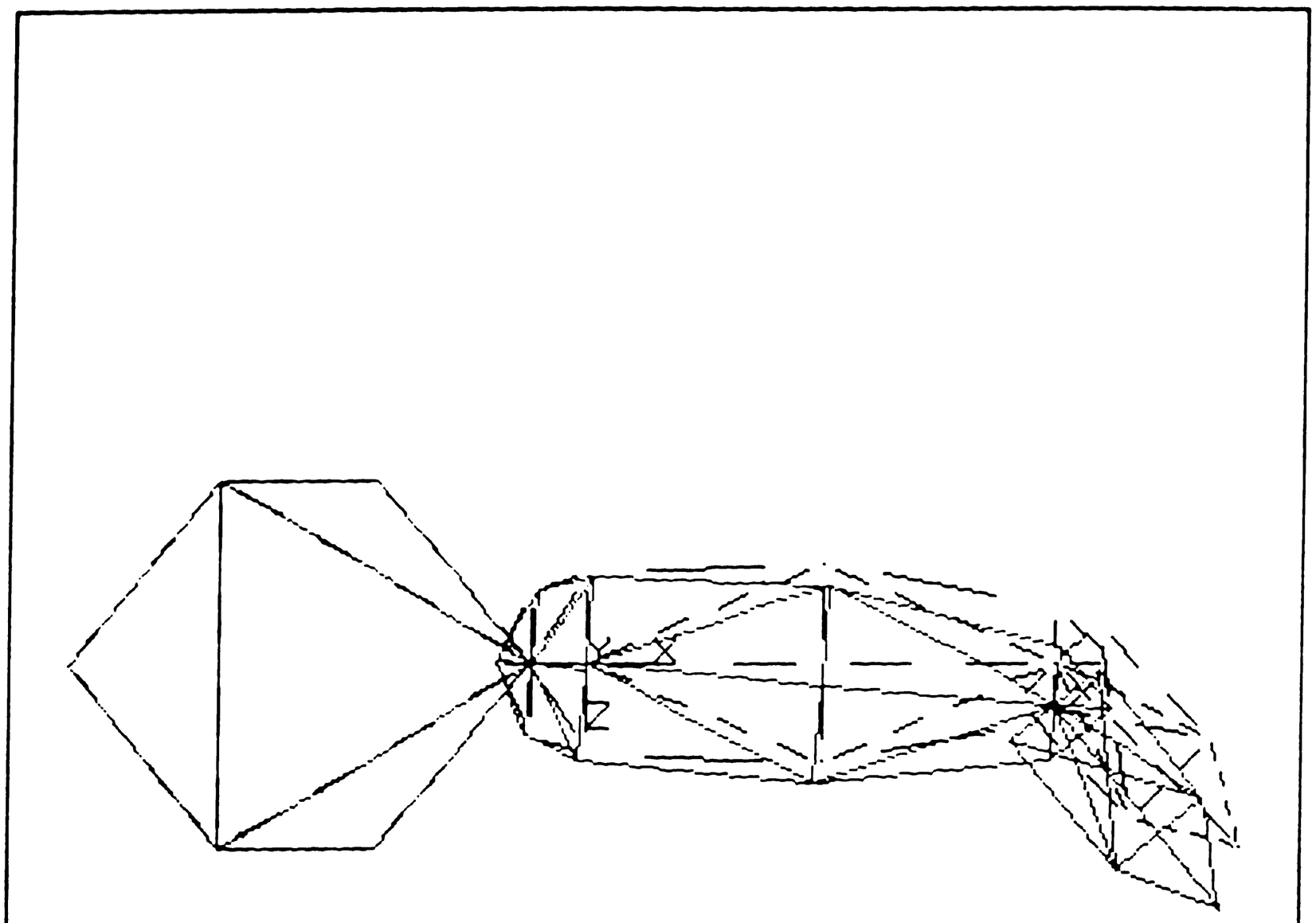

1 SP34 : 1/10TH: STATIC: ROTATED 45: FY=0: BRAKES OF

FOR LOAD STEP= 1 ITERATION= 1 SECTION= 1
FREQ= 0.262065 LOAD CASE= 1
TITLE= SP34 : 1/10TH: STATIC: ROTATED 45: FY=0: BR

Fig 3.43 : Tenth scale -- Modal Analysis (45° rotated, No load, Brakes off)

(b) Mode Shape #2

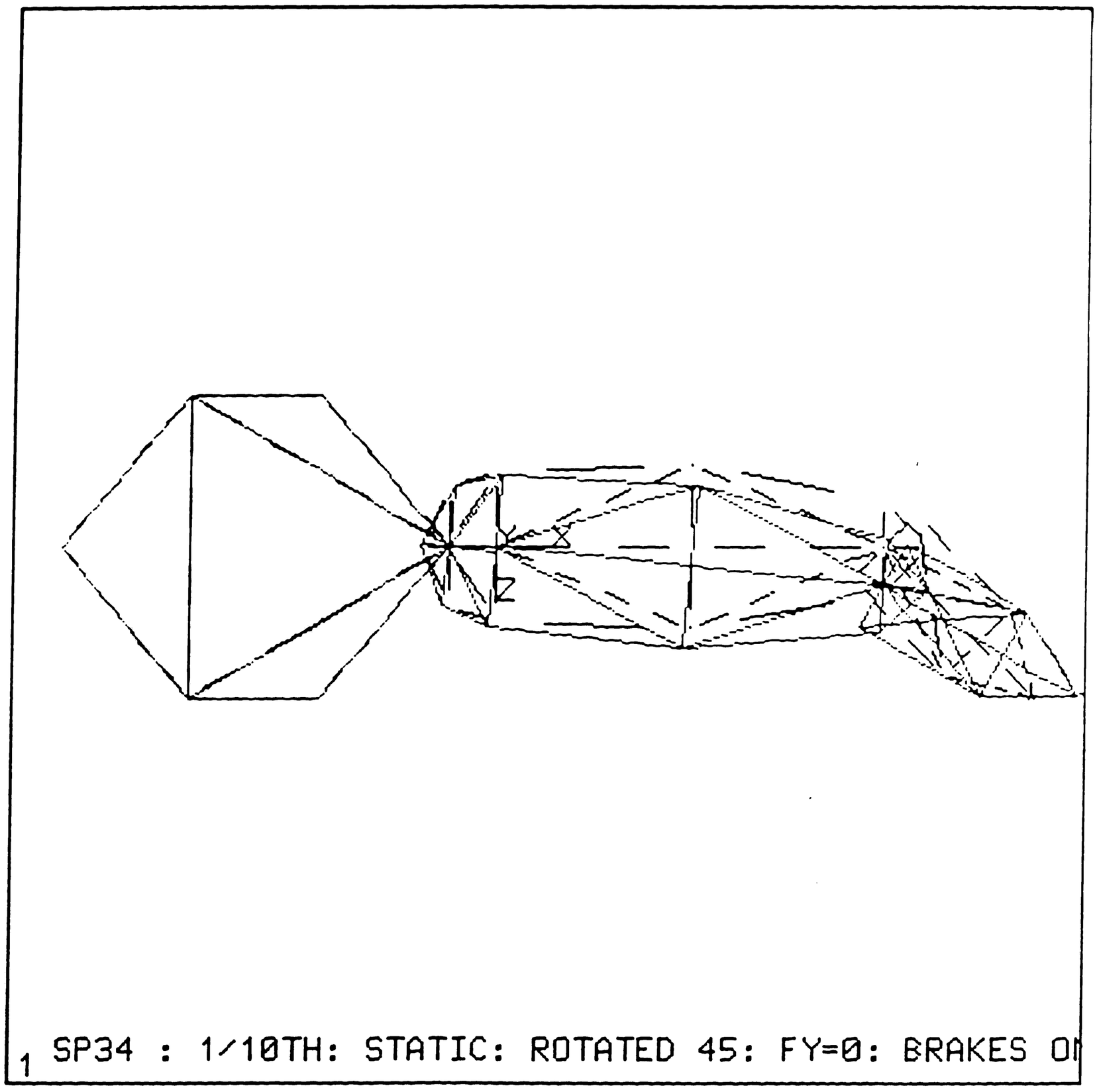

FOR LOAD STEP= 1 ITERATION= 2 SECTION= 1
FREQ= 1.55224 LOAD CASE= 1
TITLE= SP34 : 1/10TH: STATIC: ROTATED 45: FY=0: BR

Fig 3.43 : Tenth scale -- Modal Analysis (45° rotated, No load, Brakes off)

(c) Mode Shape #3

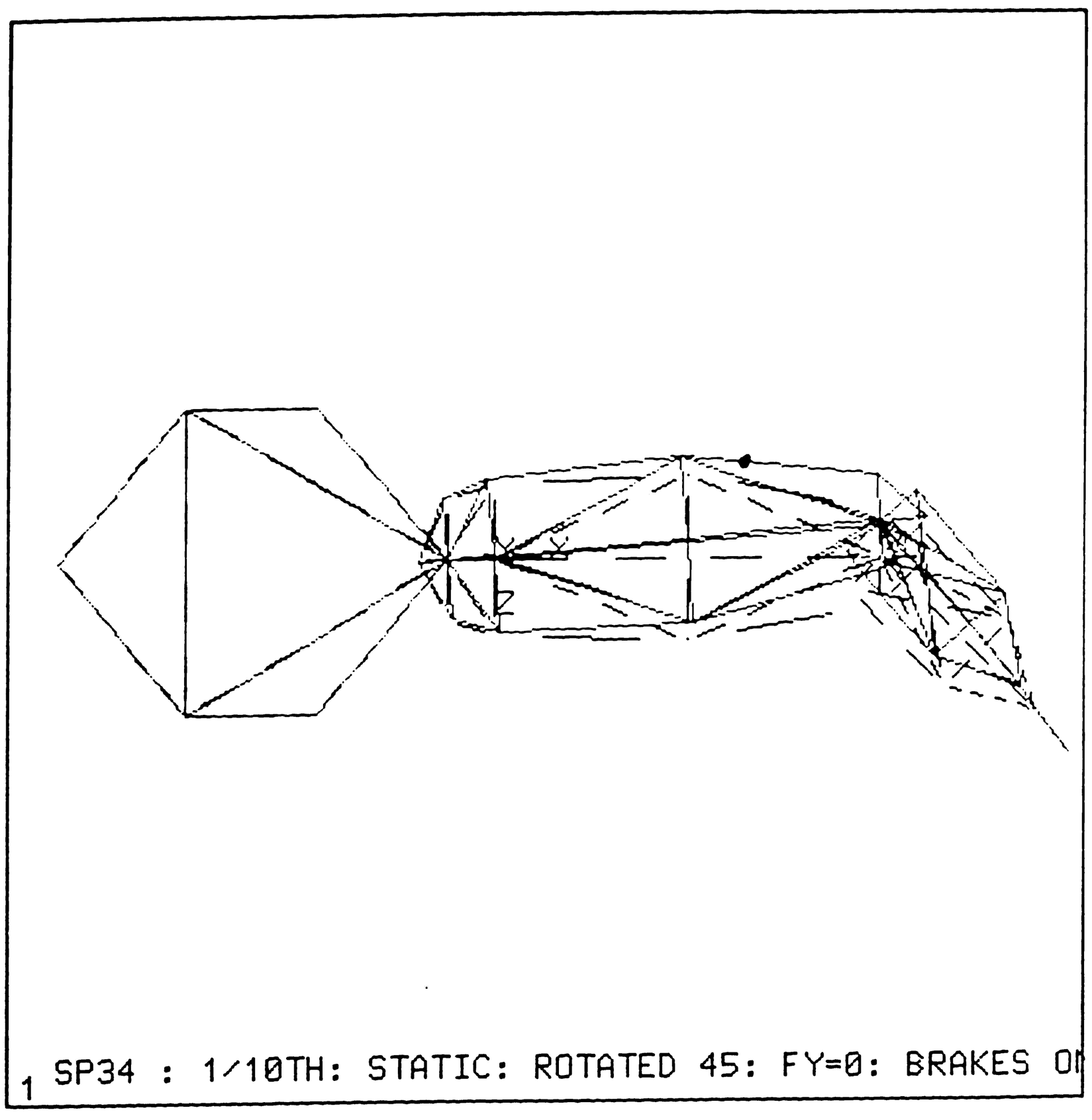

Fig 3.43 : Tenth scale -- Modal Analysis (45° rotated, No load, Brakes off)

(d) Mode Shape #4

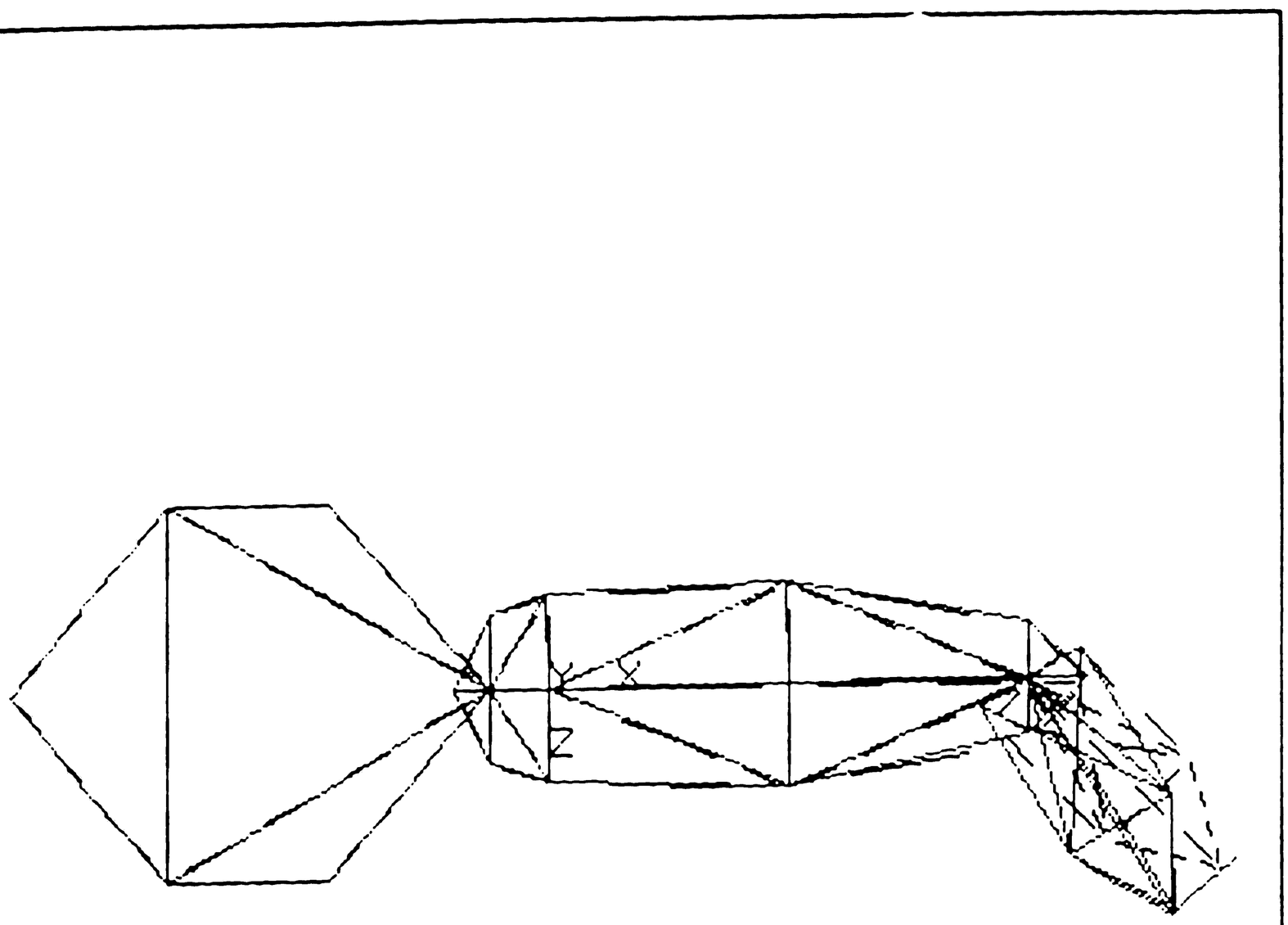

Fig 3.43 : Tenth scale -- Modal Analysis (45° rotated, No load, Brakes off)

(e) Mode Shape #5

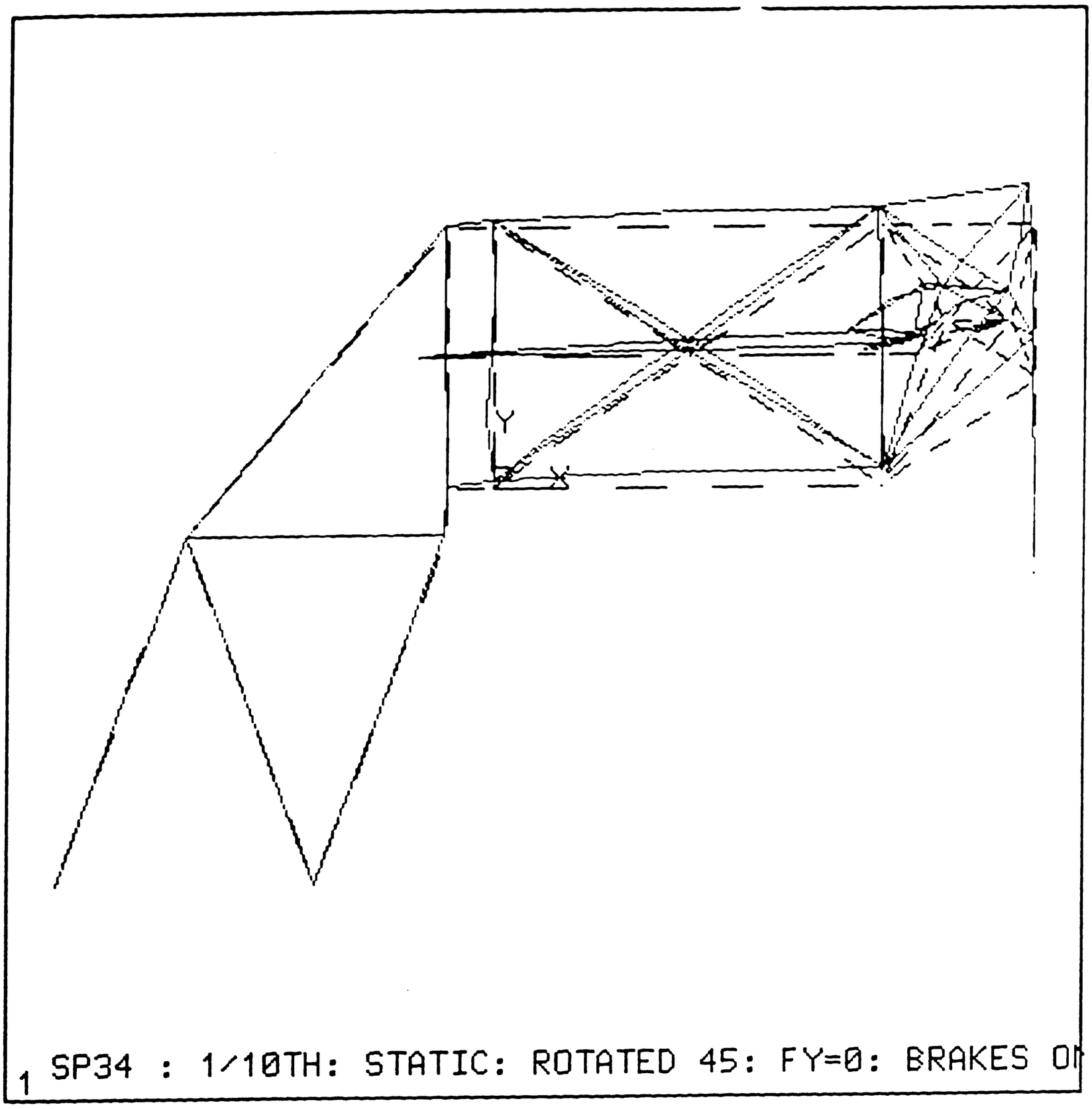

Fig 3.43 : Tenth scale -- Modal Analysis (45° rotated, No load, Brakes off)

(f) Mode Shape #6

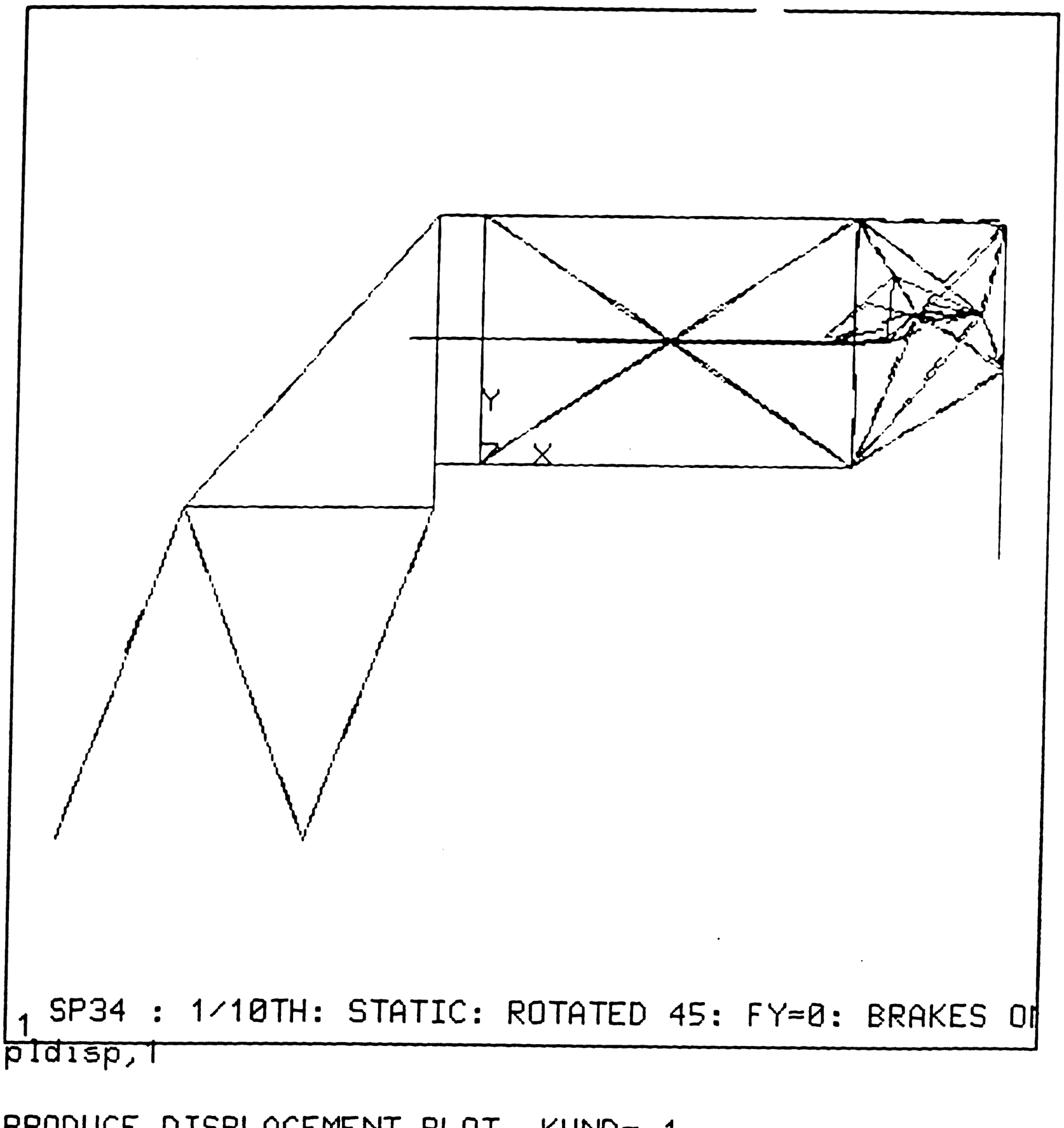

Fig 3.43 : Tenth scale -- Modal Analysis (45° rotated, No load, Brakes off)

Table 3.8 : Tenth Scale Preliminary Design -- General Mode shapes.

Type # & Name	Features	Shape Schematic (Top View unless mentioned otherwise)
I. <u>Swinging Door</u>	* Rotation about Z at torque-tube or upperarm brake. * No bending. * Relative angles between arms are maintained.	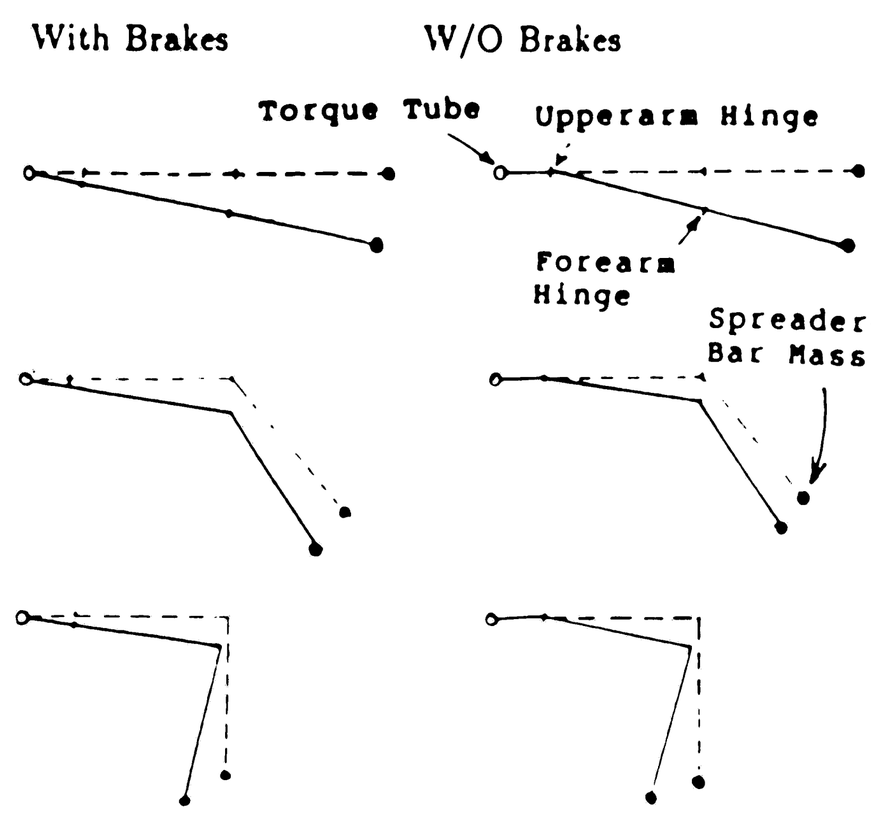
II. <u>Fishing Pole</u>	* Vibration of Spreaderbar (like a fishing pole -- slender rod) nearly in the plane of forearm. * If the upper & fore arms move, they do so in out-of-phase fashion; and the spreaderbar remains out-of-phase with the upperarm. * With brakes, if the forearm moves, it bends. Without brakes, if the forearm moves, it rotates	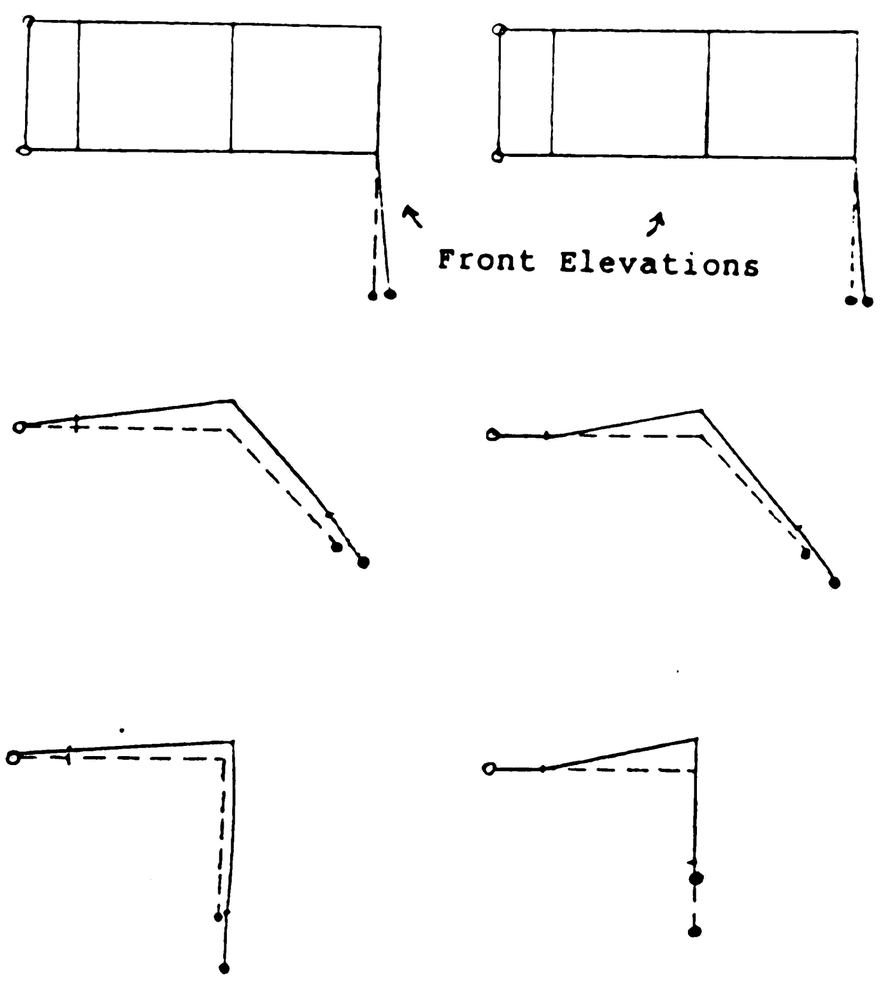

Table 3.8 : General Mode shapes -- Continued.

Type # & Name	Features	Shape Schematic
III. <u>Out-of-plane Fishing-pole Forearm Assist</u>	* Spreaderbar vibrates out-of-plane of forearm. * Forearm & upperarm move in out-of-phase fashion. * Spreaderbar remains <u>in-phase</u> with forearm. * With brakes, forearm bends; Without, forearm rotates.	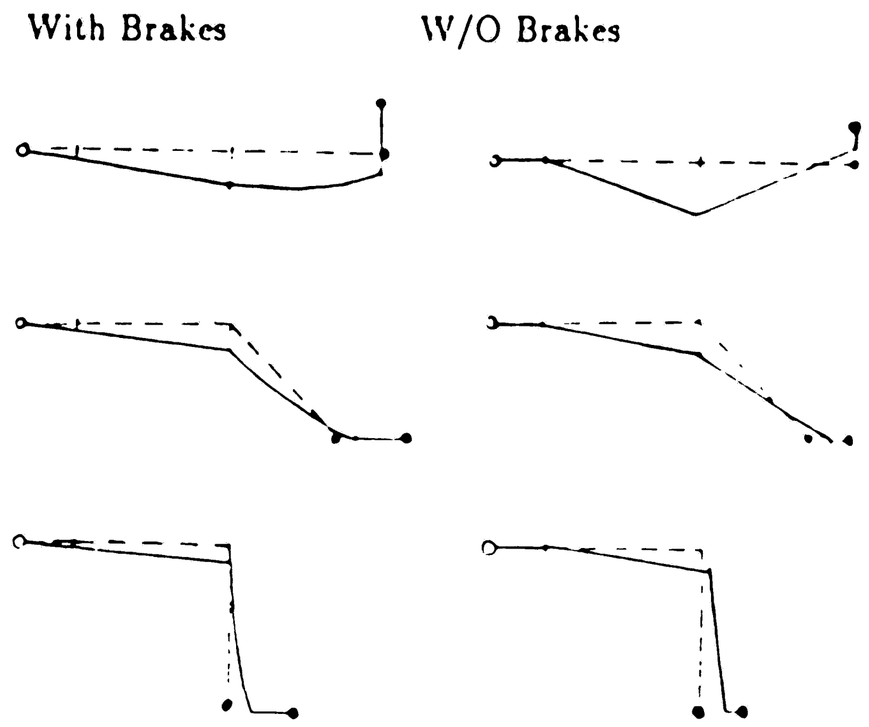
V. <u>Out-of-plane Fishing-pole Forearm Resist</u>	* Spreaderbar vibrates out-of-plane of forearm. * Forearm & upperarm move in out-of-phase fashion. * Spreaderbar remains <u>out-of-phase</u> with forearm. * With brakes, forearm bends; Without, forearm rotates.	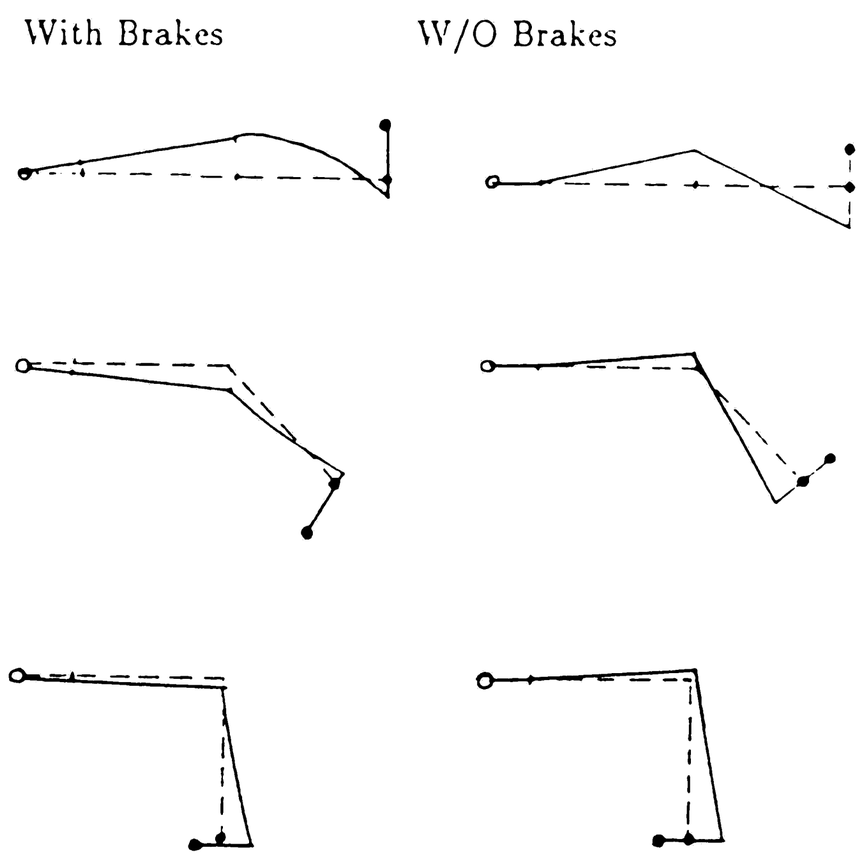

Table 3.8 : General Mode shapes -- Continued.

Type # & Name	Features	Shape Schematic (Front Elevations)
V. <u>Vertical</u> - <u>Assisted</u>	* Whole structure moves up and down in a chopping motion. * Forearm drive mechanism is in-phase with rest of the structure. * Upperarm gets twisted in the rotated positions.	With Brakes / W/O Brakes: 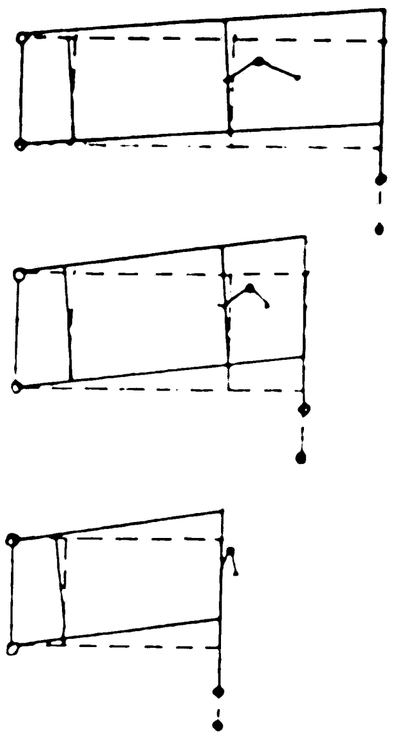 Same
VI. <u>Vertical</u> - <u>Resisted</u>	* Whole structure moves up and down in a chopping motion. * Forearm drive mechanism is out-of-phase with rest of the structure. * Upperarm gets twisted in the rotated positions.	With Brakes / W/O Brakes: 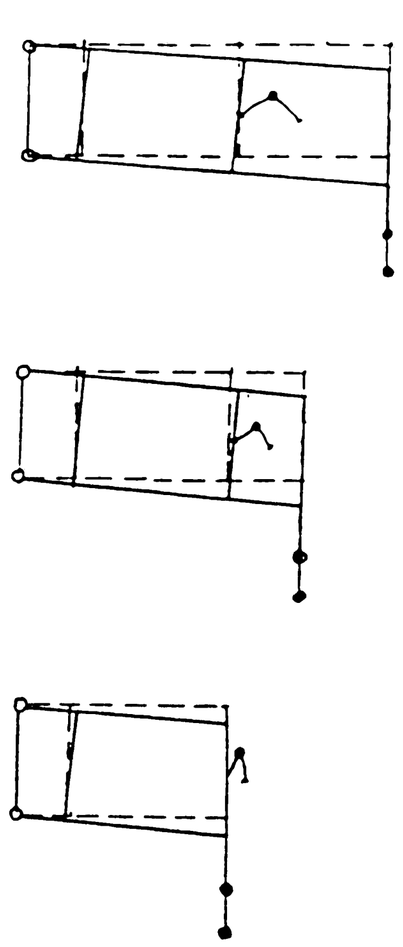 Same

Mode shape I, the Swinging Door mode (Fig 3.44) shows a consistent drop in mode frequencies for all load conditions with the release of brakes due to the reduction in stiffness (rotational about Y axis) of the manipulator. The drop of frequency with an increase of load is to be expected since frequency is inversely proportional to the mass. An increase in the angle of rotation is accompanied by an increase in frequency, since the center of gravity of the manipulator moves closer to the pivot point, thus reducing the effective vibratory arm length.

Mode Shape II, In-plane Fishing Pole mode (Fig 3.45) shows no variation of frequency with or without brakes for the 0° configuration. For other configurations, however, the frequencies drop with the brakes OFF.

Mode Shape III, Out-of-plane Forearm Assist mode (Fig 3.46) shows a different trend in that the frequency drops with an increase of the angle of rotation, indicating a decrease in stiffness with forearm rotation. This is attributed to a reduction in the torsional stiffness and an increase in moment of inertia (about X-axis) of the system with increasing angle of rotation. The same observations can be applied to Mode Shape IV, Out-of-plane Forearm Resist mode (Fig 3.47).

Mode Shapes V & VI (Vertical Chop Assisted & Resisted -- Fig 3.48 & 3.49) show similar characteristics to mode shapes III and IV with regard to mode frequency variations. Although vibration is not totally of twisting nature, some twisting is induced in the structure by the eccentricity due to forearm rotation.

The graphs in Figs 3.44 to 3.49 provide a detailed indication of the effect of various changes in load, braking and arm configuration on some of the lowest mode frequencies of the tenth scale arm. Although time did not permit such detailed analysis to be done with the full-scale arm, a few full-scale arm modal analyses were carried out as a basis for extrapolation from the tenth-scale curves.

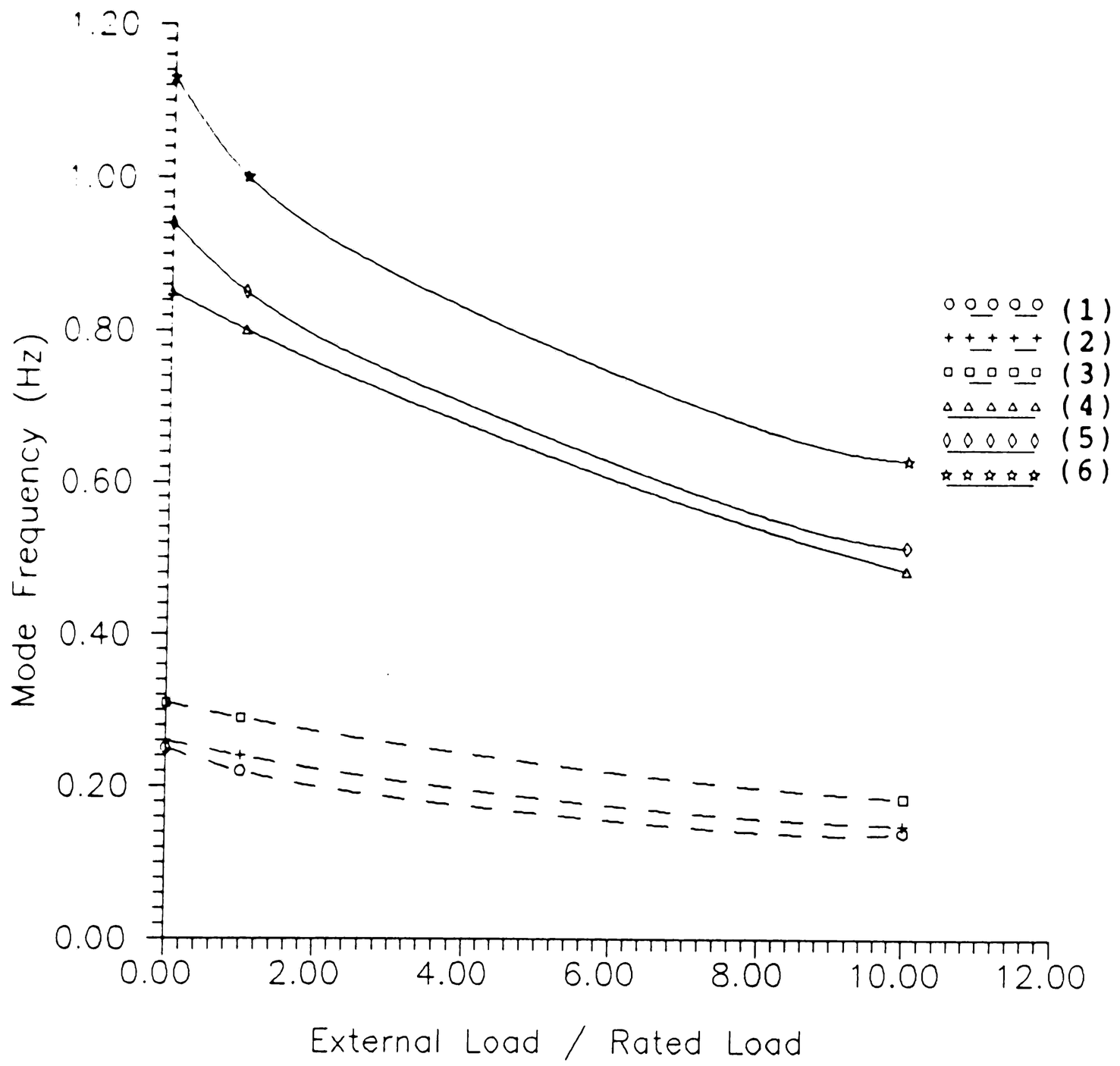

(1) Brakes OFF : 0 deg
(2) Brakes OFF : 45 deg
(3) Brakes OFF : 90 deg
(4) Brakes ON : 0 deg
(5) Brakes ON : 45 deg
(6) Brakes ON : 90 deg

Fig 3.44 : Mode Frequencies for Shape I [Swinging Door Mode]

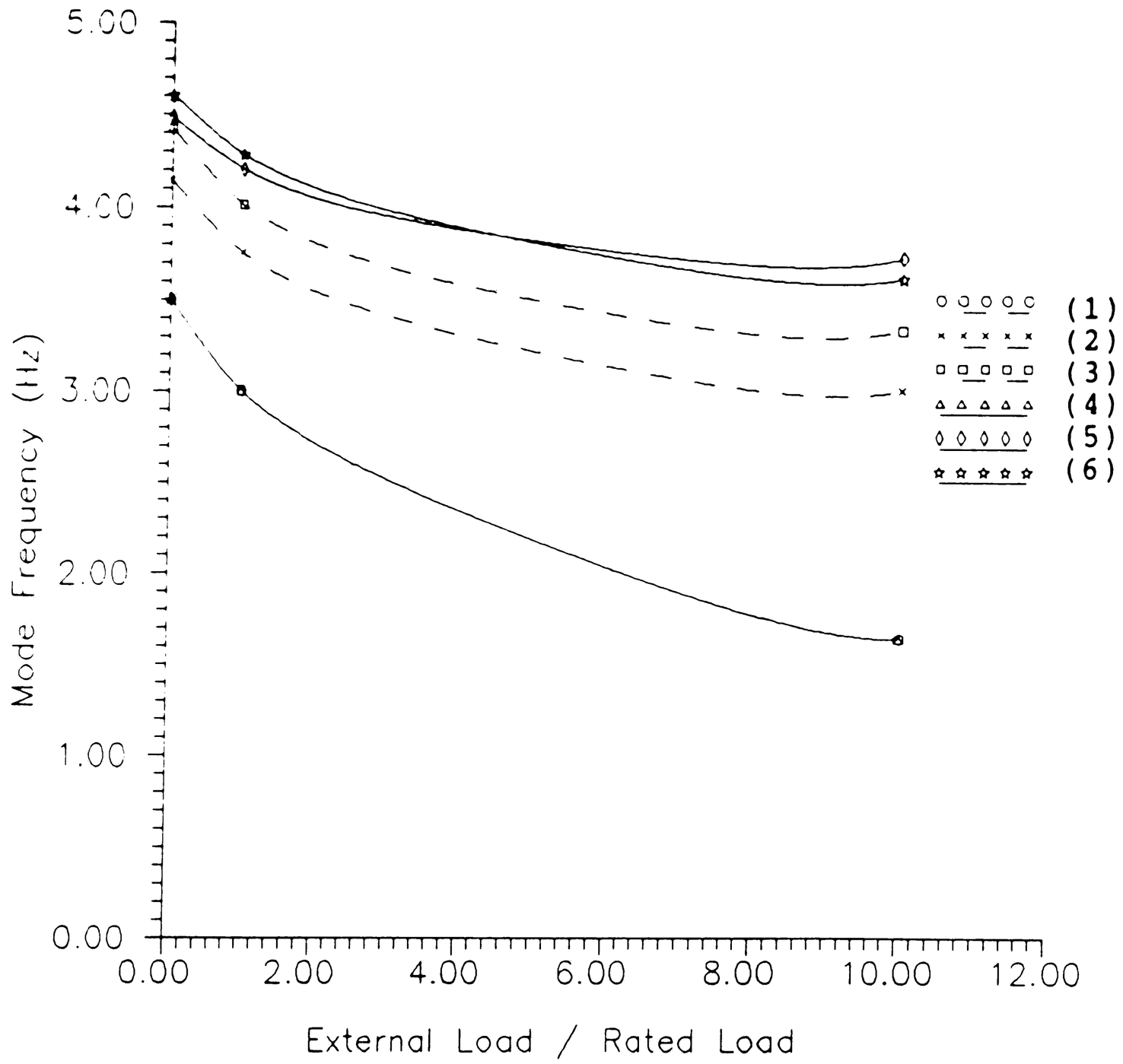

(1) Brakes OFF : 0 deg
(2) Brakes OFF : 45 deg
(3) Brakes OFF : 90 deg
(4) Brakes ON : 0 deg
(5) Brakes ON : 45 deg
(6) Brakes ON : 90 deg

Fig 3.45 : Mode Frequencies for Shape II [In-plane Fishing Pole]

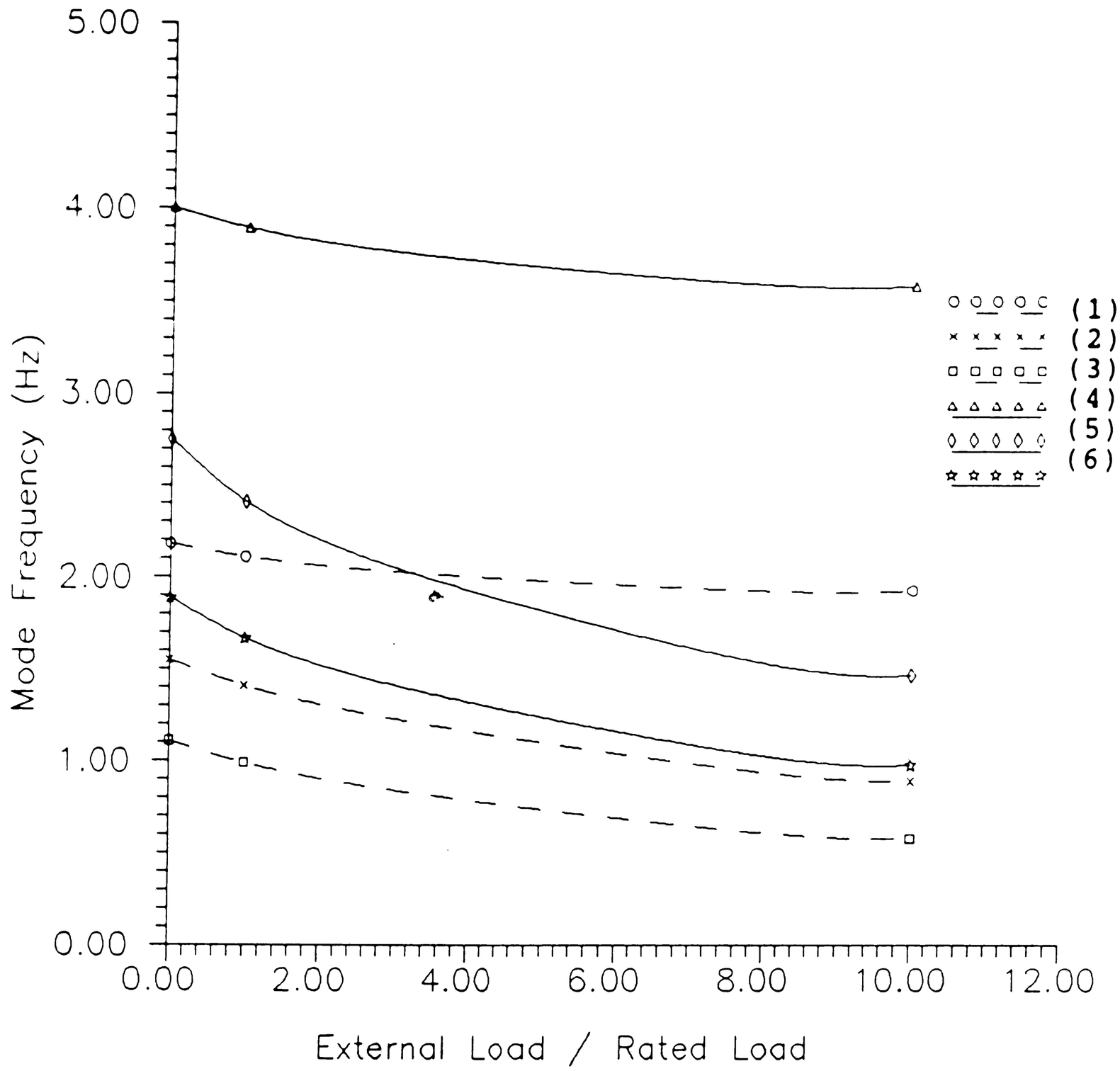

(1) Brakes OFF : 0 deg
(2) Brakes OFF : 45 deg
(3) Brakes OFF : 90 deg
(4) Brakes ON : 0 deg
(5) Brakes ON : 45 deg
(6) Brakes ON : 90 deg

Fig 3.46 : Mode Frequencies for Shape III [Out-of-plane Assist]

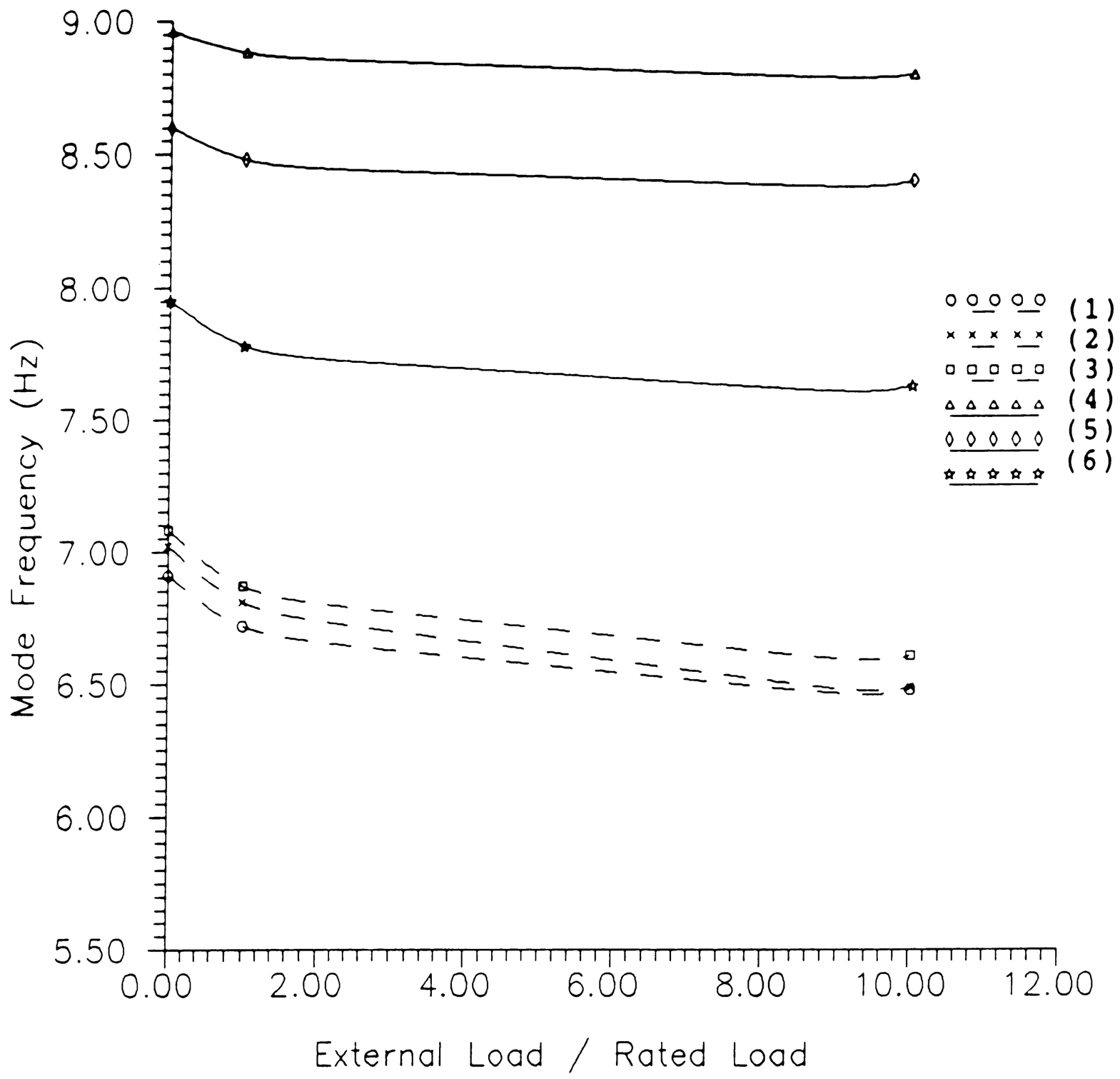

(1) Brakes OFF : 0 deg
(2) Brakes OFF : 45 deg
(3) Brakes OFF : 90 deg
(4) Brakes ON : 0 deg
(5) Brakes ON : 45 deg
(6) Brakes ON : 90 deg

Fig 3.47 : Mode Frequencies for Shape IV [Out-of-plane Resist]

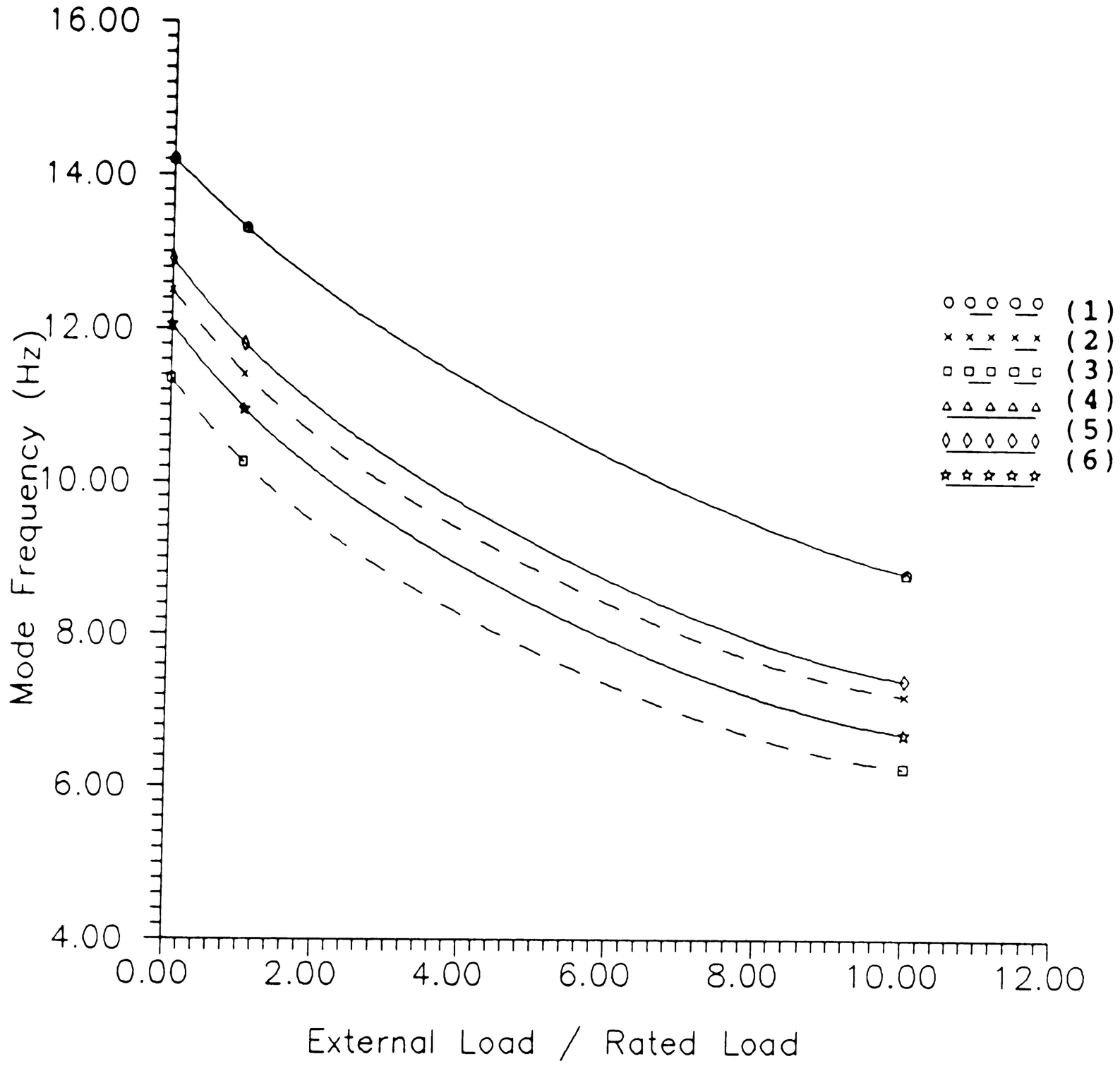

(1) Brakes OFF : 0 deg
(2) Brakes OFF : 45 deg
(3) Brakes OFF : 90 deg
(4) Brakes ON : 0 deg
(5) Brakes ON : 45 deg
(6) Brakes ON : 90 deg

Fig 3.48 : Mode Frequencies for Shape V [Vertical Chop Assist]

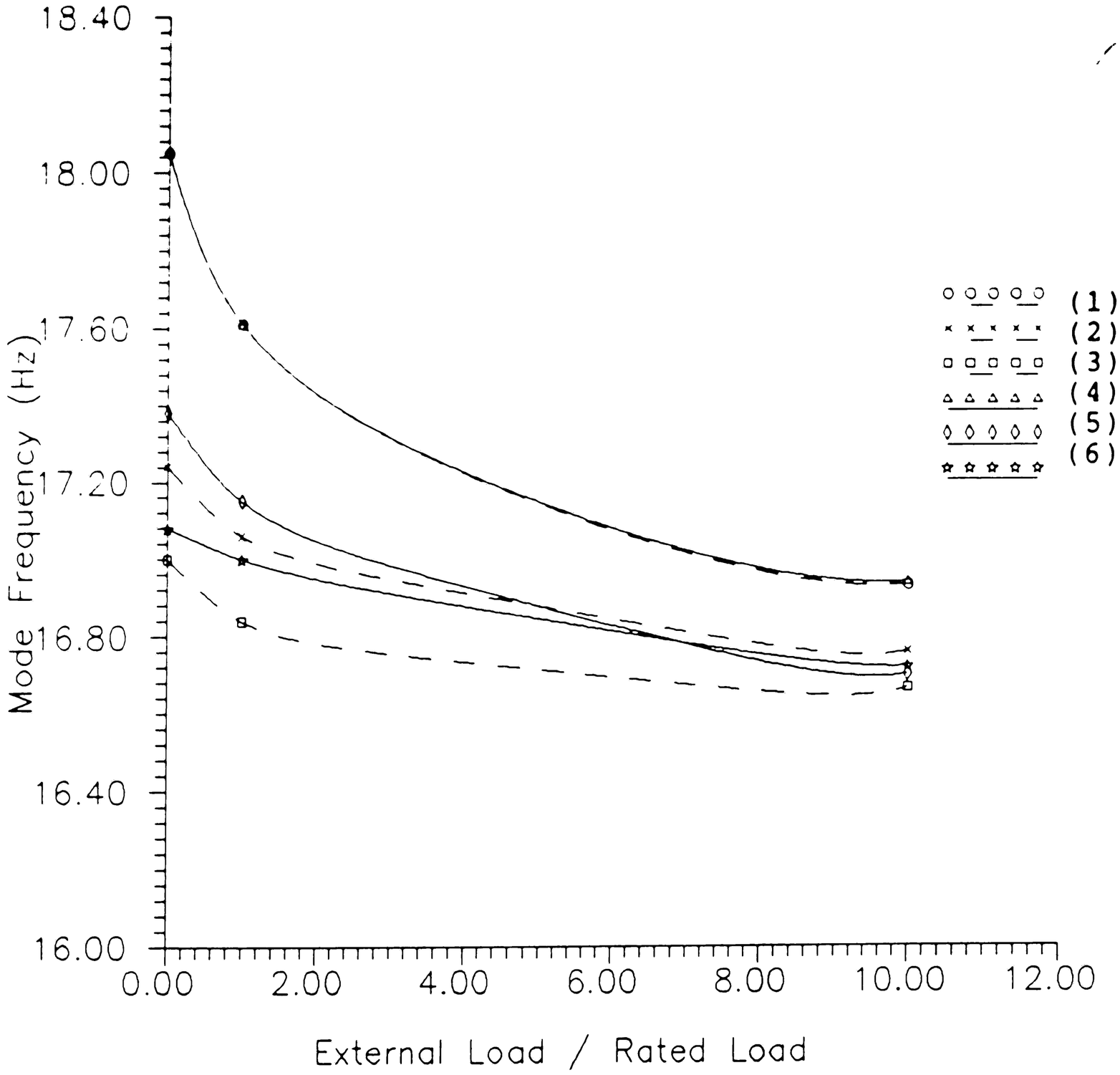

(1) Brakes OFF : 0 deg
(2) Brakes OFF : 45 deg
(3) Brakes OFF : 90 deg
(4) Brakes ON : 0 deg
(5) Brakes ON : 45 deg
(6) Brakes ON : 90 deg

Fig 3.49 : Mode Frequencies for Shape VI [Vertical Chop Resist]

3.4.1.2.3 Drive System Torque Calculations

Calculations were made to determine the torque required (at the supports at nodes # 1 & 3) to rotate the manipulator arm a full 180° within two minutes in the fully extended configuration. A maximum velocity of 24 ft/min was assumed. The centroid location and the various Moments of Inertia were also calculated (in the fully extended position) as follows --

Centroid Location (inch)	Moment of Inertia about Origin ($lb\text{-}sec^2.in$)	Moment of Inertia about Centroid ($lb\text{-}sec^2.in$)
X = 104.76 Y = 19.661 Z = 0.0	Ixx = 2858. Iyy = 25540 Izz = 28230 Ixy = -1856. Iyz = 0.0 Izx = 0.0	Ixx = 2168. Iyy = 5943. Izz = 7942. Ixy = 1822. Iyz = 0.0 Izx = 0.0

The angular displacement curve for the manipulator arm can be assumed to consist of three regions : an initial region of constant acceleration, a region of constant angular velocity, and a region of constant deceleration.

From Fig 4.50,

Angular Displacement is given as

$$\theta = 1/2\ \alpha\ t_{acc}^2 + \omega\ (T - 2t_{acc}) + 1/2\ \alpha\ t_{acc}^2$$

Angular Velocity is given as

$$\omega = \alpha\ t_{acc}$$

Hence by substitution we get,

$$\theta = \omega\, t_{acc} + \omega\,(T - 2t_{acc})$$

$$= \omega\,(T - t_{acc})$$

Now we know that the limiting linear velocity for the system is 24 ft/min.

Hence we get,

$$\omega = \frac{24 \text{ ft/min}}{14 \text{ ft}} * \frac{\text{min}}{60 \text{ sec}}$$

$$= 0.0286 \text{ rad /sec}$$

Therefore, by rearranging and substitution:

$$t_{acc} = T - \theta / \omega$$

$$= 120 - \pi / .0286$$

$$= 10.15 \text{ sec}$$

$$\alpha = \omega / t_{acc}$$

$$= 0286 / 10.15$$

$$= .0286 / 10.15$$

$$= .002817 \text{ rad/sec}^2$$

Hence the torque required about the vertical axis at link 1-3, is given as

$$T_y = Iyy * \alpha$$

$$= 25540 \text{ lb-sec}^2\text{in} * .002817 \text{ rad/sec}^2$$

$$= 71.83 \text{ lb-in}$$

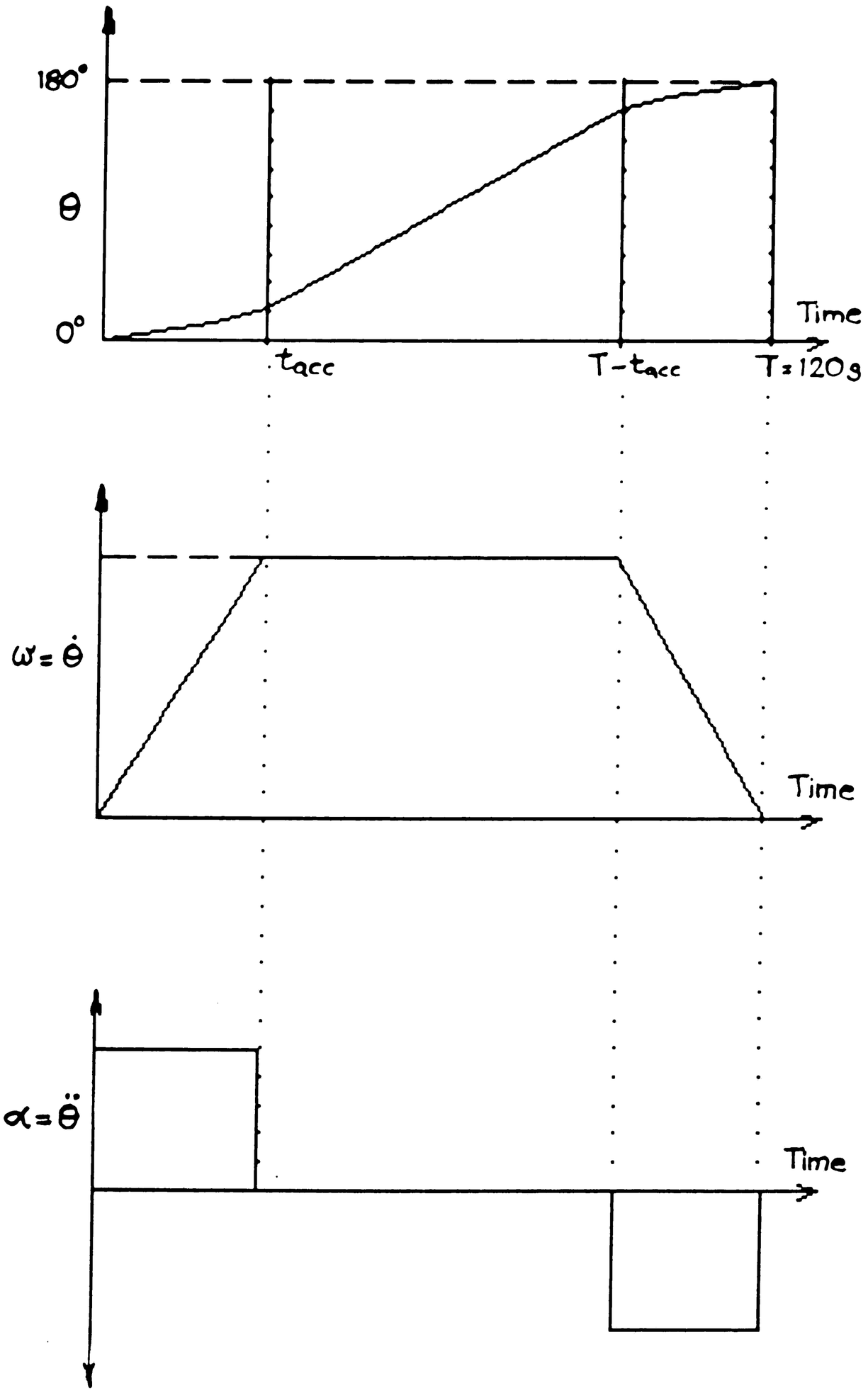

Fig 4.50 : Tenth Scale Arm -- Angular Displacement, Velocity and Acceleration at Upper Arm Support

3.4.2 Full Scale Manipulator Arm Design

3.4.2.1 Design Details

The preliminary design of the manipulator arm was kept similar to both the original conceptual design and the preliminary design of the tenth scale model. Conceptual design studies showed relatively high static and dynamic stresses in most members of the upper arm and steps were therefore taken to lighten the load on the upper arm by reducing the weight of the members of the forearm.

Structural steel angles were changed to be aluminium pipe sections, since this shape is best for resisting side loads in any direction and the moment of inertia is higher for any given cross sectional area. The depth of the horizontal basic-frame structures of the upperarm were are increased in the middle section to reduce the stress under bending loads due to self-weight. Aluminium was found to be a better choice for material when the structural weight is a problem. Aluminium pipe is available as 6061-T6 alloy/temper in drawn condition with an ultimate tensile strength of 42,000 psi and yield strength of 35,000 psi[53]. Since the yield strength of the 6061-T6 Aluminium is equal to that of most hot formed carbon steel shapes, a significant weight and stress reduction should be possible by switching to aluminium tubing for building up the basic-frame structures.

The top and bottom basic-frame structures of the upperarm are conservatively designed using 8" schedule 40 aluminium pipe, 6061-T6 drawn condition as the longitudinal members. The depth of the section of the subassemblies varied from 24 inches at the ends to 96 inches at the center. The diagonal and transverse members are 3 1/2" schedule 40 pipe, with the general arrangement being similar to the original

design in other respects. The number of transverse elements was increased to provide a brace at each node, providing a degree of redundancy. Some transverse members may, however, be removed in the final design.

The support structure must provide a rigid support for the manipulator arm as it moves to various configurations, and it must also provide a rigid attachment point for the upper arm drive system. The initial approach for the tenth scale arm, using an offset torque tube and brackets to support the two bearing assemblies, had a significant vertical displacement of the arm under loading. This tendency is reduced by eliminating the brackets and directly supporting the arm at the bearing assemblies, as shown in Fig 3.51. Links 1-3 and 2-4 were replaced by an octahedral element for added rigidity between the bearing assemblies at both upper and fore arm attachment points.

The dimensional changes made to the conceptual full-scale design to arrive at the preliminary design are summarized as in Table 3.9.

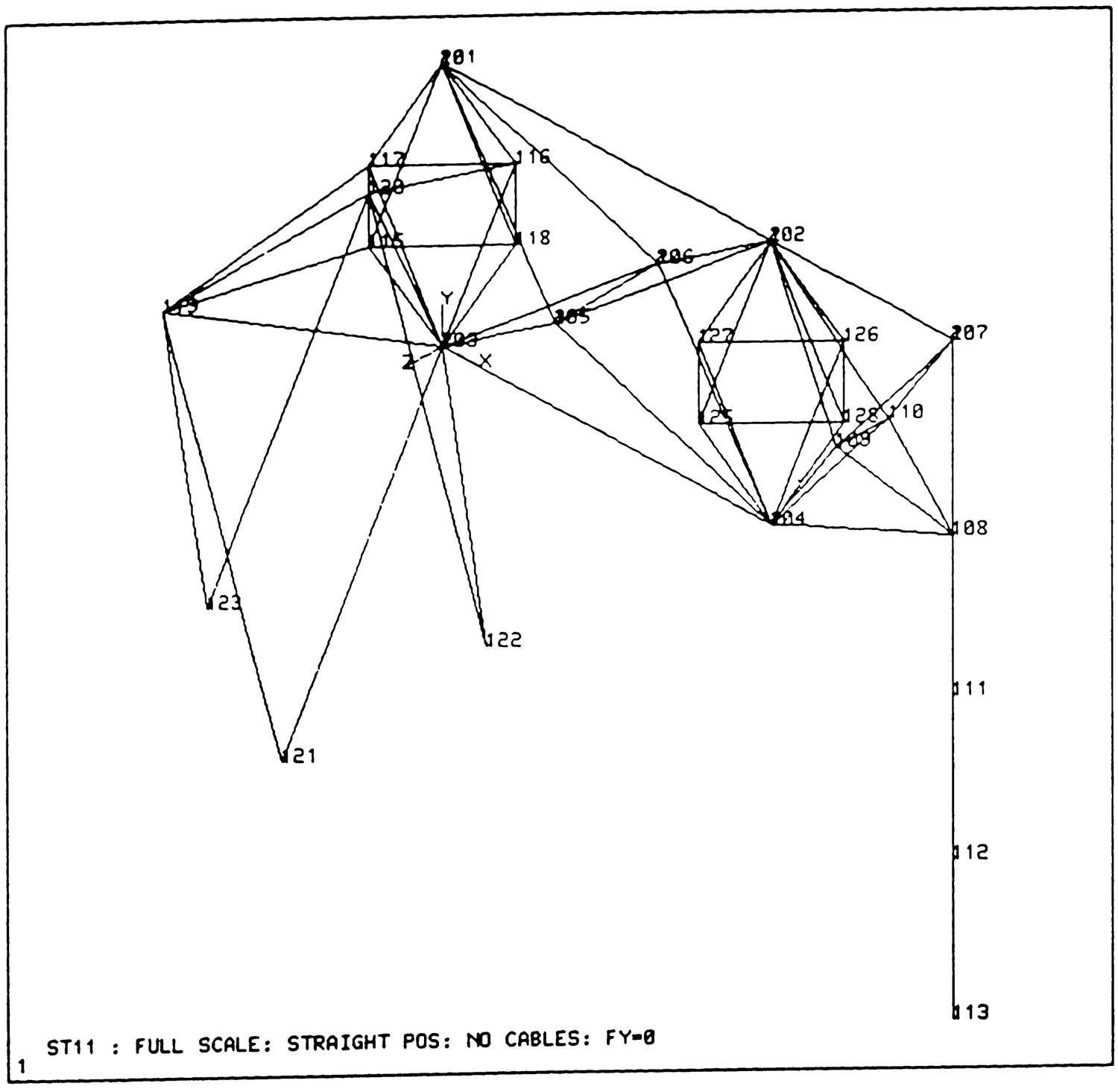

Fig 3.51 : Full Scale Arm -- Preliminary Design

Table 3.9 : Full-scale Arm Design Changes.

	CONCEPTUAL DESIGN	PRELIMINARY DESIGN
MATERIAL	Steel	Aluminium
SUBASSEMBLIES		
* Main Members	5x5x3/8 angle	8 in Schedule 40 pipe
. Min. rad of gyration	0.99 in	2.94 in
. Area	3.41 in^2	8.40 in^2
. Moment of Inertia	8.70 in^4	12.36 in^4
. Weight	12.3 lb/ft	9.88 lb/ft
* Auxiliary Members	3x3x5/16 angle	3 1/2 in Schedule 40 pipe
. Min. rad of gyration	0.59 in	1.34 in
. Area	1.78 in^2	2.68 in^2
. Moment of Inertia	1.50 in^4	4.78 in^4
. Weight	6.10 lb/ft	3.15 lb/ft
* Overall	60 in square	84 in square Max.
. Min. rad of gyration	24.5 in	34.3 in
. Area (Effective)	14.44 in^2	33.6 in^2
. Moment of Inertia	11695 in^4	77448 in^4
. Weight	90 lb/ft	60.5 lb/ft

3.4.2.2 Design Analysis

3.4.2.2.1 Static Analysis

Static analysis (Force / stress / displacement) was performed on the preliminary design of the full-scale manipulator arm for the following conditions :

A. Without drive system cables (fully extended and rotated configuation) --

1. Self-weight of manipulator arm only.

2. Self-weight + 70,000 lb at spreader bar.

3. Self-weight + 700,000 lb at spreader bar.

B. With drive system cables (fully extended configuration only) --

1. No self-weight or external load, but with a cable preload of 500 lb.

The drive system cables were not included in the Group A analysis to exclude the effect of their prestress on the behavior of the manipulator. Since the prestress on the cable would be applied only after erecting the manipulator, one should take the cumulative effect of Group B results with the appropriate category in Group A to get an estimate of the effect of prestress.

The results of the static analysis can be summed as follows --

Table 3.10 : Full Scale Preliminary Design -- Static Analysis Results.

	Load Condition					
	NO LOAD		70 kip		700 kip	
Forearm Position	Extended	Rotated	Extended	Rotated	Extended	Rotated
Max. σ_1	5733	6834	8439	10727	32795	45759
Min. σ_1	-5105	-6255	-7736	-9857	-31419	-42278
Y Disp. @ 13	-4.189	-5.848	-6.105	-9.137	-23.36	-38.74

Details of displacements and stress variations for the above conditions are shown in Fig 3.52 - 3.57. Fig 3.58 (a & b) shows the effect of cable prestress. The results show that the cables do not have a significant effect on the manipulator displacements or stresses and hence the figures given in Fig 3.52 through 3.57 can be considered an accurate representation of the overall performance of the manipulator.

3.4.2.2.2 Modal Analysis

A modal analysis was run for the full-scale manipulator arm in the no load condition, with brakes off, for comparison with the similar results for the tenth scale arm. This condition was selected since it gave the lowest mode frequency amongst all other conditions for the tenth scale design. Each of the first seven modes for the full-scale arm are plotted and compared with the six general mode shapes obtained in the tenth-scale analysis. Plots of the mode shapes are shown in Fig 4.59 (a-g).

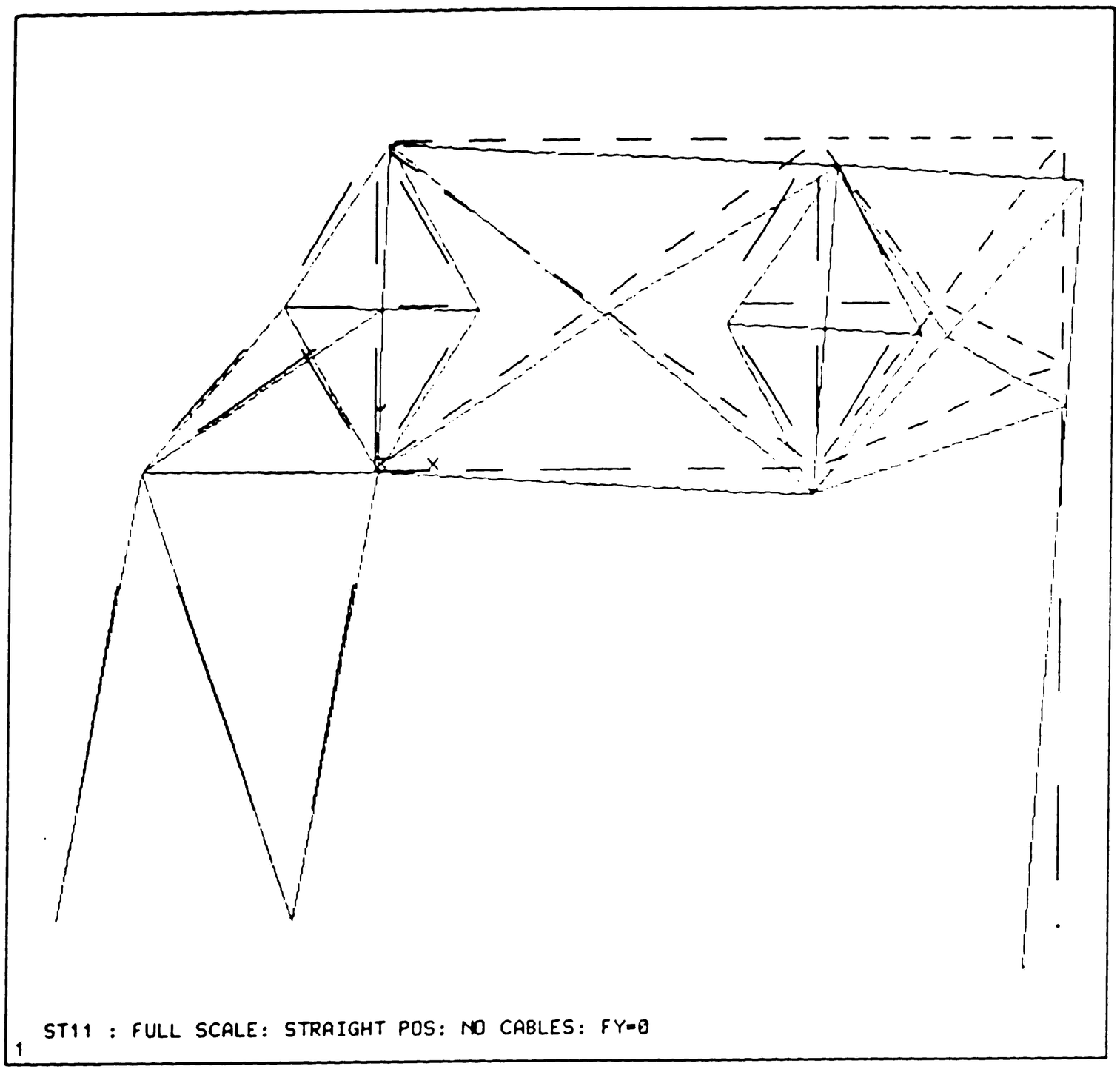

MAXIMUMS

NODE	113	113	119	509	409	403
VALUE	-3.093	-4.189	-0.1519E-01	-0.9348E-02	-0.1271E-01	-0.2879E-02

POST1 -INP=

Fig 3.52 (a) : Full Scale Arm -- Displacements with Self-weight Only

[Extended Position]

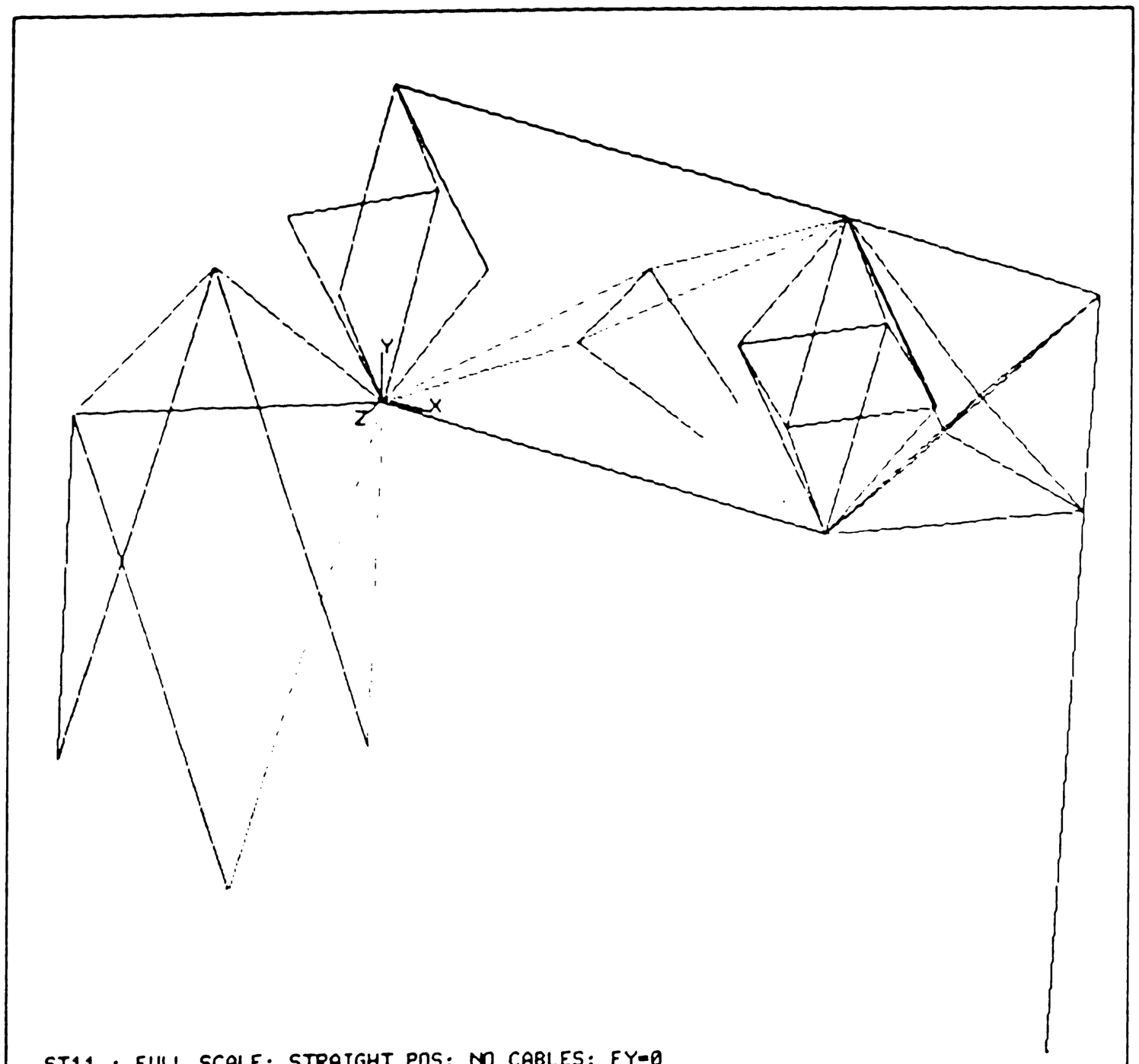

ANSYS 4.3
AUG 12 1988
14:44:24
POST1 STRESS
STEP=1
ITER=1
CIG1 (NOAUG)

XV=.5
YV=.7
ZV=1
DIST=1204
XF=473
YF=-252
ZF=34.3
MX=5733
MN=-5105
A=-3303
B=-2638
[illegible]
D=-223
E=317
F=2122

I=5733

NODE	FX	FY	FZ	MX	MY	MZ
121	0.3938E+05	0.5347E+06	-0.1226E+06			
122	0.3938E+05	0.5347E+06	0.1226E+06			
123	-0.7875E+05	-0.4531E+06	-0.2547E-10			
TOTAL	0.3775E-07	0.6164E+06	0.5821E-10	0.0000E+00	0.0000E+00	0.0000E+00

Fig 3.52 (b) : Full Scale Arm -- Stresses with Self-weight Only

[Extended Position]

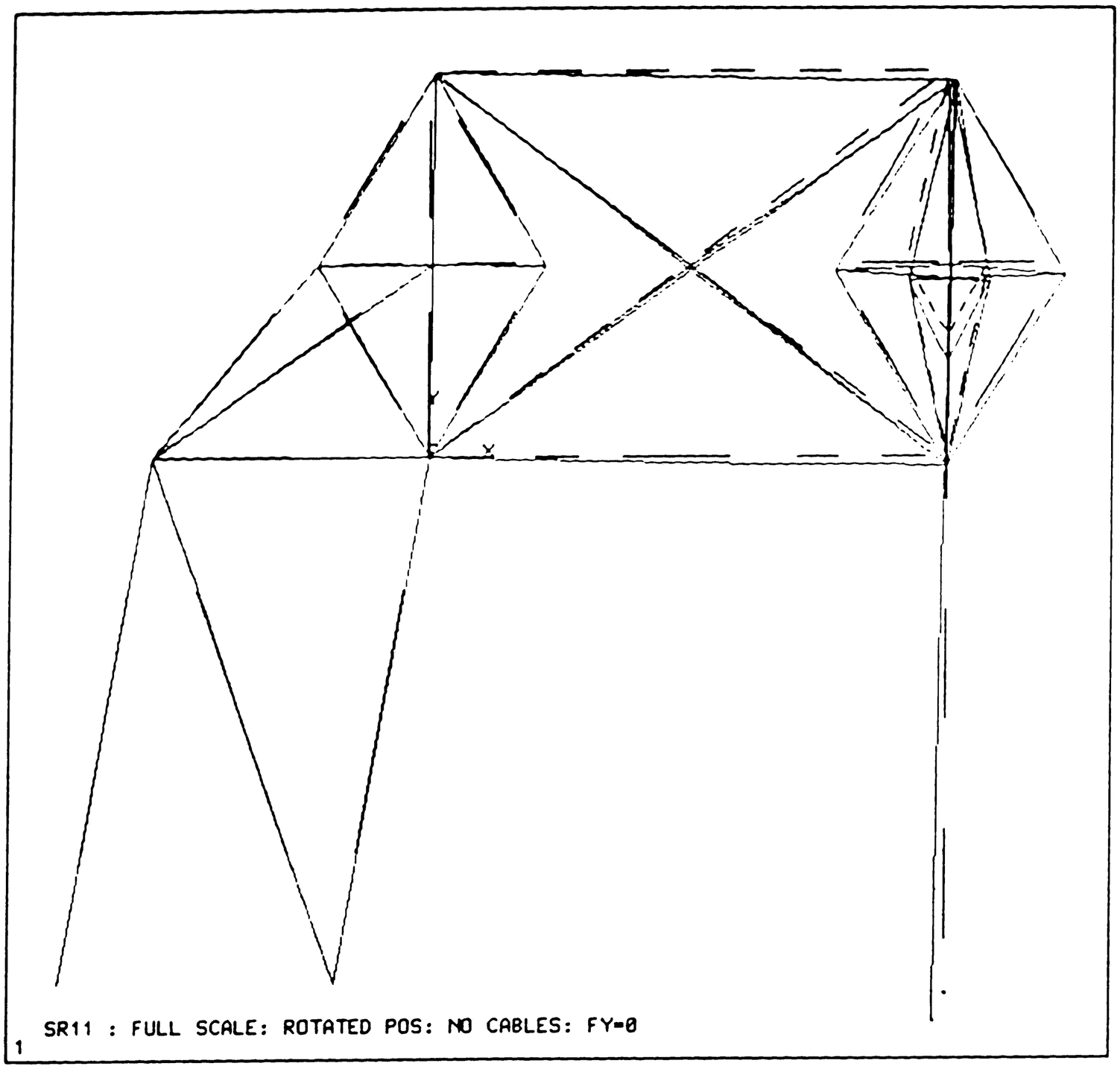

MAXIMUMS

NODE	113	113	113	110	1023	702
VALUE	-2.409	-5.848	-9.508	3.316	-0.2734E-02	-43.93

```
POST1 -INP=
pldisp,1
```

Fig 3.53 (a) : Full Scale Arm -- Displacements with Self-weight Only [Rotated Position]

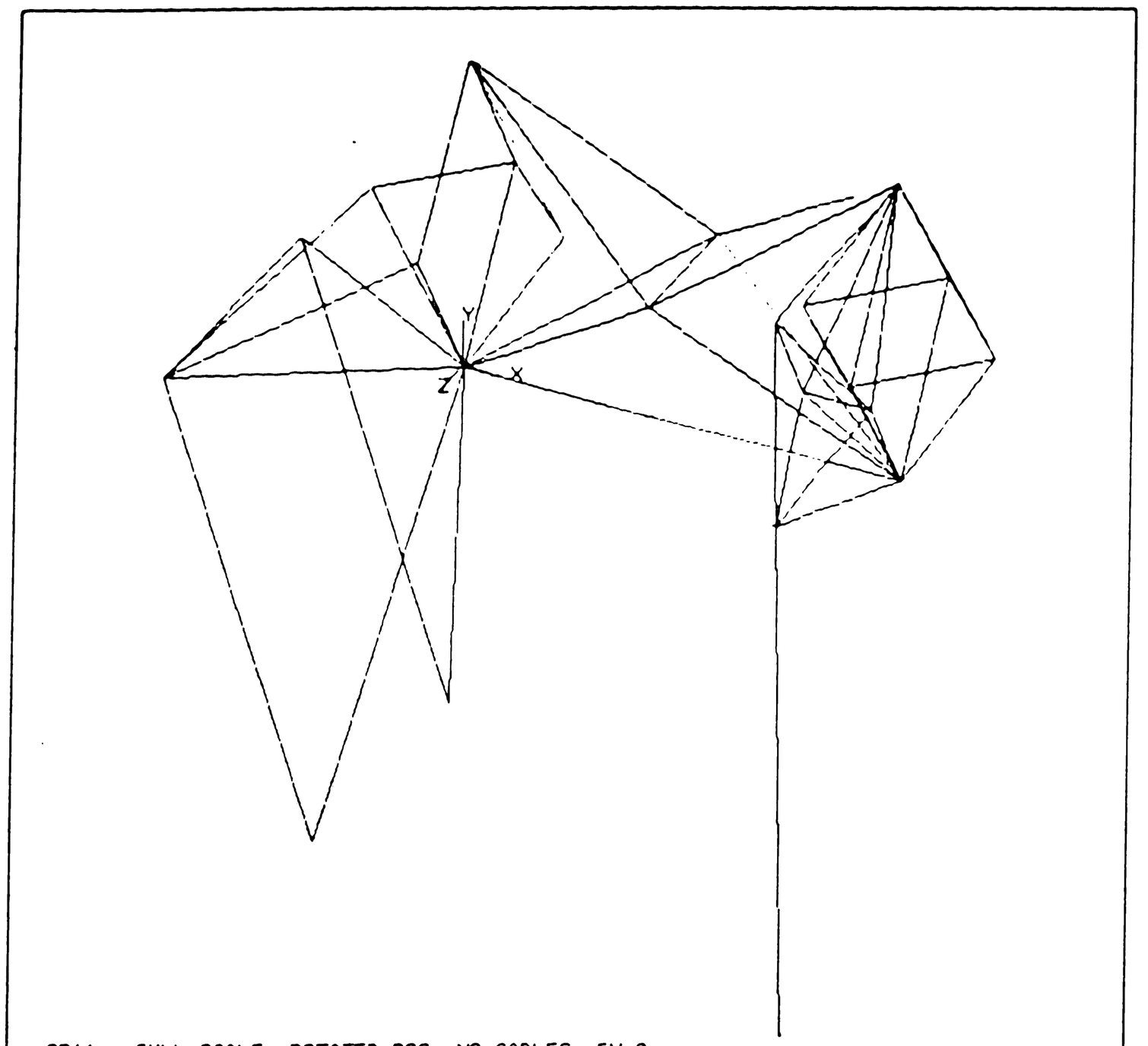

ANSYS 4.3
AUG 12 1988
17:12:43
POST1 STRES
STEP=1
ITER=1
CIG1 (NOAUG

XV=.5
YV=.7
ZV=1
DIST=1237
XF=389
YF=-252
ZF=226
MX=6834
MN=-6255
A=-4803
B=-3348
C=-1893
D=-438
E=1017
F=2472

I=6834

NODE	FX	FY	FZ	MX	MY	MZ
121	0.1462E+05	0.5740E+06	-0.1157E+06			
122	0.4580E+05	0.3853E+06	0.9748E+05			
123	-0.6042E+05	-0.3430E+06	0.1819E+05			
TOTAL	0.3401E-07	0.6164E+06	0.4899E-08	0.0000E+00	0.0000E+00	0.0000E+00

Fig 3.53 (b) : Full Scale Arm -- Stresses with Self-weight Only [Rotated Position]

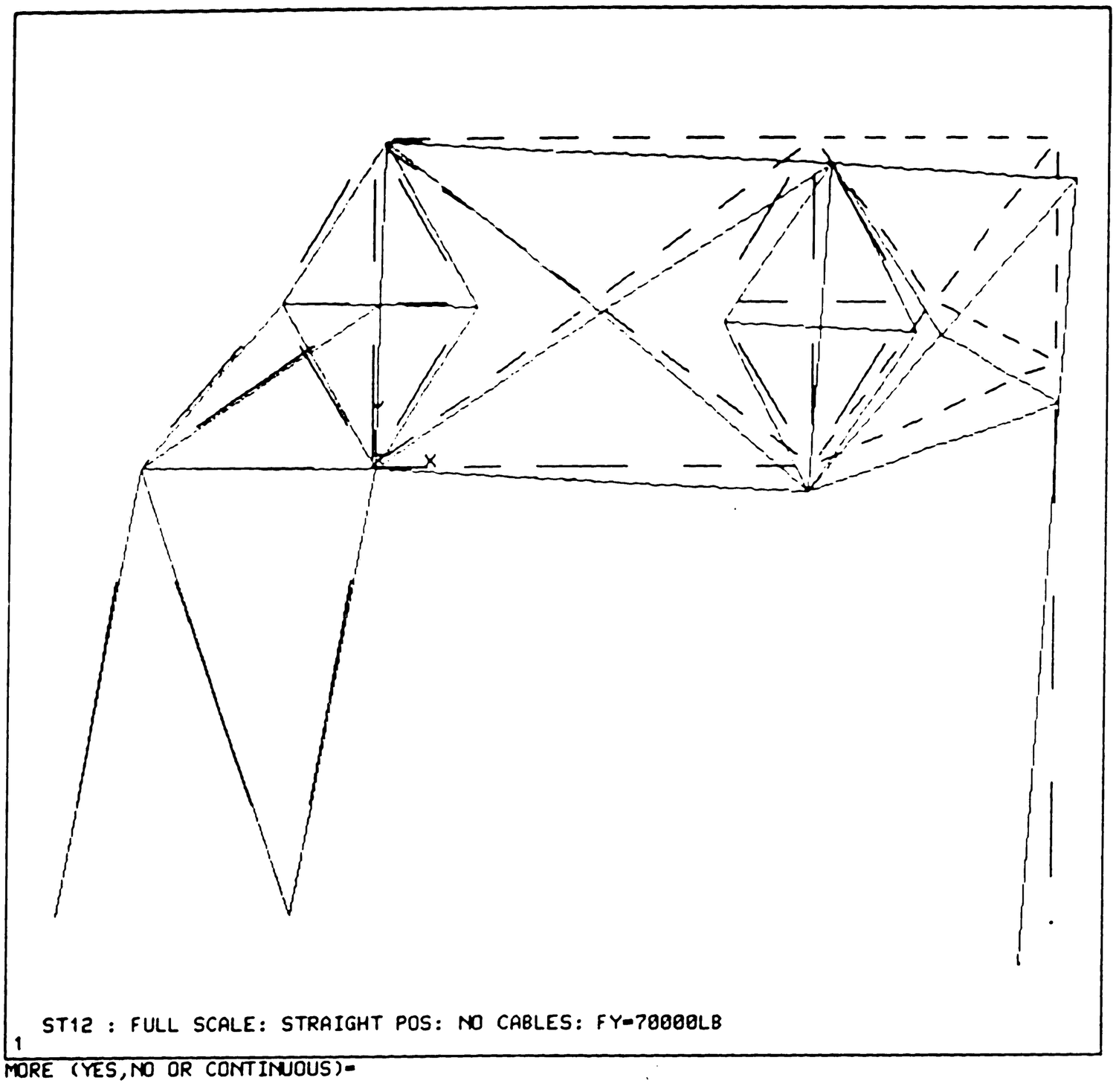

MAXIMUMS

NODE	113	113	119	509	409	505
VALUE	-4.627	-6.105	-0.2179E-01	-0.1389E-01	-0.1876E-01	-0.4029E-02

POST1 -INP=

Fig 3.54 (a): Full Scale Arm -- Displacements with Self-weight & 70 kips [Extended Position]

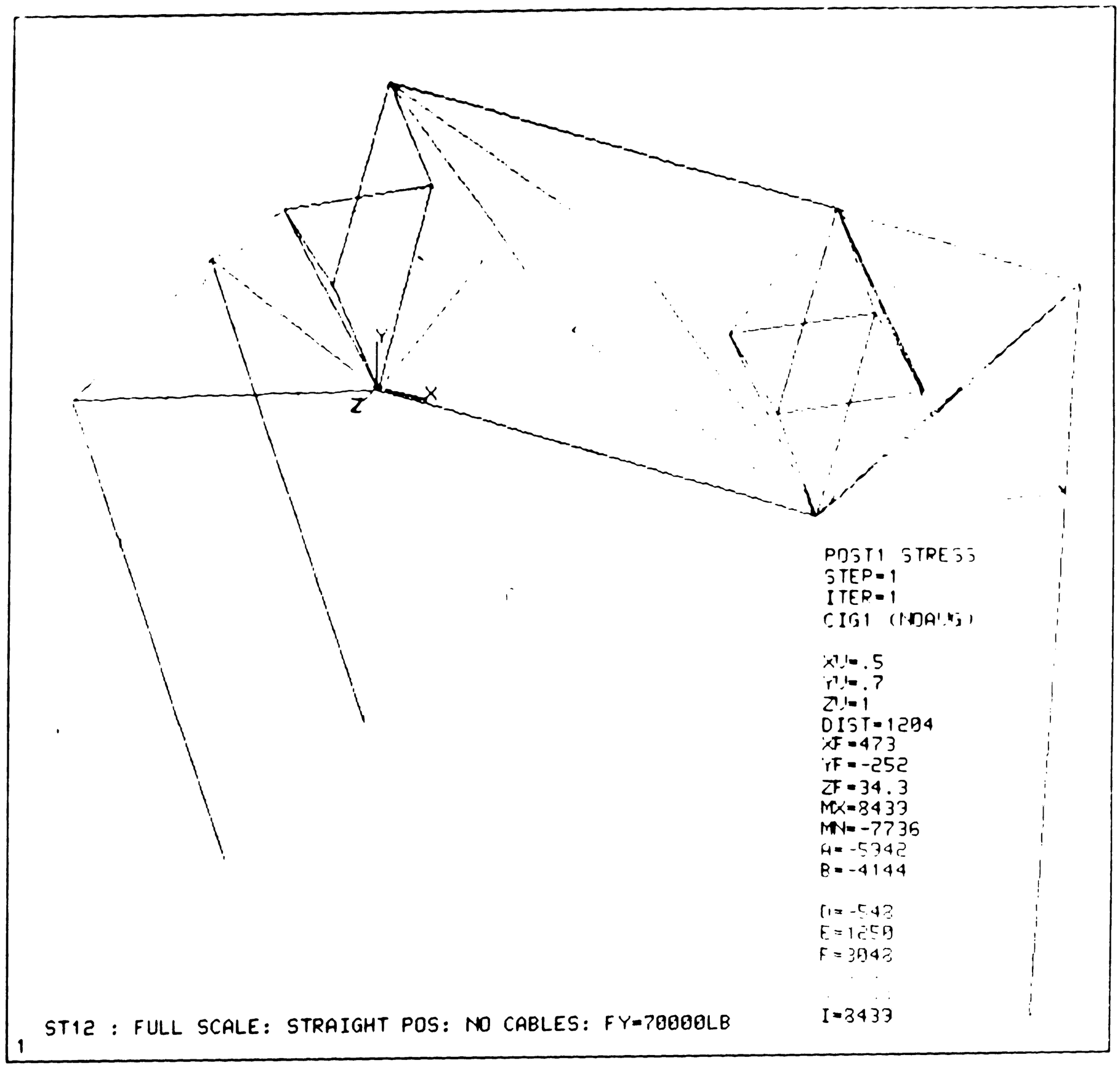

NODE	FX	FY	FZ	MX	MY	MZ
121	0.5831E+05	0.6835E+06	-0.1625E+06			
122	0.5831E+05	0.6835E+06	0.1625E+06			
123	-0.1166E+06	-0.6806E+06	-0.2728E-10			
TOTAL	0.3795E-07	0.6864E+06	0.8185E-10	0.0000E+00	0.0000E+00	0.0000E+00

Fig 3.54(b): Full Scale Arm -- Stresses with Self-weight & 70 kips

[Extended Position]

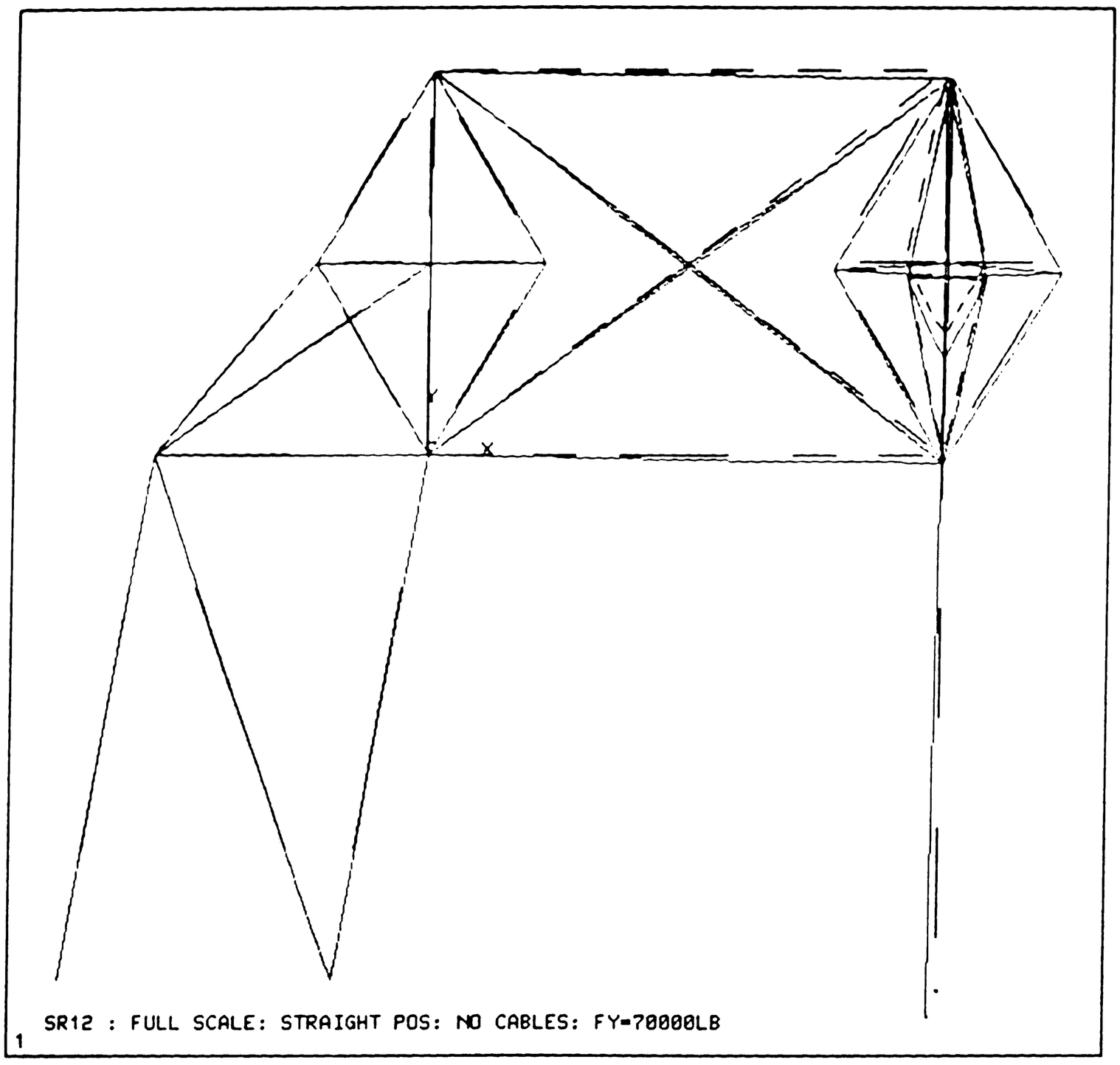

MAXIMUMS

NODE	113	113	113	110	1023	702
VALUE	-3.487	-9.137	-15.81	3.316	-0.4543E-02	-67.96

POST1 -INP=

Fig 3.55(a): Full Scale Arm -- Displacements with Self-weight & 70 kips [Rotated Position]

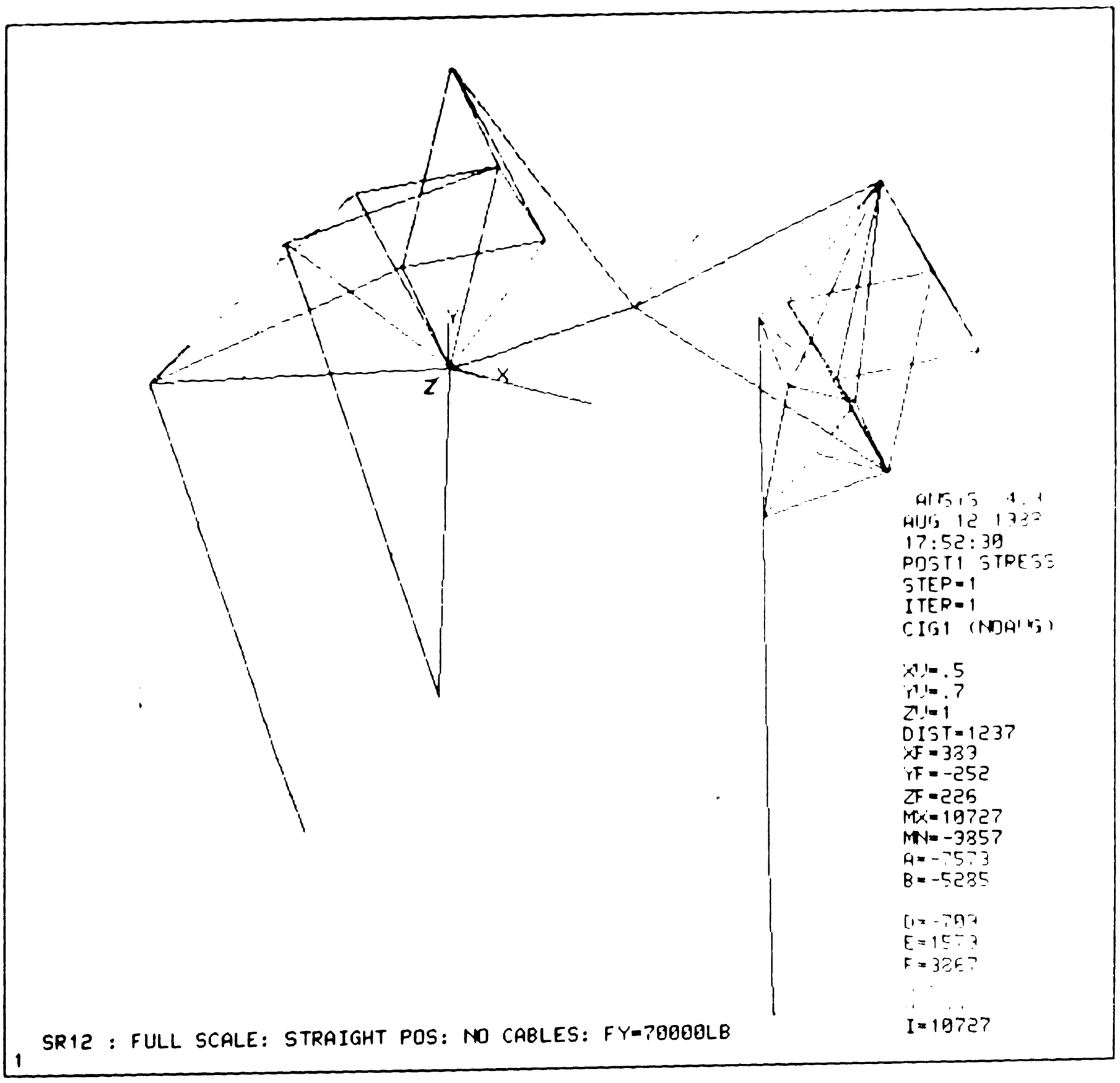

NODE	FX	FY	FZ	MX	MY	MZ
121	0.1716E+05	0.7488E+06	-0.1510E+06			
122	0.6899E+05	0.4350E+06	0.1208E+06			
123	-0.8615E+05	-0.4975E+06	0.3024E+05			
TOTAL	0.3425E-07	0.6864E+06	0.5578E-08	0.0000E+00	0.0000E+00	0.0000E+00

Fig 3.55(b): Full Scale Arm -- Stresses with Self-weight & 70 kips

[Rotated Position]

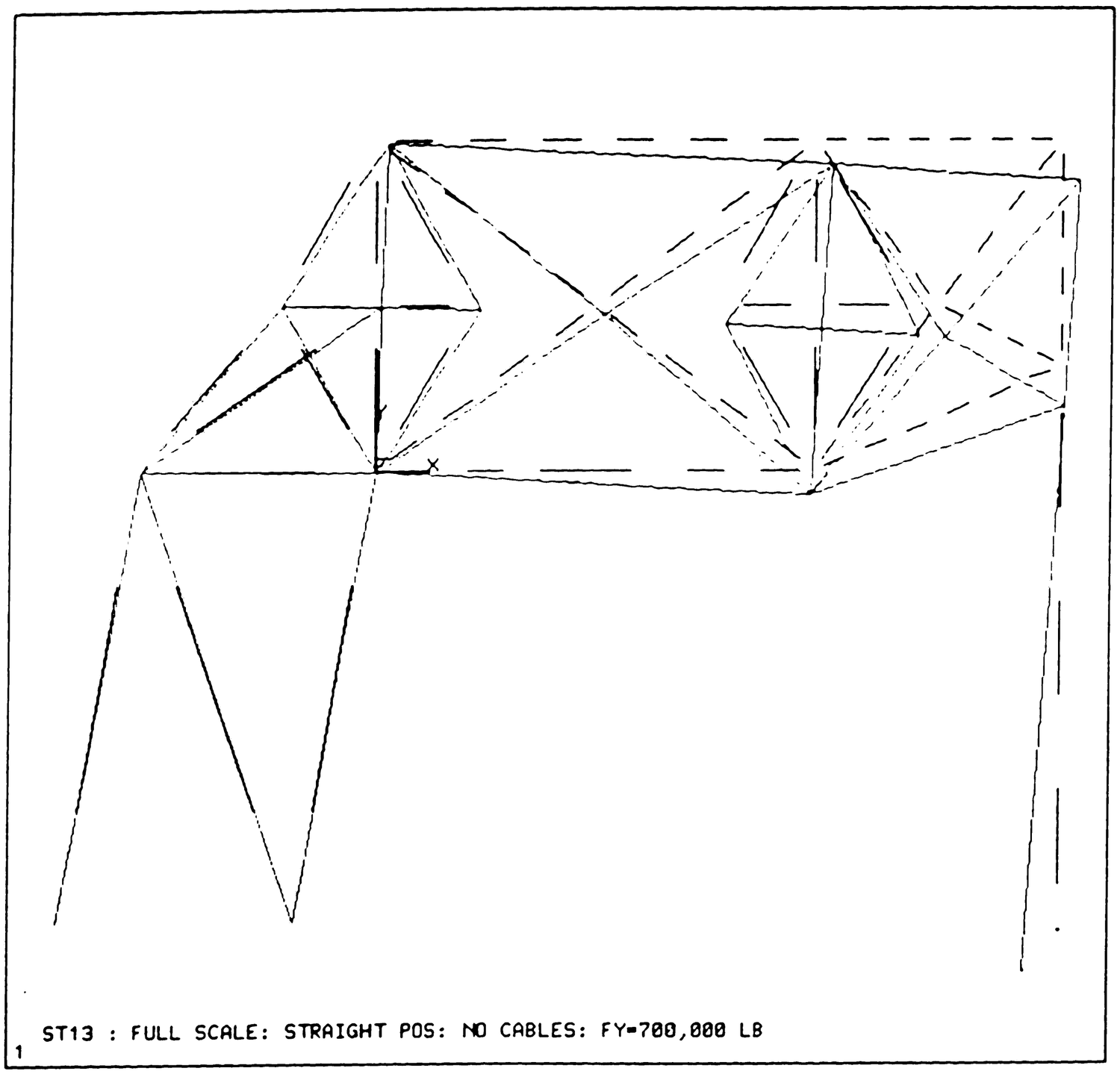

MAXIMUMS

NODE	113	113	119	509	409	702
VALUE	-18.44	-23.36	-0.8122E-01	-0.5476E-01	-0.7317E-01	-0.1525E-01

POST1 -INP=

Fig 3.56(a): Full Scale Arm -- Displacements with Self-weight & 700 kips [Extended Position]

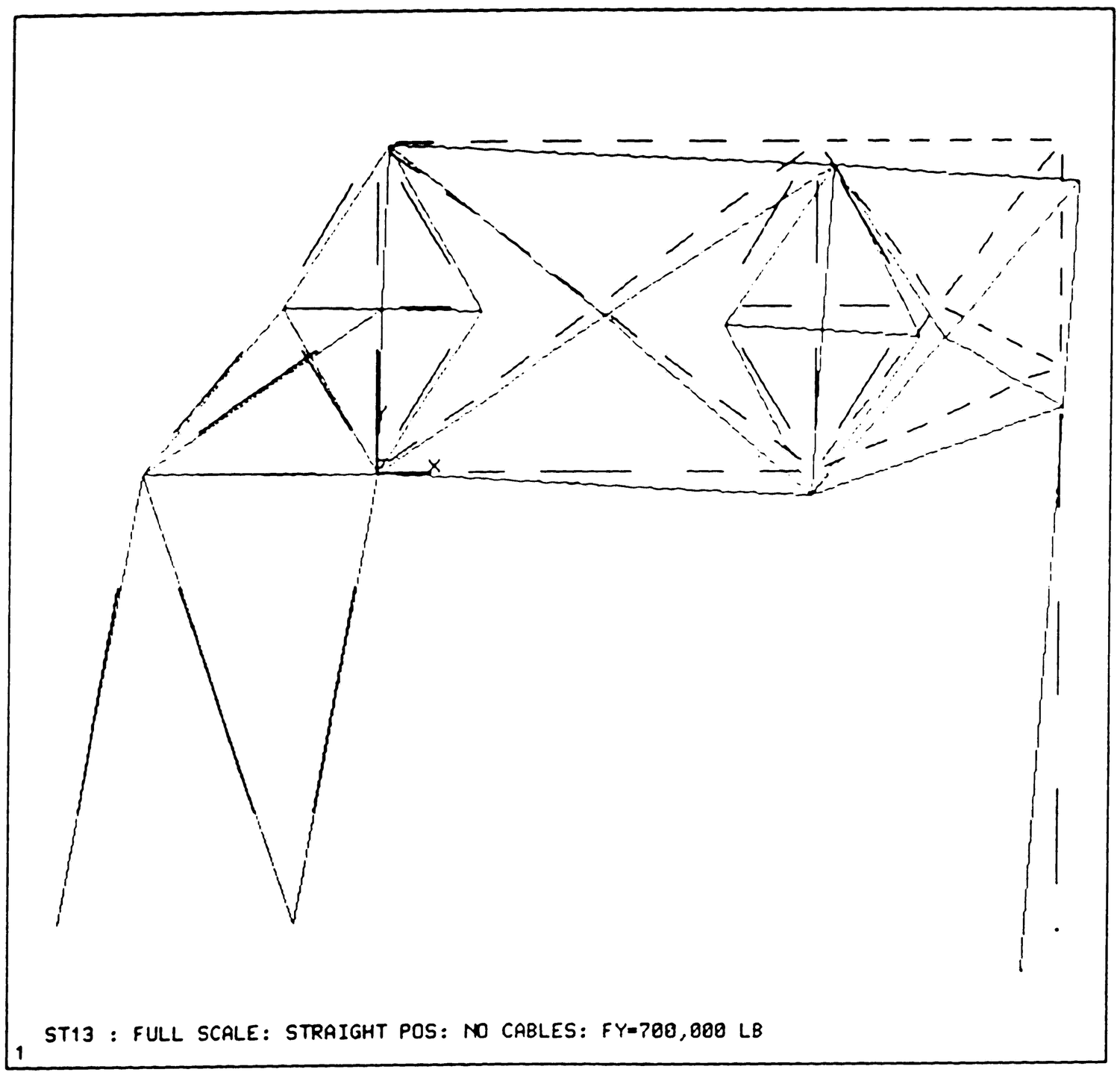

MAXIMUMS

NODE	113	113	119	509	409	702
VALUE	-18.44	-23.36	-0.8122E-01	-0.5476E-01	-0.7317E-01	-0.1525E-01

POST1 -INP=

Fig 3.56(a): Full Scale Arm -- Displacements with Self-weight & 700 kips

[Extended Position]

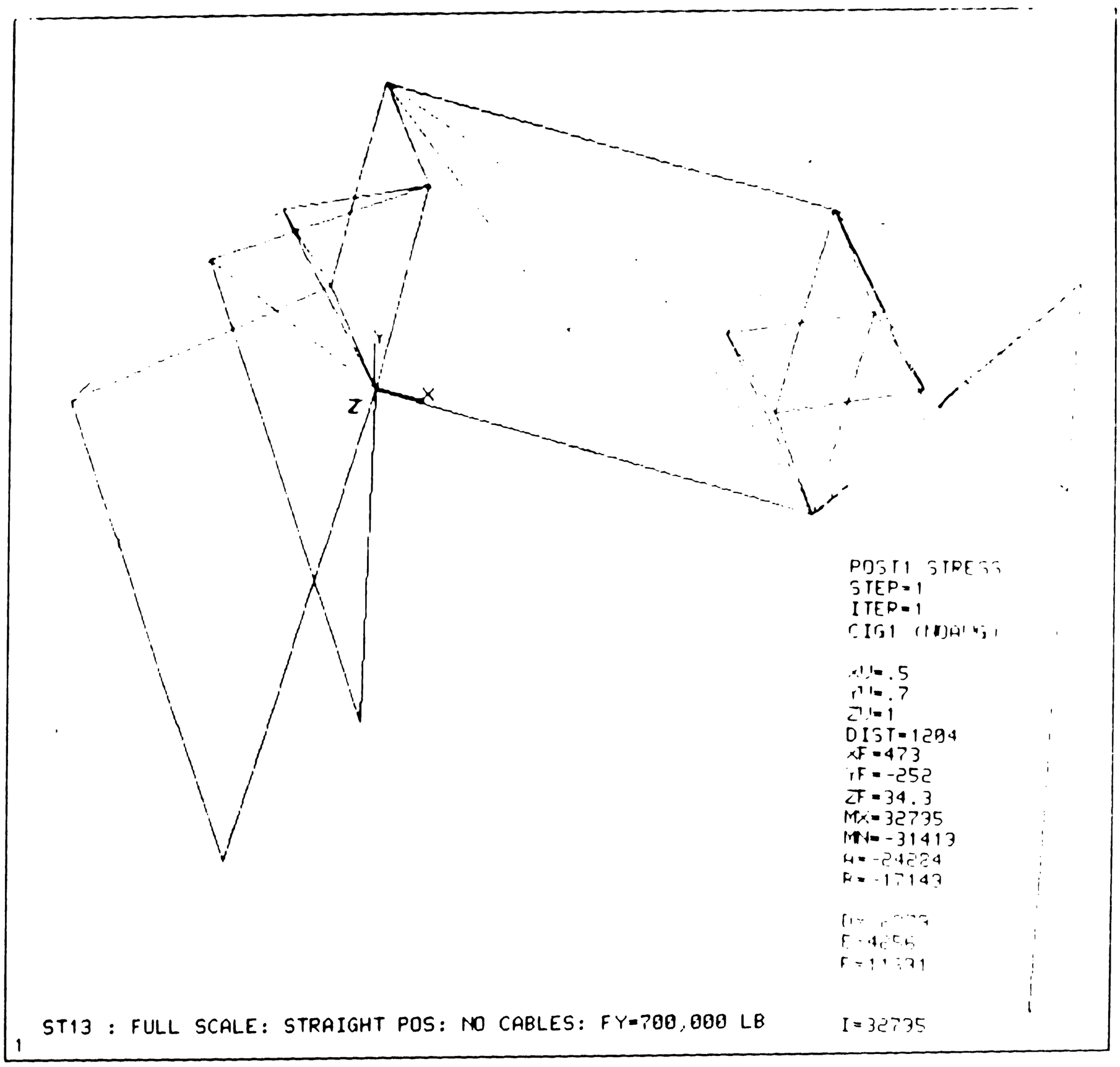

NODE	FX	FY	FZ	MX	MY	MZ
121	0.2287E+06	0.2022E+07	-0.5217E+06			
122	0.2287E+06	0.2022E+07	0.5217E+06			
123	-0.4575E+06	-0.2728E+07	-0.1091E-09			
TOTAL	0.4005E-07	0.1316E+07	0.2619E-09	0.0000E+00	0.0000E+00	0.0000E+00

Fig 3.56(b): Full Scale Arm -- Stresses with Self-weight & 700 kips

[Extended Position]

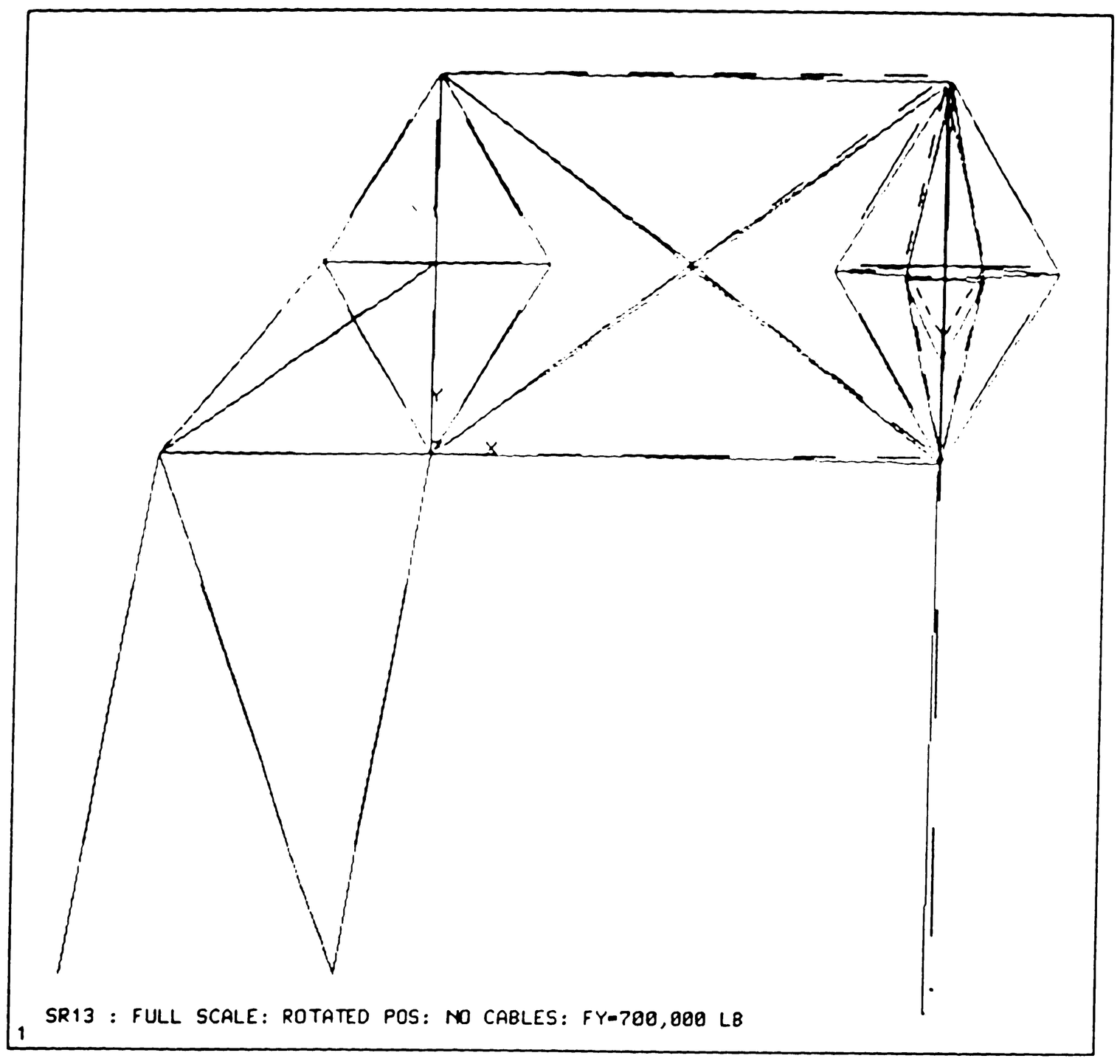

MAXIMUMS

NODE	113	113	113	110	1023	702
VALUE	-13.19	-38.74	-72.54	3.316	-0.2082E-01	-284.3

POST1 -INP=

Fig 3.57(a): Full Scale Arm -- Displacements with Self-weight & 700 kips [Rotated Position]

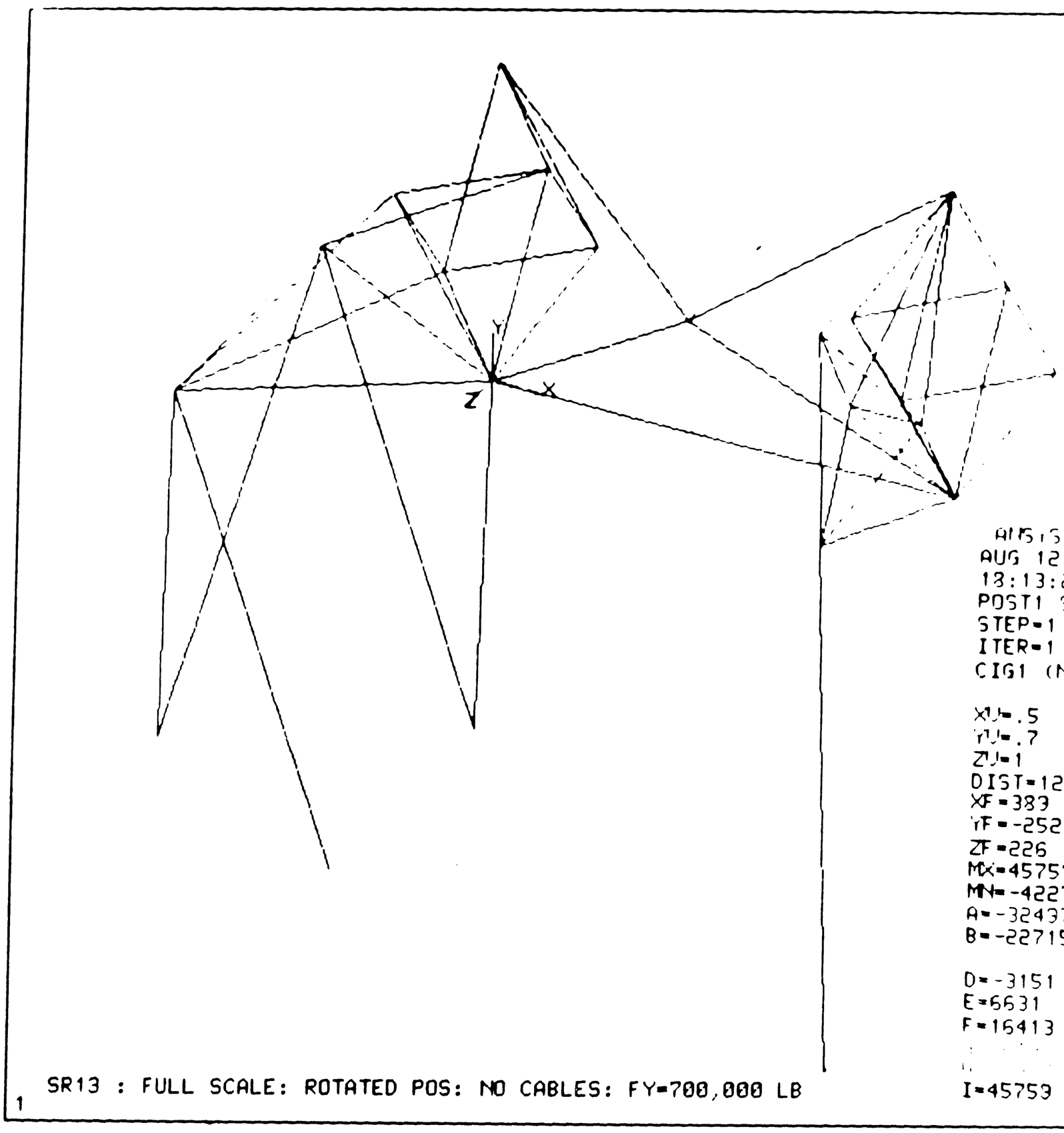

AUG 12 1988
18:13:28
POST1 STRESS
STEP=1
ITER=1
CIG1 (NOAUG)

XF=.5
YF=.7
ZF=1
DIST=1237
XF=383
YF=-252
ZF=226
MX=45753
MN=-42278
A=-32437
B=-22715

D=-3151
E=6631
F=16413

I=45753

SR13 : FULL SCALE: ROTATED POS: NO CABLES: FY=700,000 LB

NODE	FX	FY	FZ	MX	MY	MZ
121	0.4003E+05	0.2322E+07	-0.4689E+06			
122	0.2777E+06	0.8832E+06	0.3302E+06			
123	-0.3177E+06	-0.1889E+07	0.1386E+06			
TOTAL	0.3655E-07	0.1316E+07	0.1158E-07	0.0000E+00	0.0000E+00	0.0000E+00

Fig 3.57(b): Full Scale Arm -- Stresses with Self-weight & 700 kips [Rotated Position]

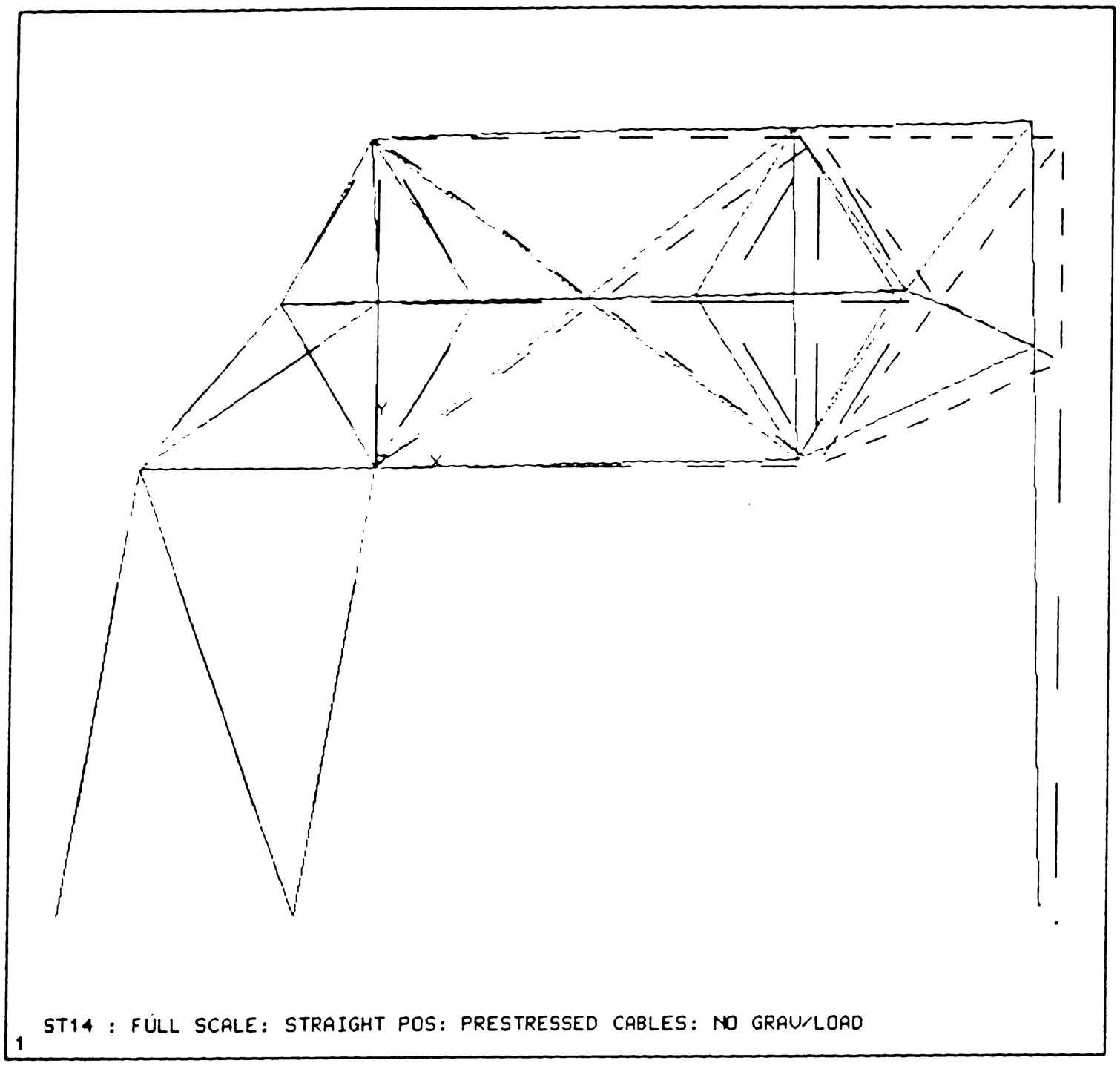

MAXIMUMS

NODE	110	108	125	308	510	604
VALUE	-0.1631E-02	0.8472E-03	-0.2071E-03	0.3782E-05	0.1933E-05	0.1531E-05

POST1 -INP=

Fig 3.58(a) : Full Scale Arm -- Effect of Cable Prestress on Displacements

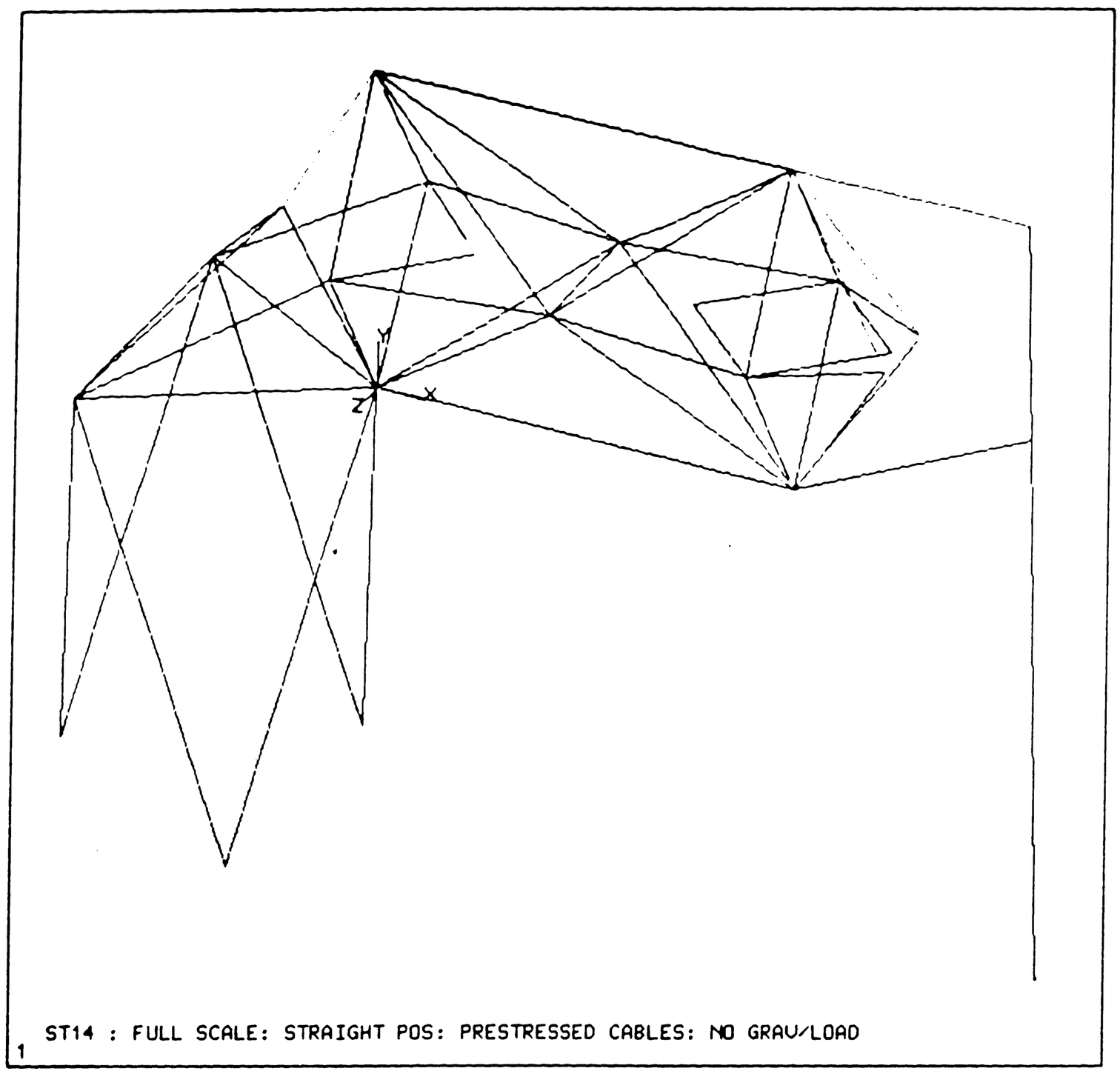

ANSYS 4.
AUG 12 19
16:27:13
POST1 STRE
STEP=1
ITER=1
CIG1 (NOAL

XV=.5
YV=.7
ZV=1
DIST=1284
XF=473
YF=-252
ZF=34.3
MX=7.26
MN=-8.97
A=-7.86
B=-5.86
D=-1.35
E=.141
F=2.14

I=7.26

ST14 : FULL SCALE: STRAIGHT POS: PRESTRESSED CABLES: NO GRAV/LOAD

1

NODE	FX	FY	FZ	MX	MY	MZ
121	-0.2792E-01	0.6308E-11	0.4895E-01			
122	-0.2792E-01	0.6626E-11	-0.4895E-01			
123	0.5584E-01	-0.1063E-10	-0.8427E-13			
TOTAL	-0.1119E-11	0.2306E-11	0.8117E-13	0.0000E+00	0.0000E+00	0.0000E+00

Fig 3.58(b) : Full Scale Arm -- Effect of Cable Prestress on Stresses

(a) Mode Shape #1

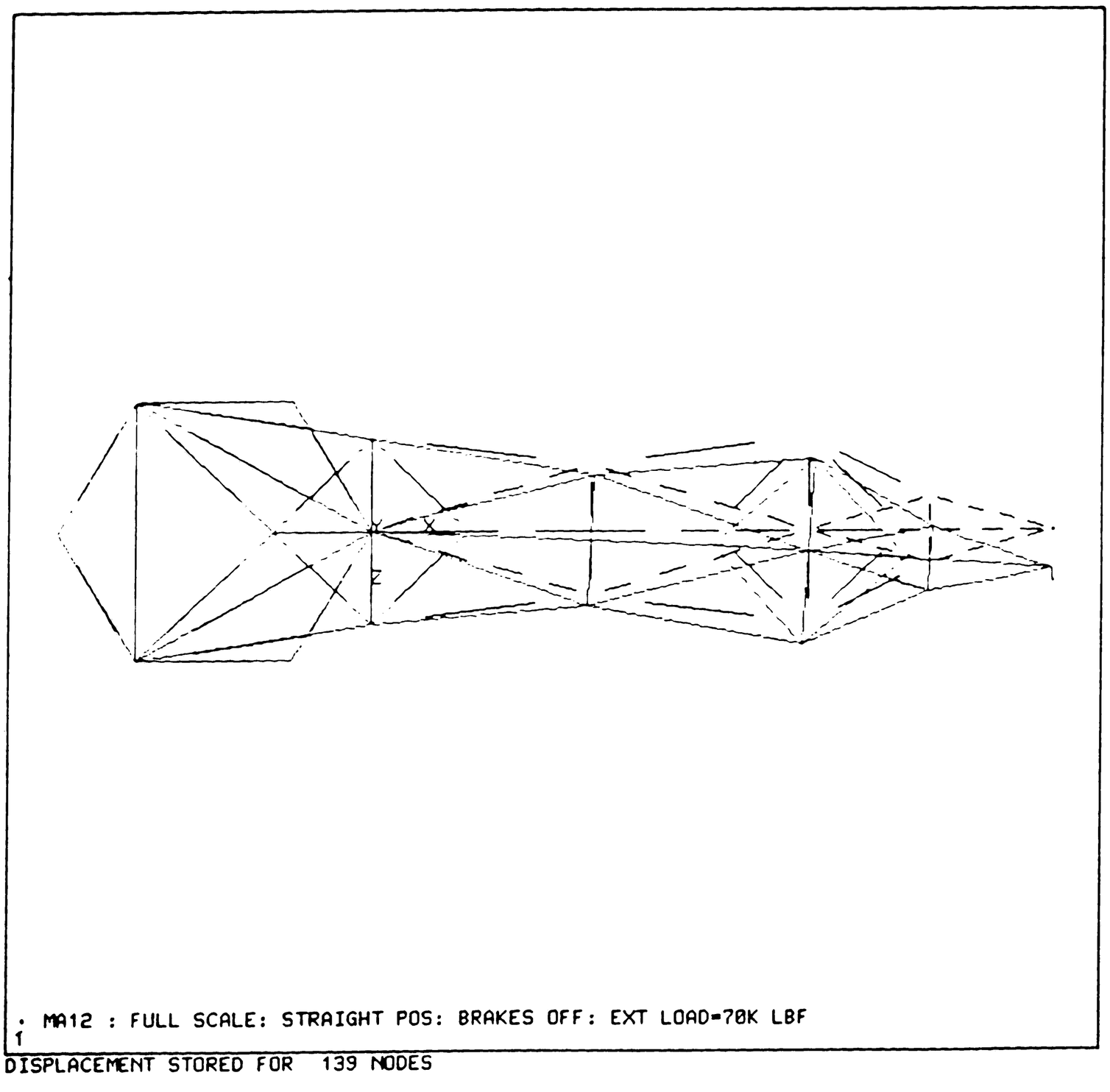

Fig 3.59 : Full Scale Arm -- Mode Shapes

(b) Mode Shape #2

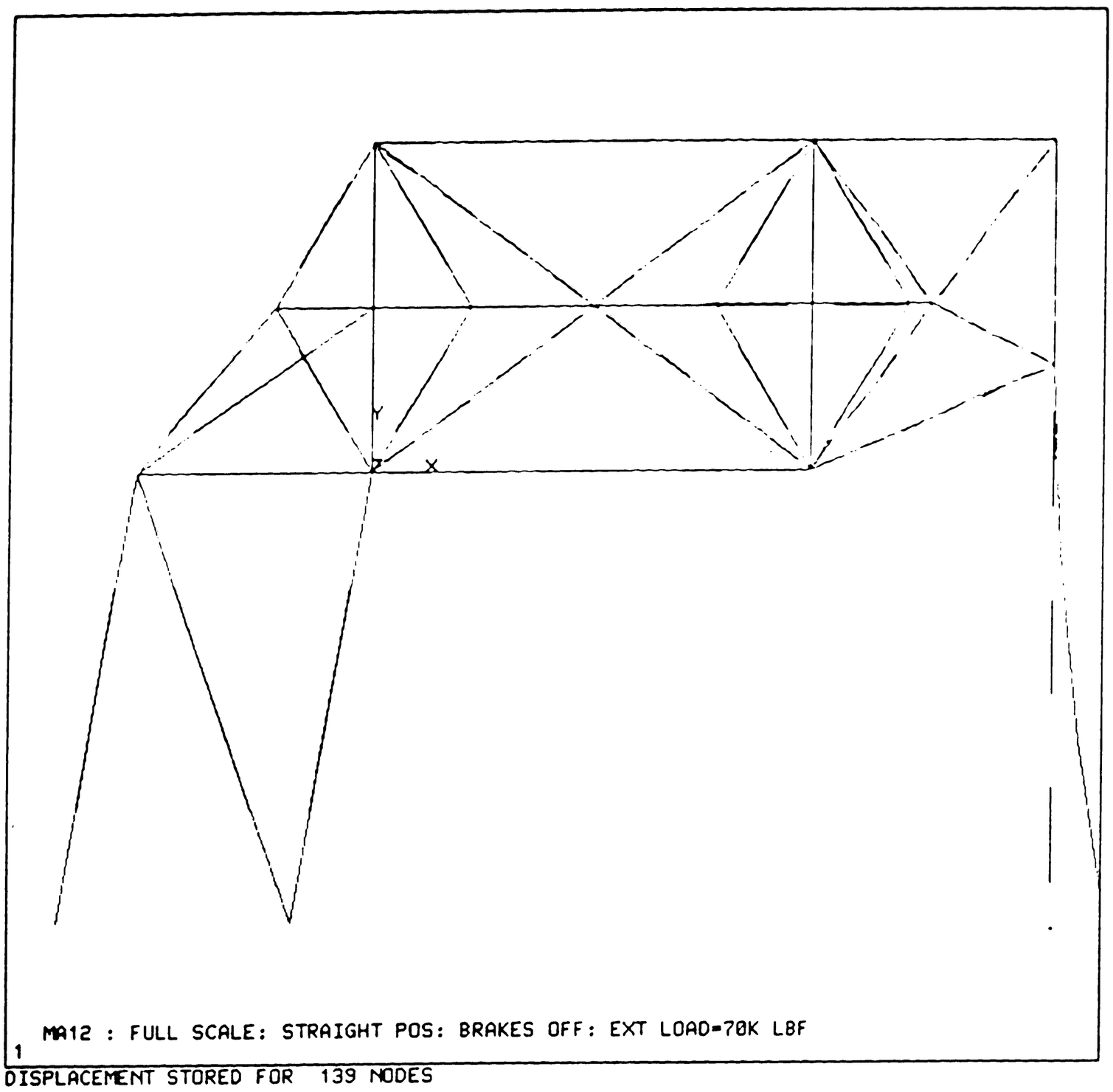

DISPLACEMENT STORED FOR 139 NODES

FOR LOAD STEP= 1 ITERATION= 2 SECTION= 1
FREQ= 0.159636 LOAD CASE= 1
TITLE= MA12 : FULL SCALE: STRAIGHT POS: BRAKES OFF: EXT LOAD=70K LBF

Fig 3.59 : Full Scale Arm -- Mode Shapes

(c) Mode Shape #3

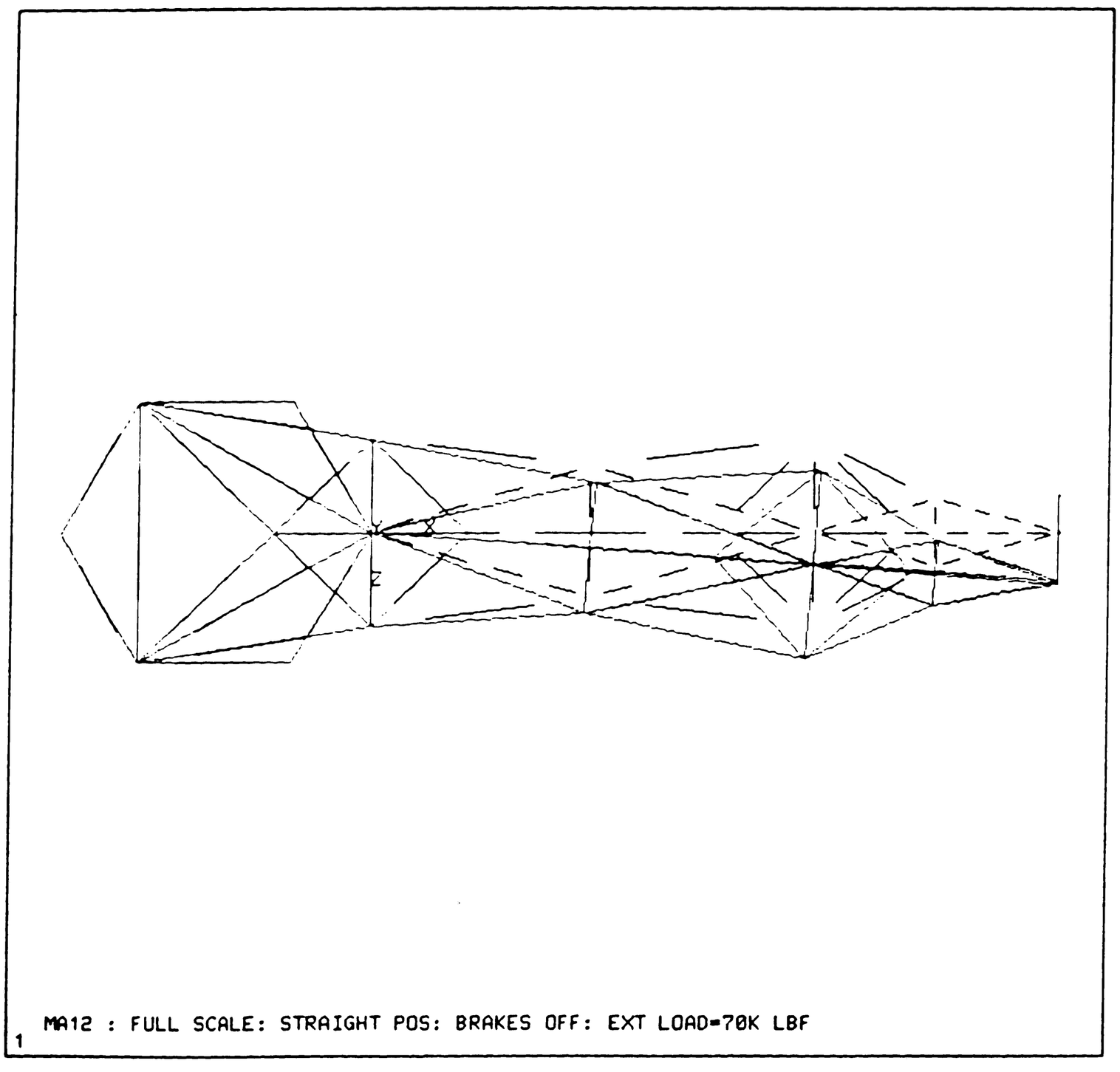

FOR LOAD STEP= 1 ITERATION= 3 SECTION= 1
FREQ= 0.246353 LOAD CASE= 1
TITLE= MA12 : FULL SCALE: STRAIGHT POS: BRAKES OFF: EXT LOAD=70K LBF

Fig 3.59 : Full Scale Arm -- Mode Shapes

(d) Mode Shape #4

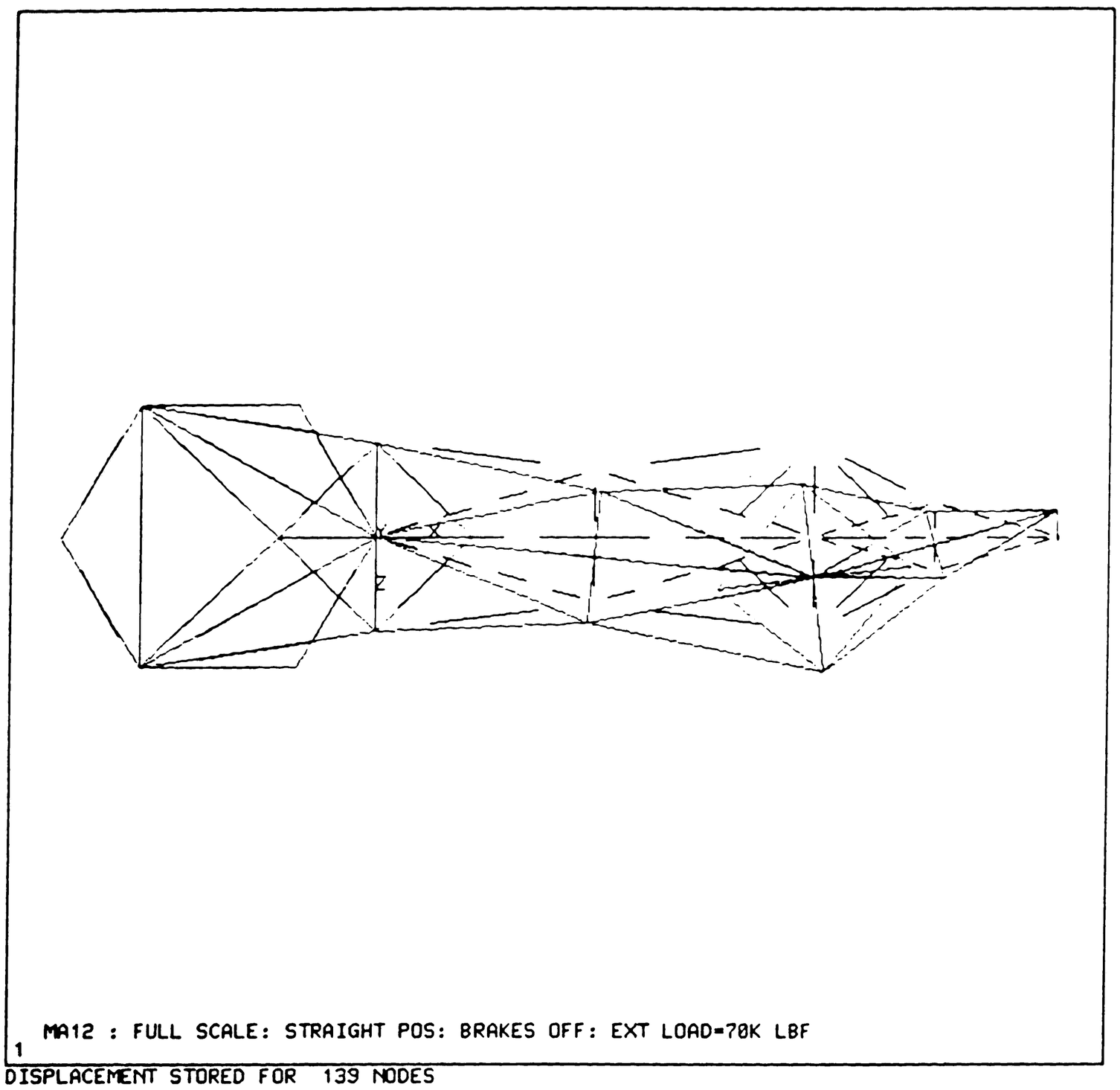

DISPLACEMENT STORED FOR 139 NODES

FOR LOAD STEP= 1 ITERATION= 4 SECTION= 1
FREQ= 0.660556 LOAD CASE= 1
TITLE= MA12 : FULL SCALE: STRAIGHT POS: BRAKES OFF: EXT LOAD=70K LBF

Fig 3.59 : Full Scale Arm -- Mode Shapes

(e) Mode Shape #5

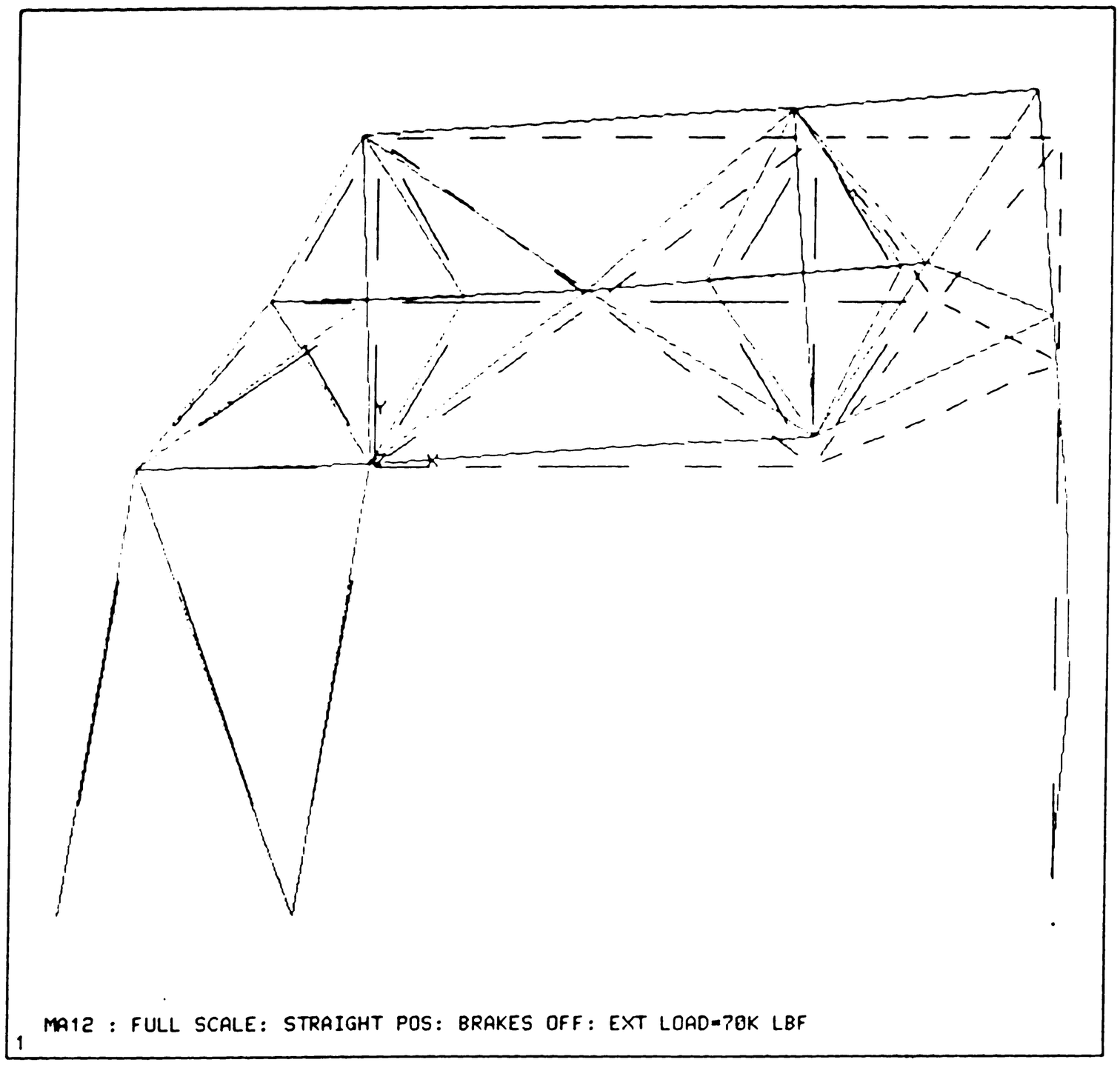

FOR LOAD STEP= 1 ITERATION= 5 SECTION= 1
FREQ= 1.30543 LOAD CASE= 1
TITLE= MA12 : FULL SCALE: STRAIGHT POS: BRAKES OFF: EXT LOAD=70K LBF

Fig 3.59 : Full Scale Arm -- Mode Shapes

(f) Mode Shape #6

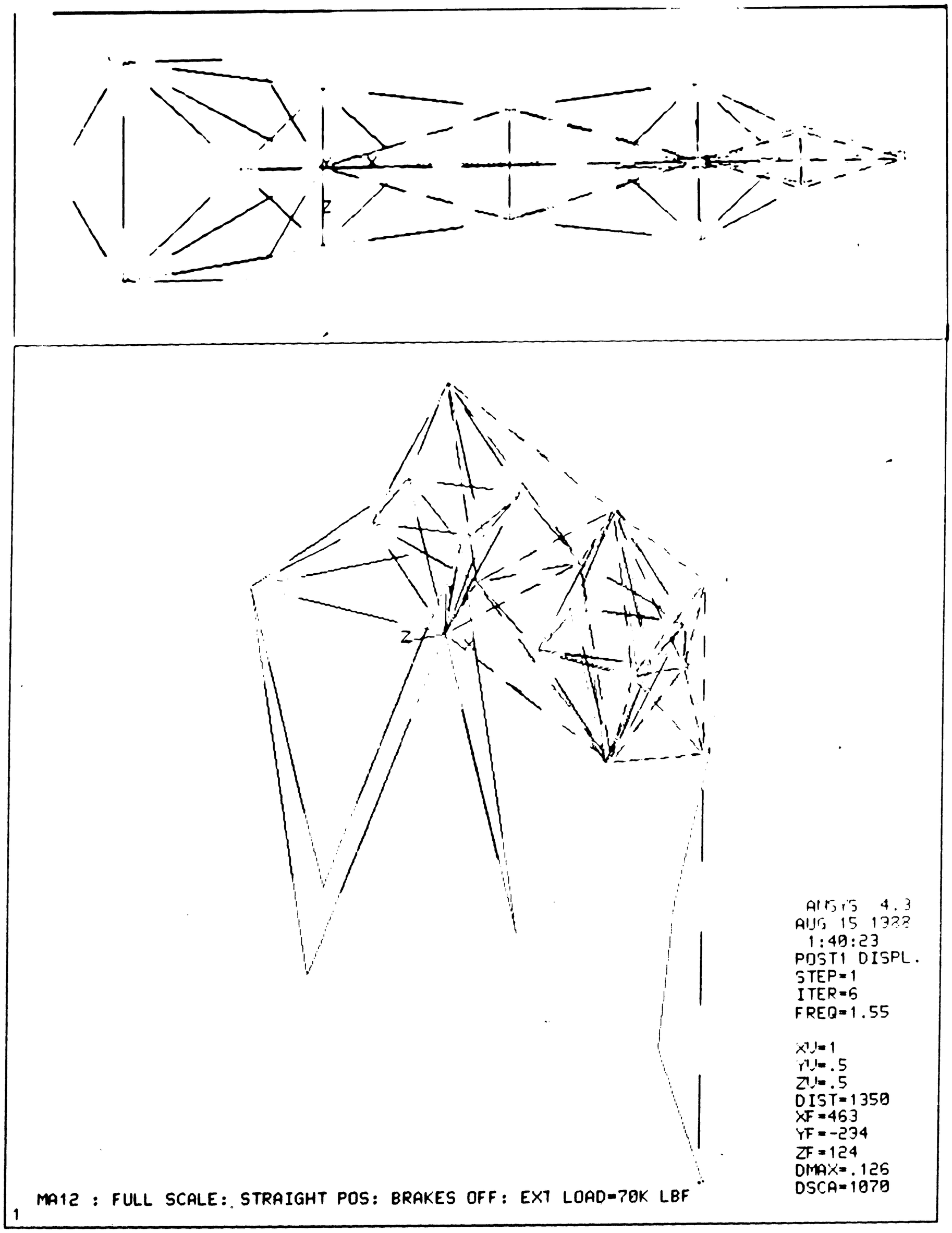

Fig 3.59 : Full Scale Arm -- Mode Shapes

(g) Mode Shape #7

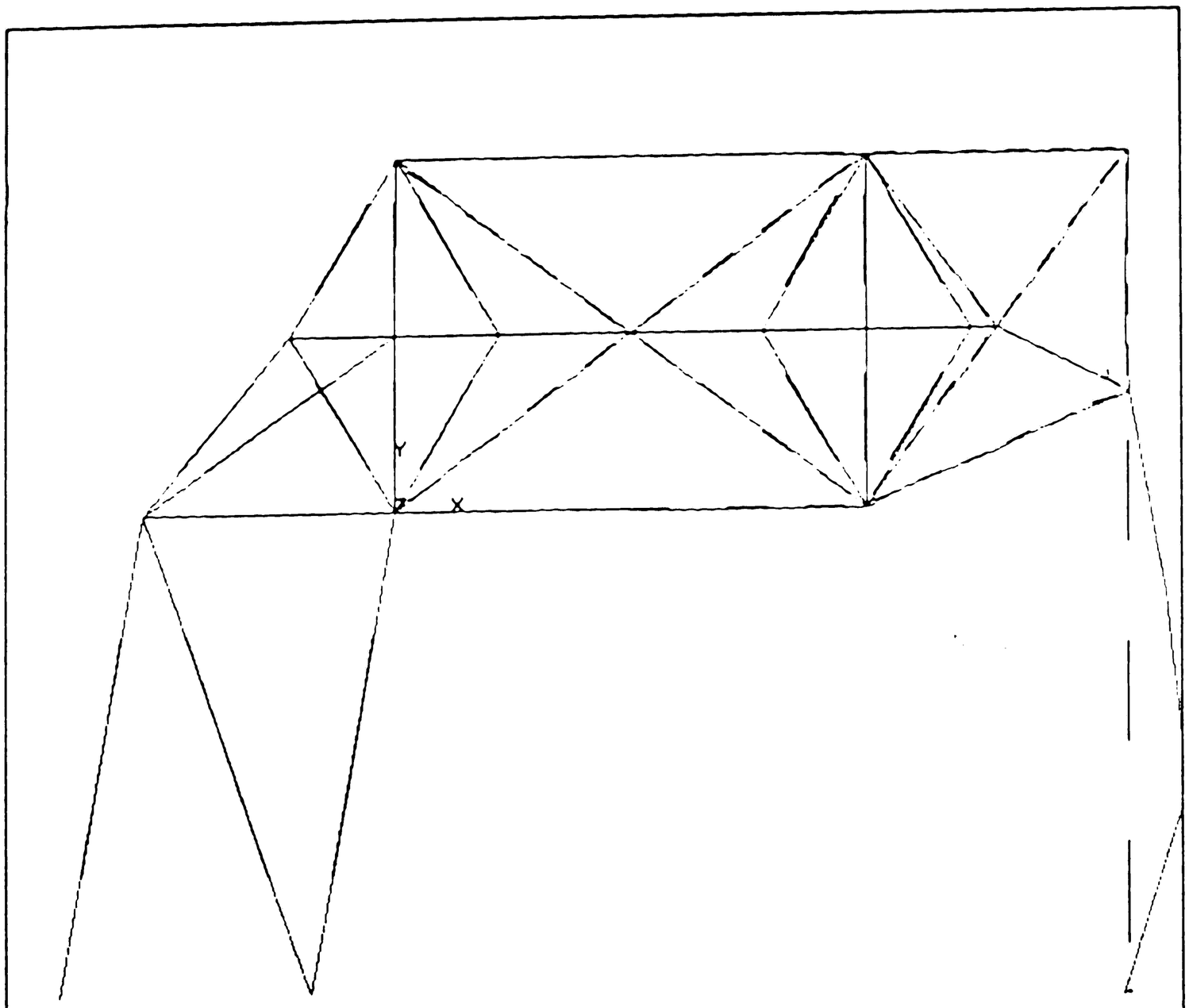

Fig 3.59 : Full Scale Arm -- Mode Shapes

A brief summary of the mode shapes is as follows --

Table 3.11 : Full Scale Preliminary Design -- Modal Analysis Results.

Mode	Name	Frequency (Full / Tenth)	Comments
1.	Swinging Door	.0742/.25	Similar shapes, lowest frequency mode
2.	In-plane Fishing Pole	.16/3.5	Similar shapes, hoist length ratios are 30:1
3.	Out-of-plane Fishing Pole Forearm Assist	.246/2.18	Similar shapes, longer hoist is more flexible
4.	Out-of-plane Fishing Pole Forearm Resist	.661/6.91	Similar shapes
5.	Vertical Chop Assisted / Resisted	1.31/16 (+/-)	Combines Types V & VI -- no forearm drive system
6.	Similar to 3	1.55/-	Hoist vibrates half wave vs quarter wave in type 3
7.	Similar to 2	1.62/-	Hoist vibrates half wave vs quarter wave in type 3

3.4.2.3 Centroid and Moment of Inertia properties for the Full-scale Arm

The centroid and mass moment of inertia properties for the manipulator arm and its major subassemblies are as listed below. Torque calculations can be made for the full-scale arm on the same lines of the tenth-scale arm using the (see 3.4.1.2.3)

A. Fully extended manipulator arm

Centroid Location (inch)	Mom. of Inertia about Origin ($lb\text{-}sec^2in$)	Mom. of Inertia about Centroid ($lb\text{-}sec^2in$)
X = 1330.4 Y = 86.331 Z = 0.0	Ixx = 0.1924E+09 Iyy = 0.9694E+09 Izz = 0.1159E+10 Ixy = -0.8038E+06 Iyz = 0.0 Izx = 0.0	Ixx = 0.1888E+09 Iyy = 0.9526E+08 Izz = 0.2808E+09 Ixy = 0.5592E+08 Iyz = 0.0 Izx = 0.0

B. Upperarm Only (Without Column 2-4)

Centroid Location (inch)	Mom. of Inertia about Origin ($lb\text{-}sec^2in$)	Mom. of Inertia about Centroid ($lb\text{-}sec^2in$)
X = 537.85 Y = 410.91 Z = 0.0	Ixx = 0.1974E+08 Iyy = 0.2877E+08 Izz = 0.4752E+08 Ixy = -0.1657E+08 Iyz = 0.0 Izx = 0.0	Ixx = 0.7123E+07 Iyy = 0.7159E+07 Izz = 0.1330E+08 Ixy = -0.5965E+05 Iyz = 0.0 Izx = 0.0

C. Forearm Only (With Column 2-4; Without any External Load)

Centroid Location (inch)	Mom. of Inertia about Origin ($lb\text{-}sec^2in$)	Mom. of Inertia about Centroid ($lb\text{-}sec^2in$)
X = 1471.7 Y = 28.432 Z = 0.0	Ixx = 0.1727E+09 Iyy = 0.9406E+09 Izz = 0.1111E+10 Ixy = -0.1579E+08 Iyz = 0.0 Izx = 0.0	Ixx = 0.1724E+09 Iyy = 0.3279E+08 Izz = 0.2029E+09 Ixy = 0.3332E+08 Iyz = 0.0 Izx = 0.0

4.0 Summary and Conclusions

4.1 Summary

4.1.1 Design of Robotic Manipulators

A design procedure is recommended for robotic manipulators, based on Fraser's[1] definition of design of structures. Robotic manipulators are treated as structures so that the procedure is catered towards design of large manipulators which can be considered as mechanisms as well as structures. Design process is defined as an essentially trial and error procedure consisting of three interacting aspects : conceptual design or decision making, preliminary kinematic and structural (static and dynamic) analyses, proportioning members and subsequent detailed design. Constraints and parameters to be considered for design of manipulators are discussed. Numerical solution techniques such as finite element analysis are recommended for complex analysis problems.

4.1.2 Design/Analysis of "Large" Robotic Manipulators

Definition for "large"ness of a robotic manipulator has been provided based on the relative size of the manipulator compared to the size of an average human arm. "Large"ness leads to contradicting manipulator design conditions. Manipulators are required to have high structural stiffness with minimum weight, whereas largeness leads to lower stiffness and higher natural frequencies and greater weight. The effect of largeness on stresses, deflections and natural frequencies are discussed by means of simple representative problems. Conventional and unconventional methods are outlined for increasing stiffness/weight ratio of large manipulators, with the emphasis being on latter. Unconventional methods in manipulator design include use of trusses and space frames, embedded closed chains, space frames with variable size members, use of cables for tension members and use of kinematic refinement techniques for stiffness

enhancement. Mechanism design techniques including use of macro- and micro-positioners, and bracing are discussed. Considerations for structural analyses of manipulators have also been included.

4.1.3 Analysis/Design of a "Very Large" Robotic Manipulator

4.1.3.1 Background

One of the main purposes of this study was to analyze the structural characteristics of a 140 ft long and 35 t load capacity SCARA-type manipulator arm, a key component of AACTS. The manipulator can be considered as a "very large" manipulator, and provided a challenging problem of achieving maximum stiffness for minimum weight and adequate performance under dynamic loading conditions.

4.1.3.2 Structural Analyses

Structural analyses were done on both the full-scale and the tenth-scale designs of the manipulator arm. The tenth-scale design was included for analysis for reasons of model building and experimental testing and to serve as a proof-of-concept. Various static and dynamic analysis were done in order to accurately simulate the working conditions. Static analyses of the full-scale design involved force/stress/displacement analysis, linear and non-linear buckling analysis, and detailed basic-frame structure analysis. Modal analysis, harmonic response analysis and transient dynamic response analysis were performed for the dynamic analyses of the full-scale design. The tenth-scale design was evaluated by performing the force/stress/displacement and the modal analyses. Modifications were made to improve the design as the analysis was in process. The cross-section characteristics (area, section modulus and constituent members) were changed to improve the stress and displacement characteristics for the manipulator arm.

A finite element analysis package (ANSYS) was used to perform the various

analyses. The finite element model was built by using equivalent beam members for individual basic-frame structures making up the manipulator arm. A force/stress/-displacement static analysis was first performed for the forearm portion of the manipulator arm, followed by the upperarm portion and then the combined manipulator arm in various relative configurations of the two arm portions. This step-by-step build up of the maniupulator provided a better insight to the characteristics and performance of the manipulator.

The force/stress/displacement analysis provided an indication of the displacement and stress distributions in the manipulator arm, while the detailed basic-frame structure analysis was used for analysis of the critical portions of the arm. The detailed basic-frame structure analysis was used to establish the correct values of cross-sectional areas and moments of inertia to be used for equivalent beam members used to model the basic-frame structure itself. The linear buckling analysis, or the eigen-value buckling, provided an upper boundary indication of the buckling load, assuming that the basic-frame structure was linear in behaviour. The nonlinear analysis provided a more accurate indication of the stability of the structure under applied loads.

Modal analysis was selected as the first dynamic analysis to be performed because the results would provide a good guideline for carrying out the remaining dynamic analyses. Several of the lowest mode frequencies were calculated and mode shapes were characterized. A comparison of the vibration characteristics of the full-scale and the tenth-scale manipulator arms showed good correlation in mode shapes. Differences in the mode frequencies were as expected.

Harmonic analysis of the manipulator arm provided an indication of the steady-state behaviour of the arm under the application of a harmonic/periodic exciting force or

displacement. A harmonic excitation was first applied as a displacement at the tip of the vertical hoist followed by a similar displacement profile at the support points. The arm performance was evaluated as a function of the excitation location. The transient dynamic response analysis was done with the force histories shaped to simulate the effect of step loads and impact loads at the tip of the vertical hoist. The performance of the manipulator arm was then compared with that demonstrated during the static analysis.

4.2 Conclusions

4.2.1 Effectiveness of Design Guide-lines for "Large" Manipulators

The "very large" robotic manipulator analyzed in this study is a SCARA, space frame, macro- and micro-positioner type manipulator. The end point of the manipulator (at which the micro-positioner is attached) displaces by about 2.5 inches while lifting a load of 70,000 lb in the fully extended position (i.e. at a distance of 140 ft from the support). The high structural rigidity obtained can be attributed basically to the space frame nature of the manipulator. A further accuracy in location is possible due to the locating and orienting capability of the micro-positioner and related sensing and control system. Active control can also be used to damp out vibrations experienced at the end effector. A low self-weight is also achieved alongwith high structural stiffness. The manipulator structure weighs about 190,000 lb, which when compared to the payload gives a self-weight to payload ratio of less than 3:1.

4.2.2 Sample Analysis of a Large Manipulator

The finite element method of analysis did prove to be of great help in analyzing the performance of the manipulator arm, a structure of considerable complexity. Since, the method is numerical in nature, some approximations were made in carrying out the analysis in order to simplify the model and to reduce computation time. These

approximations were principally in the representation of the individual basic-frame structures of the manipulator arm by equivalent beam members. Analyses verified that equivalent members could be used to accurately represent more complex structural shapes.

In the conceptual design of the manipulator arm, the individual basic-frame structures were made of structural steel angles. However, the analysis showed that the use of aluminium pipe and slightly deeper basic-frame sections gave a much lighter structure with lower stresses and high rigidity.

Buckling analysis of the manipulator basic-frame structures indicated that the basic-frames would behave as short columns, failing in yielding rather than buckling. The nonlinear analysis showed the effect of eccentric loading (due to manufacturing tolerances) on the buckling performance of the structure.

The variation in performance with rotation of the forearm was quite noticable in the course of the analyses. The 90° rotated configuration lead to the highest induced stresses in the diagonal basic-frame members in the upperarm. In modal analysis, a change in arm configuration led to changes in mode frequencies and, to a certain extent, changes in the mode shapes.

Inclusion of additional basic-frame members between the intersections of the diagonals of the upperarm lead to no appreciable improvements in rigidity, but did provide a degree of redundancy in the manipulator design. A support structure for the manipulator, developed during the analysis, proved to be of good rigidity and suitablity for tenth-scale design testing.

The cable drive system, also developed during the analysis, proved to be of importance in terms of vibration characteristics of the manipulator. Modal analyses indicated that the stiffness of the cables can be effectively used to alter the lowest mode frequencies when the manipulator vibrated without the brakes being set.

The mode shapes of the full and tenth scale manipulator arm showed good correlation. Load conditions, application of brakes and configuration of the manipulator arm, all showed a marked effect on the mode frequencies. However, it was possible to identify and characterize basic mode shapes such that the effect of various conditions on mode frequencies could be studied. The lowest mode frequency was obtained in the fully extended configuration, with ten times the rated load at the vertical hoist and the brakes off at the bearing supports.

The modal analysis showed that several of the mode frequencies were in the range of frequencies which could be excited by the normal working conditions of the manipulator. The harmonic analysis indicated that damping elements would be required in the design of the manipulator arm, since inherent structural damping was not sufficient to limit the induced stresses due to resonance. The induced stresses were higher when the manipulator was excited at the supports than when excited at the vertical hoist.

The transient dynamic response analysis indicated that the stresses induced by step loads could be twice as high as those induced by gradual loading. The ringing of the manipulator upon step or impact loading took a long time to decay, indicating a need for increased damping.

4.3 Suggestions for Further Work

A better understanding of the vibrational characteristics of the manipulator arm under earthquake and seastate conditions can be obtained by the using nonspectrum option of modal analysis provided by ANSYS. In this option, it is possible to excite the structure at the base or any other point on the structure, providing the force or displacement spectra actually observed during the conditions to be simulated.

A transient dynamic analysis of both full-scale and tenth scale designs is suggested to examine the induced stresses when various torque histories are applied at the upperarm and forearm supports. This would give an estimate of the maximum torques allowable in order to obtain greater working speeds. Dynamic analyses can also be done to determine the torque histories needed to obtain required displacement (hence velocity and acceleration) histories at particular points on the arm.

More precise static and dynamic structural analysis can be obtained with the "superelement" analysis technique of ANSYS. For this technique, a repeatable component of the whole structure/system is identified as the superelement. In this case it would be the basic-frame structure used throughout the manipulator arm. This superelement is first modeled separately and then the whole structure is built by using many such superelements. This leads to higher accuracy of solution but does require the use of increased computational resources.

5.0 References

1) Fraser, Donald J.; "Conceptual Design and Preliminary Analysis of Structures"; Pitman Publishing Inc., Marshfield, Massachusetts, 1981.

2) Nnaji, Bartholomew O., "Computer-Aided Design, Selection and Evaluation of Robots";Elsevier Science Publishing Company, Inc., New York, 1986.

3) Rivin, Eugene I.; "Mechanical Design of Robots"; McGraw-Hill Book Company, New York, 1988.

4) Critchlow, Arthur J.; "Introduction to Robotics"; Macmillan Publishing Company, New York, 1985.

5) Dorf, Richard C.; "International Encylopedia of Robotics : Applications and Automation" Vol. 2; John Wiley & Sons, Inc., New York, 1988.

6) Hennessey M. P., Priebe J. A., Huang P. C., Grommes R. J; "Design of a Lightweight Robotic Arm and Controller"; Proc. 1987 IEEE International Conference on Robotics and Automation, pp.779-785, Raleigh, NC, March-April 1987.

7) Book, Wayne J.; "New Concepts in Lightweight Arms"; The 2nd International Symposium on Robotics Research, pp. 203-205, Kyoto, Japan, Aug. 1984.

8) Kiedrzynski A.; "Mass-Stiffness Analysis of Robot Links"; 16th International Symp. on Indl. Robots, pp. 151-158, Brussels, Belgium, 1986.

9) Weck M., Stave H.; "A Method of Optimizing Gantry Robot Stiffness"; 16th International Symp. on Indl. Robots, pp.159-173, Brussels, Belgium, 1986.

10) Chedmail P.; "Robot Structures and Actuators Optimization"; 16th International Symp. on Indl. Robots, pp. 185-195, Brussels, Belgium, 1986.

11) Armstrong B.; "Friction : Experimental Determination, Modeling and Compensation"; Proc. 1988 IEEE International Conference on Robotics and Automation, pp.1422-1427, Philadelphia, PA, April 1988.

12) Singer N. C., Seering W. P.; "Using Acausal Shaping Techniques to Reduce Robot

Vibration"; Proc. 1988 IEEE International Conference on Robotics and Automation, pp. 1434-1439, Philadelphia, PA, April 1988.

13) Gogoussis A., Donath M.; "Couloub Friction Joint and Drive Effects in Robot Mechanisms"; Proc. 1987 IEEE International Conference on Robotics and Automation, pp. 828-836, Raleigh, NC, March-April 1987.

14) Sunada W. H., Dubowsky S.; "On the Dynamic Analysis and Behavior of Industrial Robotic Manipulators with Elastic Members"; Trans. ASME - Journal of Mechanisms, Transmissions, and Automation in Design, vol. 105 pp. 42-51, March 1983.

15) Sunada W. H., Dubowsky S.; "The Application of Finite Element Methods to the Dynamic Analysis of Flexible Spatial and Co-planar Linkage Systems"; Trans. ASME - Journal of Mechanical Design, vol. 103 pp. 643-650, July 1981.

16) Everett L. J., McCarroll D. R.; "Using Finite Element Methods to Approximate Kinematic Solutions of Robotic Manipulators when Closed Form Solutions are Unobtainable"; Proc. IEEE 1986 International Conference on Robotics and Automation, pp. 1164-1167, San Francisco, CA, April 1986.

17) Thomas J., Abbas B. A. H.; "Dynamic Stability of Space Frames by Finite Element Method"; 2nd International Conference on Space Structures, pp. 128-135, Guildford, England, Sept. 1975.

18) Muto M., Matsushita F., Tamamatsu K.; "Travelling Space Structures"; 2nd International Conference on Space Structures, pp. 360-368, Guildford, England, Sept. 1975.

19) Mullord P.; "A Review of Collapse Analysis of Space Structures"; 3rd International Conference on Space Structures, pp. 647-649, Guildford, England, Sept. 1984.

20) Shun J., Tesar A.; "Dynamic Stability of Space Structures"; 3rd International Conference on Space Structures, pp. 446-451, Guildford, England, Sept. 1984.

21) Thomas J., Abbas B. A. H.; "Dynamic Stability of Three-Dimensional Frames Structures"; 3rd International Conference on Space Structures, pp. 642-646, Guildford,

England, Sept. 1984.

22) Dado M., Soni A. H.; "A Generalized Approach for Forward and Inverse Dynamics of Elastic Manipulators"; Proc. IEEE 1986 International Conference on Robotics and Automation, pp. 359-364, San Francisco, CA, April 1986.

23) Shaik M. A., Datseris P.; "A Workspace Optimization Approach to Manipulator Linkage Design"; Proc. IEEE 1986 International Conference on Robotics and Automation, pp. 75-81, San Francisco, CA, April 1986.

24) Vukobratovic M., Potkonjak V.; "Dynamics of Manipulation Robots - Theory and Application"; Springer-Verlag, New York, 1982.

25) Vukobratovic M., Potkonjak V.; "Applied Dynamics and CAD of Manipulation Robots"; Springer-Verlag, New York, 1985.

26) Warnecke H. J., Schraft R. D., Wanner M. C.; "Application of the Experimental Modal-Analysis in the Performance Testing Procedure of Industrial Robots"; Robot technology and Applications - Proc. 1st Robtics Europe Conference, pp.45-53, Brussels, Belgium, June 1984.

27) Asada H., Slotine J-J. E.; "Robot Analysis and Control"; John-Wiley and Sons, Inc., New York, 1986.

28) Corkill P. A., Puderbaugh H. L., Sawyers H. K.; "Structure and Architectural Design"; Sernoll, Inc., Iowa City, Iowa, 1965.

29) Timoshenko S., Young D. H.; "Elements of Strength of Materials", 4th Edition; D. Van Nostrand Company, Inc., Princeton, NJ, 1962.

30) Warnecke H. J., Schraft R. D. (eds.); "Industrial Robots : Application Experience", I.F.S. (Publications) Ltd., Bedford, 1982.

31) Earl C. F., Rooney J.; "Some Kinematic Structures for Robot Manipulator Designs"; ASME Transactions - Journal of Mechanisms, Transmissions, and Automation in Design, vol. 105, pp. 15-22, March 1983.

32) Gupta K. C., Roth B.; "Design Considerations for Manipulator Workspace";

ASME Transactions - Journal of Mechanical Design, vol. 104, pp. 704-711, October 1982.

33) Kobrinskii A. E., Korendiasev A. I., Salamandra B. L., Tyves L. I.; "Programmable Automatic Manipulators (Industrial Robots)", Stanki i Instrument,11, pp. 4-11 (in Russian), 1974.

34) Norris C. H., Hansen R. J., Holley M. J., Biggs J. M., Namyet S., Minami J. K.; "Structural Design for Dynamic Loads"; McGraw-Hill Book Company, Inc., New York, 1959.

35) Sugimoto K.; "An Approach to Structural Synthesis of Robots"; 9th International Symposium on Industrial Robots, pp 641-655, Washington, D.C., March 1979.

36) Burckhardt C. W., Helms D.; "3rd Conference on Industrial Robot Technology & 6th International Symposium on Industrial Robots", pp E4-49 to E4-58, University of Nottingham, U.K., March 1976.

37) Kohnke P. C. (ed.); "ANSYS Engineering Analysis System Theoretical Manual - Revision 4.3"; Swanson Analysis Systems, Inc., Houston, PA, Nov. 1987.

38) S.Timoshenko, D.H.Young; "Elements of Strength of Materials", Fourth Edition; D. Van Nostrand Company, Inc., Princeton, New Jersey; 1962.

39) Seering W. P.; "Directions in Robot Design"; Trans, ASME - Journal of Mechanisms, Transmissions, and Automation in Design, vol. 105, pp 12-13, March 1983.

40) Baumeister T., Avallone E. A., Baumeister III T.; "Mark's Standard Handbook for Mechanical Engineers" Eight Edition; McGraw-Hill Book Company, New York, 1978.

41) Zhang C., Grandin H. T.; "Optimum Design of Flexible Mechanisms"; ASME Transactions - Journal of Mechanisms, Transmissions, and Automation in Design, vol. 105, pp 267-272, June 1983.

42) Beards C. F., Woovat A.; "Control of Frame Vibration by Friction Damping in Joints"; Trans. ASME - Journal of Vibration, Acoustics, Stress, and Reliability in Design, vol. 106, pp 26-32, Jan. 1985.

43) Meirovitch L.; "Elements of Vibration Analysis"; pp 212, McGraw-Hill, Inc., New

York, 1975.

44) Giannotti J. G.; "A Dynamic Simulation of Wave Impact Loads on Offshore Floating Platforms"; Trans. ASME - Journal of Engineering for Industry, pp 550-557, May 1976.

45) Lee D. E., Perreira N. D; Private Consultation, Department of Mechanical Engineering and Mechanics, Lehigh University, Bethlehem, PA.

46) Perreira N. D., Colson J. C.; "Kinematic Arrangements Used in Industrial Robots", Proceedings of the 13th International Symposium on Industrial Robots, Chicago, pp 20-1 to 20-18, April 1983.

47) Address by Vice Admiral Walter T. Piotti, Jr., Commander Sealift Command 10/28/87 at the Military Sealift Technology Conference, Arlington, VA page 19.

48) Dan J. Beakey; "Logistics Over The Shore : Do We Need It?", National Security Affairs Monograph Series No. 82-6, National Defense University Press, Fort Lesley J. McNair, Washington, DC 20319.

49) Ibid., page 45.

50) D. E. Lee, E. J. Dougherty, G.R. Holiday; Automated All-Weather Cargo Transfer System (AACTS) Final Technical Report; August Design and Development Final Report TR C860102 F for Belvoir RD&E Center, March 1987.

51) Private Consultation : Dr. Peter Mueller, Prof. of Civil Engineering, Lehigh University.

52) Gabriel DeSalvo, Robert Gorman; "ANSYS Engineering Analysis System User's Manual", Vol I, Swanson Analysis Systems, Inc., PA, p 2.14.3, 1987.

53) Kilsby-Roberts Stock Catalog, page 85.

Biography

Name : Udaykumar (Uday) G. Parshionikar

Date of Birth : June 8, 1963

Place of Birth : Pune, India

Father's Name : Gunwant E. Parshionikar

Mother's Name : Prabha G. Parshionikar

Education :

- Master of Science (Mechanical Engineering)

  Lehigh University, Bethlehem, PA. [June 1989]

- Bachelor of Engineering (Mechanical Engineering)

  University of Bombay, Bombay, India. [May 1984]

Academic Honors :

- NSF-ATLSS Scholar, Lehigh University, 8/87-1/89.
- Sir Mangaldas Nathubai Scholarship, University of Bombay, 1984.
- National Merit Scholarship, Government of India, 1978.

Professional Interest :

Design/Analysis, Modeling & Simulation of Mechanical Engineering Systems and Processes using CAD/CAE techniques including Finite Element Analysis and Solids Modeling.

Professional Experience :

- Technical Development Engineer, Structural Dynamics Research Corp., Milford, OH. [3/89 - Present]
- Research Assistant, Lehigh University, Bethlehem, PA, and, Ohio University, Athens, OH. [8-86 - 1/89]
- Assistant Systems Analyst & Programmer, Tata Consultancy Services, Bombay, India. [6/84 - 7/86]